University of Southampton

School of Biological Sciences.

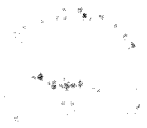

The Nramp family of transition metal transporters in *Arabidopsis thaiiana*.

Russell John Vaughan.

Ph.D. Thesis.

UNIVERSITY OF SOUTHAMPTON

ABSTRACT

FACULTY OF MEDICINE, HEALTH AND LIFE SCIENCES
SCHOOL OF BIOLOGICAL SCIENCES

Doctor of Philosophy

THE NRAMP FAMILY OF TRANSITION METAL TRANSPORTERS IN *ARABIDOPSIS THALIANA*

By Russell John Vaughan

Transition metals such as Cu, Fe, Mn and Zn are essential micronutrients although when present in excess they can be toxic to cells. The uptake and sequestration of these metals therefore requires careful regulation. Natural resistance associated macrophage proteins (Nramps) have been shown to be involved in transition metal homeostasis and are found in many diverse organisms including bacteria, yeast, mammals and plants. The conservation of these proteins suggests an evolutionary advantage for their role in transition metal transport. Analysis of the AtNramp sequences and comparison to other Nramps suggests that they contain 12 transmembrane domains and a conserved signature motif implicated in transport activity. The tissue-specific expression patterns of the *AtNramp* genes have been studied using RT-PCR and quantitative PCR performed on root, leaf, stem, flower and silique material. The *AtNramps* were detected in all tissues with the exception of *AtNramp5*, which was only found in flowers. Upon Fe starvation, *AtNramp3* transcript increased in roots while *AtNramp6* increased in stem. No changes were observed in the other *AtNramp* genes. The function of the AtNramps has been studied using yeast mutants deficient in Fe uptake. *AtNramp3* and *AtNramp4* were able to rescue the *fet3/fet4* Fe uptake mutant while *AtNramp5* and *AtNramp6* have not successfully complemented this mutant. Radiolabelled Fe uptake assays in the same cells showed that AtNramp3 and AtNramp4 are capable of transporting Fe and that this transport is pH dependent in *AtNramp4* transformed cells. A lower level of uptake activity was also observed with AtNramp5 in some experiments. Plant lines containing T-DNA inserts within the *AtNramp* genes have been identified in order to allow the future investigation of the effect of lack of function of the AtNramps. The data presented suggest that members of the AtNramp family play different roles in transition metal homeostasis in *Arabidopsis thaliana*.

Table of contents.

Acknowledgements.

I would very much like to thank my supervisors, Dr. Lorraine Williams and Prof. John Hall for their help and guidance throughout this PhD.

I would also like to thank Dr. Thelma Biggs, Dr. Melanie Logan-Smith, Dr. Aram Buchanan, Dr. Gerard Krijger, Dr. Rebecca Mills, Dr. Pedro Rocha, Dr. Alex McCormac, Dr. Francis Chee, Dr. Vasileios Fotopoulos, Dr. Duncan Legge, Paul Baccarini, Melissa Aylett, David Renville and Lucy Reiman for their assistance and friendship during my time in the laboratory.

Thanks also to my parents, John and Gwen, for all their support over the years.

Abbreviations

ABC	ATP Binding Cassette
ATP	Adenosine Tri-Phosphate
bp	Base Pairs
Ca	Calcium
CAX	Calcium Exchanger
CCCP	Carbonyl Cyanide m-Chlorophenylhydrazone
Cd	Cadmium
Col 0	Columbia 0
COPT	Copper Transporter
C(t)	Cycle Threshold
Cu	Copper
DCT	Divalent Cation Transporter
dH_2O	Deionised H_2O
DIG	Digoxygenin
DMT	Divalent Metal Transporter
DNA	De-oxyribonucleic Acid
DTT	Dithiothreitol
EDTA	Ethylene Diamine Tetra Acetic Acid
EGTA	Ethylene Glycol Tetra Acetic Acid
Fe	Iron
Fet	Ferric Transporter
GFP	Green Fluorescent Protein
GUS	β-glucuronidase

h	Hours
HCl	Hydrochloric Acid
HMA	Heavy Metal ATPase
IRT	Iron Regulated Transporter
Kb	Kilo-base pairs
M	Molar
Min	Minutes
Mn	Manganese
mRNA	Messenger Ribonucleic Acid
MS	Murashige and Skoog
NA	Nicotianamine
Ni	Nickel
Nramp	Natural Resistance Associated Macrophage Protein
PAA	P-type ATPase of *Arabidopsis*
Pb	Lead
PCR	Polymerase Chain Reaction
PEG	Polyethylene Glycol
PPT	Phosphinothricin
qPCR	Quantitative Polymerase Chain Reaction
RAN	Responsive to Antagonist
RNA	Ribonucleic Acid
RT	Reverse Transcriptase
RT-PCR	Reverse Transcriptase Polymerase Chain Reaction
SC	Synthetic Complete
SDS	Sodium Dodecyl Sulfate

Sec	Seconds
SOD	Super Oxide Dismutase
Taq	*Thermus aquaticus*
TMHMM	Transmembrane Hidden Markov Model
TMPred	Transmembrane Prediction
Tris	1-[bis(2,3-dibromopropoxy)phosphinoyloxy]-2,3-dibromo-propane
UTR	Untranslated Region
WT	Wild type
YPD	Yeast Peptone Dextrose
YS	Yellow Stripe
YSL	Yellow Stripe-Like
ZIP	Zinc Iron regulated Protein
Zn	Zinc
Zrt	Zinc Regulated Transporter

1. General introduction.

1.1. Nutrient transport.

All organisms require various nutrients such as sugars, amino acids and inorganic ions for growth and normal cellular function. In order to obtain these nutrients organisms have evolved a range of transport proteins, enabling them to take up nutrients from the medium upon which they live. Pumps move solutes against their electrochemical potential gradient using energy derived from ATP while carriers are coupled to Na^+ or H^+ gradients across the membrane. These ion gradients are maintained by pumps that are also driven by ATP hydrolysis. Carriers are generally high affinity, high specificity and low capacity transporters and usually bind their substrate before moving it through the membrane. Channel proteins are usually low affinity, low specificity and high capacity transporters, which allow the passive diffusion of molecules down their concentration and electrochemical gradients (Epstein and Bloom, 2005). Transition metals identified as essential to plant growth include Fe, Cu, Mn and Zn (Graham and Stangoulis, 2003). These transition metal ions are vital to all organisms since they play roles in many processes within the cell, such as oxidative phosphorylation, free-radical homeostasis and gene regulation (Gunshin *et al.*, 1997). Many of the transition metals are involved in electron transfer chains, due to their ability to donate and receive electrons. Fe and Cu are found in cytochrome oxidase, allowing the protein to reduce oxygen in respiration by carrying electrons (Babcock and Wikström, 1992). Fe is also found in iron-sulphur proteins such as ferredoxin, an electron carrier involved in photosynthesis (Arnon *et al.*, 1964), while Mn is associated with the water-splitting enzyme in photosystem II (Debus, 1992, Sauer and Yachandra, 2004), in components of the cell division cycle (Supek *et al.*, 1997) and in superoxide dismutase (Luk and Culotta, 2001). Zn is known to be a co-factor in many enzymes and proteins (Clarke and Berg, 1998). A summary of the essential micronutrients is shown in Table 1.1. These examples highlight the importance of micronutrients for normal plant growth and survival and the deficiency of a particular micronutrient can result in visible symptoms such as reduced growth and chlorosis. However, although most of the transition metals are essential for life they also have toxic effects on organisms when present in excess. Other transition metals, such as Cd, which are not

Table 1.1. Summary of essential plant micronutrients. (Adapted from Epstein and Bloom, 2005).

Micronutrient	Function	Typical amount in plant cells (Dry weight)	Deficiency symptoms
Boron	Contributes to cell wall stability by binding to pectic polysaccharides of the cell wall.	0.2-800 (ppm)	Growing tips damaged, tissues are hard, dry and brittle. Flowering affected.
Copper	Several metalloenzymes.	2-50 (ppm)	Chlorotic or deep blue-green leaves, margins rolled up.
Iron	Part of heme proteins, ferredoxin and iron-sulphur proteins.	20-600 (ppm)	Chlorosis of young leaves.
Manganese	Part of water splitting enzyme in Photosystem II and in Super Oxide Dismutase.	10-600 (ppm)	Interveinal chlorosis, necrotic spots and streaks. The leaves of certain species become malformed.
Nickel	Constituent of one enzyme: Urease.	0.05-5 (ppm)	Marginal chlorosis of leaves, premature senescence and diminished seed yield.
Zinc	Present in a few metalloenzymes, activates some enzymes but is not specific.	10-250 (ppm)	"Little leaf" (leaves fail to expand) and "Rosette" (internodes fail to elongate) phenotypes. Flowering and fruiting also reduced.

required for plant growth, can also be toxic. These effects include the generation of super-oxide radicals, which damage various cellular organelles and molecules (Srivastava *et al.*, 1989, Briat *et al.*, 1995, Meneghini, 1997, Wang *et al.*, 2004). Cd has also been shown to inhibit the activation of photosystem II by competing for the Ca binding site (Faller *et al.*, 2005). Therefore, although the organism requires a ready supply of some of the transition metals, it is necessary for the plant to maintain tight control over the levels of these metal ions within its tissues. It is now known that the transition metals are almost entirely, if not completely, present within the plant bound to various ligands and not as free ions (Clemens, 2001).

Despite being required in only small quantities many of these micronutrients can be growth limiting. A good example of this problem is Fe, which is required at concentrations of approximately 10^{-4} to 10^{-8} M by the plant. However, in alkaline soils the amount of available Fe can be orders of magnitude lower than this, in the region of 10^{-10} or less (Briat and Lobreaux, 1997, Mori, 1999). Although Zn is also required in similar concentrations to Fe (around 10^{-9} M) it is generally more readily available (Norvell and Welch, 1993, Cohen *et al.*, 2004). Toxic effects of the essential transition metals such as Cu and Fe are generally seen at high μM ranges (Caro and Puntaralo, 1996, Weckx and Clijsters, 1996) and result in oxidative damage to plant tissues. Cd can have toxic effects at concentrations as low as 5 μM, resulting in reduced plant growth, altered uptake of other essential metals, increases in antioxidative enzymes and other signs of abiotic stress (Metwally *et al.*, 2005). Plants capable of tolerating normally toxic levels of these micronutrients have been identified and of particular interest are species termed hyperaccumulators. This term refers to plants that are able to accumulate greater than 1% Zn, 0.1% Ni, Co or Pb, or 0.01% Cd, in shoots when measured as dry weight (Clemens, 2001). These species have the potential to be used for phytoremediation; the reduction or removal of toxic minerals from contaminated soil (Clemens *et al.*, 2002). The most commonly studied species are the Ni hyperaccumulators *Thlaspi goesingense* and *Thiaspi caerulescens* and the molecular mechanisms of this phenomenon are beginning to be identified (Pence *et al.*, 2000, Assuncao *et al.*, 2001, Persans *et al.*, 2001, Bernard *et al.*, 2004, Papoyan and Kochian, 2004). In most cases the mechanism of increased accumulation is the high expression levels of metal transporters and the subsequent sequestration of these metal ions within the plant vacuole. Highly expressed transporters have been

identified from more than one family, including TgMTP1 from the CDF family (Persans *et al.*, 2001) and TcHMA4 from the P_{1B}-type ATPase family (Bernard *et al.*, 2004).

In plants, transporters must exist at the root systems for the uptake of metal nutrients. Other transporters exist for the distribution of essential metal micronutrients to organs and cells where they are required for normal growth and development. Also, plants require transporters to allow them to control the levels of toxic metal ions within cells and organs. This means that plants (and all other complex organisms) require an array of transporters, each with different localisations and specificities, in order to achieve homeostasis. Most nutrients required by plants are obtained from the soil by specific transport systems in the roots. They are then transferred to the xylem vessels via two pathways, termed apoplastic (extracellular) and symplastic (intracellular). Ions being passed through the apoplastic pathway must eventually be transported into cells of the endodermis since a layer of cell wall secondary thickening, known as the Casparian strip, prevents further movement into the stele. Once transported into the endodermal cells ions are transferred to and loaded into xylem vessels for distribution around the plant (Tester and Leigh, 2001). The movement of nutrient ions into and out of the xylem vessels also requires transport proteins, located at the plasma membrane of cells adjacent to the vessels. Once at a sink organ, the ions must then be transported out of the vasculature in order for the nutrients to reach the cells where they are required. A similar process occurs when nutrients are redistributed through the plant via the phloem sieve elements, for example when transporting nutrients to developing seeds (Patrick and Offler, 2001). Specific transport proteins allow nutrients to be passed directly into the phloem vessels, or to the companion cells of the phloem that then load the phloem sieve elements via the plasmodesmata that connect them. Once nutrient ions have been transported into a specific cell these ions are then distributed between the various intracellular organelles where they are required. This process again requires specific transport systems.

The Iron Regulated Transporter 1 (IRT1) of *Arabidopsis thaliana* has been identified as the transport protein primarily responsible for the uptake of Fe from the soil environment by the root system (Eide *et al.*, 1996, Vert *et al.*, 2002). IRT1 was first identified by functional expression in a yeast strain deficient in Fe uptake capacity and was localised to the roots of *Arabidopsis* (Eide *et al.*, 1996). By fusing green fluorescent protein (GFP) to the C-terminus of IRT1 Vert *et al.* (2002) were able to demonstrate that IRT1 was plasma membrane bound. Vert *et al.* (2002) also made

use of the *uidA* gene, which encodes β-glucuronidase (GUS), under the control of the *IRT1* promoter to show that *IRT1* was expressed in cells of the root epidermis and was induced by Fe deficiency. *IRT1* mRNA is detectable 24 h following transfer to Fe deficient conditions and peaks after 72 h (Connolly *et al.*, 2002). IRT1 is also down-regulated (but not induced) by Zn and Cd and plants overexpressing *IRT1* accumulate higher concentrations of these metals than wild type *Arabidopsis* plants (Connolly *et al.*, 2002). In summary, IRT1 appears to be a plasma membrane bound transporter involved in the uptake of Fe, Zn and Cd from the soil into cells of the root epidermis.

The controlled distribution of metal ions within the cell is also important for plant growth and survival. The *responsive to antagonist 1* (*RAN1*) gene, which encodes a Cu transporting ATPase, has been suggested to be important for the transport of Cu into post-Golgi vesicles where this metal ion is incorporated into ethylene receptors before they are transferred to the plasma membrane (Hirayama *et al.*, 1999, Woeste and Kieber, 2000). Plants lacking functional *RAN1* show symptoms such as a rosette-lethal phenotype and a constitutively activated ethylene response pathway, consistent with the lack of functional ethylene receptors (Woeste and Kieber, 2000). A closely related protein, P-type ATPase of *Arabidopsis* (PAA1), also a Cu transporting ATPase, appears to have a similar role in the supply of Cu to chloroplasts (Tabata *et al.,* 1997, Shikanai *et al.,* 2003). Plants lacking functional PAA1 transporters showed reduced levels of active holoplastocyanin, decreasing photosynthetic electron transport. The lack of PAA1 mediated Cu transport in these plants also resulted in insufficient formation of active Cu/Zn SOD isozyme within the stroma of the chloroplasts. From these findings, Shikanai *et al.* (2003) suggested that PAA1 is located within the chloroplast inner envelope and transports Cu across the plastid envelope. PAA1 has since been shown to be located in the chloroplast envelope by GFP fusions, while another protein, named PAA2, has been identified and localised to the thylakoid membrane, the two proteins functioning in sequence to supply the chloroplast and its internal structures with Cu (Abdel-Ghany *et al.*, 2005).

It is generally considered that one of the functions of the plant cell vacuole is in the storage of various solutes, including the sequestration of metal ions in order to reduce their toxic effects (Hall, 2002). Two cation/H^+ antiporters, Ca^{2+} exchanger 1 and 2 (CAX1 and CAX2) have been identified and localised to the tonoplast (Hirschi *et al.*, 1996, Hirschi *et al.*, 2000). CAX1 has been shown to be important for maintaining low cytosolic Ca^{2+} concentrations by pumping Ca^{2+} into the vacuole (Hirschi *et al.,* 1996)

while CAX2 can also transport Mn and Cd and confers enhanced Mn tolerance, albeit for a limited time (Hirschi *et al.*, 2000).

Two different strategies have evolved to tackle the problem of Fe uptake, a divalent cation required for normal plant growth but one that is of relatively low availability in the soil environment. Most higher plants use a method involving a plasma membrane bound ferric chelate reductase (Robinson *et al.*, 1999) to reduce Fe from Fe^{3+} to the more accessible Fe^{2+} form and an Fe transport protein (Eide *et al.*, 1996) to allow uptake into the root system. This approach is known as strategy I. Strategy II is utilised by the grasses (Poaceae) and involves the production of Fe^{3+} chelating agents known as phytosiderophores. These molecules bind Fe^{3+} and are then taken into the plant by Fe^{3+}/phytosiderophore specific transporter systems such as YS1 (Curie *et al.*, 2001) and Fe is released from the complex within the cell.

1.2. Transition metal transport in plants.

Reviews of the mechanisms of transition metal transport in higher plants can be found in Fox and Guerinot (1998), Guerinot (2000), Williams *et al.* (2000), Maser *et al.*, (2001) and Hall and Williams (2003). Families of transport proteins implicated in transition metal homeostasis in plants include members of a number of different gene families, summarised below. The Nramp family is reviewed in more detail in section 1.4.

1.2.1. ABC family.

Members of the ABC (ATP Binding Cassette) family are found in a wide range of organisms and use the energy derived from ATP to drive transport. In addition to an ATP binding domain they also contain between 4 to 6 transmembrane helices although the arrangement of these domains is not always consistent between different members of the family (Theodoulou, 2000). ABC transporters are able to transport a variety of substrates such as ions, peptides, sugars, heavy metal chelates, lipids, inorganic acids and glutathione conjugates. Evidence for a role in transition metal transport by members of this family has been obtained in the fission yeast where the *heavy metal tolerance 1* (*HMT1*) gene has been shown to alleviate Cd-sensitivity of a

mutant strain. The HMT1 sequence shares some similarity with other members of the ABC family (Ortiz *et al.*, 1992). More recently it has been shown that *Arabidopsis thaliana multidrug resistance-related protein* (*MRP*) genes are induced by Cd treatment indicating they may be involved in Cd transport in plants (Bovet *et al.*, 2003). Furthermore, an Fe-regulated ABC transporter, Fe-deficiency induced 7 (IDI7), has been identified in barley roots; its expression closely follows the Fe nutritional status of the plant, although it may play a role in the production of phytosiderophores, rather than transporting Fe itself (Yamaguchi *et al.*, 2002). A role in Fe transport for an ABC transporter has been identified previously in yeast. Strains with an *ABC transporter of mitochondria 1* (*ATM1*) deletion were found to accumulate approximately 30-fold higher levels of Fe in mitochondria than wild-type cells, indicating a role in mitochondrial Fe homeostasis (Kispal *et al.*, 1997). As yet, the data obtained for this family has not conclusively shown transition metal transport activity in plants but does suggest a role in metal homeostasis in some cases.

1.2.2. P_{1B}-type ATPases.

P-type ATPases form a large superfamily of transporters found in bacteria, fungi, plants and animals and as with the ABC family make use of ATP to obtain the energy needed for transport (Axelsen and Palmgren, 2001). Within the P-type ATPase superfamily five different families have been identified by their transport specificity or homology to other P-type ATPases (Palmgren and Axelsen, 1998). These five families can also be further sub-divided according to their transport specificity. The P-type ATPases implicated in the transport of transition metals form the type IB sub-family or heavy metal ATPases (HMAs), also known as the CPx-type ATPases due to the presence of cysteine-proline-cysteine/histidine/serine motifs within the sequence (Solioz and Vulpe, 1996). This sub-family can also be divided into two groups: one able to transport Cu or Ag cations, the other Zn, Co, Cd or Pb (Axelsen and Palmgren, 2001, Mills *et al.*,2003). In *A. thaliana* eight HMA ATPase sequences have been identified (Mills *et al.*, 2003), some of which have been suggested to function in the transport of Cu (Hirayama *et al.*, 1999, Shikanai *et al.*, 2003) or Zn and Cd (Mills *et al.*, 2003, 2005). More recently it has been shown that *athma2/athma4* double mutants contain lower than wild-type levels of Zn and exhibited Cd sensitivity in phytochelatin-deficient plants, suggesting a role for these proteins in Zn and Cd homeostasis

(Hussain *et al.*, 2004). To date, only two of these proteins have been assigned specific functions in *Arabidopsis.* RAN1 has been suggested to transport Cu into post-golgi vesicles to allow the production of active ethylene receptors (Hirayama *et al.*, 1999, Woeste and Kieber, 2000) while PAA1 transports Cu into chloroplasts across the plastid envelope (Shikanai *et al.*, 2003).

1.2.3. CNGC family.

The CNGC (Cyclic Nucleotide-Gated Channels) family consists of sequences with calmodulin and cyclic nucleotide binding domains (Maser *et al.*, 2001). CNGCs are generally plasma membrane bound and are non-selectively permeable to monovalent and divalent cations. Plant members of this family are possibly able to transport Pb and Ni since transgenic tobacco over-expressing the *calmodulin binding protein* (*NtCBP4*) gene show tolerance to Ni and sensitivity to Pb (Arazi *et al.*, 1999). Leng *et al.* (2002) found that AtCNGC1 and NtCBP4 are able to transport Ca and K and may function in the uptake of these minerals from the soil along with non-essential metals such as Pb.

1.2.4. CDF family.

The CDF (Cation Diffusion Facilitator) family (also given the name cation efflux, CE, or metal tolerance protein, MTP, family) comprises proteins with six transmembrane domains, a signature sequence at the N-terminus and a C-terminal cation efflux domain (Maser *et al.*, 2001). The evidence accumulated to date suggests that CDF proteins play a role in the transport of Zn, Mn or Cd. In *A. thaliana,* eight members of this family have been identified by sequence similarity (Maser *et al.*, 2001). Of these, the *Zn transporter of Arabidopsis thaliana* (*ZAT,* also referred to as *MTP1*) gene has been shown to be induced by increased Zn levels and, when over-expressed, leads to Zn resistance and a higher Zn content (Van der Zaal *et al.*, 1999). ZAT (MTP1) has been localised to the tonoplast and shown to transport Zn into the vacuole (Kobae *et al.*, 2004). Interestingly, it was also shown that MTP1 appears to be specific for Zn and does not have a broad substrate range unlike many other metal transporters. Novel members of this family, the MTPs from *Arabidopsis halleri,* have also been shown to be localised at the vacuolar membrane, are regulated by Zn at the

transcript level and are responsible for detoxification of Zn in the cell vacuole (Drager *et al.*, 2004). An MTP has also been identified in *Stylosanthes hamata,* a tropical legume that often grows in soils high in Mn (Delhaize *et al.*, 2003). It was found that this protein (named ShMTP1) also localises to the tonoplast and is capable of conferring Mn tolerance to *Arabidopsis thaliana* by transporting excess Mn into internal organelles, indicating a role in tolerance to Mn. A CDF protein, TgMTP1, has also been identified in the hyperaccumulator, *Thlaspi goesingense* (Persans *et al.*, 2001). It was found that the single genomic sequence gave rise to two transcripts, one spliced, the other unspliced. Expression of these two transcripts in yeast showed that the unspliced transcript provided the highest tolerance to Cd, Co and Zn while the spliced transcript resulted in higher tolerance to Ni. Both transcripts are highly expressed in *T. goesingense* and may contribute to the plants ability to hyperaccumulate metal ions within shoot vacuoles.

1.2.5. ZIP family.

The ZIP (ZRT, IRT-like Protein) family contains many members found in bacteria and all types of eukaryotes. They are predicted to contain 8 transmembrane domains (Guerinot, 2000) and can be grouped into four sub-families based on sequence similarity (Maser *et al.*, 2001). The first member of this family (Iron regulated transporter, IRT1) was identified in *A. thaliana* by screening cDNAs for their ability to rescue an Fe uptake-deficient yeast mutant (Eide *et al.*, 1996). More recent and similar findings show that this protein is up-regulated on Fe-deficiency and is responsible for Fe uptake at the root although it is also able to transport Cd and Zn (Connolly *et al.*, 2002, Vert *et al.*, 2002). Plants lacking a functional *IRT1* gene are chlorotic and show impaired growth but can be rescued by supplying Fe (Vert *et al.*, 2002). A closely related gene, *IRT2*, has also been cloned from *A. thaliana* roots and shown to transport Fe and Zn but not Cd or Mn by yeast functional complementation (Vert *et al.*, 2001). *IRT2* was found to be expressed in the outer cell layers of the root, suggesting a role in uptake from the soil (Vert *et al.*, 2001). The rice homologue of *IRT1* (*OsIRT1*) has also been identified specifically in root tissue; it rescues yeast deficient in Fe uptake and is upregulated in rice plants deficient in Fe or Cu (Bughio *et al.*, 2002). ZIPs 1 to 3 have been identified as potential Zn uptake proteins since they are expressed in roots of Zn-deficient plants and have been shown to complement the

yeast Zn-uptake mutant *zrt1/zrt2* (Grotz *et al.*, 1998, Guerinot, 2000). LeIRT1 and LeIRT2 have also been identified in tomato and appear to be differentially regulated by Fe, *LeIRT1* being up-regulated by Fe deficiency while *LeIRT2* expression was not altered (Bereczky *et al.*, 2003).

1.2.6. Cation/H^+ antiporter family.

Plant members of this family generally contain between 10 and 14 transmembrane domains and a number of repeated residues (Maser *et al.*, 2001). While they have been implicated in transport of Ca and Na there is evidence that some members of this family, such as the Ca^{2+}/H^+ exchanger 2 (CAX2), can transport Cd (Hirschi *et al.*, 2000, Hirschi, 2001) and Mn (Shigaki *et al.*, 2003). Maser *et al.* (2001) observed that many of the sequences related to CAX2 possess organellar-targeting sequences suggesting some members of this family may reside in the membranes of intracellular organelles. Expression of CAX2 in tobacco resulted in the accumulation of Ca, Cd and Mn as well as increased resistance to Mn toxicity (Hirschi *et al.*, 2000). Vacuolar Mn transport by CAX2 was also shown by Shigaki *et al.* (2003).

1.2.7. Copper transporter family.

Putative Cu transporters have been identified in many eukaryotes including yeast (Dancis *et al.*, 1994, Marjorette *et al.*, 2000) and *A. thaliana* (Kampfenkel *et al.*, 1995). In *A. thaliana* five members of this family have been identified, named Cu transporter 1-5 (COPT1-5), some of which show functional complementation of yeast mutants deficient in Cu transport (Kampfenkel *et al.*, 1995, Sancenon *et al.*, 2003). The expression of these genes was generally found to be lower in roots than shoots but it remains unclear if these proteins function in Cu uptake or in distribution around the plant.

1.2.8. YSL proteins.

Although not a family, the yellow stripe-like (YSL) proteins are of importance in the uptake of Fe, especially in plants utilising strategy II for Fe uptake (as discussed in section 1.1). Eight predicted YSL proteins exist in *A. thaliana* and maize *yellow stripe 1*

(*YS1*) has been shown to be capable of Fe^{3+}-phytosiderophore complex transport in yeast Fe uptake deficient mutants and is up-regulated by Fe deficiency in maize (Curie *et al.*, 2001). More recently YS1 has also been shown to be capable of transporting nicotianamine (NA) chelates, such as Fe-NA and Cu-NA, in addition to Fe-phytosiderophores (Roberts *et al.*, 2004). Since NA (a precursor to phytosiderophores) is produced by all higher plants and is also found in the phloem this may explain the function of YSL proteins in plants such as *Arabidopsis* that lack phytosiderophore production and strategy II uptake of Fe.

1.3. Transition metal transport in yeast.

The characterisation of transition metal transporters in yeast has helped pave the way for heterologous expression of plant proteins in metal uptake deficient yeast mutants allowing the identification of candidate metal transporters by functional complementation (Dreyer, 1999). This approach led to the identification of the *A. thaliana* root Fe transporter, IRT1, thought to be largely responsible for uptake of Fe from the soil (Eide *et al.,* 1996). In yeast, Fe is first reduced to the Fe^{2+} form by ferri-reductases (Eide *et al.*, 1992) and its transport mediated by both high affinity and low affinity uptake systems (Askwith *et al.*, 1994, Dix *et al.*, 1994). The low affinity Fe transporter is encoded by the *FET4* gene (Dix *et al.*, 1994, 1997) while the high affinity transport system comprises of a multi-copper oxidase (FET3) and an Fe transporter (FTR1) (Askwith *et al.*, 1994, Stearman *et al.*, 1996). Zn uptake is also mediated by high and low affinity transport systems encoded by the *ZRT1* and *ZRT2* genes respectively (Zhao and Eide, 1996a, b). While ZRT2 is responsible for low affinity transport under Zn replete conditions, ZRT1 is induced in yeast when Zn is available in low concentrations and mediates high affinity transport of this cation. Following reduction by metalloreductases, Cu transport in yeast appears to be attributed to a low affinity transporter, CTR2, and to two functionally redundant proteins, CTR1 and CTR3, both high affinity copper transporters expressed at the plasma membrane and regulated at the transcriptional level by Cu (Dancis *et al.*, 1994, Marjorette *et al.*, 2000). Members of the Nramp family in yeast, SMF1 and SMF2 have been shown to transport a range of divalent cations but are most likely to function in the uptake of Mn, Zn or Cu (Supek *et al.*, 1996, Chen *et al.*, 1999, Cohen *et al.*, 2000). The *SMF* genes are discussed further in section 1.4.

1.4. The Nramp family.

Natural resistance-associated macrophage proteins (Nramps) and the genes that encode them are found in a wide range of organisms, including bacteria, yeast, plants, insects and mammals (Vidal *et al.,* 1993; Belouchi *et al.,* 1995; Rodrigues *et al.,* 1995; Supek *et al.,* 1996; Agranoff *et al.,* 1999; Williams *et al.,* 2000). They appear to be a highly conserved family of proteins that are thought to function in the transport of a number of divalent metal ions, including Fe^{2+}, Zn^{2+}, Mn^{2+} and Cu^{2+}, all of which are essential for plant metabolism. When high concentrations of these ions, along with Cd^{2+} (a non-essential metal), are encountered they can be extremely toxic to the plant, indicating the importance of metal homeostasis for normal cellular function. The high degree of conservation observed, even between Nramp proteins from animals and plants, suggests that the Nramp family may belong to an ancient class of membrane transporters (Cellier *et al.*, 1995). Much of the similarity between the proteins of the Nramp family is found in the first 10 hydrophobic transmembrane domains (of a predicted maximum of 12) while the other regions, including the amino and carboxy termini, are much more variable, possibly reflecting different modes of regulation and/or specificity (Cellier *et al.*, 1995). Conserved regions have also been found in some of the intra and extracytoplasmic domains between transmembrane segments, including a conserved region of predicted N-linked glycosylation sites between transmembrane segments 7 and 8 (Belouchi *et al.,* 1997). The intracytoplasmic loop between transmembrane segments 8 and 9 was found to contain a conserved sequence motif of unknown function, known as a binding-protein-dependent transport system inner membrane component signature, also found in many other membrane proteins (Cellier *et al.*, 1995; Belouchi *et al.,* 1997). This region is commonly referred to as a consensus transport signature, is highly conserved in the Nramp gene family and could be important for their function, although this remains to be demonstrated (Williams *et al.*, 2000).

Nramp was first identified by Vidal *et al.* (1993) when they found that a dominant gene given the name *Bcg* controlled resistance to intracellular parasites in mice. This gene was found to affect the ability of macrophages to destroy engulfed bacteria. The authors were able to identify that *Nramp* (later named *Nramp1*, see review by Cellier *et al.,* 1996) was a strong candidate for *Bcg* since a Gly to Asp

substitution at position 105 of the *Nramp* was associated with the susceptible *Bcg* phenotype. Also, both *Bcg* and *Nramp* mapped to the same position on chromosome 1 and were found to be expressed specifically in macrophages. *Nramp2* was later identified, shown to be expressed in a number of tissues and cell types and capable of complementing the yeast *SMF* mutants suggesting that Nramp2 is capable of transporting Mn^{2+} (Pinner *et al.*, 1997). Working on the rat, Gunshin *et al.* (1997) identified a ubiquitously expressed, 561 amino acid protein with 12 transmembrane domains and found it to be a metal ion transporter, coupled to the proton gradient across the cell membrane. Proton coupled transport of Fe^{2+} was shown by simultaneously monitoring changes in intracellular pH and Fe^{2+}-evoked currents in *Xenopus* oocytes injected with the mRNA encoding this protein. The protein was given the name divalent cation transporter (DCT1) and was shown to be a member of the Nramp family due to its high similarity to other Nramps. Although capable of transporting a wide range of divalent cations, DCT1 was found to be upregulated by iron deficiency in the diet and is most noticeably active in the proximal duodenum. It was proposed that DCT1 functions in iron uptake in the gut, a suggestion which was confirmed when Nramp2 (the human homologue of DCT1) was shown to be localised in the apical membrane of intestinal epithelial cells using antibodies and capable of transporting radioactive $^{55}Fe^{2+}$ in uptake studies (Tandy *et al.*, 2000). Nramp2 has also been shown to have a role in transport of iron out of intracellular endosomes in both the rat and the mouse (Fleming *et al.*, 1998). Since then, Nramp homologues have been identified in a number of other organisms, such as *Mycobacterium tuberculosis* Mramp (Agranoff *et al.*, 1999), *Escherichia coli* MntH (Makui *et al.*, 2000), Yeast SMF1 (Supek *et al.*, 1996), SMF2 and 3 (reviewed by Cellier *et al.*, 1995, Chen *et al.*, 1999, Cohen *et al.*, 2000), *Drosophila melanogaster* Malvolio (Rodrigues *et al.*, 1995), *Caenorhabditis elegans* (Cellier *et al.*, 1995), *Oryza sativa* (Belouchi *et al.*, 1995, Belouchi *et al.*, 1997, Cellier *et al.*, 1995,), *A. thaliana* (Curie *et al.*, 2000, Thomine *et al.*, 2000, Williams *et al.*, 2000), *Lycopersicon esculentum* (Bereczky *et al.*, 2003), *Glycine max* (Kaiser *et al.*, 2003) and *Hordeum vulgare* (Finkemeier *et al.*, 2003).

Studies conducted using yeast and its Nramp homologue, SMF1, have identified another gene, *Bsd2*, whose product is able to regulate the activity of SMF1. It was proposed that the *Bsd2* gene product is able to redirect traffic of SMF1 proteins to the vacuole of the yeast when metal ions are abundant. At the vacuole the SMF1

protein is degraded by vacuolar proteases. When metal ions are in short supply it was suggested that SMF1 undergoes a conformational change and is no longer recognised by the Bsd2 protein, therefore allowing SMF1 to accumulate in the plasma membrane and transport metal ions into the cell (Liu and Culotta, 1999a). It was later confirmed that this post-translational control of SMF1 does occur in yeast (Liu and Culotta, 1999b). Differing roles and cellular locations for the three SMF proteins so far identified in yeast have been suggested by Portnoy *et al.* (2000). While SMF1 and 2 seem to function in the uptake of Mn^{2+} across the plasma membrane and are regulated by Bsd2, SMF3 is targeted to the vacuolar membrane and is down-regulated by Fe^{2+}. It is proposed that SMF3 functions in maintaining Fe^{2+} homeostasis by transporting it into and out of the vacuole (Portnoy *et al.*, 2000).

In *A. thaliana* six genes have been identified with homologies to members of the Nramp family and have been named AtNramp1-6 (Curie *et al.*, 2000, Thomine *et al.*, 2000, Williams *et al.* 2000, Maser *et al.*, 2001). So far, the data for proteins of the Nramp family expressed in plants have only shown broad substrate specificities. Curie *et al.* (2000) sequenced five *Nramp* genes from *A. thaliana* and discovered that there appear to be two different groups based on the comparison of their sequences. In *Arabidopsis thaliana Nramp2, 3, 4* and *5* share a high sequence similarity and group together while *Nramp1* is separate. Curie *et al.* (2000) also showed that Nramp1, but not Nramp2, is capable of restoring the function of the yeast *fet3/fet4* mutant, which lacks high (*fet3*) and low (*fet4*) affinity iron transporters, indicating the ability of Nramp1 to transport Fe^{2+}. However, Thomine *et al.* (2000) found that both Nramp3 and 4 are also capable of complementing the yeast *fet3/fet4* mutant possibly suggesting that, although they group with Nramp2 due to sequence similarity, they do not necessarily share the same function and that the grouping proposed by Curie *et al.* (2000) could be misleading. For *AtNramp6*, two cDNA transcripts have been identified in our laboratory by RT-PCR, one of which retains an intron (Pittman *et al.*, unpublished). Thomine *et al.* (2000) also showed that Nramps might be capable of transporting Mn^{2+} (by complementing a *smf1/smf2* yeast mutant deficient in Mn^{2+} uptake) and Cd^{2+} (by showing that *AtNramp3* disruption in *A. thaliana* led to Cd^{2+} toxicity resistance and over-expression resulted in Cd^{2+} sensitivity). Curie *et al.* (2000) were able to show that iron deficiency in *A. thaliana* roots leads to accumulation of the *AtNramp1*, but not the *AtNramp2,* transcript, while over-expression of *AtNramp1* can result in resistance of transgenic *A. thaliana* plants to normally toxic levels of iron. More recently, Thomine *et*

al. (2003) have shown that *AtNramp3* is expressed in vascular bundles of the roots, stem and leaves under Fe-replete conditions by using promoter-GUS fusions. *AtNramp3* is also expressed in vascular bundles and is up-regulated under Fe- limited conditions. AtNramp3::GFP fusions were also used to show that AtNramp3 is targeted to the tonoplast of *A. thaliana* cells. Overexpression of AtNramp3 was shown to reduce manganese accumulation as well as down-regulating the expression of IRT1 and FRO2 while disruption of AtNramp3 resulted in increased accumulation of manganese and zinc. These changes were only observed in Fe-deficient plants. The data obtained by Thomine *et al.* (2003) led them to suggest that AtNramp3 is involved in mobilization of metal pools to or from the vacuole of cells in the vascular bundles. All these results suggest that the AtNramps may be able to transport a range of divalent cations. However, much still remains to be understood of the function of the Nramps in plants and further studies of the substrate specificity and localisation of the *A. thaliana* Nramps are therefore required.

1.5. Aims.

The aims of this study are to identify the potential roles of the Nramps from *Arabidopsis thaliana* in transition metal homeostasis at the whole plant, tissue and cellular level. This includes the elucidation of their functional activity, their pattern of expression within the plant and their localisation within individual cells under varying environmental conditions such as metal-deficiency or toxicity. This information is to be used to help place the Nramps within the overall picture of transition metal transport and homeostasis in higher plants, relative to other families of transport proteins.

Experiments will be performed with the aim to further characterise the substrate specificity and tissue and cellular localisation of AtNramp5 and AtNramp6 isolated from *A. thaliana* and to identify their potential role in transition metal uptake and transport. In order to study the function of the AtNramps, yeast mutant complementation and radioactive Fe uptake studies will be performed. Complementation involves transforming mutant yeast cells, deficient in endogenous uptake systems for certain divalent metal ions, with Nramps from *A. thaliana*. Any AtNramps capable of rescuing the yeast mutant are therefore capable of transporting the ions for which the yeast lacks uptake systems. Radioactive studies allow the uptake of specific metal ions to be traced and rates of uptake measured. In addition,

competition studies with other metal cations can be performed in order to aid identification of the substrate specificity of each Nramp. RT-PCR methods will be used to identify the expression pattern of these genes in various *A. thaliana* tissues, while *A. thaliana* plants transformed with promoter-GUS constructs will be used to study the localisation of the various AtNramps using the GUS assay.

Chapter 2. Materials and Methods.

2.1. Plating *Arabidopsis thaliana* seeds.

Once dried, the stems of *Arabidopsis thaliana* ecotype Columbia 0 were cut off into a tray lined with white paper and the siliques stripped off by hand. Seeds and debris were then poured into a fine sieve and debris ground by hand to release seeds into a tray lined with white paper. Seeds and remaining debris were sieved once again and stored at 4°C. Enough seeds to plate out 200 seeds per plate were weighed out; assuming 2000 seeds have a mass of approximately 40 mg. Seeds were washed in 1 ml 10% (v/v) bleach for 15 min while shaking. They were pulsed in a Sorvall MC 12 V microfuge and the bleach removed by pipette. Seeds were washed in 1 ml sterile distilled H_2O and pulsed again. This was repeated until all bleach was removed. Seeds were resuspended in 1 ml 0.1% (w/v) agarose per 10 mg of seeds. Seeds were plated in 400 µl volumes onto 0.5 × Murashige and Skoog salts, 0.8% (w/v) agar (pH 5.8) plates with 10 µg/ml phosphinothricin in order to select transformed seedlings. Seedlings were left to grow on plates in a growth room at 23°C with a 16 h photo-period and a light intensity of approximately 100 µmol. m^{-2} s^{-1} for approximately 2 weeks. Surviving seedlings were transferred to soil composed of equal parts Levingtons F2s, John Innes No. 2 and Vermiculite. Plants were placed in individual pots and bags placed around each pot to prevent cross pollination and seed dispersal.

2.2. Growth of *Arabidopsis* in hydroponic culture.

Arabidopsis thaliana ecotype Columbia 0 seed were sterilised as described above and individually transferred to black 0.5 ml microfuge tubes containing 300 µl of 0.6% (w/v) agar with the bottom 0.5 cm cut off. These were placed into black foam rafts, approximately 70 tubes per raft. These were floated on a hydroponic culture medium based on Arteca and Arteca (2000) (1.25 mM KNO_3, 0.5 mM $Ca(NO_3)_2$-$(H_2O)_4$, 0.5 mM $MgSO_4$-$(H_2O)_7$, 42.5 µM FeNaEDTA, 0.625 µM KH_2PO_4, 2 mM NaCl, 0.16 µM $CuSO_4$-$(H_2O)_5$, 0.38 µM $ZnSO_4$-$(H_2O)_7$, 1.8 µM $MnSO_4$-(H_2O), 45 µM H_3BO_3, 0.015 µM $(NH_4)_6Mo_7O_{24}$-$(H_2O)_4$, 0.01 µM $CoCl_2$-$(H_2O)_6$ and NaOH pH 5.6). Once the plants reached the 6 leaf stage the tubes containing the plants

were transferred to smaller floats holding 5 plants in magenta culture vessels (Sigma, UK) for treatment with 100 μM ferrozine, which was added directly to the hydroponic culture medium.

2.3. Extraction of RNA from *Arabidopsis*.

Arabidopsis tissues were harvested from plants grown in hydroponic medium and frozen in liquid N_2 before being ground to powder using a pestle and mortar chilled with liquid N_2. Up to 2.5 g of the powder was transferred to a 50 ml centrifuge tube to which 10 ml of a 1:1 volume mix of RNA extraction buffer (0.1 M LiCl, 100 mM Tris-HCl, pH 8.0, 10 mM EDTA and 1% (w/v) SDS) and phenol was added per 1g of powder. The mix was shaken and then vortexed for 2 min before adding 1 volume of chloroform and vortexing again for 30 s. The mix was centrifuged in a Sorvall legend RT benchtop centrifuge at 3000 x *g* for 10 min and the aqueous phase transferred to a clean 50 ml centrifuge tube. An equal volume of 4 M LiCl was then added and the samples incubated at -20°C for 16 h. The samples were then decanted into baked Corex centrifuge tubes and centrifuged in a Sorvall SS34 rotor cooled to 4°C at 8000 x *g* for 20 min. The supernatant was removed and the pellet washed with 70% (v/v) ethanol followed by 100% (v/v) ethanol, centrifuging as above after each wash. After air-drying the pellet it was resuspended in 1.5 ml sterile de-ionised water. 0.1 volume of 3 M sodium acetate (pH 5.2) and 2.5 volumes of 100% (v/v) ethanol were added and incubated at -20°C for 2 h. The samples were centrifuged at 9500 rpm for 20 min at 4°C and washed with 70% (v/v) and then 100% (v/v) ethanol as before. The pellets were again air-dried and dissolved in 100 μl sterile de-ionised water at -70°C.

2.4. Extraction of genomic DNA from *Arabidopsis*.

Genomic DNA preparations were extracted from *Arabidopsis* tissues using the DNAmite plant genomic DNA extraction kit (Microzone, UK). 1 leaf from each plant was removed and ground using a pestle in a 1.5 ml microfuge tube and processed following the manufacturer's instruction provided in the kit. Once complete the DNA was resuspended in 30 to 50 μl sterile de-ionised water.

2.5. GUS histochemical staining and fluorometric assay.

GUS histochemical staining

Plant tissues were submerged in GUS histochemical stain consisting of 0.1 mg/ml X-glu (5-bromo-4-chloro-3-indolyl glucuronide), 0.5% (v/v) dimethyl formamide, 0.5 M Na_2EDTA (pH 7.7 with NaOH), 200 mM sodium phosphate buffer (pH 7.0), 0.5% (v/v) Triton X-100, 500 mM potassium ferrocyanide and 500 mM potassium ferricyanide. Tissues were incubated at 37°C in this solution for 16 to 18 h and then cleared and fixed in 80% (v/v) ethanol, 5% (v/v) formaldehyde solution, which was changed frequently. Once cleared, tissues were stored in 50% (v/v) ethanol and viewed under a Nikon light microscope.

GUS fluorometric assay

Plant tissues were ground in a GUS fluorometric solution containing 50 mM sodium phosphate pH 7.0, 10 mM EDTA, 0.1% (v/v) Triton X-100, 0.1% (v/v) sarkosyl and 10 mM β-mercaptoethanol and incubated at 37°C for 16 to 18 h. Preparations were then viewed under UV light to check for possible positive GUS-promoter plants.

2.6. Spectrophotometric determination of nucleic acid concentration.

To calculate the amount of DNA or RNA in a given sample, optical density (OD) readings were taken at 260 nm and 280 nm. A nucleic acid sample was diluted 1:250 in dH_2O in a quartz cuvette and measured in a Hitachi U-2001 UV absorbance spectrophotometer. The OD_{260} reading gave the concentration of nucleic acid. The concentrations were calculated according to $OD_{260} = 1$ for 50 μg/ml of DNA and $OD_{260} = 1$ for 40 μg/ml of RNA. A calculation of the ratio OD_{260}/OD_{280} gave an estimate of the purity of the sample. A pure sample has a ratio of 1.8-2.0.

2.7. Gel electrophoresis of DNA.

DNA was separated on a 1.0% (w/v) agarose gel, containing 1 × TAE (40 mM Tris/acetate (pH 8.0), 1 mM EDTA). The running buffer also consisted of 1 × TAE. Both the gel and the running buffer contained 1 μM ethidium bromide. DNA was loaded in gel loading buffer containing 0.25% (w/v) bromophenol blue and 15% (w/v) Ficoll 400 in distilled H_2O (1 μl of loading buffer per 5 μl of DNA sample) and electrophoresis was carried out at 100 V for 1 h. DNA was visualised under UV light.

2.8. Purification of DNA from agarose gel.

Gel extraction and purification of DNA from agarose gels was performed using the Qiagen PCR purification kit. Each block of agarose containing the DNA to be extracted was first transferred to microfuge tubes and weighed. 3 μl of Qiagen buffer QG to every mg of agarose was then added. The preparations were then incubated at 50°C for 10 min, vortexing every 2 to 3 min. Each sample was then transferred to Qiagen spin columns and centrifuged in a microfuge for 1 min at 10,000 x *g*. The flow through was discarded and 500 μl of Qiagen buffer QG added to each spin column. The columns were centrifuged again for 1 min at 10,000 x *g*. The flow through was discarded and 750 μl of Qiagen buffer PE added to each column followed by centrifugation at 10,000 x *g* for 1 min. The flow through was discarded and the columns centrifuged 2 more times, each at 10,000 x *g* for 1 min in order to remove all traces of ethanol from the columns. The spin columns were then removed from the collection tubes and placed in 1.5 ml microfuge tubes. 50 μl of sterile distilled H_2O was then added to each column and left to stand at room temperature for 2 min. The columns were then centrifuged for 1 min at 10,000 x *g* to elute the DNA.

2.9. Transfer of DNA from agarose gel to membrane.

The position of the DNA ladder (Smartladder supplied by Eurogentec, Romsey, UK) was marked on the gel by making small incisions with a blade while

viewed under UV light. Unused areas of the agarose gel were cut off and discarded. The agarose gel containing the DNA to be transferred was then washed in depurination solution (0.25 M HCl) for 5 min with gentle shaking. The gel was then rinsed twice in distilled H_2O and washed in denaturation solution (1.5 M NaCl, 0.5 M NaOH) for 20 min with gentle shaking. The gel was again rinsed twice in distilled H_2O and washed in neutralisation solution (1.5 M NaCl, 0.5M Tris-HCl, pH 7.5) for 15 min with gentle shaking. The gel was then rinsed twice more in distilled H_2O and set up for transfer of the DNA. The agarose gel was laid with the wells facing downwards on a ceramic tile. A single piece of Hybond membrane was then cut to fit and placed on the agarose gel. Three layers of filter paper (3MM) were then placed on top of the Hybond membrane. A roughly one inch thick layer of blue paper towels (Kimwipe) was then placed on top of the 3MM paper and a tile placed on top of the blue paper towels. A weight (such as a water-filled container) was then placed on the top tile and the set-up left overnight to allow the DNA to transfer to the Hybond membrane. Following transfer overnight, the Hybond membrane was removed and baked at 85°C for 2 h.

2.10. Digoxygenin probing of DNA membrane.

A pre-hybridisation mix was prepared containing 40 ml of distilled H_2O, 24 ml of 20 × SSC (3 M NaCl, 340 mM tri-sodium citrate, HCl, pH 7.0), 8 ml of 10% (w/v) SDS and 8 ml of 10 × blocker (Roche Diagnostics) and heated to the hybridisation temperature of 65°C. The DNA membrane to be probed was then placed between 2 sheets of fine mesh, rolled up and placed in a cylindrical hybridisation tube with 20 ml of the pre-hybridisation mix. The membrane was incubated in a rotary oven at 65°C for 2 h. The pre-hybridisation mix was then poured out and discarded and 10 ml of pre-hybridisation mix and 2 µl of digoxygenin (DIG) labelled DNA probe added to the hybridisation tube containing the membrane. The tube was returned to the rotary oven and incubated overnight at 65°C. The digoxygenin probe was then poured out of the tube and stored for future use (up to 3 or 4 times) at -20°C. The DNA membrane was removed from the hybridisation tube and incubated in low stringency wash (2 × SSC, 0.1% (w/v) SDS) at room temperature for 15 min with gentle shaking. The low stringency wash was poured away and fresh low

stringency wash added for a further 15 min at room temperature with gentle shaking. The low stringency wash was again discarded and replaced with high

stringency wash (0.1 × SSC, 0.1% (w/v) SDS), in which the membrane was incubated for 15 min at 65°C with gentle shaking. The high stringency wash was then discarded and replaced with fresh high stringency wash for another 15 min at 65°C with gentle shaking. The membrane was rinsed in maleic acid buffer (100 mM maleic acid, 150 mM NaCl, pH 7.5) and washed in 20 ml of 1 × blocker (Roche Diagnostics) for 1 h at room temperature with gentle shaking. The blocker was then poured away and 10 ml of a 1 in 10,000 dilution of anti-DIG conjugate in 1 × blocker was added and the membrane incubated at room temperature for 30 min with gentle shaking. The blocker and antibody were discarded and the membrane washed in excess maleic acid buffer at room temperature while shaking. The maleic acid buffer was replaced 4 times at 15 min intervals. The membrane was then placed DNA side up and between 250 and 1000 µl (depending on the size of the membrane) of a 1 in 100 dilution of CSPD (disodium 3-(4-methoxyspiro(1,2-dioxetane-3,2'-(5'-chloro) tricyclo [3,3.1.1^{3,7}] decan}-4-yl) phenyl phosphate) (Roche Diagnostics) in detection buffer (0.1 M Tris-HCl, 0.1 M NaCl pH 9.5) was added directly to the membrane and spread across the membrane by tilting it. The membrane was then placed in an unsealed plastic bag and the CSPD solution wiped out. The bag was then sealed and the membrane incubated at 37°C for 15 min. Kodak X-ray film was then placed on top of the membrane under red light and exposed for varying lengths of time in total darkness.

2.11. Polymerase Chain Reaction (PCR) amplification of DNA.

PCR reactions were carried out using *AtNramp* cDNAs, *Arabidopsis thaliana* Col 0 genomic DNA and/or *Arabidopsis thaliana* cDNA as a template. Oligonucleotide primers with *Eco*RI, *Sac*II or *Kpn*I ends (see Table 4.1) designed to *AtNramp3*, *5* and *6* genomic sequences were obtained from MWG Biotech, Germany. For each PCR, a bulk mix of 10 µl of 10 × *Taq* DNA polymerase buffer, 10 µl of *Taq* enhancer, 1.5 mM $MgCl_2$, 5 µM of each primer, 200 µM of each dNTP and 2.5 units of AGS Gold *Taq* DNA polymerase (Hybaid, UK) was added to a final volume of 100 µl, made up with sterile distilled H_2O. This bulk mix was then

aliquoted into PCR tubes (Axygen, distributed by Thistle Scientific Ltd, Glasgow, UK) in 9.5 μl volumes and 0.5 μg of cDNA in 0.5 μl distilled H_2O added to each reaction. The reactions were cycled using Biometra UNO II or PE Applied Biosystems GeneAmp 9700 thermocyclers. For PCR using the Wisconsin facility's primers a different protocol was used. To each PCR tube 4 μl of Takara Ex *Taq* 10 × buffer, 4 μl of Takara dNTP mix, 5 μM of each primer, 2 μl of DNA template and 28 μl of sterile distilled H_2O was added. A bulk mix (enough for 10 reactions) of 85 μl sterile distilled H_2O, 10μl Takara Ex Taq 10 × buffer and 5μl Takara Ex Taq was prepared and 10μl of this bulk mix added to each reaction after the initial melting step (hot start). This gave a final reaction volume of 50 μl. In order to prepare the digoxygenin-labelled probes for *AtNramp5* and *AtNramp6* 1.6 μl of the digoxygenin stock was added to each PCR tube. The remaining components were added as above and the PCR run as normal. Before use the digoxygenin-labelled probes were denatured at 95°C for 5 min.

2.12. Colony PCR.

For PCR amplification directly from bacterial or yeast cell plate cultures a sample of each colony was picked off using a sterile pipette tip and transferred to 25 μl of sterile de-ionised water. 1 μl of this suspension was then transferred to a PCR tube containing 4 μl sterile de-ionised water and mixed. These samples were then heated to 95°C for 5 min (for bacteria) or 15 min (for yeast). 1 μl of 1 x buffer, 5 μM of each primer, 200 μM of each dNTP and 0.1 μl Takara EX *Taq* was added to each sample with sterile de-ionised water to make a final reaction volume of 10 μl. PCR was then performed as above.

2.13. Reverse transcription.

Reverse transcriptase (RT) reactions were performed using the Invitrogen Super Script I kit. 1 μl oligo $dT_{12\text{-}18}$ primer and 1 μl Invitrogen dNTP mix were added to 0.5 μg of RNA, mixed and briefly centrifuged at 10,000 x *g* in a microfuge. This mix was then incubated at 65°C for 15 min, placed on ice, centrifuged once again and returned to ice. 4 μl of 5 x 1^{st} strand buffer, 2 μl of 0.1M DTT and 1 μl RNase guard were then added to each reaction mix and the contents mixed by

centrifugation as above before incubating at 37°C for 2 min. The reactions were returned to ice, centrifuged once again and 1 µl Superscript RT added to each. The samples were again centrifuged to mix the contents and then incubated at 37°C for 50 min and then at 70°C for 15 min. The samples were then stored at -20°C before use in PCR.

2.14. Quantitative real time PCR.

Quantitative real time PCR (qPCR) was carried out using the DyNamo SYBR green kit (Finnzymes). Reactions were performed in 20 µl volumes in 96 well white plates sealed with optical caps (GRI, UK). Each reaction contained 10 µl SYBR green master mix, cDNA (sample or standard) in a maximum volume of 5 µl and 0.4 µM of each primer. For blank reactions the cDNA template was replaced with sterile de-ionised water. The plate was centrifuged at 3000 x *g* in a Sorvall Legend benchtop centrifuge for 1 min to collect the samples at the bottom of the wells. The reactions were then cycled 35 to 40 times in an MJ Research Opticon 2 lightcycler (GRI, UK). For all reactions an initial melting step of 95°C for 10 min was performed followed by cycles of 95°C 30 s (melting), 58°C 30 s (annealing), 72°C 1 min (elongation) and a final elongation step of 72°C for 5 min. The optical read was performed after the elongation phase of each cycle when double stranded product is present. Melting curve analysis was performed after completion of the specified number of cycles and ranged from 55°C to 95°C in 0.2°C increments, each held for 1 s to allow reading of each sample. The data was processed using Opticon monitor 2 software using standard deviation over maximum cycle range to set the cycle threshold.

2.15. Sequence analysis.

DNA, mRNA and protein sequences were obtained from the MIPS database (http://mips.gsf.de/proj/thal/db/search/search_frame.html), the *Arabidopsis* Membrane Protein Library (http://www.cbs.umn.edu/*arabidopsis*/) or from the EMBL database using the SRS6 website (http://srs.ebi.ac.uk/) and were converted to FASTA format using the LOADSEQ program on the World Wide Web at

http://bioweb.pasteur.fr/seqanal/interfaces/loadseq-simple.html. Alignments of the sequences were performed using CLUSTALW (Thompson *et al*, 1994 http://bioweb.pasteur.fr/seqanal/interfaces/clustalw-simple.html) and BOXSHADE (http://bioweb.pasteur.fr/seqanal/interfaces/boxshade-simple.html) used to convert the CLUSTALW alignment output to a postscript file, which was viewed using the GHOSTSCRIPT program (http://www.cs.wisc.edu/~ghost/). BOXSHADE was also used to convert the CLUSTALW output to rich text format (.rtf) files, which were viewed using Microsoft Word. TREEVIEW32 (http://taxonomy.zoology.gla.ac.uk/rod/treeview.html) was used to construct phylogenetic trees from the CLUSTALW .dnd output file.

2.16. Yeast strains.

The *Saccharomyces cerevisiae fet3 fet4* double mutant, DEY1453 (genotype: MATa/MATα *ade2/+can1/can1 his3/his3 leu2/leu2 trp1/trp1 ura3/ura3 fet3-2::HIS3/fet3-2::HIS3 fet4-1::LEU2/fet4-1::LEU2*) was a kind gift from Dr. E. Rogers, Dartmouth College, New Hampshire, USA. Also used were the *zrt1/zrt2* (MATα ade6 can1 his3 leu2 trp1 ura3 zrt1::LEU2 zrt2::HIS3) double mutant and *smf1/smf2* (*MAT*a *ura*3-52 *leu*2-3 -112 *gal*2 *SMF1*::*LEU2*, *SMF2*::*LEU2*, 19) double mutant. Growth of yeast strains was monitored by measuring optical density (OD) at 600 nm.

2.17. Transformation of yeast using PEG method.

Yeast were transformed using a sorbitol/polyethylene glycol transformation method. A 5 ml overnight yeast culture in YPD (1% (w/v) yeast extract, 2% (w/v) peptone and 2% (w/v) dextrose) media grown at 30°C, was used to inoculate 100 ml of YPD media in a 500 ml conical flask. The cells were grown shaking at 30°C until they reached an OD_{600nm} of 0.6 to 1.0. The cells were recovered by centrifuging at 3000 × *g* for 5 min in an MSE Centaur 1 centrifuge, then resuspended in 20 ml of ice cold storage buffer containing 1 M sorbitol, 10 mM bicine (pH 8.35) and 3% (v/v) ethylene glycol. The cells were pelleted as before, then resuspended in 2 ml of storage buffer and aliquoted into 200 μl and stored at –70°C until use. For the transformation, 50 ng to 2 μg of plasmid DNA (Fig.2) and 50 μg of herring sperm DNA were added to the top of the frozen cell aliquot. The cells were defrosted at 37°C while shaking for 5 min. After thawing, 1 ml of

transformation buffer, containing 40% (w/v) PEG 1000 and 200 mM bicine (pH 8.35) was added and the cells incubated at 35°C for 1 h. Following incubation, the cells were centrifuged at 3000 × *g* for 5 min in a Sorvall MC 12V microfuge and resuspended in 800 μl resuspension buffer, containing 150 mM NaCl and 10 mM bicine (pH 8.35). The cells were centrifuged again as before and resuspended in 300 μl of sterile distilled H_2O, then plated onto selection media.

2.18. Transformation of Yeast using PLATE solution method.

A single colony (2 to 3 mm in diameter) of yeast was transferred from a fresh plate to a sterile 1.5 ml microfuge tube using a 200 µl pipette tip. 10 µl of carrier DNA (10 µg/µl herring sperm DNA) and transforming DNA (in 10µl) were added to the microfuge tube and the contents vortexed well. 0.5 ml of PLATE solution (40% (w/v) polyethylene glycol MW 3350, 0.1 M lithium acetate, 10 mM Tris-HCl pH 7.5, 1 mM EDTA) was added to the microfuge tube and vortexed well. The tube and contents were incubated at room temperature for 96 h. The cells were then heat shocked at 42°C for 15 mins. Cells were then pelleted for 10 s at 10,000 x *g* in a microfuge. The supernatant was discarded and the cells resuspended in 200 µl of sterile distilled H_2O. The cells were then plated onto selective media.

2.19. Yeast growth and selection conditions.

Following transformation, yeast cells were grown on synthetic complete (SC) media without uracil, comprising 0.17% (w/v) yeast nitrogen base without amino acids (DIFCO), 18 g/l bacto-agar (DIFCO), 2% (w/v) dextrose (DIFCO) as a carbon source, 1.4 g/l drop-out mix (without uracil, histidine, leucine or tryptophan) (Sigma-Aldrich, UK), tryptophan, leucine, histidine, 50 µM $FeCl_3$ and adjusted to pH 5.5 with hydrochloric acid (HCl). The cells were grown at 30°C. Uracil only was omitted from the first selection media. Transformants which grew on the first selection media were plated onto a second selection media containing 0.17% (w/v) yeast nitrogen base, 18 g/l bacto-agar, 2% (w/v) dextrose, 1.4 g/l drop-out mix (without uracil, histidine, leucine or tryptophan) and 1 mM EDTA. Uracil, histidine, leucine and tryptophan were omitted from the second selection media. No $FeCl_3$ was supplied. There was no second selection for yeast transformed with the vector alone. Cells that grew on second selection plates were transferred to liquid second selection media shaking at

30°C. For complementation yeast transformed with AtNramp5 in Nev-N or the vector alone were grown on SC –ura plates or in liquid media (as above but with 0.5 mM EDTA) with or without 50 μM $FeCl_3$.

2.20. Isolation of plasmid DNA from yeast.

Plasmid DNA was isolated from yeast using a method adapted from Hoffman and Winston (1987). 5 ml of overnight culture of yeast cells grown in YPD media or selection media was centrifuged at 10,000 × *g* for 5 min in an MSE microfuge. The cells were resuspended in 300 μl of cell resuspension solution containing 2% (v/v) Triton X100, 1% (w/v) SDS, 100 mM NaCl, 10 mM Tris/HCl (pH 8.0) and 1 mM EDTA. An equal volume of sterile glass beads (0.45-0.60 mm diameter) and phenol/chloroform/isoamyl alcohol (25:24:1) was added to the cells then vortexed for 30 s. The sample was extracted twice with equal volumes of phenol/chloroform/isoamyl alcohol (25:24:1) then the aqueous phase was treated with 10 μg/ml RNase for 1 h at 37°C and precipitated in 2 volumes of ethanol and 0.1 volume of sodium acetate (pH 5.2) solution at –20°C. Following ethanol precipitation, the DNA was recovered by centrifugation at 10,000 × *g* for 20 min in an MSE microfuge, washed in 70% (v/v) ethanol then resuspended in 50 μl of sterile distilled H_2O.

2.21. Isolation of RNA from yeast.

Yeast cells were grown in the appropriate selection media at 30°C until reaching an OD_{600nm} of approximately 1.0. The cells were pelleted at 3000 x *g* for 5 min in a Sorvall legend RT benchtop centrifuge cooled to 4°C before resuspending in 1 ml of ice cold sterile de-ionised water. The cells were then pelleted in a microfuge at 10,000 x *g* for 10 s, the supernatant removed and the cells resuspended in 400 μl ice cold TES buffer (10 mM Tris-HCl pH 7.5, 10 mM EDTA, 0.5% (w/v) SDS). To this 400 μl of acid phenol was added and the samples vortexed for 10 s before incubating at 65°C for 60 min with occasional vortexing. Samples were then placed on ice for 5 min, centrifuged for 5 min at 10,000 x *g* at 4°C and the aqueous phase of each transferred to clean microfuge tubes. 400 μl of acid phenol was added to each, vortexed, placed on ice for 5 min and then centrifuged for 5 min at 10,000 x *g* at 4°C. The aqueous phase was once again transferred to a clean microfuge tube and 400 μl chloroform

added before vortexing and centrifuging at 10,000 x *g* at 4°C. The aqueous phase was transferred to a new microfuge tube and 40 µl 3 M sodium acetate pH 5.3 with 1 ml ice cold 100% (v/v) ethanol added to each. The samples were again centrifuged at 10,000 x *g* at 4°C, washed by vortexing briefly in 1 ml 70% (v/v) ethanol and centrifuged again to pellet the RNA. Once dried, the pellet was resuspended in 50 µl sterile de-ionised water and stored at -70°C.

2.22. Uptake of radioactive Fe into yeast cells.

Yeast *fet3fet4* cells were grown in liquid selection media in 500 ml flasks at 30°C on a rotary shaker and grown to OD_{600nm} of between 0.8 and 1.2. The cells were pelleted by centrifuging at 3000 x *g* for 5 min in a Sorvall legend RT benchtop centrifuge and resuspended in 5 ml ice cold 2% (w/v) galactose, 10 mM Mes-NaOH, pH 5. This was repeated two more times to wash the cells. The cells were pelleted as above and weighed in 1.5 ml microfuge tubes. The cells were resuspended in ice cold 2% (w/v) galactose, 10 mM Mes-NaOH, pH 5 to a density of 0.5 mg/µl. The cells were then immediately added to the uptake assay mix in a volume of 44.4 µl. The assay mix contained 2% (w/v) galactose, 10 mM Mes-NaOH pH 5, 1mM sodium ascorbate, 10 µM $^{55}FeCl_3$ (to give 0.05 MBq of radioactivity) and cold $FeCl_3$ added to give a final $FeCl_3$ concentration of 50 µM. 50 µl was removed at each time point, placed onto Whatman GF/C filter discs and 3 x 5 ml of wash buffer (1 mM NaEDTA, 1 mM NaCl, 5 mM $MgSO_4$, 1 mM $CaCl_2$ and 1 mM KH_2PO_4) drawn through using a suction pump. The discs were then placed in 20 ml plastic scintillation vials (Amersham, UK) and 5 ml scintillation fluid (Fisher, UK) added to each. The samples were then analysed in a liquid scintillation counter (Beckman, High Wycombe, UK).

2.23. Transformation of *E. coli*.

Escherichia coli DH5α cells were used for all experiments presented in this work. *E. coli* DH5α cells (Invitrogen) were thawed on ice and aliquoted into 50 µl volumes in microfuge tubes. 2 µl of transforming DNA was added to each and the cells left on ice for 30 min. The cells were then heat shocked at 37°C for 15 s and returned to ice for 2 min. 950 µl of Luria broth (LB) (Sigma, UK) media was added to each and the cells incubated at 37°C for 60 min. The cells were then pelleted in a microfuge at 10,000 x *g* for 10 s and resuspended in 150 µl sterile de-ionised water

before plating onto LB agar with 50 μg/ml ampicillin. Plates were incubated at 37°C for 16 h. Colonies were picked off and grown in liquid LB with 50 μg/ml ampicillin to check for the presence of the plasmid DNA.

2.24. Isolation of plasmid DNA from *E.coli.*

A 5ml LB overnight culture of *E.coli* containing the required plasmid and insert DNA was chilled on ice and pelleted at 2,000 x *g* at 4°C for 5 min. The supernatant was discarded and the cells resuspended in 100 μl TEG (10 mM Tris, 1.5 mM EDTA, 10% (v/v) glycerol, pH 7.6) and left to stand at room temperature for 5 min. A stock solution of 4 μl of 10 M NaOH, 20 μl 10% (w/v) SDS, 176 μl sterile distilled H_2O was prepared and 200 μl of this added to each suspension of bacteria. The cells were left on ice for 5 min before adding 150 μl of 3 M potassium acetate. The cells were then left on ice for a further 10 min before being centrifuged at 10,000 x *g* for 10 min. The supernatant was transferred to fresh 1.9 ml microfuge tubes and an equal volume (usually 300μl) of phenol/chloroform/isoamyl alcohol (25:24:1 mixture), pH 5.2 (Fisher Scientific, UK) added. The samples were centrifuged at 10,000 x *g* for 5 min and the aqueous (top) layer pipetted off and transferred to fresh 1.9 ml microfuge tubes. Another 300 μl of phenol chloroform isoamyl alcohol was added to each sample and again centrifuged at 10,000 x *g* for 5 min. The aqueous phase was again extracted and transferred to fresh 1.9 ml microfuge tubes. 600 μl of 100% (v/v) ethanol and 30 μl 3 M sodium acetate pH 5.2 was added to each tube and the DNA allowed to precipitate overnight at -20°C. The samples were then centrifuged at 10,000 x *g* for 20 min, the supernatant removed by pipette and 600 μl of 70% (v/v) ethanol added. The samples were centrifuged at 10,000 x *g* for 1 min and the ethanol removed by pipetted. Remaining traces of ethanol were allowed to evaporate. The DNA pellet was then resuspended in 50 μl of sterile distilled H_2O.

2.25. Restriction digest of DNA.

Between 1 and 5 μg of DNA (in distilled H_2O) to be cut was added to 2 μl of the appropriate 10 × enzyme buffer (Promega, Southampton, UK) and pulsed in a Sorvall MC 12 V microfuge. 10 μg/ml acetylated bovine serum albumin (Promega) and 5 units of the desired restriction endonuclease (Promega) were then added. The reaction volume was then made up to 20 μl with sterile distilled H_2O and incubated at

37°C for between 3 and 18 h, depending on the enzyme used (refer to manufacturer's manual).

2.26. Transformation of *Agrobacterium.*

Transformation of *Agrobacterium* was performed using a method based on that of McCormac *et al* (1997). *Agrobacterium tumefaciens* (strain GV3101) cells were grown in 5 ml YPD (1% (w/v) bacto-yeast extract, 2% (w/v) bacto-peptone, 2% (w/v) dextrose) pH 5.5 with 50 μg/ml rifampicin and 25 μg/ml gentamycin for 16 to 18 h on a rotary shaker at 28°C. 2 ml of growing cultures were then taken and used to inoculate 18 ml of YPD (without antibiotics) and grown for a further 16 to 18 h on a rotary shaker at 28°C. Cultures were allowed to equilibrate with atmosphere for 30 s in a flow cabinet and then returned to the rotary shaker at 28°C for 4 h. The cells were put on ice for 5 min and then harvested by centrifugation at 3000 x *g* for 5 min at 4°C in a Sorvall RC2B centrifuge and SLA600 rotor. The supernatant was then discarded and the cells resuspended in 5 ml of ice cold sterile 10% (v/v) glycerol. This was repeated two more times. The cells were then centrifuged at 3000 x *g* for 5 min, the supernatant discarded and the cells gently resuspended in 200 μl ice cold sterile 10% (v/v) glycerol. The cells were then aliquoted in 40 μl volumes and stored at -70°C until transformation or used immediately. Once thawed, each 40 μl aliquot of cells was transferred to 0.2 mm gap electroporation cuvettes (Flowgen, UK) and about 2 μg of plasmid DNA added. *Agrobacterium* cells were then transformed by pulsing at 2.5 KV using the Bio-Rad E.coli pulser. Cells were then plated onto YPD agar (1% (w/v) bacto-yeast extract, 2% (w/v) bacto-peptone, 2% (w/v) dextrose, 2% (w/v) agar) plates with 50 μg/ml rifampicin, 25 μg/ml gentamycin and 50 μg/ml kanamycin by pipette in 50 to 250 μl volumes and spread using a metal loop sterilised with ethanol and flamed. Plates were incubated in a 28°C oven for approximately 72 h. Colonies were picked off of selection plates with an inoculation loop and grown in 6 ml 1% (w/v) tryptone, 0.5% (w/v) bacto-yeast extract, 0.5% (w/v) NaCl with 50 μg/ml rifampicin, 25 μg/ml gentamycin and 50 μg/ml kanamycin. *Agrobacterium* cells were stored in 15% (v/v) glycerol at -70°C.

2.27. *Agrobacterium tumefaciens* mediated transformation of *Arabidopsis.*

Arabidopsis Col 0 plants were transformed with GUS-promoter constructs using a floral dip method adapted from that of Clough and Bent (1998). Transformed *Agrobacterium tumefaciens* (strain GV3101) cells were grown in 6 ml 1% (w/v) tryptone, 0.5% (w/v) bacto-yeast extract, 0.5% (w/v) NaCl with 50 μg/ml rifampicin, 25 μg/ml gentamycin and 50 μg/ml kanamycin for 16 to 18 h. 2 ml of growing cultures was used to inoculate 200 ml 1% (w/v) tryptone, 0.5% (w/v) bacto-yeast extract, 0.5% (w/v) NaCl. Cultures were returned to a rotary shaker until reaching an OD_{600nm} of approximately 0.4. The cells were then pelleted at 3000 x *g* for 10min in a Sorvall RC2B centrifuge and SLA600 rotor. *Agrobacterium* cells were then resuspended in 300 ml 1 × Murashige and Skoog media, pH 5.7, 5% (w/v) sucrose, 0.02% (v/v) Silwet 77. After cutting floral shoots 4 to 8 days prior to the transformation in order to promote bolting, *Arabidopsis* Col 0 plants were dipped in the *Agrobacterium* cell suspension for 5 min. The plants were placed in a plastic tray, sealed in a plastic bag to maintain humidity and placed in a growth room at 23°C with a 16 h photoperiod and a light intensity of approximately 100 μmol. m^{-2} s^{-1}. After 1 or 2 days the plants were removed from the plastic bag and watered regularly for 2 weeks. As production of siliques began, the plants were placed inside tall plastic bags, 1 pot to a bag, in order to prevent seed dispersal. Seed was collected and seed plated out as outlined in section 2.1. For selection of transformed seedlings the plates contained 10 μg/ml phosphinothricin. Seedlings that produced roots and continued to grow while on the selection media were gently removed and placed into pots of soil for growing on.

2.28. *Agrobacterium*-mediated transient transformation of tobacco.

Agrobacterium cells were grown in LB with 50 μg/ml kanamycin, 50 μg/ml rifampicin and 50 μg/ml gentamycin for 16 h at 28°C before pelleting the cells by centrifugation at 3000 x *g* in a Sorvall Legend benchtop centrifuge. The cell pellets were resuspended in 9.5 ml virulence induction medium (9.76 g/l MES NaOH pH 5.6, 5 g/l glucose, 0.276 g/l Na_2HPO_4-(H_2O), 0.24 g/l NaH_2PO_4, 1 g/l NH_4CL, 0.3 g/l $MgSO_4$-$(H_2O)_7$, 0.15 g/l KCl, 10 mg/l $CaCl_2$ and 2.5 mg/l $FeSO_4$-$(H_2O)_7$) and grown for 2 to 3 h at 28°C. The cells were then diluted to an OD_{600nm} of 0.2 and 0.5 ml of 50 mM acetosyringone was added to each cell suspension shortly prior to injection of tobacco leaves. *Agrobacterium* cells were then injected into *Nicotiana tabacum* tobacco leaves

using a plastic syringe (without needle) by applying the syringe to the upper leaf surface and depressing the syringe gently to infiltrate the leaf with *Agrobacterium*. GUS expression was visualised after 2 days of plant growth.

2.29. Chemicals.

Chemicals were from Sigma-Aldrich Co. Ltd. (Poole, Dorset, UK), Fisher Scientific Ltd. (Loughborough, Leicestershire, UK), Difco (Becton Dickinson, Oxford, UK), GibcoBRL Life Technologies Ltd. (Paisley, Scotland) and Roche Diagnostics (Lewes, East Sussex, UK). Molecular biology enzymes were from Promega (Southampton, Hampshire, UK), Hybaid Ltd. (Ashford, Middlesex, UK), Stratagene Ltd. (Cambridge, UK), Invitrogen (Paisley, UK), Bioline (London, UK), Takara (Cambrex Bio Science, Wokingham, UK), GRI (Braintree, UK), Eurogentec (Romsey, UK). Radiolabelled chemicals were from Amersham Life Science Ltd. (Buckinghamshire, UK).

Chapter 3. Sequence analysis of the AtNramp family.

3.1. Introduction.

3.1.1. Sequence analysis.

Computational analysis of DNA and protein sequences can be a valuable tool in the investigation of both the function and regulation of proteins and the genes that encode them. A number of different analyses are commonly used in order to predict various characteristics of proteins, genes and other regulatory sequences. One of the most common methods employed to gain information about DNA or amino acid sequences is to perform an alignment of the sequence of interest with others of known structure or function. In many cases this approach can assist in identifying the type of sequence and assigning the gene or protein to a family of related sequences. Geisler *et al.* (2000) used this method to suggest that additional Ca^{2+}-ATPases were present in the *Arabidopsis thaliana* genome by identifying expressed sequence tags with similarity to the Ca^{2+}-ATPases known at the time. The *AtNramp* sequences were also identified by comparison to known *Nramps* from other organisms (Alonso *et al.,* 1999, Curie *et al.,* 2000, Thomine *et al.,* 2000, Williams *et al.,* 2000). The most common method used to align DNA or amino acid sequences to others in a database is the BLAST algorithm (Altschul *et al.*, 1997). Others such as FASTA can also be used to align sequences to those in a database (Pearson, 1990) while CLUSTAL W allows multiple sequences to be aligned to one another (Higgins *et al.*, 1994, Thompson *et al.*, 1994).

Alignments of DNA or protein sequences can give further information when used to construct phylogenetic trees to show the sequence similarity relationships between members of gene or protein families. This analysis can often show relationships not immediately obvious from sequence alignments alone. Guerinot (2000) performed phylogenetic analysis of the ZIP family of proteins from various organisms and showed that they fall into two distinct groups. Another example is the P-type ATPase family, which forms five distinct major groups in phylogenetic

analysis (Palmgren and Axelsen, 1998). In this case the groupings reflect functional differences between the proteins since members in the same group are known to transport similar ions while members of other groups transport different ones.

These approaches generally identify possible evolutionary relationships between sequences with similarity to each other. The assumption that genes or proteins with similar sequences will also have similar structures and function is central to this method of analysis. Any predictions made should therefore be treated with some caution since this assumption may not always be accurate. Another very common method of obtaining information about protein structure is to perform hydropathy analysis in order to identify possible membrane spanning regions. A great many algorithms are available to predict transmembrane number and length as well as the position of N and C termini with relation to the interior and exterior of the cell from the amino acid sequence. This also makes it possible to identify possible intra and extracellular loops which may include functional domains within the protein. The majority of these prediction methods are available on the world wide web, for example, TMPred (http://www.ch.embnet.org/software/TMPRED.form.html, Hofmann and Stoffel, 1993), TMHMM (http://www.cbs.dtu.dk/services/TMHMM, Sonnhammer *et al.*, 1998) and TopPred (http://www.bioweb.pasteur.fr/seqanal/interfaces/toppred.html, von Heijne, 1992). However, individually, these prediction methods are not always accurate and are probably better used together and in conjunction with other methods, for example, by comparison to similar sequences with established tertiary structure.

Where both genomic DNA and cDNA (or amino acid) sequences are available for a particular gene it is possible to compare the two sequences and identify introns within the genomic DNA. This information can often suggest relationships between sequences with relatively low identity as in the case of the lipocalin gene family. While the amino acid sequence of many lipocalins is not highly conserved, their exon and intron number and arrangement is often strikingly similar (Salier, 2000) and can be used to infer evolutionary relationships.

Once translated from mRNA, the amino acid sequence of a protein can be subject to a range of further modifications that may affect the function or expression of the mature polypeptide. A commonly studied modification is that of N-linked glycosylation in which oligosaccharide chains are attached to an asparagine residue within the protein. This kind of modification has been shown to affect the expression of the modified protein in some cases. For example, mutations at the asparagine residue, which prevents glycosylation, resulted in decreased expression of the gonadotrophin-releasing hormone receptor in COS-1 cells (Davidson *et al.*, 1995). It is possible to predict asparagine residues that may be glycosylated in proteins by the consensus sequence Asn-X-Ser/Thr (Kornfeld and Kornfeld, 1985). Identification of possible N-linked glycosylation sites within the extracellular domains of a protein can assist in the direction of mutational analysis to determine the function or regulation of a protein.

3.1.2. Sequence analysis of the Nramps.

To date, limited analysis of the *AtNramp* sequences has been performed. Sequence analysis has been carried out for the *Oryza sativa* Nramp family by Belouchi *et al.* (1997) who identified possible N-linked glycosylation sites, transmembrane domains and a conserved signature motif in the amino acid sequences. Thomine *et al.* (2000) and Maser *et al.* (2001) have also performed some analysis of the AtNramp sequences by constructing phylogenetic trees. They showed that the AtNramps appear to cluster in two distinct groups in phylogenetic analysis. One group consists of AtNramp1 and 6 while the other group consists of AtNramp2 to 5. Gross *et al.* (2003) identified more predicted Nramp genes in the *Oryza sativa* genome to bring the total number to eight. Phylogenetic analysis of these sequences together with the AtNramps and yeast SMF1 and 2 also suggested the presence of a division within the Nramp family. The functional significance (if any) of this division between the AtNramps is not clear, especially since members from both groups (AtNramp1, AtNramp3 and AtNramp4) are capable of rescuing the low Fe-sensitive phenotype of the yeast *fet3/fet4* iron uptake mutant (Curie *et al.*, 2000, Thomine *et al.*, 2000).

Liu and Culotta (1999a) performed mutational analysis of the yeast SMF1 protein and showed that certain amino acids in the putative fourth transmembrane domain and the conserved signature motif are important for transport activity and the correct targeting of the protein to the plasma membrane under low manganese conditions. Cohen *et al.* (2003) identified three amino acids in the putative first external loop of the mammalian DCT1 protein that are involved in metal binding and specificity. Substitution of these amino acids resulted in the loss of transport activity in *Xenopus* oocytes and completely abolished functional complementation of the yeast *smf1* Mn uptake mutant.

The aim of the work described in this chapter was to further analyse the DNA and amino acid sequences of the AtNramps in order to discover any possible similarities with members of the Nramp family from other organisms and to identify features that may give some insight as to their function and localisation within the plant.

3.2. Results.

3.2.1. Nramps in *Arabidopsis thaliana*.

Six genes with homology to members of the Nramp family can be identified in the genome of *Arabidopsis thaliana* by searching sequence databases. Of the six *AtNramp* genes, named *AtNramp1* to *6*, there is functional information for *AtNramp1* to *4* (Curie *et al.*, 2000, Thomine *et al.*, 2000, Thomine *et al.*, 2003).

Table 3.1 shows the protein entry codes, accession numbers and the position of the six *AtNramp* genes. *AtNramp1*, *2*, *3* and *4* were cloned independently prior to the start of this project by other groups (Alonso *et al.*, 1999, Curie *et al.*, 2000, Thomine *et al.*, 2000) while *AtNramp5* and *AtNramp6* were cloned by members of our group (Pittman, Hall and Williams, unpublished). For *AtNramp6*, two cDNA transcripts were cloned, one is the correctly spliced cDNA (herein referred to as *AtNramp6a*) and the other retains the sixth intron (referred to as *AtNramp6b*), which would result in a truncated protein due to the presence of stop codons in each reading frame within this intron.

3.2.2. Sequence alignments.

The percentage amino acid sequence identities between the AtNramps were obtained from FASTA alignment scores available on the MIPS website (http://mips.gsf.de/proj/thal/db/search/search_frame.html) and are shown in Table 3.2. An amino acid sequence alignment of the six Nramps from *Arabidopsis thaliana* is shown in Fig.3.1 and a cDNA alignment in Fig.3.2. Both alignments were performed using CLUSTAL W. These illustrate the high degree of identity and similarity between the AtNramps. However, it can be seen that AtNramp2, 3, 4 and 5 share more similarity with each other than they do with AtNramp1 and 6. AtNramp1 and 6 also share areas of identity to each other that are not shared with the other AtNramps. There are many similarities however, and many of the amino acid sequences are conserved in all six of the AtNramps, the longest sequence

Table 3.1. Database accession numbers and position of the *Nramp* genes within the genome of *Arabidopsis thaliana*.

Gene Name	Chromosome No.	Protein Entry Code	DNA accession	Protein accession	BAC clone No.
AtNramp1	1	At1g80830	AF165125	Q9SAH8	F23A5
AtNramp2	1	At1g47240	AF141204	Q9C6B2	F8G22
AtNramp3	2	At2g23150	AF202539	Q9SNV9	T20D16
AtNramp4	5	At5g67330	AF202540	Q9FN18	K8K14
AtNramp5	4	At4g18790	ATH292076 AJ292076	Q9SN36	F28A21
AtNramp6	1	At1g15960	ATH291831 AJ291831	Q9S9N8	T24D18

Table 3.2. Percentage amino acid identities of the AtNramp family in *Arabidopsis thaliana*. Amino acid sequence identities were obtained using FASTA alignment values from the MIPS website at http://mips.gsf.de/proj/thal/db/search/search_frame.html.

	AtNramp1	AtNramp2	AtNramp3	AtNramp4	AtNramp5	AtNramp6
AtNramp1	-	40	42	42	40	88
AtNramp2	40	-	76	72	72	39
AtNramp3	42	76	-	76	66	42
AtNramp4	42	72	76	-	63	42
AtNramp5	40	72	66	63	-	39
AtNramp6	88	39	42	42	39	-

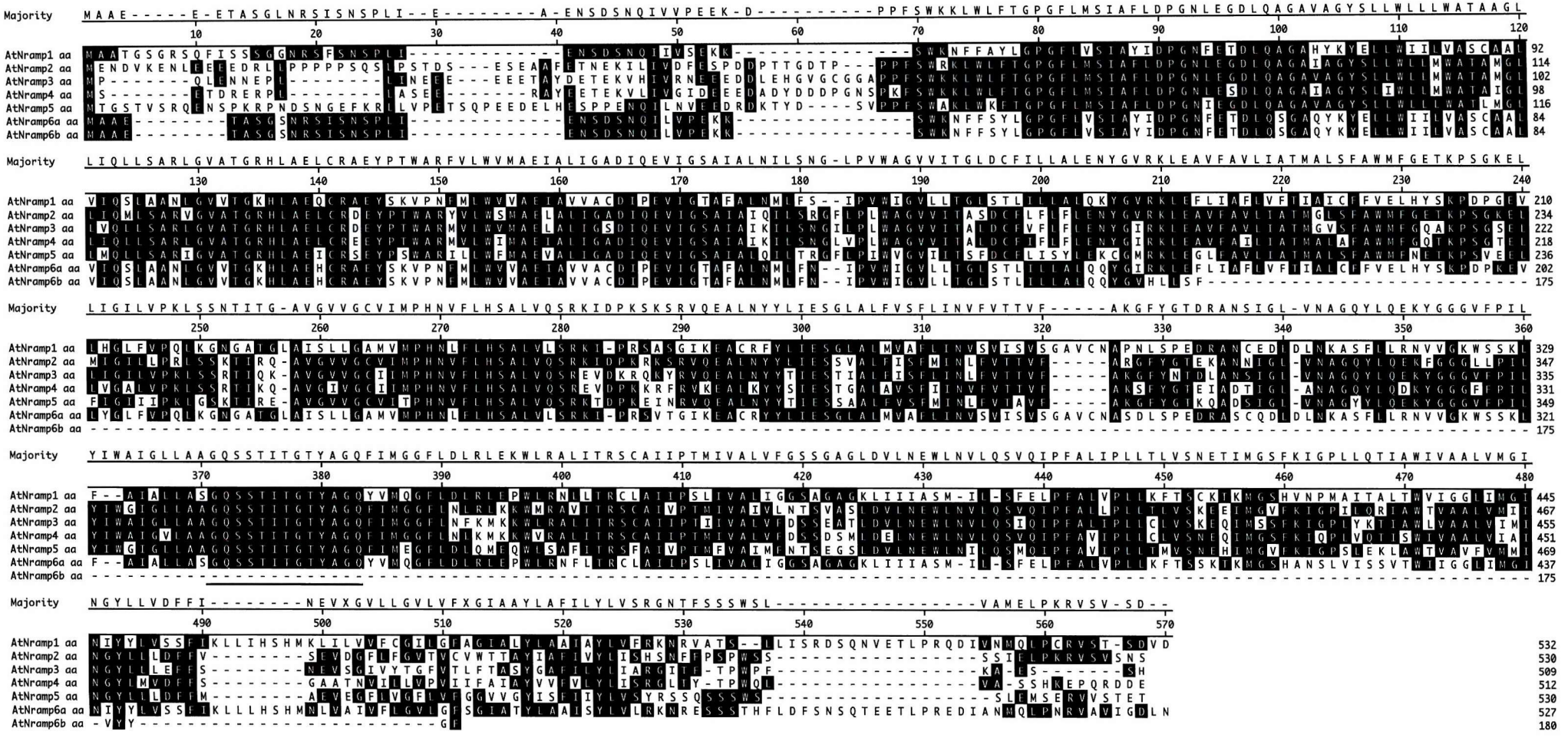

Fig.3.1. Amino acid sequence alignment of the AtNramps. The amino acid sequences were obtained from the MIPS database at http://mips.gsf.de/proj/thal/db/search/search_frame.html and aligned using CLUSTAL W. The conserved motif is underlined. Asterisks above the alignment indicate amino acids conserved in mammalian DCT1 (accession O54902) shown to be involved in metal ion binding and specificity (Cohen *et al*, 2003). The consensus sequence is given above the alignment. Shading shows residues conserved between the Nramp sequences. Dashes indicate gaps in the alignment.

Fig.3.2. cDNA sequence alignment of the *AtNramps*. The cDNA sequences were obtained from the MIPS database at http://mips.gsf.de/proj/thal/db/search/search_frame.html and aligned using CLUSTAL W. Shading shows bases conserved between the *Nramp* sequences.

being the conserved signature motif (GQSSTITGTYAGQ) first identified by Belouchi *et al.* (1997) in *Oryza sativa*. This sequence is identical in all six AtNramps and is also highly conserved in many members of the Nramp family identified so far in a variety of different organisms.

Also, shown on Fig.3.1 by asterisks above the sequence are the positions of three amino acids conserved between the AtNramps and mammalian DCT1 which have been shown to be involved in metal ion binding and specificity of DCT1 (Cohen *et al.*, 2003). All three are located within the putative first external loop of the DCT1 protein and align exactly with those in the AtNramps.

3.2.3. Transmembrane domains.

Predicted transmembrane domains of the six AtNramps were obtained from The Arabidopsis Membrane Protein Library (http://www.cbs.umn.edu/arabidopsis) and their position highlighted on a protein sequence alignment. Twelve transmembrane domains are predicted for each of the AtNramps by this database. The predicted positions of the transmembrane domains are highlighted in Fig.3.3 in blue (for AtNramp2, 3, 4 and 5) and yellow (AtNramp1 and 6). Comparing Fig.3.1 with Fig.3.3 it can be seen that the AtNramps appear to be more conserved in regions predicted to be transmembrane domains.

Other transmembrane prediction programs were also used to analyse the AtNramp protein sequences. TMHMM (http://www.cbs.dtu.dk/services/TMHMM), TopPred (http://www.bioweb.pasteur.fr/seqanal/interfaces/toppred.html) and TMpred (http://www.ch.embnet.org/software/TMPRED.from.html) each give different predictions as to the number of transmembrane domains present in the AtNramps, varying between 10 to 12 transmembrane domains.

TopPred gives a prediction of 10 transmembrane domains at the upper cut off point or 12 transmembrane domains at the lower cut off point for AtNramp5, this is shown diagrammatically in Fig.3.4. This indicates that 10 of the predicted transmembrane domains are highly likely to be membrane spanning regions while another 2 regions of the protein could be transmembrane domains but are not so

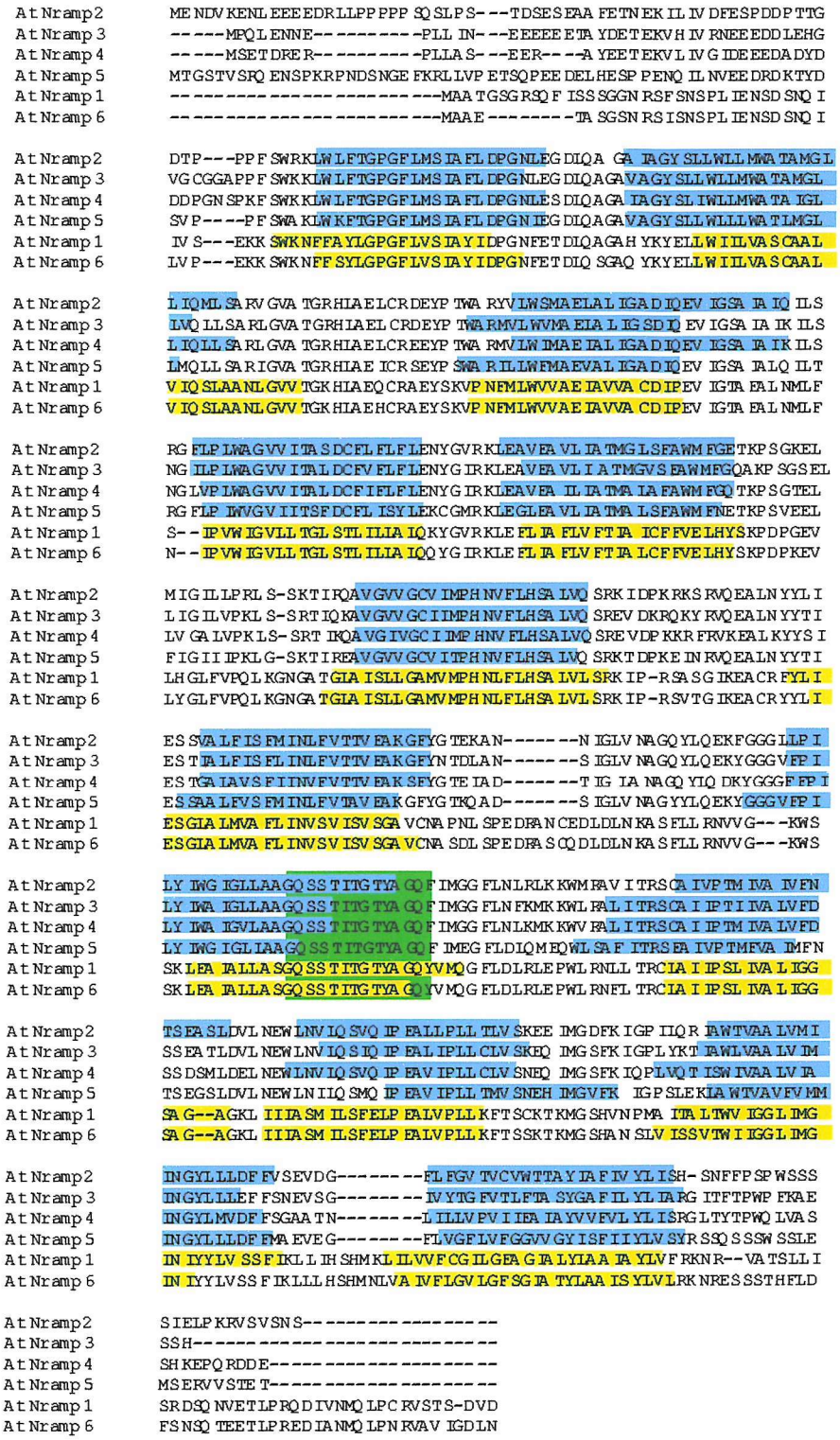

Fig.3.3. Sequence alignment of the Nramps from *Arabidopsis thaliana* showing the predicted transmembrane regions. Predicted transmembrane domains of AtNramp1 and 6 are highlighted in yellow while those of AtNramp2, 3, 4 and 5 are highlighted in blue. The conserved signature motif is highlighted in green. Predicted transmembrane domains of the six *AtNramps* were obtained from the Arabidopsis Membrane Protein Library (http://www.cbs.umn.edu/arabidopsis).

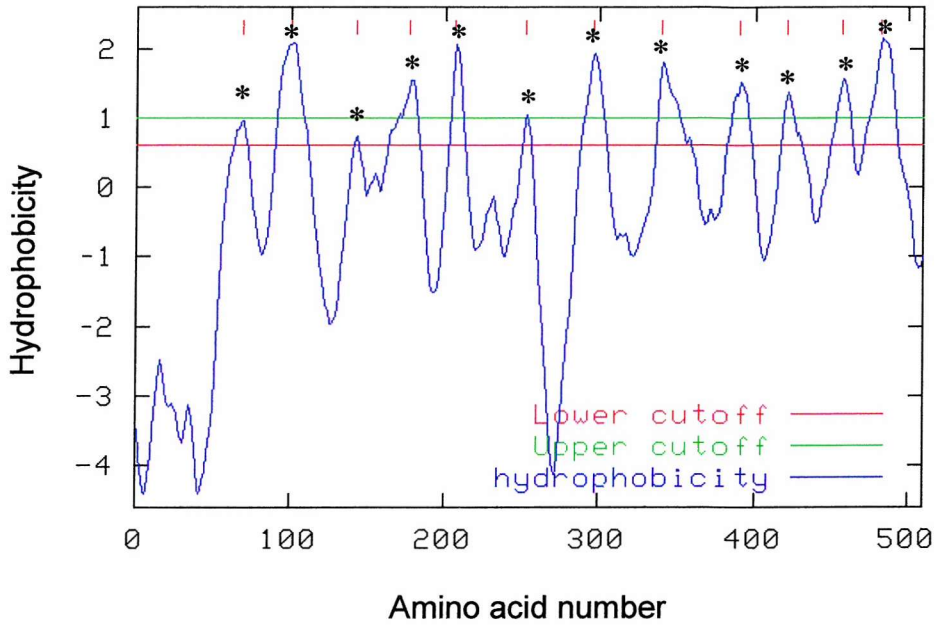

Fig.3.4. Hydrophobicity plot of AtNramp5 produced using TopPred (http://www.bioweb.pasteur.fr/seqanal/interfaces/toppred.html). 12 hydrophobic peaks are above the lower cut-off point while 10 peaks are above the upper cut-off point indicating that this program predicts 10 or possibly 12 transmembrane domains (indicated by asterisks).

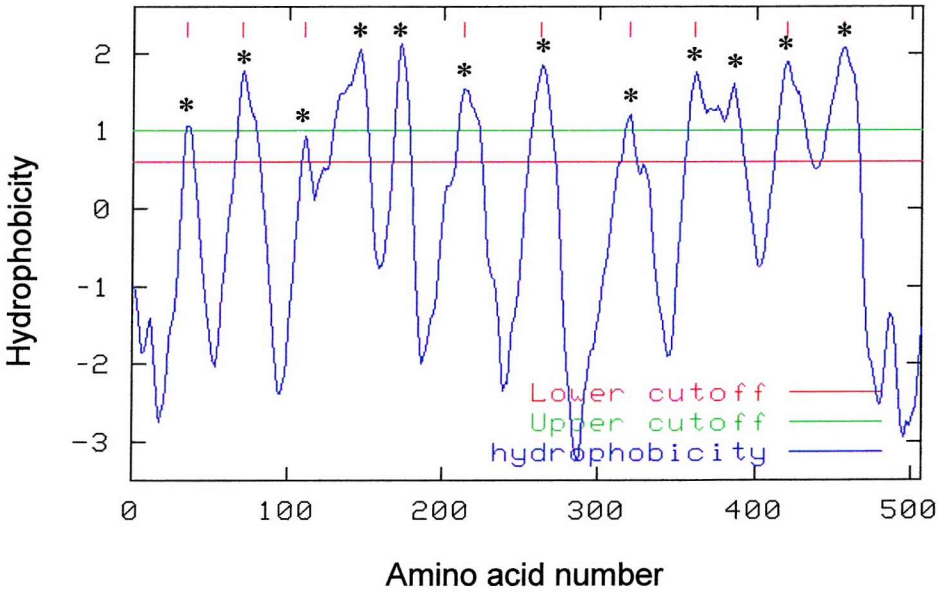

Fig.3.5. Hydrophobicity plot of AtNramp6 produced using TopPred (http://www.bioweb.pasteur.fr/seqanal/interfaces/toppred.html). 12 hydrophobic peaks are above the lower cut-off point while 11 peaks are above the upper cut-off point indicating that this program predicts 11 or possibly 12 transmembrane domains (indicated by asterisks).

hydrophobic. Fig.3.5. shows the TopPred output for AtNramp6. In this case 11 regions are highly likely to be transmembrane domains while 1 region is possibly a membrane-spanning domain. Making use of cytoplasmic and periplasmic reporter fusions and functional assays Pascal *et al.* (2003) determined the transmembrane topology of the *Escherichia coli* Nramp ortholog, MntH. This is currently the only member of the Nramp family for which topological data of the entire sequence exists. Their results indicated that *E. coli* MntH has 11 transmembrane domains with the N-terminus of the protein inside the cytoplasm and the C-terminus exposed on the outside of the cell. A CLUSTAL W alignment of the AtNramps with the *E. coli* MntH amino acid sequence (accession P77145) is shown in Fig.3.6. The position of the transmembrane domains determined experimentally for MntH is shown underneath the sequence alignment. It can be seen that there is still high homology between the *Arabidopsis* Nramps and the *E. coli* MntH, often in areas shown to be transmembrane spanning regions in MntH. The same alignment with the MntH transmembrane domains under the alignment is seen in Fig.3.7 while the TMHMM transmembrane prediction for each sequence is shown as highlighted text. Overall, the TMHMM predictions are relatively accurate and most of the predicted transmembrane domains are a few amino acids away from the position of the experimentally deduced transmembrane regions. It is particularly important to note that TMHMM predicts the correct number of transmembrane domains for MntH and correctly places the N-terminus within the cytoplasm. However, there are occasions when TMHMM predicts transmembrane domains with less accuracy in the MntH sequence. For example TM2 differs by 5 amino acids while TM8 differs by 9 amino acids when compared to the experimental evidence. In some cases the TMHMM program fails to predict a transmembrane region as can be seen in the case of TM1 for AtNramp2 and 5, TM3 for AtNramp2, 3 and 5 and TM10 of AtNramp2. Given the high homology to the other AtNramps (AtNramp2 is identical to 3 and 4, AtNramp5 differs by only 2 amino acids in this region) and the homology to MntH in these particular regions, it seems likely that these also represent transmembrane domains. All six of the AtNramps are also predicted to contain a twelfth transmembrane domain by TMHMM. This occurs at the C-

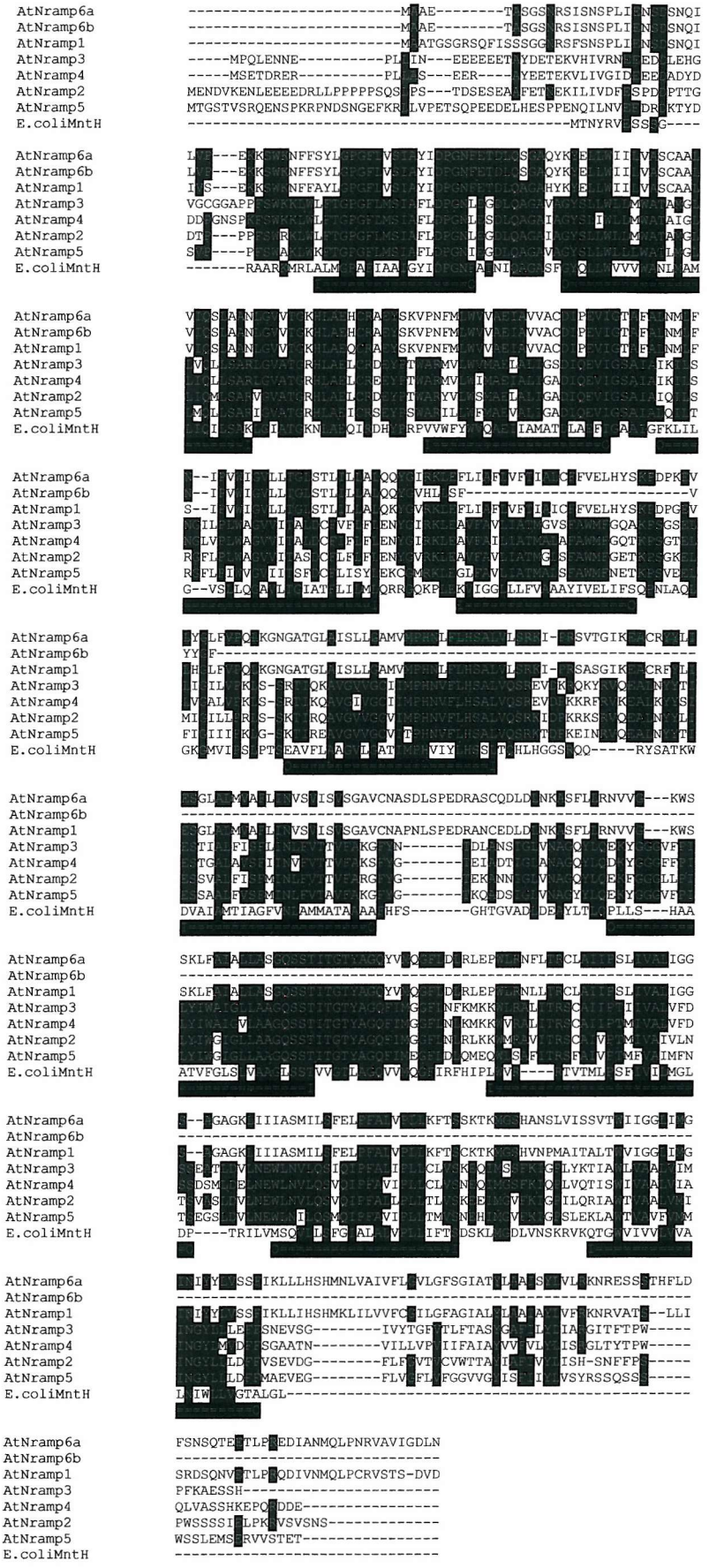

Fig.3.6. Amino acid alignment of AtNramps with *E. coli* MntH (accession P77145). Sequences were aligned using CLUSTAL W. Highlighted text represents identical amino acids between the sequences. The experimentally determined transmembrane topology (Pascal *et al*, 2003) is shown underneath the alignment. I=inside, O=outside, ========= = membrane spanning region.

Fig.3.7. Amino acid alignment of AtNramps with *E. coli* MntH (accession P77145). Sequences were aligned using CLUSTAL W. Highlighted text represents membrane-spanning regions as predicted by TMHMM. The experimentally determined transmembrane topology (Pascal *et al*, 2003) is shown underneath the alignment. I=inside, O=outside, ======= = membrane spanning region.

terminus of the protein, which appears to be extended when compared to MntH. An alignment of the AtNramps with MntH showing the TMPred transmembrane predictions is shown in Fig.3.8. While most of the transmembrane regions are predicted to within a few amino acids of the experimentally determined domains, TMPred fails to predict TM3 and TM9 of MntH. As with TMHMM, TMPred fails to detect TM3 in all the sequences except AtNramp4 and 5 despite the high sequence identity in this region. Although TMPred does not detect TM9 in MntH, it does predict this region to be membrane spanning in the AtNramps. However, in AtNramp1 and 6, the predicted TM9 overlaps with the predicted TM10, shown on Fig.3.8 as a single, long transmembrane region. As with the TMHMM predictions, a twelfth (or eleventh in the case of AtNramp1 and 6) transmembrane domain is predicted by TMPred at the C-termini of all the AtNramps after the MntH sequence has ended.

3.2.4. Phylogenetic analysis.

For phylogenetic analysis of the Nramps, sequences from various organisms were obtained from the Pfam protein family database (http://www.sanger.ac.uk/Software/Pfam/), the Ward laboratory predicted protein databases for *Arabidopsis* (http://www.cbs.umn.edu/arabidopsis/) and Rice (http://www.cbs.umn.edu/rice/) and by searching general databases such as EMBL and SWISSPROT. The amino acid sequences were aligned using CLUSTAL W 1.83 (Thompson *et al.*, 1994; http://bioweb.pasteur.fr/seqanal/interfaces/clustalw-simple.html) and a phylogenetic tree generated using the PHYLIP 3.6a.3 neighbour joining method with the dataset bootstrapped 500 times (Felsenstein, 1985). The tree was rooted at a sequence from an archaebacterium *Sulfolobus solfataricus* and displayed using treeview 1.6.6 (Page, 1996). This tree is shown in Fig.3.9. Bootstrap values are shown only where a branch occurred less than 300 times. The plant Nramps appear to cluster in two distinct groups; AtNramp1 and 6 group with OsNramp1, OsNramp3, three unnamed OsNramp homologs and LeNramp1 while the other plant Nramps, AtNramp2, 3, 4, 5, OsNramp2, an OsNramp homolog, LeNramp3 and TjNramp form a separate group on the tree. Separated

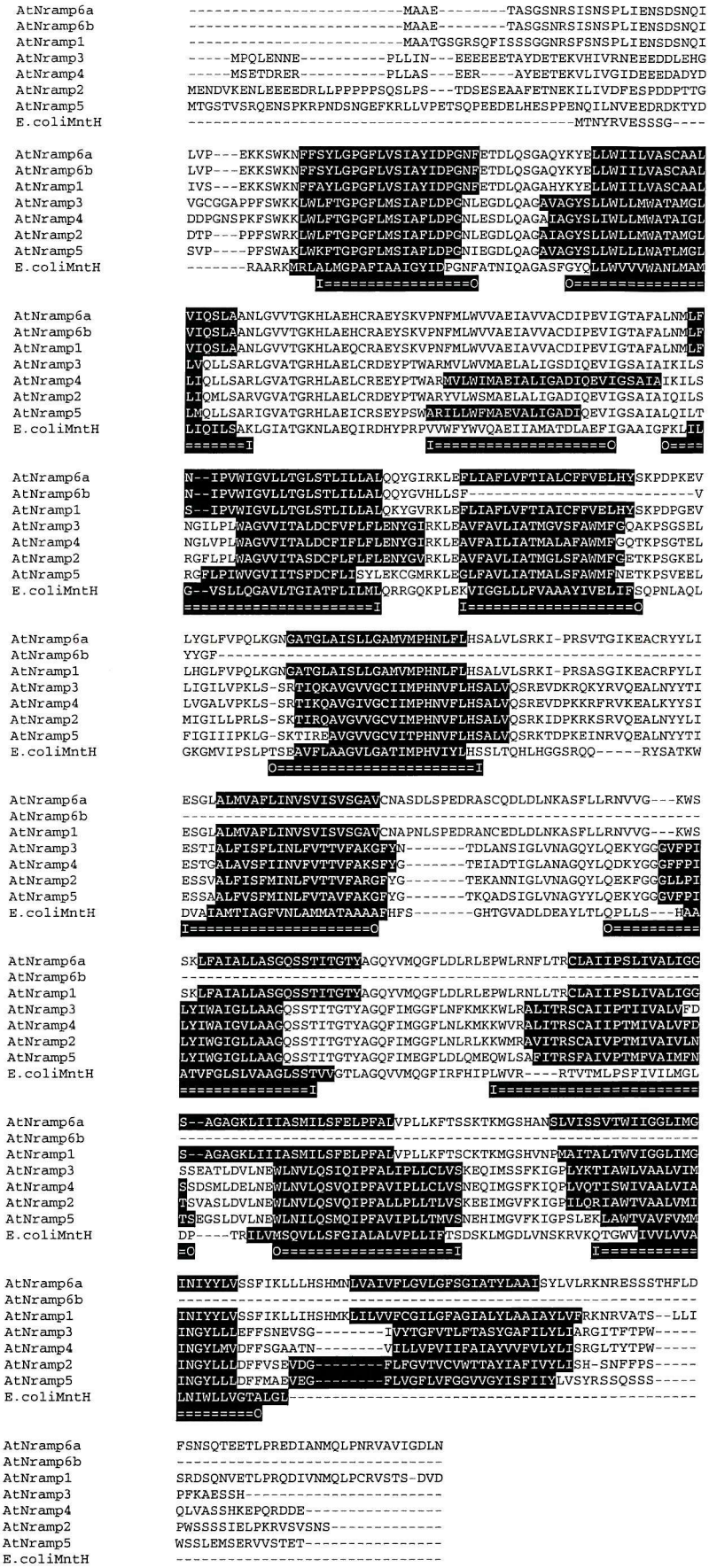

Fig.3.8. Amino acid alignment of AtNramps with *E. coli* MntH (accession P77145). Sequences were aligned using CLUSTAL W. Highlighted text represents membrane-spanning regions as predicted by TMPred. The experimentally determined transmembrane topology (Pascal *et al*, 2003) is shown underneath the alignment. I=inside, O=outside, ======= = membrane spanning region.

Fig.3.9. (A). Phylogenetic tree of the Nramp family of proteins from various organisms. The phylogenetic tree was generated from CLUSTALW alignments of full-length amino acid sequences (except where indicated below) and generated using PHYLIP. The number of times a branch occured is shown only for branches that were present in fewer than 300 of the 500 data sets. The organism names and sequence accession numbers are: 1. *Sulfolobus solfataricus* hypothetical protein P95854, 2. *Sulfolobus solfataricus* Putative manganese transporter Q97UL0, 3. *Sulfolobus tokodaii* ST1901 Q96ZD0, 4. *Thermoplasma acidophilum* Conserved membrane protein Q9HKW5, 5. *Thermoplasma volcanium* hypothetical protein Q97AG8, 6. *Rhizobium meliloti* RA0604 (SMA1115) Q92Z88, 7. *Burkholderia cepacia* genomovar III Q8VP26 8. *Ralstonia solanacearum* MNTH2? Q8XTS7, 9. *Mycobacterium leprae* MLCB1886.05C Q9ZBE5, 10. *Mycobacterium leprae* ML2667 Q9CCY6, 11. *Clostridium acetobutylicum* putative Nramp Q97L77, 12. *Clostridium acetobutylicum* putative Nramp Q97DZ1, 13. *Natronomonas pharaonis* ORF1 (fragment) O07292, 14. *Chlorobium tepidum* Nramp Q8KDN5, 15. *Clostridium acetobutylicum* putative Nramp Q97LD4, 16. *Thermoanaerobacter tengcongensis* MNTA Q8RBX2, 17. *Corynebacterium diptheriae* putative transmembrane protein Q8RMJ9, 18. *Bifidobacterium longum* AAN24094 Q8G7L2, 19. *Mycobacterium leprae* MNTH Q50103, 20. *Mycobacterium tuberculosis* MNTH O05916, 21. *Mycobacterium bovis* MNTH O69443, 22. *Bacillus subtilis* MNTH P96593, 23. *Thermoanaerobacter tengcongensis* MNTA2 Q8R7S2, 24. *Clostridium acetobutylicum* MNTH (MNTA) Q97TN5, 25. *Deinococcus radiodurans* MNTH Q9RTP8, 26. *Yersinia pestis* MNTH Q8ZCK2, 27. *Escherichia coli* MNTH P77145, 28. *Salmonella typhi* MNTH Q9RPF4, 29. *Dictyostelium discoideum* metal ion transporter Q8MXP7, 30. *Chlamydomonas reinhardtii* Nramp Q8LKG7, 31. *Brucella melitensis* MNTH Q8YI76, 32. *Agrobacterium tumefaciens* MNTH AI2789, 33. *Agrobacterium tumefaciens* MNTH Q8UEM1, 34. *Anabaena* Sp. MNTH Q8ZSB0, 35. *Listeria innocua* MNTH Q92BT1, 36. *Listeria monocytogenes* MNTH Q8Y773, 37. *Pseudomonas aeurignosa* MNTH2 Q9RPF2, 38. *Rhizobium loti* MNTH Q98I99, 39. *Xylella fastidiosa* XF1015 Q9PEL3, 40. *Xanthomonas campestris* SMF2 Q8P8R8, 41. *Xanthomonas axonopodis* SMF2 Q8PKX1, 42. *Burkholderia cepacia* MNTH (fragment) Q9RPF1, 43. *Pseudomonas aeurignosa* MNTH1 Q9RPF3, 44. *Ralstonia solanacearum* MNTH1? Q8XSF6, 45. *Neurospora crassa* ESP1 Q9P4X9, 46. *Schizosaccharomyces pombe* Nramp Q10177, 47. *Saccharomyces cerevisiae* SMF1 P38925, 48. *Saccharomyces cerevisiae* SMF2 P38778, 49. *Saccharomyces cerevisiae* SMF3 Q12078, 50. *Staphylococcus aureus* SAV1105 Q931T9, 51. *Lactobacillus brevis* HITA Q93V04, 52. *Streptococcus agalactiae* AAM99632 Q8E0I6, 53. *Lactococcus lactis* YKJB (LL1082) Q9CGL4, 54. *Streptococcus agalactiae* AAN00884 Q8DX33, 55. *Oryza sativa* Nramp homolog #3 Q67G85, 56. *Oryza sativa* Nramp homolog #2 Q6IMS4, 57. *Lycopersicon esculentum* Nramp1 Q84LR0, 58. *Oryza sativa* Nramp homolog #1 Q6IMS6, 59. *Oryza sativa* Nramp1 Q41268, 60. *Oryza sativa* Nramp3 Q6IMS7, 61. *Arabidopsis thaliana* Nramp6 At1g15960, 62. *Arabidopsis thaliana* Nramp1 At1g80830, 63. *Dictyostelium discoideum* Nramp Q8MYI4, 64.*Oryza sativa* Nramp2 O24209, 65. *Oryza sativa* Nramp homolog #4 Q6IMS3, 66. *Arabidopsis thaliana* Nramp4 At5g67330, 67. *Thlaspi japonicum* Nramp Q7XB56, 68. *Lycopersicon esculentum* Nramp3 Q84LR1, 69. *Arabidopsis thaliana* Nramp5 At4g18790, 70. *Arabidopsis thaliana* Nramp2 At1g47240, 71. *Glycine max* Nramp Q7X9B8, 72. *Arabidopsis thaliana* Nramp3 At2g23150, 73. *Sparus aurata* Nramp fragment Q8UUI6, 74. *Morone saxatilis* Nramp (fragment) Q9DET9, 75. *Takifugu rubripes* Nramp Q8AUT2, 76. *Ictalurus punctatus* Nramp Q8JFC9, 77. *Brachydanio rerio* Nramp Q9PUF1, 78. *Cyprinus carpio* Nramp Q9PU93, 79. *Pimephales promelas* Nramp (fragment) Q9IAJ3, 80. *Perca flavescens* Nramp (fragment) Q9PTE1, 81. *Oncorhynchus mykiss* Nramp beta Q9W666, 82. *Oncorhynchus mykiss* Nramp alpha Q9W665, 83. *Homo sapiens* Alternative Nramp2 AB004857, 84. *Macaca fascicularis* Nramp2a Q9MZV1, 85. *Macaca fascicularsis* Nramp2 Q9MZV2, 86. *Homo sapiens* Nramp2 P49281, 87. *Mus musculus* Nramp2 P49282, 88. *Rattus norvegicus* Nramp2 O54902, 89. *Gallus gallus* Nramp1 P51027, 90. *Sus scrofa* Nramp1 O77741, 91. *Equus caballus* Nramp1 Q95N75, 92. *Homo sapiens* Nramp1 P49279, 93. *Canis familiaris* Nramp1 Q9XT74, 94. *Rattus norvegicus* Nramp1 (fragment) P70553, 95. *Mus musculus* Nramp1 P41251, 96. *Ovis aries* Nramp1 P49280, 97. *Cervus elaphus* Nramp1 P56436, 98. *Bubalus bubalis* Nramp Q27946, 99. *Bison bison* Nramp1 Q95102, 100. *Bos taurus* Nramp1 Q27981, 101. *Anopheles gambiae* Nramp (fragment) Q7Q7L5, 102. *Drosophila heteroneura* Malvolio (fragment) O45125, 103. *Drosophila melanogaster* Malvolio P49283, 104. *Drosophila melanogaster* Malvolio alternative seq Q95TT7, 105. *Caenorhabditis elegans* Y69A2AR.4. Q95XG8, 106. *Caenorhabditis elegans* K11G12.3. Q21433, 107. *Caenorhabditis elegans* NRAMP-like transporter K11G12.4. 108. *Pagrus major* Nramp fragment Q9IB49, 109. *Oryza sativa* EIN2 homolog Q6TJY0, 110. *Arabidopsis thaliana* EIN2 At5g03280.

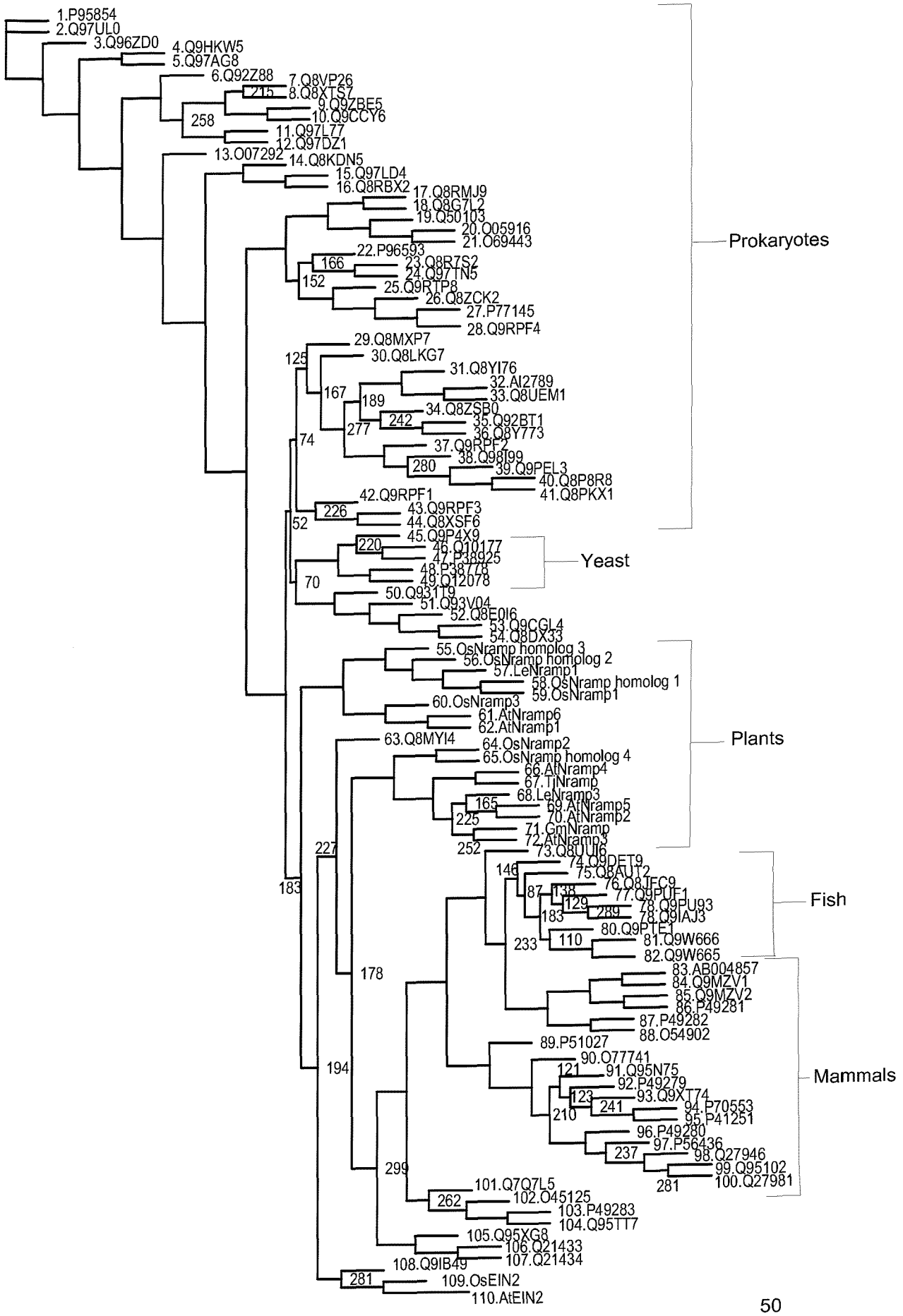
1.P95854
2.Q97UL0
3.Q96ZD0
4.Q9HKW5
5.Q97AG8
6.Q92Z88
7.Q8VP26
8.Q8XTS7
9.Q9ZBE5
10.Q9CCY6
11.Q97L77
12.Q97DZ1
13.O07292
14.Q8KDN5
15.Q97LD4
16.Q8RBX2
17.Q8RMJ9
18.Q8G7L2
19.Q50103
20.O05916
21.O69443
22.P96593
23.Q8R7S2
24.Q97TN5
25.Q9RTP8
26.Q8ZCK2
27.P77145
28.Q9RPF4
29.Q8MXP7
30.Q8LKG7
31.Q8YI76
32.AI2789
33.Q8UEM1
34.Q8ZSB0
35.Q92BT1
36.Q8Y773
37.Q9RPF2
38.Q98I99
39.Q9PEL3
40.Q8P8R8
41.Q8PKX1
42.Q9RPF1
43.Q9RPF3
44.Q8XSF6
45.Q9P4X9
46.Q10177
47.P38925
48.P38778
49.Q12078
50.Q931T9
51.Q93V04
52.Q8E0I6
53.Q9CGL4
54.Q8DX33
55.OsNramp homolog 3
56.OsNramp homolog 2
57.LeNramp1
58.OsNramp homolog 1
59.OsNramp1
60.OsNramp3
61.AtNramp6
62.AtNramp1
63.Q8MYI4
64.OsNramp2
65.OsNramp homolog 4
66.AtNramp4
67.TjNramp
68.LeNramp3
69.AtNramp5
70.AtNramp2
71.GmNramp
72.AtNramp3
73.Q8UUI6
74.Q9DET9
75.Q8AUT2
76.Q8JFC9
77.Q9PUF1
78.Q9PU93
78.Q9IAJ3
80.Q9PTE1
81.Q9W666
82.Q9W665
83.AB004857
84.Q9MZV1
85.Q9MZV2
86.P49281
87.P49282
88.O54902
89.P51027
90.O77741
91.Q95N75
92.P49279
93.Q9XT74
94.P70553
95.P41251
96.P49280
97.P56436
98.Q27946
99.Q95102
100.Q27981
101.Q7Q7L5
102.O45125
103.P49283
104.Q95TT7
105.Q95XG8
106.Q21433
107.Q21434
108.Q9IB49
109.OsEIN2
110.AtEIN2
Prokaryotes
Yeast
Plants
Fish
Mammals

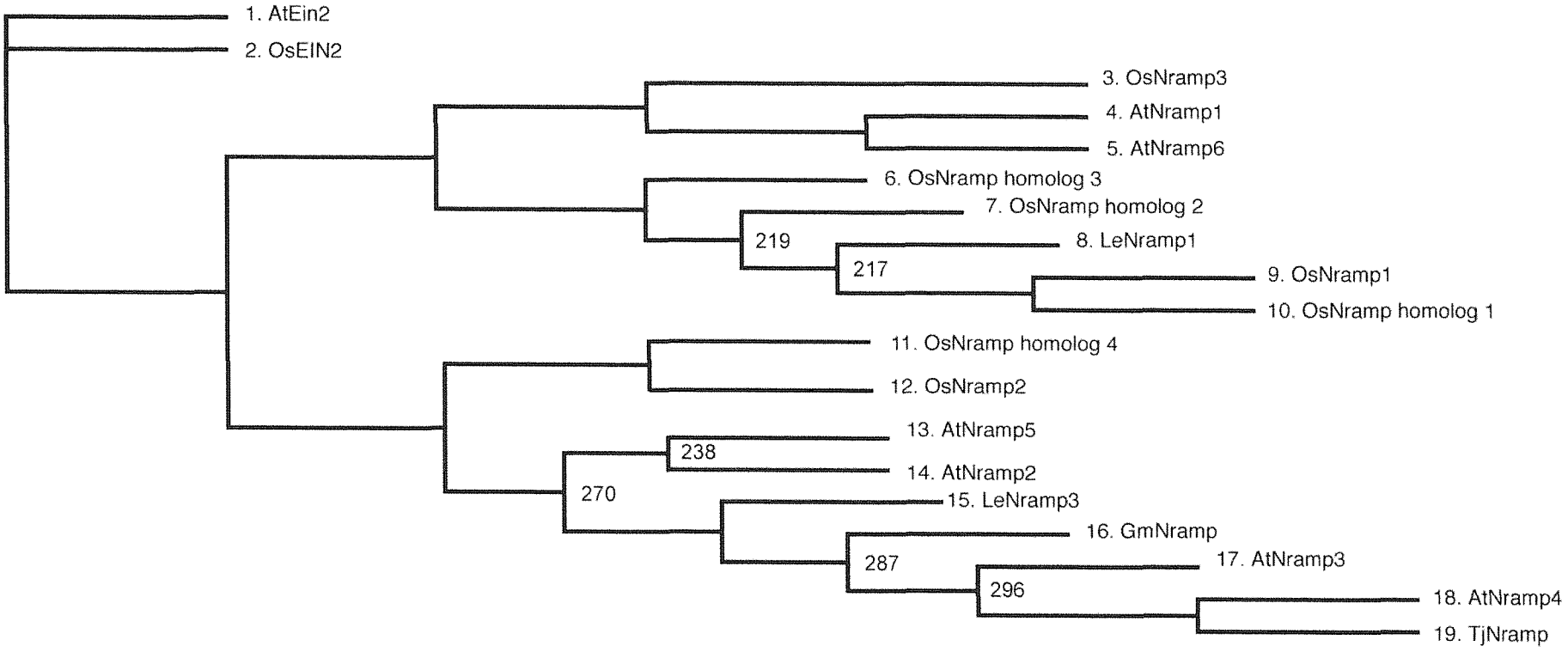

Fig. 3.9. (B). Phylogenetic tree of the Nramp family of proteins identified in plants to date. 1. Arabidopsis thaliana EIN2 At5g03280, 2.Oryza sativa EIN2 homolog Q6TJY0, 3. Oryza sativa Nramp3 Q6IMS7, 4. Arabidopsis thaliana Nramp1 At1g80830, 5. Arabidopsis thaliana Nramp6 At1g15960, 6. Oryza sativa Nramp homolog #2 Q6IMS4, 7. Oryza sativa Nramp homolog #3 Q67G85, 8. Lycopersicon esculentum Nramp1 Q84LR0, 9. Oryza sativa Nramp1 Q41268, 10. Oryza sativa Nramp homolog #1 Q6IMS6, 11. Oryza sativa Nramp homolog #4 Q6IMS3, 12. Oryza sativa Nramp2 O24209, 13. Arabidopsis thaliana Nramp5 At4g18790, 14. Arabidopsis thaliana Nramp2 At1g47240, 15. Lycopersicon esculentum Nramp3 Q84LR1, 16. Glycine max Nramp Q7X9B8, 17. Arabidopsis thaliana Nramp3 At2g23150, 18. Arabidopsis thaliana Nramp4 At5g67330, 19. Thlaspi japonicum Nramp Q7XB56.

from these are AtEIN2 and the rice homolog, OsEIN2. The mammalian Nramps also seem to divide into two groups. One group is made up of the Nramp1 proteins (89-100 on the tree), which are expressed in macrophages, while the other is made up of the Nramp2 proteins (83-88 on the tree), which are expressed in the apical membranes of cells lining the intestine. The plant Nramps are also shown in a separate tree in Fig.3.9 constructed using the same methods as for the full tree.

3.2.5. Topology.

A general model of the possible topology of the AtNramps is shown in Fig.3.10. Predicted N-linked glycosylation sites shown here are only present on AtNramp1 and 6 and are in similar positions to those in OsNramp1 and 3 (Belouchi *et al.*, 1997). AtNramp3 and 4 have no predicted glycosylated sites while AtNramp2 and 5 possess one each, between TM9 and 10 in AtNramp5. The only possible predicted site in AtNramp2 lies within the predicted TM9 and so would not be glycosylated if the protein assumes the conformation shown here. The positions of the conserved amino acids required for the function of DCT1 (Cohen *et al.*, 2003) are also indicated. These are found in all six AtNramps.

3.2.6. Intron/exon structure.

The intron and exon structures of the six *AtNramps* were obtained from the MIPS database at (http://mips.gsf.de/proj/thal/db/search/search_frame.html) which gives the predicted spliced and unspliced sequences. From these sequences the predicted splice sites of the introns can be identified. The structure of the introns and exons of the *AtNramps* are shown diagrammatically in Fig.3.11. *AtNramp2, 3, 4* and *5* possess far fewer introns than *AtNramp1* and *6*. *AtNramp4* is predicted to have only two introns while *AtNramp2, 3* and *5* have three. Of these, *AtNramp2* and *3* appear to share a much more similar pattern of introns and exons than *AtNramp4* and *5*. The main difference is in the length of the first intron, in

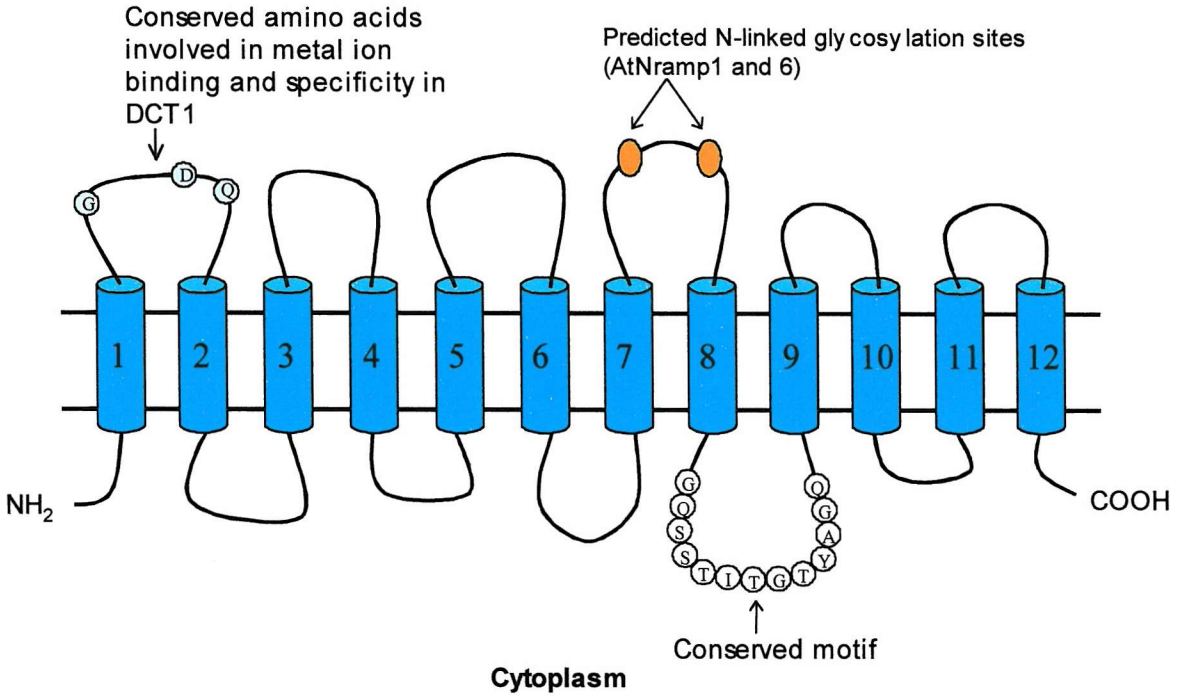

Fig.3.10. Predicted topology of the AtNramps. 12 transmembrane domains (identified by comparison to *E. coli* MntH topology by Pascal *et al*, 2003), possible N-linked glycosylation sites in AtNramp1 and AtNramp6 (identified by the consensus sequence N X S/T and comparison to OsNramp analysis by Belouchi *et al*, 1997), conserved amino acids required for function of mammalian DCT1 (Cohen *et al*, 2003) and the conserved signature motif are shown. This model also shows the N and C-termini positioned inside the cytoplasm.

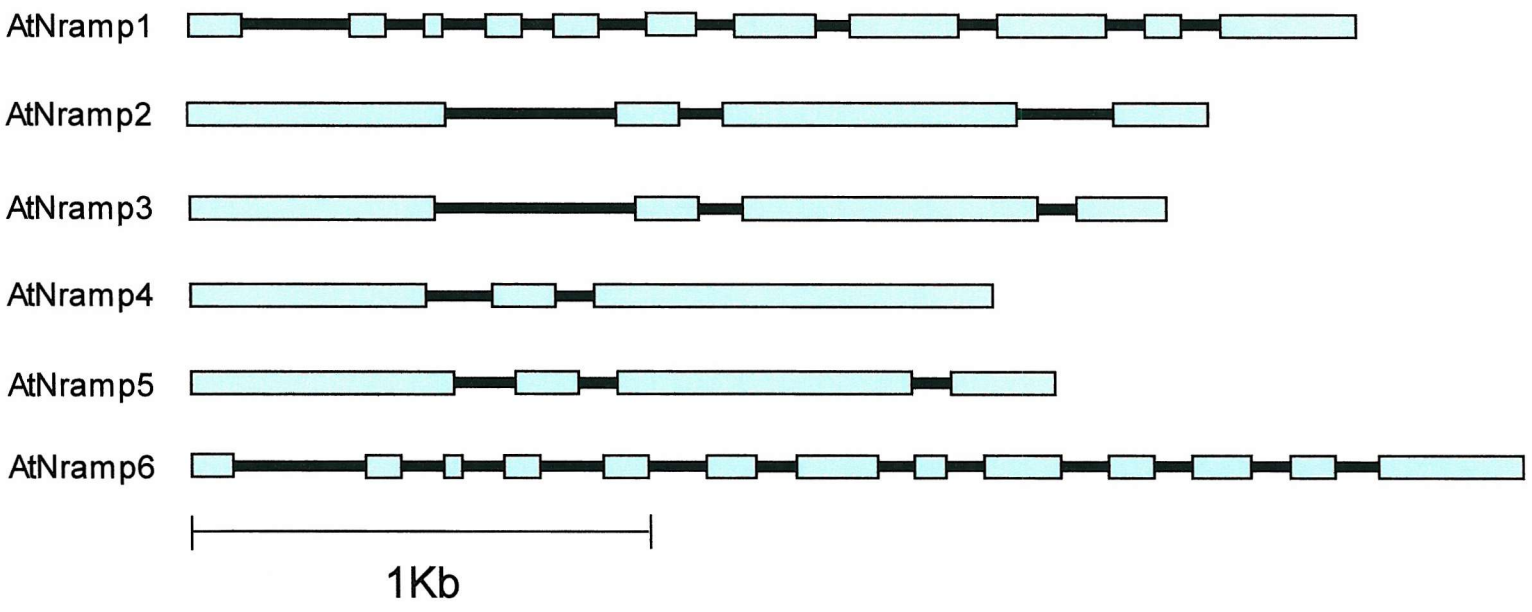

Fig.3.11. Predicted intron and exon positions in the six *AtNramps*. Exons are shown as blocks while introns are shown as horizontal black lines. Both introns and exons are shown to scale. The predicted intron/exon structures were obtained from the MIPS database (http://mips.gsf.de/proj/thal/db/search/search_frame.html).

AtNramp2 and *3* it is noticeably longer than *AtNramp4* and *5*. The remaining introns and exons are of similar lengths except there is no third intron in *AtNramp4*. *AtNramp1* has ten introns while *AtNramp6* has twelve making them appear quite different when compared to the other *AtNramps* with regard to intron and exon structure and number. Although the introns occur in slightly varying positions within *AtNramp1* and *6* most of the introns and exons are of similar lengths and share a similar overall pattern. The main difference between *AtNramp1* and *6* appears at exons 8 and 9 (of *AtNramp1*). In *AtNramp6* it seems that these exons have both been split by extra introns resulting in *AtNramp6* possessing two more exons than *AtNramp1*. The other exons are approximately the same length in both these genes. Fig.3.12 shows the lengths and positions of the exons of the *AtNramps* more clearly than Fig.3.11 since the intron lengths are not included. This shows that apart from *AtNramp2* and *AtNramp5* (which are near identical in exon length and position) there is some variation in the length and positioning of exons when comparing the *AtNramp* sequences.

3.2.7. Signal peptide analysis.

The six AtNramp amino acid sequences were analysed for the presence of putative signal peptides in order to make predictions as to their subcellular locations. Data from the online programs, iPSORT, (http://hypothesiscreator.net/iPSORT), Predotar (www.inra.fr/predotar) and TargetP (www.cbs.dtu.dk/services/TargetP), are shown in Table 3.3. The iPSORT program predicts AtNramp1 to contain signal sequences that may indicate a mitochondrial location within the cell. The other AtNramp sequences are predicted to contain no signal sequences and so would be localised to the plasma membrane of the cell. Predotar does not detect any signal sequences within the AtNramps while TargetP predicts weak signal sequences for chloroplast localisation in AtNramp1 and AtNramp5.

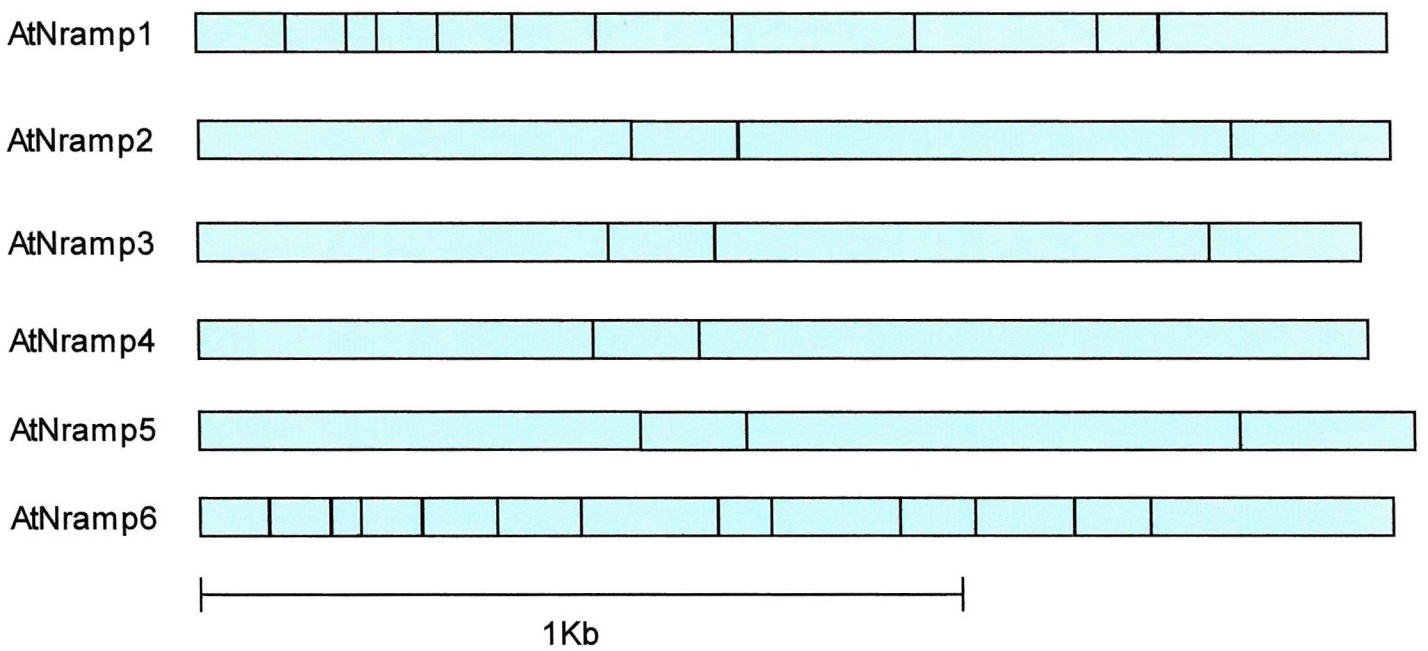

Fig.3.12. Predicted intron and exon positions in the six *AtNramps*. Exons are shown as blocks while introns are shown as vertical black lines. Exons are shown to scale. The predicted intron/exon structures were obtained from the MIPS database (http://mips.gsf.de/proj/thal/db/search/search_frame.html).

Table 3.3. Signal peptide predictions for the amino acid sequences of the six Nramps from *Arabidopsis thaliana*. The full length amino acid sequences were used in each case.

	Signal	Chloroplast/Mitochondrial	Mitochondrial	Result
AtNramp1	iPSORT -0.93 (No) Predotar 0.00 (No) TargetP 0.103 (No)	iPSORT 0.03 (Yes) Predotar 0.29 (No) TargetP 0.492 (weak)	iPSORT 6.1 (Yes) Predotar 0.03 (No) TargetP 0.19 (No)	Mitochondrial
AtNramp2	iPSORT -1.73 (No) Predotar 0.00 (No) TargetP 0.058 (No)	iPSORT 0.3 (No) Predotar 0.00 (No) TargetP 0.197 (No)	iPSORT 4.9 (No) Predotar 0.01 (No) TargetP 0.104 (No)	None
AtNramp3	iPSORT -1.62 (No) Predotar 0.00 (No) TargetP 0.142 (No)	iPSORT 0.36 (No) Predotar 0.00 (No) TargetP 0.121 (No)	iPSORT 5.1 (No) Predotar 0.01 (No) TargetP 0.052(No)	None
AtNramp4	iPSORT -1.18 (No) Predotar 0.00 (No) TargetP 0.174 (No)	iPSORT 0.3 (No) Predotar 0.00 (No) TargetP 0.061 (No)	iPSORT 5.6 (No) Predotar 0.01 (No) TargetP 0.146 (No)	None
AtNramp5	iPSORT -2.24 (No) Predotar 0.00 (No) TargetP 0.046 (No)	iPSORT 0.13 (No) Predotar 0.00 (No) TargetP 0.493 (Weak)	iPSORT 6.5 (No) Predotar 0.01 (No) TargetP 0.118 (No)	Possibly chloroplast
AtNramp6	iPSORT -0.925 (No) Predotar 0.11 (No) TargetP 0.194 (No)	iPSORT 0.1 (No) Predotar 0.31 (No) TargetP 0.017 (No)	iPSORT 5.9 (No) Predotar 0.16 (No) TargetP 0.193 (No)	None

3.3. Discussion.

To date, six Nramps have been identified in *Arabidopsis thaliana,* eight in *Oryza sativa,* two in *Lycopersicum esculentum* and one in *Glycine max* (Belouchi *et al.*, 1997, Curie *et al.,* 2000, Thomine *et al.*, 2000, Williams, 2000, Bereczky *et al.*, 2003, Kaiser *et al.*, 2003). More putative Nramp sequences from various organisms are also present in the databases and it seems likely that these and other species will express more genes that fit into the Nramp family. This chapter provides a detailed analysis of the *Arabidopsis* Nramp sequences. Sequence analysis can often give insights into the relationship of genes within a family or between members of different families. From these types of analyses the possible functions of these genes and the proteins they encode can be predicted and then tested experimentally. Certain regions of the DNA or amino acid sequences may be similar to regions of previously characterised genes or proteins thus giving insight into the mechanisms and function of the genes of interest. Such regions include transmembrane domains, metal-binding motifs, glycosylation sites, signal sequences and other characterised motifs in the sequence.

Sequence analysis performed by Belouchi *et al.,* (1997) on three members of the *Oryza sativa* (Os) Nramp family has identified 12 predicted transmembrane domains, possible N-linked glycosylation sites and a conserved motif with some similarity to a motif found in animal shaker type K^+ channels (Wood *et al.*, 1995). These characteristics were found in all three OsNramps studied. Belouchi *et al.* (1997) concluded that the high degree of conservation in the transmembrane domains and in the conserved motif suggests the importance of these regions in a common structure and function of these proteins. It was also suggested that the N-linked glycosylation sites would be present on an extracellular loop while the conserved motif would be found in an intracellular location along with the N and C-termini. This is consistent with the topology identified for *E. coli* MntH (Pascal *et al.*, 2003).

The high degree of conservation of the conserved signature motif throughout the evolution of the Nramp family could suggest an important role for

this region of the Nramps, perhaps in transport function or regulation. Belouchi *et al.* (1997) made the observation that this motif bears some similarity to a motif found in animal K^+ channels (Wood *et al.*, 1995). Pinner *et al.* (1997) introduced three independent mutations in this motif in mouse MmNramp2 and determined the effect on the protein's ability to rescue the *SMF1/SMF2* yeast mutant. A glutamine to glutamate substitution at position 384 (Q384E) or a glycine to valine substitution at position 394 (G394V) resulted in loss of function of MmNramp2. A glutamine to glutamate mutation at position 395 (Q395E) had no effect however. In AtNramp1 these bases occur at position 339 (Q), 349 (G) and 350 (Q) respectively and are identical to those in many other Nramp sequences including mouse MmNramp2 (Pinner *et al.*, 1997). All six of the AtNramp sequences possess these amino acids in the same positions relative to each other. The high degree of conservation of these amino acids allows speculation that they may also be important in the function of the AtNramps. However, it is still unknown how this motif is important to the protein and whether it is a structural or functional feature.

It appears that the plant Nramps (highlighted in Fig.3.5) may cluster in two distinct groups in the phylogenetic tree. AtNramp1 and AtNramp6 group together with OsNramp1 and OsNramp3 (from *Oryza sativa*), while AtNramp2, 3, 4 and 5, along with OsNramp2, form a separate group. The significance of these groupings is unclear but the Nramps from the mammals also appear to cluster in two groups, the so-called Nramp1 proteins being separate from the Nramp2 proteins. It is possible this grouping may in some way reflect the differing functions of mammalian Nramp1 and 2. In mice, MmNramp1 is expressed in macrophages (Vidal *et al.*, 1993) and some neuronal cells (Evans *et al.*, 2001) and may have a more specialised function than Nramp2, which is expressed in intestinal endothelial cells and is involved in the uptake of dietary iron (Gunshin *et al.*, 1997; Picard *et al.*, 2000). If the evolutionary differences indicated by the phylogenetic tree reflect some difference in the way the mammalian Nramps function it may be possible that the two AtNramp groups also have functionally distinct roles.

So far, a specific function for a plant Nramp has only been suggested for AtNramp3. Thomine *et al.* (2000, 2003) have shown that AtNramp3 is capable of transporting Fe and Cd, affects Mn and Zn accumulation and that the protein

localises to the vacuolar membrane. They suggested that AtNramp3 mobilises vacuolar stores of Fe, Cd and other metals to control Fe acquisition genes (IRT1), Mn and Zn accumulation under Fe starvation and Cd sensitivity.

As in the phylogenetic tree, the AtNramps appear to separate into two groups with regard to their predicted transmembrane positions. In the tree, AtNramp1 groups with AtNramp6, while AtNramp2, 3, 4 and 5 form another group. Differences between these two groups are also apparent in the length and position of their predicted transmembrane domains. Many of the transmembrane domains of AtNramp1 and 6 possess a similar amino acid sequence and are of a similar length. The same appears true of the transmembrane domains of AtNramp2, 3, 4 and 5 although these are different to those of AtNramp1 and 6.

Interestingly, the conserved signature motif is almost completely contained in a predicted transmembrane domain in some of the AtNramps while in others the motif is found almost entirely outside of the transmembrane domains. It is possible that the differences in the position of this motif may perhaps indicate functional differences in the AtNramps although it is perhaps more likely that the predicted transmembrane domains are slightly inaccurate and that the position of the signature motif is similar in all the AtNramps with respect to the transmembrane domains. This remains to be tested.

Other transmembrane prediction programs, such as TMHMM and TMpred, give slightly different predictions as to the position, length and number of the transmembrane domains in the AtNramps showing that the predictions illustrated in Fig.3.3 are by no means certain. For example, the TMHMM prediction suggests only 10 transmembrane domains in AtNramp5, missing out the first and third transmembrane domains shown in Fig.3.3. The other transmembrane domains are predicted in similar, but by no means identical, positions. TMpred, however, predicts 11 transmembrane domains, missing only the third domain shown in Fig.3.3. The various predictions for AtNramp6 also showed these kinds of differences, which may be inherent in the way these programs work. When compared to the sequence of *E. coli* MntH, for which the topology has been experimentally determined (Pascal *et al.*, 2003), it seems likely that the transmembrane prediction programs are relatively accurate with the exception of a

few regions in the sequences. The sequence similarity between MntH and the AtNramps suggests that regions shown to be transmembrane domains in MntH may also be such in the AtNramps. While MntH has eleven transmembrane domains, the AtNramps are predicted to contain a twelfth, toward the C-terminus of the proteins, which is extended compared to MntH. This twelfth domain is consistently predicted in all six of the AtNramps and leads to the suggestion that the AtNramps are likely to each possess twelve transmembrane domains in total. However, the region between TM9 and TM10 in MntH does not align well to the AtNramps and AtNramp1 and 6 are different to the other AtNramps here. Also, TM9 and TM10 of AtNramp1 and 6 are predicted as one long transmembrane region. Without further evidence it is impossible to rule out that this region represents only one transmembrane domain in these AtNramp sequences and that they possess only eleven transmembrane domains.

Cohen *et al.* (2003) identified the role of three amino acids within the first external loop of the mammalian DCT1 by generating proteins with substitutions at these positions. A glycine (G) to alanine (A) substitution at position 119 (G119A) in DCT1 seems to abolish the uptake of Fe^{2+}, Mn^{2+} and Co^{2+} while increasing the affinity of the proton-binding site. The first asterisk on the AtNramp sequence alignment (Fig.3.1.) indicates this conserved glycine. An aspartate (D) to alanine (A) substitution at position 124 (D124A) retained Fe^{2+} uptake activity but failed to rescue the yeast *smf1* Mn uptake mutant on media containing EGTA. This conserved aspartate is indicated by the second asterisk on Fig.3.1. A glutamine (Q) to aspartate (D) substitution at position 126 (Q126D) in DCT1 also abolished Fe^{2+}, Mn^{2+} and Co^{2+} uptake in oocytes. This conserved glutamine is indicated by the third asterisk on Fig.3.1. The double mutant D124A/Q126D suppresses the Q126D phenotype and is able to transport Fe^{2+} and Co^{2+}. The triple mutant G119A/D124A/Q126D shows no transport activity (Cohen *et al*, 2003). The identity between DCT1 and the AtNramps with regard to the positioning of these residues suggests these amino acids may also have a functional significance in the AtNramps. Amino acid substitutions of these residues in the AtNramps would be required to ascertain if this hypothesis is correct however.

The position of introns and exons in genes and the similarities in this pattern between members of a gene family can give an insight into the degree of relatedness between different genes and their evolutionary order. Fig.3.7 shows the predicted intron splice sites of the six *Arabidopsis Nramps*. The intron patterns seem to divide the *AtNramps* into two distinct groups; *AtNramp2, 3, 4* and *5* have few introns while *AtNramp1* and *6* contain noticeably more. Perhaps the increase in the number of introns and exons is indicative of a split in the family leading to functional or regulatory differentiation. Duplication events may have then led to the multiple members of each sub-group. For example, AtNramp1 and AtNramp6 may have resulted from a duplication event since they are closely related with regard to sequence similarity and intron splice pattern. Further evidence for this possibility is the fact that both AtNramp1 and AtNramp6 are preceded by a cinnamoyl Co A reductase-like gene, perhaps indicating that a region of the chromosome was duplicated at some point in the evolution of the *Arabidopsis* genome. Without functional studies of the *AtNramps* (and *Nramps* from other species) there is no evidence to support the idea that the existence of two phylogenetic sub-groups means there are two functionally different groups.

It seems that many features of the AtNramp sequences point to the existence of two subgroups, one comprising AtNramp1 and 6 and the other comprising AtNramp2, 3, 4 and 5. AtNramp1 and 6 do not align so well to the other AtNramps as they do to each other, possess more introns and exons, contain more N-linked glycosylation consensus sequences and may have one fewer transmembrane domains than the other AtNramps. It is impossible to know whether these groupings reflect any real differences between the AtNramps in functional terms however. The observation that Nramps from both of these two groups are able to complement a Fe-uptake deficient yeast mutant (*fet3/fet4*) (Curie *et al.*, 2000, Thomine *et al.*, 2000) leads to speculation that the differences are not necessarily reflected in the protein's function with regard to substrate. However, it is still possible that there are differences in their regulation or expression that do reflect the relationships between the sequences. Also, although some Nramps can rescue the Fe-uptake deficient yeast mutant it does not necessarily follow that they transport Fe in the plant under all conditions, but are

perhaps dependent on the nutrient status of the plant. One group of Nramps may be altered in their expression levels under some conditions while the other group may be altered under others. Of course, it cannot be ruled out that the multiple members of the Nramp family in Arabidopsis are merely functionally redundant proteins and all have similar roles within the plant.

As more studies are performed on the Nramp family and important regions and motifs in the proteins are identified it may be possible to make more educated predictions as to differences and similarities between the AtNramps and how these relate to their functions in the plant. The results of sequence analysis of the AtNramps does provide avenues for investigation into their function by identifying various potentially important regions of the DNA and amino acid sequences on the basis of similarity to regions identified experimentally in other Nramps.

Chapter 4. Tissue specific expression of the *AtNramps.*

4.1. Introduction.

Determining the expression pattern of a gene can give insight into its function or role in the organism. A gene found in only one tissue or organ is likely to have some role that may differentiate that tissue from others. For example, expression only in roots could suggest a role in uptake from the soil since this is one of the primary functions of the root system. However, if a gene is found in all tissue types this can suggest that it plays a part in a more fundamental process that is required in all cells or organs of the organism. A number of methods are commonly used to ascertain gene expression patterns in different organs and cells. Reverse transcriptase-PCR (RT-PCR) makes use of reverse transcriptase to synthesize cDNA from mRNA. Once cDNA is obtained, PCR using standard reaction components can be used to amplify specific genes to identify which ones are present in the mRNA and are therefore being expressed in the tissue at that time. It can be used semi-quantitatively to identify the expression pattern of a gene or changes in its expression under various environmental conditions. For example, Yamaji *et al.* (2001) used this method to show that Zn caused an increase in the mRNA levels of Divalent Metal Transporter 1 (DMT1) in human intestinal Caco cells. Quantitative real-time PCR involves monitoring the progress of the reactions by the use of fluorescent probes and PCR lightcyclers capable of detecting the fluorescence produced (Wittwer *et al.*, 1997). In the case of the experiments presented here, the fluorescent dye SYBR green has been used. This molecule binds only to double-stranded DNA and fluoresces only when bound. Therefore as more double-stranded DNA is formed in the elongation step of each PCR cycle, more fluorescence is produced since more of the dye will be bound. This can be a cost effective method but care must be taken since the dye will also bind to primer-dimers and other unwanted, non-specific products giving a spurious signal. This can be investigated by analysing the melting temperatures of the products (Ririe *et al.*, 1997). Alternatively, specific probes to the gene of interest can be synthesized, which incorporate a fluorescent dye, such as 5-carboxyfluorescein (FAM), and a molecule such as methyl red that quenches the fluorescence when attached to the probe. The probe anneals to the gene of

interest but the polymerase removes the quenching part of the probe as it synthesizes the new DNA strand thus allowing fluorescence to be produced and detected. These fluorescent probes allow the early stages of amplification to be measured giving more accurate quantification. This is due to the reactions still being in the exponential phase and lower quantities of unwanted or competing products such as primer-dimers are present at the early stages of PCR.

RT-PCR methods are only one way of identifying where genes are expressed and also cannot give information about protein expression. Another method of determining gene expression profiles is the use of the β-glucuronidase assay. This technique was developed by Jefferson *et al.* (1986) in order to provide an alternative to β-galactosidase and other marker genes. The β-glucuronidase (*uid*A) gene, often termed "GUS", is fused to the promoter sequence of the gene of interest and the fusion transformed into plants. Wherever the promoter is active the β-Glucuronidase gene product will be expressed. This allows the activity of the promoter to be assayed histochemically or fluorometrically. Schulze *et al.* (2000) used GUS-promoter fusions to identify the expression of the low affinity sucrose transporter *SUT1* in major leaf veins and flowers of *Arabidopsis*. Green fluorescent protein (GFP) can also be tagged to the protein by creating GFP-gene fusions and inserting them into the genome of the organism. The fluorescence of the GFP-gene fusion product can then be visualised by UV microscopy and can often give more detailed information as to the location of the protein of interest within the cells of the organism. Thomine *et al.* (2003) used *AtNramp3::GFP* gene fusions to show that the AtNramp3 protein is located in the vacuolar membrane in *Arabidopsis* leaf and root cells.

The aim of the work presented in this chapter was to characterise the expression patterns of the *AtNramps* and identify if *AtNramp5* and *AtNramp6* expression is regulated by Fe availability.

4.2. Results.

4.2.1. PCR analysis.

4.2.1.1. Primer design.

To monitor expression of the *AtNramps* the first step was to design suitable primers for their amplification from *Arabidopsis* tissues. These primers are shown in Table 4.1. The initial primers designed to the 5′ and 3′ untranslated region (UTR) of AtNramp1 failed to produce consistent results and amplified many unwanted products over a range of annealing temperatures. New primers were designed to the 5′ region of the cDNA sequence, which produced better results. *AtNramp2* primers required optimisation by performing PCR using various annealing temperatures. A hot-start method was used to reduce primer-dimer formation and the amplification of unwanted products. Fig.4.1 shows the results of this gradient PCR using *AtNramp2* primers. *AtNramp3*, *AtNramp4* and *AtNramp5* primers required no optimisation since they gave good amplification using an annealing temperature a few degrees under the melting temperature of the primers. The *AtNramp6b* primer was used in conjunction with the *AtNramp6* fwd primer and gave good amplification under the same conditions as the standard *AtNramp6* primers. Attempts to design and optimise primers to produce short products for quantitative PCR amplification of *AtNramp5* were unsuccessful. Primers that were suitable on paper did not perform adequately in PCR as shown in Fig.4.2. A gradient PCR using these primers at various annealing temperatures shows that a single specific band is not amplified under any of the conditions tested, although the correct sized 250bp product was obtained, among others, at 60.9ºC. The Nramp5 fwd and rev primers used in RT-PCR were therefore used to obtain data for *AtNramp5* in quantitative real-time PCR. Fig.4.2 also shows that the *AtNramp6* quantitative real-time PCR primers produce the correct sized products from both flower cDNA and cDNA clones of the gene in the NEV E vector. This product is approximately 250bp in size.

Table 4.1. Primers used in RT-PCR for amplification of *AtNramp*, *IRT1* and *Actin2* genes from *Arabidopsis* tissues. Base pair distances from start indicate the number of bases from the A residue of the ATG start codon to the first and last residue of each primer.

Gene	Primer Name	Sequence	Position	TM(ºC)	GC(%)
AtNramp1	Nr1bfwd	5' AGGCCCTGGTTTTCTTGTTT 3'	cDNA (202-221bp from start)	66	55
	Nr1brev	5' TTCAGCAACGACCCATAACA 3'	cDNA (423-442bp from start)	63	47
AtNramp2	Nr2fwd	5' CGCTCGAGGCGTCTTCTTCTTCTTTTATCCC 3'	5' UTR	64	52
	Nr2rev	5' CGCTCGAGTGCACATCCTCTTAACAAAAACA 3'	3' UTR	62	45
AtNramp3	NRMP.fwd	5' CGGAATTCATAACGTGTTAAACTAAAACC 3'	5' UTR	56	34
	NRMP.rev	5' CGGAATTCTAAGGATTACAAGACATAGCT 3'	3' UTR	57	38
AtNramp4	Nramp4cd-fwd	5' GAAGAAGAAGACGCTGATTACGA 3'	5' cDNA (91-113bp from start)	53	43
	Nramp4cd-rev	5' TGTACGTGAGTCCTCGTGAGATA 3'	3' cDNA (1681-1703bp from start)	55	48
AtNramp5	NRMP5KPN1.F	5' CGGGGTACCTCACGTCGTCAGTAACGCCGA 3'	5' UTR	68	63
	NRMP5KPN1.R	5' CGGGGTACCCGACCTTCTGATTTTGCTCAG 3'	3' UTR	66	57
AtNramp6 (a+b)	NRMP6.F	5' CGGAATTCCTCTGCATGTAAATTGTTGAT 3'	5' UTR	57	38
	NRMP6.R	5' CGGAATTCTGCAATAGATTACAATAAGTA 3'	3' UTR	54	31
AtNramp6 (b only)	NRMP6b.rev (used with NRMP6.F)	5' GCCATAATAAACAAAACTTAACAAATG 3'	Intron 4	58	26
AtIRT1 (Atg)	IRT1-fwd	5' AATCTCTCCAGCAACTTCAACTG 3'	5' cDNA (41-64bp from start)	58.9	43
	IRT2-rev	5' GAGCATGCATTTAGAAGTCCAAC 3'	3' cDNA (843-866bp from start)	58.9	43
Actin2 (Atg)	Act-fwd	5' GGCGACTCAACCAGCTACTGA 3'	cDNA (2171-2194bp from start)	56	57
	Act-rev	5' CGGTAACTCTTCTGGTAACGA 3'	cDNA (2436-2458bp from start)	52	48
AtNramp6 (qPCR)	N6 fwd Real Time	5' ATGGTGGCATTTCTCATCAA 3'	cDNA (801-821bp from start)	48	40
	N6 rev Real Time	5' AGCTCCATTTACCCACAACG 3'	cDNA (935-955bp from start)	52	50

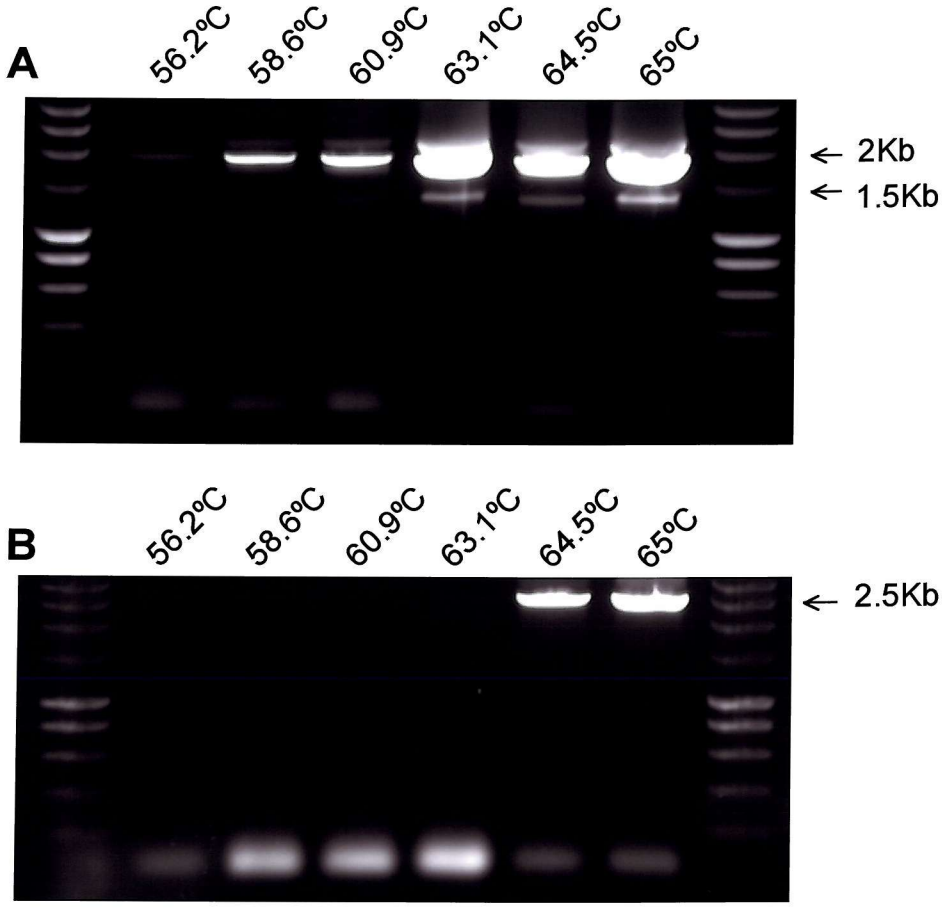

Fig. 4.1. Gel electrophoresis of gradient PCR using *AtNramp2* primers on **A**: flower cDNA and **B**: genomic DNA. Temperatures shown indicate the annealing temperature used in each reaction. A single experiment with one replicate of each temperature is shown. The expected size of *AtNramp2* product is 1.6Kb from cDNA and 2.2Kb from genomic DNA. PCR was performed with an initial melting step of 94°C for 2 min, then 40 cycles of 94°C, 30 s, annealing temperatures as shown above for 1 min, 72°C , 2 min and a final elongation step of 72°C for 5 min.

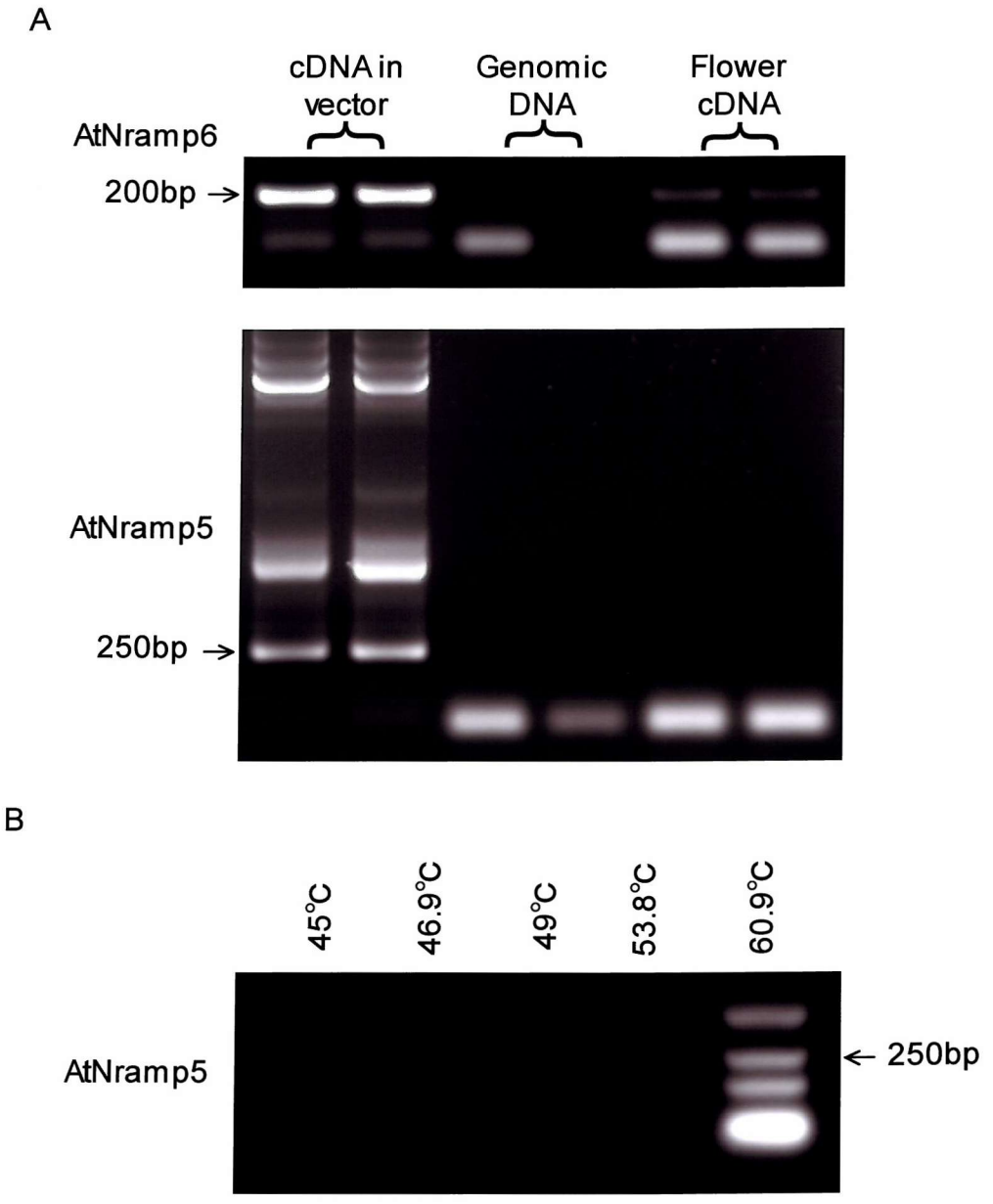

Fig. 4.2. (**A**) PCR to verify products obtained using *AtNramp5* or *AtNramp6* quantitative real-time PCR primers. PCR was performed with an initial melting step of 94°C for 2 min, then 40 cycles of 94°C, 30 s, 58°C, 1 min, 72°C , 2 min and a final elongation step of 72°C for 5 min. (**B**) Gradient PCR using *AtNramp5* quantitative real-time PCR primers on flower cDNA. A 2% agarose gel was used in all cases. Each of two replicates from one experiment is shown in each case. PCR was performed with an initial melting step of 94°C for 2 min, then 40 cycles of 94°C, 30 s, annealing temperatures as shown above for 1 min, 72°C , 2 min and a final elongation step of 72°C for 5 min.

4.2.1.2. RT-PCR

Fig.4.3 shows the results of RT-PCR using the *AtNramp* gene-specific primers described above on RNA from *Arabidopsis* roots, leaves, stem, flowers and siliques grown hydroponically under metal-replete conditions. *AtNramp1*, *AtNramp2*, *AtNramp3* and *AtNramp4* are amplified from all tissues; *AtNramp5* is amplified only from flowers, while *AtNramp6a* is found in all tissues except roots and *AtNramp6b* is found in all tissues except roots and siliques.

RT-PCR performed on cDNA from tissues treated with the specific Fe-chelator, ferrozine, is shown in Fig.4.4. Potential alterations in gene expression are indicated on Fig.4.4 by arrows under each image. *AtIRT1* was used as a control for these experiments since it has been shown to be induced upon Fe starvation in roots (Connolly *et al.*, 2002). When compared to *Actin2* controls *AtIRT1* shows up-regulation in roots in these experiments following treatment with ferrozine, the increase being more pronounced after 72 h than at 48 h. After 48 h *AtNramp3* appears slightly up-regulated in stem and flower but slightly down regulated in leaf and siliques tissues. It also seems greatly reduced in root after 48 h treatment with ferrozine. However, after 72 h *AtNramp3* is up-regulated in roots. *AtNramp6a* appears up-regulated in leaf tissue after 48 h and in stem tissue after 72 h. *AtNramp6b* also seems up-regulated in stem tissue after 72 h. No obvious changes are seen in the expression of *AtNramp5*.

4.2.1.3. Quantitative real-time PCR

Quantitative real-time PCR was performed using *AtNramp5, AtNramp6* and *AtIRT1* specific primers on the cDNA preparations used in the RT-PCR experiments described in section 4.2.1.2. The data from these experiments is shown in Fig.4.5 to Fig.4.10 and in Table 4.2 to Table 4.6. In each figure the amplification analysis graphs show the fluorescence detected against cycle number during each reaction. The fluorescence detected is indicative of the amount of double stranded PCR product formed at the end of each cycle since the SYBR green molecule only fluoresces when bound to double stranded DNA. Each coloured line on the amplification analysis graphs represents a separate amplification reaction. The dotted horizontal line shows the cycle threshold or

C(t). Optimally, this should be the initial point in each reaction at which amplification enters the log phase and it is used to cross reference the cycle number to enable comparisons between each sample in the run (e.g. lines that cross the cycle threshold at lower cycle numbers contain more starting template than those which cross the C(t) at higher cycle numbers). Instead of defining the cycle threshold arbitrarily for each run, the cycle threshold was set by using the standard deviation over the maximum cycle range with the intention to allow comparisons between runs to be made. The melting curve analysis graphs show the fluorescence detected against temperature following completion of the PCR run. This data allows the identification of single or multiple products in each reaction. Each coloured line shows the fluorescence given off from the final product of each amplification reaction shown in the amplification analysis graph as the temperature is increased. When the melting point of the double stranded product is reached it becomes single stranded, releasing the bound SYBR green and resulting in a marked drop in fluorescence. The negative slope of this line is also plotted on the same graph and forms a tall peak where the slope of the melting curve is steepest. This is the melting temperature of the final product. Narrow peaks indicate a single specific product while broad or multiple peaks indicate multiple non-specific products or primer-dimer formation. The peaks representing non-specific products or primer-dimers are often positioned at lower temperatures than those representing specific PCR products. A good example of this is seen in Fig.4.5 when comparing the melting curve analysis of the standards (a single narrow peak indicating specific product seen in all reactions) against that of the samples (some reactions show single narrow peaks while others show multiple broad peaks, most likely due to primer-dimer formation in the blank reactions). Each figure also shows the control graph in which the log of the initial template quantity (e.g. number of molecules) in each known standard is plotted against the C(t) cycle value. A line of best fit through these data points is plotted and the position of each sample along this standard line is used to calculate the quantity of initial template in each sample reaction. The data from these calculations is shown in the relevant tables following each figure. Finally, the results from gel electrophoresis of the products from each standard and sample reaction is shown in each figure.

Fig.4.5 shows the results from the first experiment using the *AtNramp6* real-time PCR primers. While the end point analysis (by agarose gel

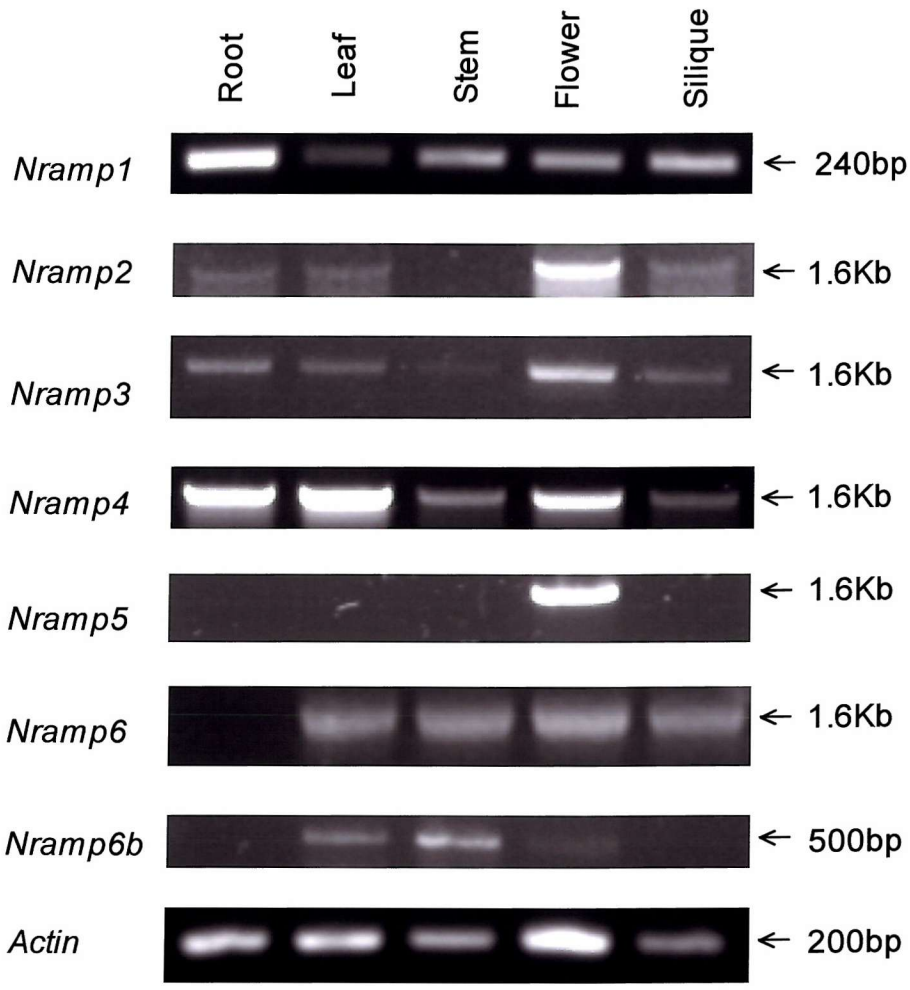

Fig. 4.3. Expression profile of *AtNramps* in roots, leaves, stems, flowers and siliques from *Arabidopsis* plants. RT-PCR products using gene specific primers were electrophoresed on 1% agarose gels or 2% agarose gels for products below 300bp in size. Results shown are representative of at least two separate experiments, each with one replicate. PCR was performed with an initial melting step of 94°C for 2 min, then 40 cycles of 94°C, 30 s, annealing temperatures as listed below for 30 s, 72°C , 1:30 min and a final elongation step of 72°C for 5 min. Annealing temperatures: *Nramp1*, 60°C. *Nramp2*, 55°C. *Nramp3*, 55°C. *Nramp4,* 55°C. *Nramp5*, 60°C. *Nramp6* and *Nramp6b,* 50°C. *Actin*, 60°C.

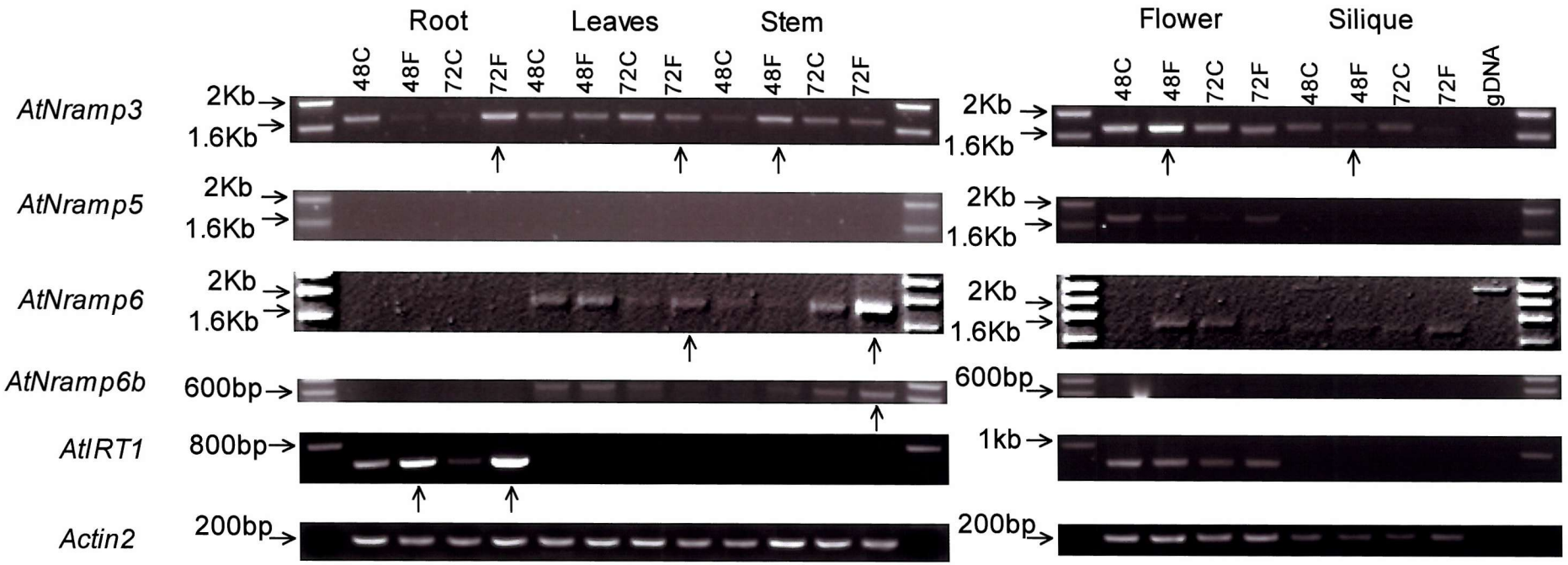

Fig.4.4. RT PCR performed on RNA from various *Arabidopsis* tissues with *AtNramp*, *IRT1* and *actin2* primers. 48C, 48h treatment control; 48F, 48h 100µM Ferrrozine treatment; 72C, 72h treatment control; 72F, 72h 100µM Ferrozine treatment; gDNA, genomic DNA control. Data shown is representative of two experiments performed on cDNA from different plants, each with two replicates. Possible changes in expression levels are indicated by upward arrows. PCR was performed with an initial melting step of 94°C for 2 min, then 40 cycles of 94°C, 30 s, annealing temperatures as listed below for 30 s, 72°C , 1:30 min and a final elongation step of 72°C for 5 min. Annealing temperatures: *AtNramp3*, 55°C. *AtNramp5*, 60°C. *AtNramp6* and *AtNramp6b,* 50°C. *AtIRT2*, 55°C. *Actin*, 60°C.

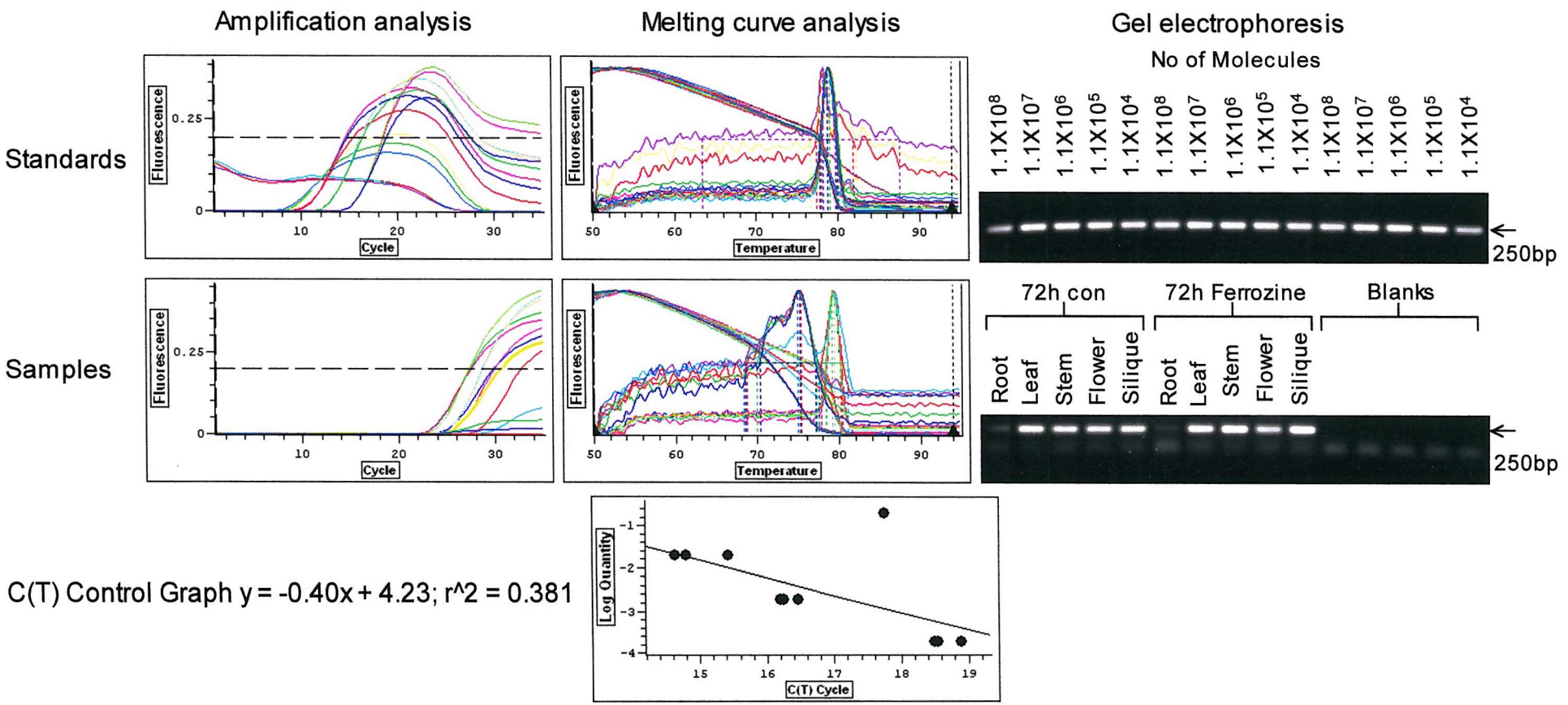

Fig. 4.5. Real time quantitative RT-PCR performed on *Arabidopsis* tissues treated with 100μM ferrozine for 72h using *AtNramp6* gene specific primers. Data from a single experiment is presented. For the standards three replicates were performed while for the samples there was one replicate. Amplification analysis graphs show fluorescence detected against cycle number while melting curve analysis graphs show the fluorescence detected against temperature. Gel electrophoresis of the PCR products is also shown. Refer to section 4.2.1.3 for a full description.

electrophoresis) shows that *AtNramp6* is amplified from both the cDNA samples and the standards, the amplification curves show that the cDNA product is amplified at a much later cycle in the samples (after approximately 26 cycles) than the standards (between 14 and 20 cycles). This indicates that *AtNramp6* is present in the cDNA at a lower copy number than any of the standards. Because of this it is not possible to calculate quantities for *AtNramp6* by comparison to the standards. The melting curve analysis shows that most of the products are the correct, specific amplicon since only one peak is present. For a few samples, a second peak is present with a lower melting temperature, indicating the presence of primer-dimers. The results of gel electrophoresis confirm this, showing primer-dimer formation, most notably in the root samples.

Fig.4.6 shows the results from a similar experiment, this time performed using standards with much lower serial dilutions, going down to approximately 10 molecules. Melting curve analysis and agarose gel electrophoresis show that for most of the standards, a single, specific product is formed. However, for the 10-molecule standard, a second peak with a lower melting temperature is seen in melting curve analysis and primer-dimer formation is visible in greater intensity than the *AtNramp6* product in gel electrophoresis. This suggests that the 10-molecule standard does not contain enough *AtNramp6* cDNA to allow reliable amplification. Some primer-dimer formation is also seen in the samples in both melting curve analysis and gel electrophoresis. The quantitative data from the experiment shown in Fig.4.6 is presented in Table 4.2. This shows that *AtNramp6* expression is most abundant in leaf and stem tissues with slightly less present in flowers and siliques. The signals from flowers treated with ferrozine and both root treatments were too low to be used in the analysis. The gel electrophoresis of the root samples does show a faint band in roots suggesting that *AtNramp6* is present.

Fig.4.7 shows the results from an experiment performed using different concentrations of the cDNA. In this case, *AtNramp6* is amplified from all tissues and cycle threshold values were high enough to calculate molecule amounts. In this experiment it seems that *AtNramp6* was amplified from roots as strongly as from other tissues. However, primer-dimer formation seems more apparent, especially in reactions with the lowest amount of cDNA added. This is most clearly shown in the gel electrophoresis of these samples and melting curve analysis also shows products with lower melting temperatures present in many

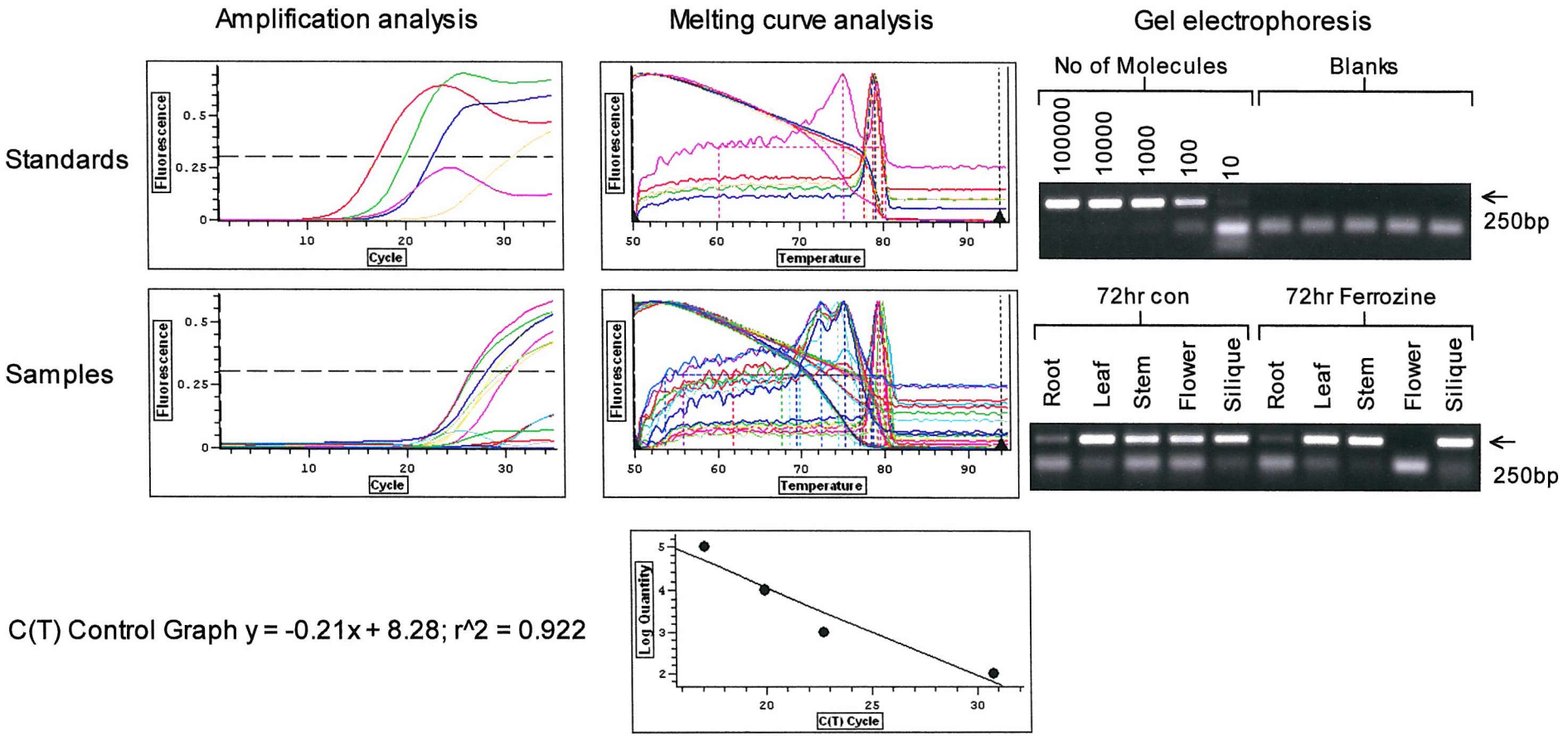

Fig. 4.6. Real time quantitative RT-PCR performed on *Arabidopsis* tissues treated with 100µM ferrozine for 72h using *AtNramp6* gene specific primers. Data from a single experiment is presented. For both standards and samples one replicate was performed. Amplification analysis graphs show SYBR green fluorescence detected against cycle number while melting curve analysis graphs show the fluorescence detected against temperature. Gel electrophoresis of the PCR products is also shown. Refer to section 4.2.1.3 for a full description.

Table 4.2. Quantification data calculated from real-time PCR experiment shown in Fig.4.6.

Sample	Cycle threshold	No. molecules
Root control	None	N/A
Root ferrozine	None	N/A
Leaf control	25.7507	429.2926
Leaf ferrozine	27.8357	155.7478
Stem control	27.0820	224.7043
Stem ferrozine	25.5190	480.5078
Flower control	29.5095	69.0125
Flower ferrozine	None	N/A
Silique control	29.4541	70.8992
Silique ferrozine	28.7412	100.2745

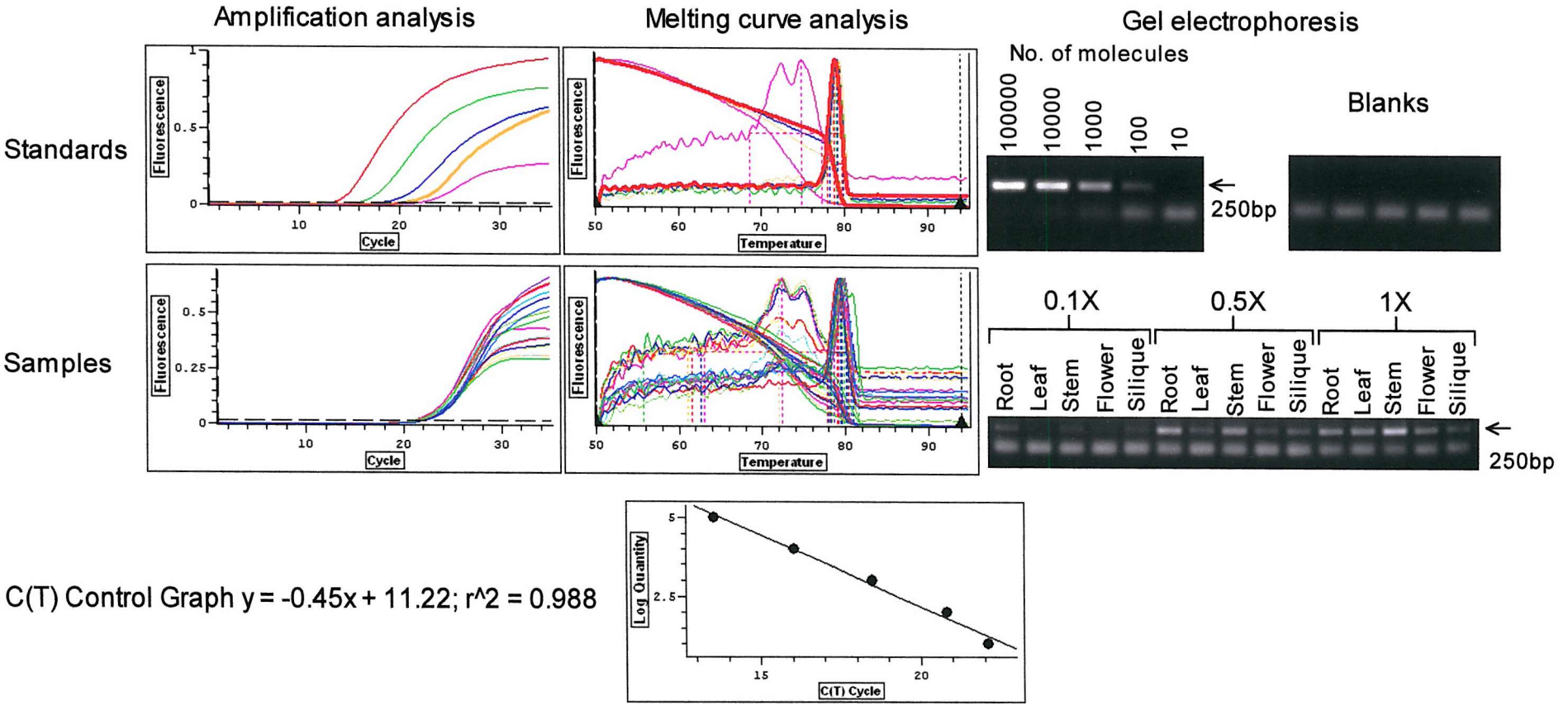

Fig. 4.7. Real time quantitative RT-PCR performed on varying quantities of cDNA from *Arabidopsis* tissues using *AtNramp6* gene specific primers. Data from a single experiment is presented. For both the standards and samples one replicate was performed. Amplification analysis graphs show fluorescence detected against cycle number while melting curve analysis graphs show the fluorescence detected against temperature. Gel electrophoresis of the PCR products is also shown. Refer to section 4.2.1.3 for a full description.

of the samples. However, a number of the samples with detectable primer-dimer formation in gel electrophoresis do not show this in the melting curve analysis. The quantitative data from the experiment shown in Fig.4.7 is presented in Table 4.3. In this experiment the level of *AtNramp6* expression appears much more consistent between the different tissues. The amount of starting template also seems to have had a minor effect on the cycle threshold of each sample, for example in the stem samples reducing the starting template by a factor of ten only increases the cycle threshold value by 0.3 of a cycle and the calculated number of molecules is reduced from 37 to 27 molecules, a factor of only 1.3. Fig.4.8 shows quantitative real-time PCR performed on cDNA synthesized with or without dithiothreitol (DTT) in the reaction mixes. The results show an improvement when DTT is omitted where *AtNramp6* is found in low levels; in this experiment *AtNramp6* was detected in roots and siliques where it is not consistently found when using DTT. As before, primer-dimer formation is seen in all samples in gel electrophoresis but is not detected in all of the melting cure analysis results. This time, primer-dimer formation is also seen in most of the standards in gel electrophoresis but again it is not detected in all the melting curves for these samples. The quantitative data for this experiment is shown in Table 4.4. In root, leaf and stem tissues there is not such a marked difference between cDNA synthesized with or without DTT but in flowers and siliques the omission of DTT has given improved results in this experiment. Since the *AtNramp6* real-time primers amplify both *AtNramp6a* and *AtNramp6b*, the results of the quantitative real-time PCR experiments suggest that both *AtNramp6a* and *AtNramp6b* are present in all tissues tested, including roots where they seem to be present at lower levels.

The results of quantitative real-time PCR using *AtNramp5* specific primers are shown in Fig.4.9 while results for *AtIRT1* are shown in Fig.4.10. *AtNramp5* and *AtIRT1* results are similar to those from standard RT-PCR in that *AtNramp5* is only detected in flowers while *AtIRT1* is detected in roots and flowers. Surprisingly, primer-dimer formation is not detected in the *AtNramp5* reactions, although it can be seen in melting curve analysis of the *AtIRT1* samples. Quantitative PCR does not detect an increase in *AtIRT1* under ferrozine treatment in roots as shown by RT-PCR. *AtNramp5* is only detected in flowers under ferrozine treatment and not in controls by quantitative real-time

Table 4.3. *AtNramp6* Quantification data calculated from real-time PCR experiment shown in Fig.4.7.

Sample	Cycle threshold	No. molecules
Root 0.1X	20.9358	20.7600
Root 0.5X	20.1208	48.4246
Root 1X	20.8913	21.7431
Leaf 0.1X	20.8686	22.2621
Leaf 0.5X	20.8485	22.7310
Leaf 1X	21.1735	16.2151
Stem 0.1X	20.6536	27.8349
Stem 0.5X	20.1265	48.1380
Stem 1X	20.3608	37.7355
Flower 0.1X	20.6473	28.0172
Flower 0.5X	20.3974	36.3255
Flower 1X	20.3570	37.8837
Silique 0.1X	20.2575	42.0134
Silique 0.5X	20.2322	43.1304
Silique 1X	21.1312	16.9443

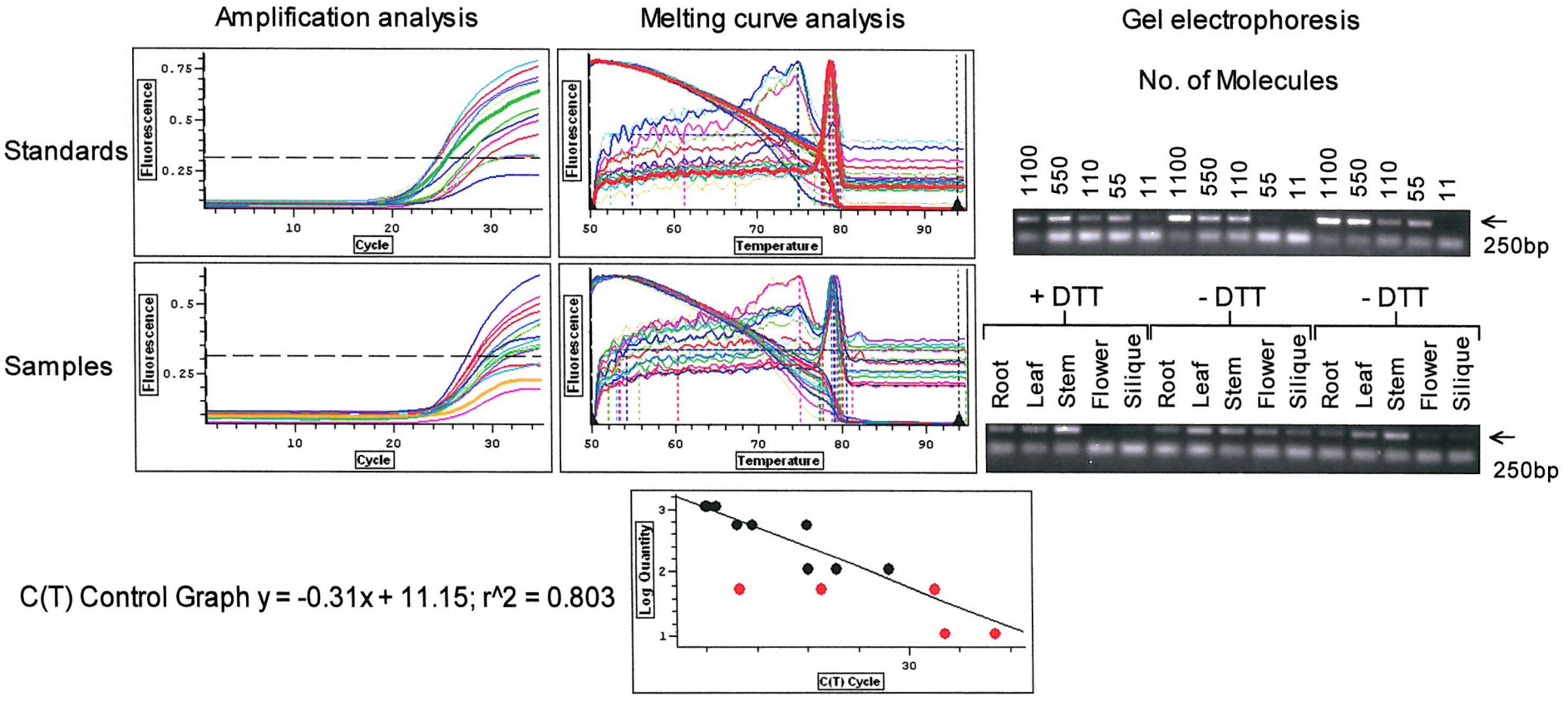

Fig. 4.8. Effect of DTT on Real time quantitative RT-PCR performed on cDNA from *Arabidopsis* tissues using *AtNramp6* gene specific primers. Data from a single experiment is presented. For each of the standards three replicates were performed while for the samples one replicate was performed . +DTT, DTT included in cDNA synthesis; -DTT, DTT omitted from cDNA synthesis. Amplification analysis graphs show fluorescence detected against cycle number while melting curve analysis graphs show the fluorescence detected against temperature. Gel electrophoresis of the PCR products is also shown. Refer to section 4.2.1.3 for a full description.

Table 4.4. *AtNramp6* Quantitation data calculated from real time PCR experiment shown in Fig.4.8.

Sample	Cycle threshold	No. molecules
Root +DTT	27.7934	76.0276
Root -DTT	29.4700	32.6240
Root -DTT	30.8620	16.1608
Leaf +DTT	28.8995	43.5077
Leaf -DTT	28.9319	42.8010
Leaf -DTT	28.4745	53.9135
Stem +DTT	26.4193	152.0945
Stem -DTT	27.2184	101.6234
Stem -DTT	27.3646	94.3950
Flower +DTT	None	N/A
Flower -DTT	30.8271	16.4475
Flower -DTT	30.1656	22.9662
Silique +DTT	None	N/A
Silique -DTT	29.8697	26.6641
Silique -DTT	28.5878	50.9174

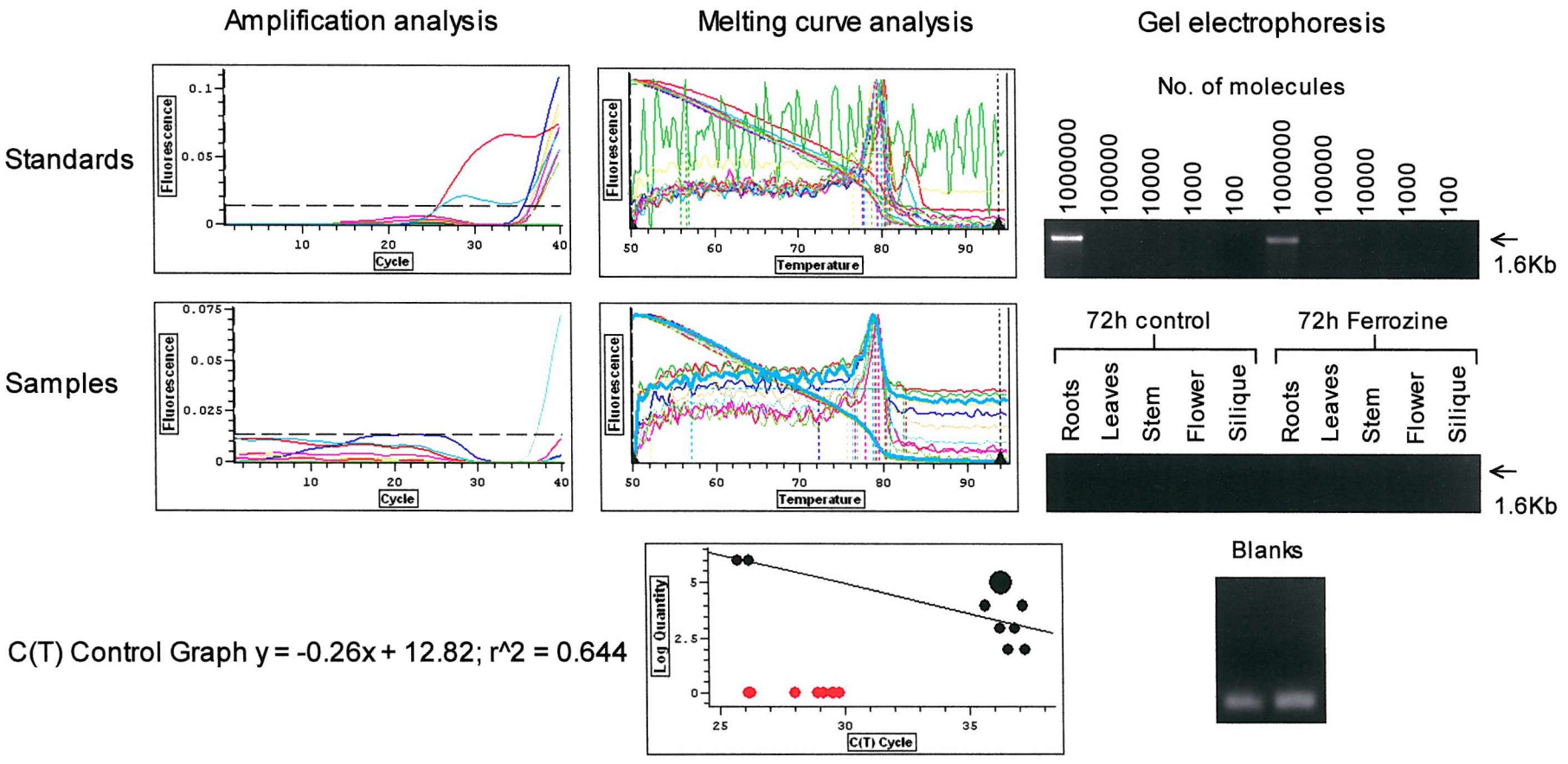

Fig. 4.9. Real time quantitative RT-PCR performed on cDNA from *Arabidopsis* tissues using *AtNramp5* gene specific primers. Data from a single experiment is presented. For the standards two replicates were performed while for the samples one replicate was performed. Amplification analysis graphs show fluorescence detected against cycle number while melting curve analysis graphs show the fluorescence detected against temperature. Gel electrophoresis of the PCR products is also shown. Refer to section 4.2.1.3 for a full description.

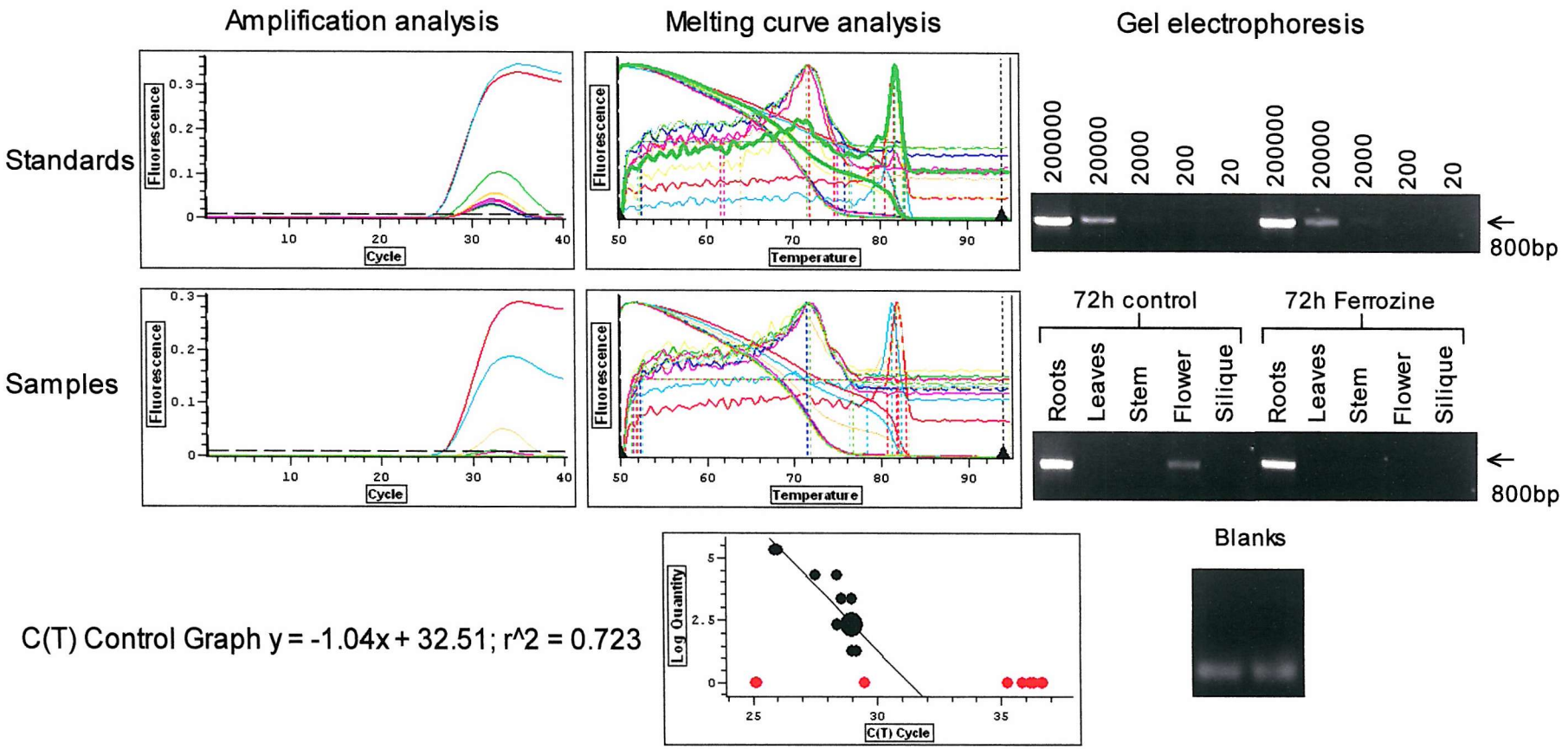

C(T) Control Graph y = -1.04x + 32.51; r^2 = 0.723

Fig. 4.10. Real time quantitative RT-PCR performed on cDNA from *Arabidopsis* tissues using *AtIRT1* gene specific primers. Data from a single experiment is presented. For the standards two replicates were performed while for the samples one replicate was performed. Amplification analysis graphs show fluorescence detected against cycle number while melting curve analysis graphs show the fluorescence detected against temperature. Gel electrophoresis of the PCR products is also shown. Refer to section 4.2.1.3 for a full description.

PCR. No product for *AtNramp5* is seen when run on an agarose gel however. The quantitative data for *AtNramp5* is shown in Table 4.5 and that for *AtIRT1* is shown in Table 4.6.

Table 4.5. *AtNramp5* Quantification data calculated from real-time PCR experiment shown in Fig.4.9.

Well Type	C(t)	molecules
Root control	None	N/A
Root ferrozine	None	N/A
Leaf control	None	N/A
Leaf ferrozine	None	N/A
Stem control	None	N/A
Stem ferrozine	None	N/A
Flower control	None	N/A
Flower ferrozine	35.9094	1426.0218
Silique control	None	N/A
Silique ferrozine	None	N/A

Table 4.6. *AtIRT1* Quantification data calculated from real-time PCR experiment shown in Fig.4.10.

Sample	Cycle threshold	No. molecules
Root control	25.6280	68976.8937
Root ferrozine	25.7079	56978.1960
Leaf control	30.2898	0.9869
Leaf ferrozine	None	N/A
Stem control	None	N/A
Stem ferrozine	None	N/A
Flower control	28.4258	85.3638
Flower ferrozine	None	N/A
Silique control	None	N/A
Silique ferrozine	None	N/A

4.2.2. Promoter-GUS fusions.

4.2.2.1. Verification of promoter-GUS fusions.

Agrobacterium tumefaciens GV3101 cells were transformed with pGPTV/*AtNramp5*promoter and pGPTV/*AtNramp6*promoter vectors, which were produced prior to the start of this work. The potentially transformed cells were then grown on selective media. The presence of the vectors was checked by first performing plasmid extractions from the cells. PCR was performed on the DNA obtained to confirm that the *AtNramp* promoters were present. In addition, the promoters were digested out of the vectors used in the transformation in order to check the vector DNA stocks. The results of these experiments are shown in Fig.4.11. *Xba*I/*Sma*I double digests successfully excise the 3Kb *AtNramp6* promoter from the pGPTV vector and the DNA extracted from the *Agrobacterium* cells is visually larger than the empty vector suggesting that the *AtNramp6* promoter is present. However, the PCR product (shown in Fig.4.11C) from the plasmid extractions is slightly larger than would be expected, running at approximately 4Kb. The expected 3Kb band of the *AtNramp5* promoter is not seen in the restriction digests and the pGPTV/*AtNramp5*promoter vector is not visible in the plasmid extractions from the cells. However, a faint band of about 3Kb is amplified from the plasmid DNA extractions.

4.2.2.2. Transient GUS expression in tobacco leaf.

Arabidopsis Col 0 plants were transformed using *Agrobacterium* containing the *AtNramp5*promoter or *AtNramp6*promoter DNA sequences in the pGPTV vector. This was performed on various occasions using plants with flowers at a range of developmental stages from bud to mature flower. However, after performing the histochemical assay no blue staining was seen in leaves, stem, root or flowers following selection for the resistance marker, PPT. In an attempt to check the activity and viability of the *AtNramp*-promoter-GUS fusions, *Agrobacterium* mediated transient transformation of tobacco leaves was carried out. Following transient transformation of tobacco leaves with *AtNramp6*promoter-GUS constructs, blue staining is seen around the area of

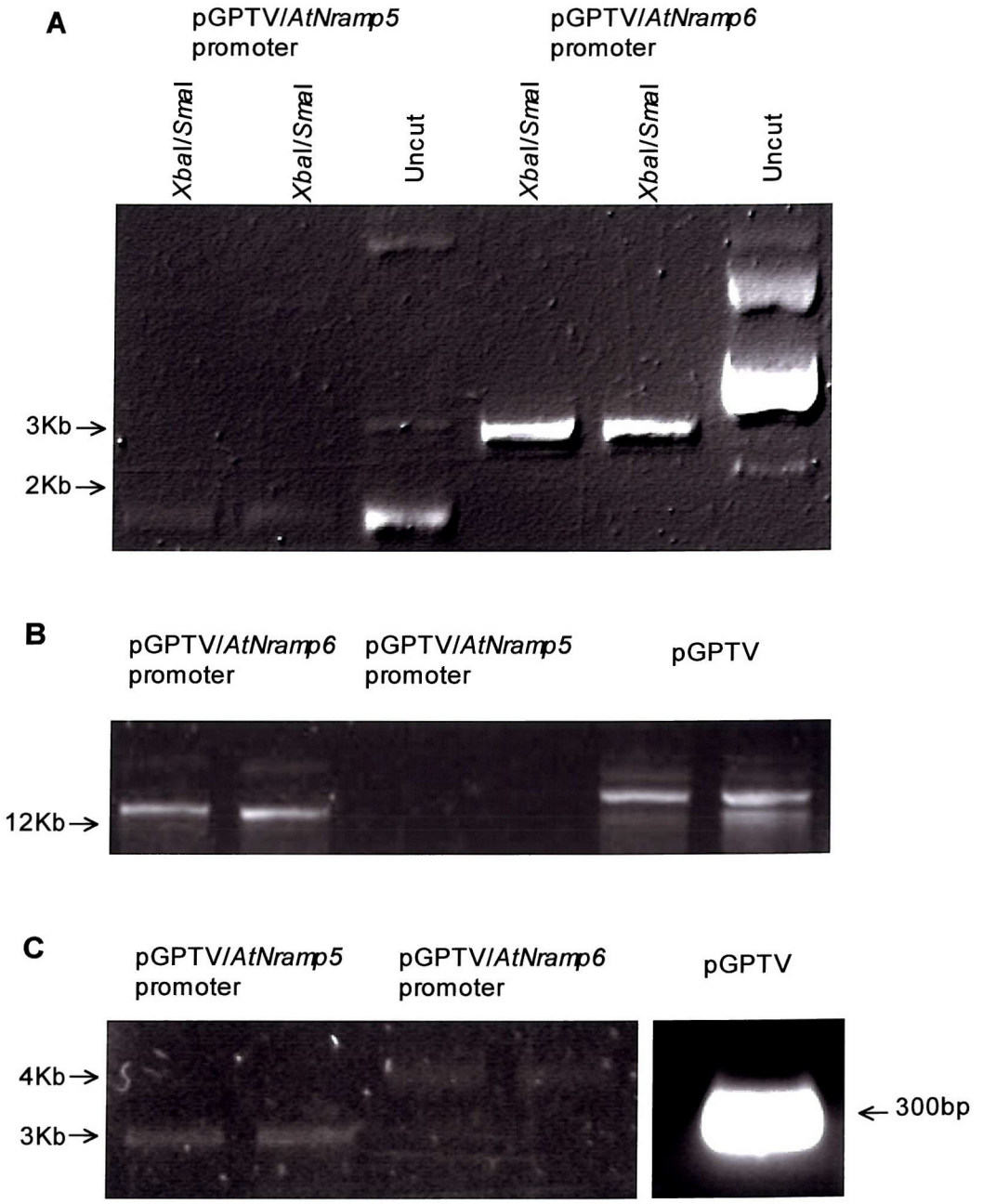

Fig.4.11. Verification of transformation of *Agrobacterium* with *AtNramp*-promoter-GUS vectors. **A**: Gel electrophoresis of *XbaI/SmaI* double restriction digests of plasmid DNA used to transform *Agrobacterium*. **B**: Gel electrophoresis of plasmid extraction from transformed *Agrobacterium* cells. **C**: Gel electrophoresis of PCR performed on DNA plasmid extractions shown in fig.4.11B using pGPTV vector specific primer that anneals either side of the cloning site. The results shown are each representative of one experiment with two replicates.

injection of *Agrobacterium* into the leaf. This appears as a blue tinted ring on the leaf surface shown in Fig.4.12.

4.3. Discussion.

The expression pattern of a gene or protein can often give information about that gene's function within the organism. It is a logical assumption that genes expressed only in certain organs or cells may have a specific function linked to the function of the tissue type. Alternatively, genes expressed throughout the organism may have a more universal role essential to all cells and organs.

The data obtained from RT-PCR experiments using *AtNramp* gene specific primers suggests that while *AtNramp1*, *2*, *3* and *4* are expressed throughout the plant, *AtNramp5* is expressed only in flowers and *AtNramp6* is expressed in all tissues except roots. Thomine *et al.* (2003) showed that the AtNramp3 protein is found in the vacuolar membrane of *Arabidopsis* cells and suggested a role in mobilization of vacuolar metal pools to the cytoplasm. It has also been proposed that *AtNramp3* and *AtNramp4* encode redundant proteins both involved in the mobilization of vacuolar metal pools (Thomine *et al.*, 2004). This is consistent with the data presented here and raises the question as to the function of AtNramp1 and AtNramp2 since they also share the same tissue distribution. The localisation of *AtNramp5* transcript strictly to flower tissues suggests a specific role not shared with the other AtNramps. AtNramp5 could be involved in processes specific to the flowers, such as the development of pollen for instance. It is interesting to note that *AtNramp5* is not found in siliques, suggesting that it is perhaps switched off as the flower tissues mature and seeds are produced.

The RT-PCR results for *AtIRT1* show that the ferrozine treatment has been effective in reducing the amount of available Fe to the plants since it is up-regulated in the roots of plants treated with ferrozine for 48 h and 72 h. *AtNramp3* also shows some up-regulation in roots under the Fe deficient conditions in these experiments (as shown previously by Thomine *et al.*, 2000).

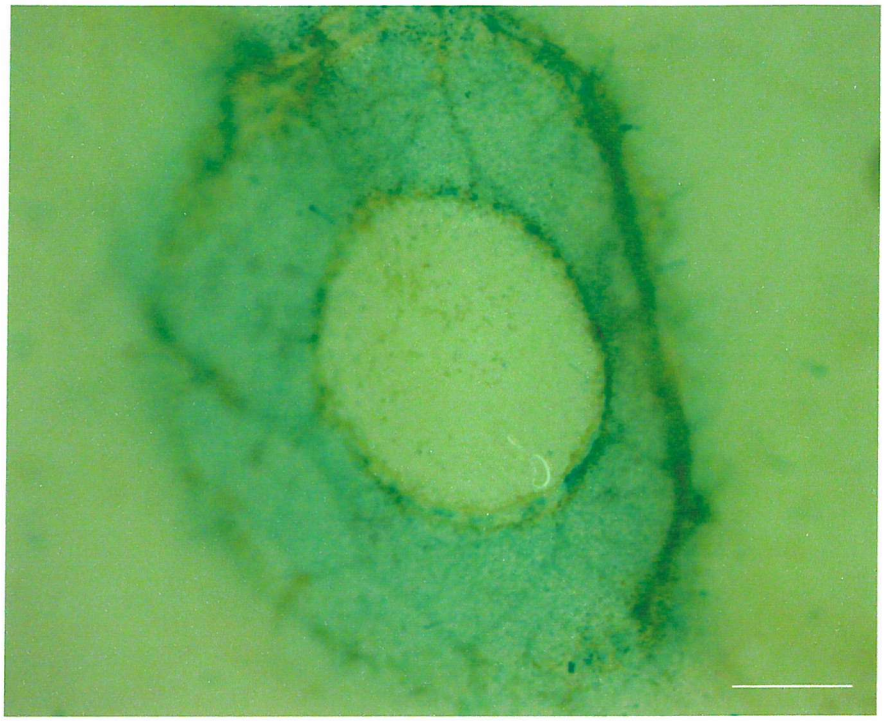

Fig.4.12. Transient GUS expression in intact whole tobacco leaf under control of the *AtNramp6* promoter. Bar = 0.5cm. Staining shown here is representative of one experiment with three replicates.

The other *AtNramps* do not show any marked changes in expression levels except *AtNramp6* in stems treated with ferrozine for 72 h. In this case there appears to be an increase in the mRNA levels of *AtNramp6* that was seen in PCR performed on separate sets of RNA. This makes it more likely that this is a real response rather than an error during PCR or gel electrophoresis.
The results of Quantitative RT-PCR seem to suggest that *AtNramp6* is also expressed in roots where RT-PCR did not amplify any product.
Omission of dithiothreitol (DTT) from the cDNA synthesis reactions has been shown to be beneficial in subsequent quantitative PCR analysis (Deprez *et al.*, 2002), since DTT may interfere with the binding of the SYBR green molecule and therefore alter the fluorescence given off. With this in mind cDNA synthesis reactions were repeated without DTT and the results of quantitative real-time PCR using *AtNramp6* primers compared to that on cDNA synthesized with DTT. However, in this case there has not been a great improvement in the quality of amplification except from flower and siliques cDNA. Altering the cDNA template concentration also seemed to have little effect on the cycle threshold, an unexpected result since lowering the starting template amount should give a higher cycle threshold. This could be due to other contaminants in the cDNA template mix, which perhaps have a greater effect when larger volumes of the cDNA are used. In other words, although the template is present in smaller quantities, the lack of inhibition of the PCR by any contaminants may mean more specific product is amplified giving a seemingly similar result to when greater quantities of template are used. However, there seems to be a much larger difference between the samples when run on an agarose gel (Fig.4.7).
AtNramp5 forward and reverse primers amplify a 1.6Kb product that may be too large for reliable quantitative real-time PCR hence the lack of visible product on the agarose gel and the lack of detection in control flowers in quantitative real-time PCR. The size of the product can cause unreliable results since the polymerase may detach from the DNA template strand before completing synthesis of the complimentary strand in some cases. This means that overall, the amount of product may not double with every subsequent PCR cycle and so the experiment will no longer be quantitatively accurate. Generally, a 200 to 300bp product is desirable to minimise this problem but in this case primers were not available for amplification of a short product. Further efforts to obtain

primers to amplify a smaller fragment of *AtNramp5* will be required to achieve better results using quantitative RT-PCR.

GUS expression in tobacco suggests that the *AtNramp6*promoter-GUS constructs are functional but can give only limited information since the promoter is not native to tobacco. The staining appears to be localised only to the area of injection with *Agrobacterium* and it is not possible to resolve which cells are being stained in the leaf. The lack of signal from *Arabidopsis* plants that survived selection suggests that only a low level of GUS activity is present. If the *AtNramp* promoters are normally of low activity under metal replete conditions then β-glucuronidase may not be expressed strongly. In *AtNramp5*promoter-GUS plants it is possible that the tissue localisation of *AtNramp5* (in flowers) makes it difficult to visualise. For example, if *AtNramp5* is only expressed in a small subset of cells in flowers and the promoter is only weakly driving expression, then β-glucuronidase may not be driven strongly enough to be visible under light microscopy.

Table 4.7 shows some microarray and proteomic data available publicly on the world wide web from various databases. Although the Nramps are poorly represented among the many experiments available to browse, some data relating to Nramp expression under different treatments does exist. The *Arabidopsis* microarray data available at TAIR (http://www.arabidopsis.org) suggests that *AtNramp1* and *AtNramp6* are not strongly regulated by Fe-deficiency although *AtNramp6* may be slightly down-regulated. For *AtNramp1* this is contradictory to previously published data (Curie *et al.*, 2000, Colangelo and Guerinot, 2004) indicating that *AtNramp1* expression is altered on Fe-deficiency. *AtNramp6* expression was not affected by application of Zn. *AtNramp1* and *AtNramp2* did not show markedly altered expression when exposed to Cd. However, *AtNramp1* was more highly expressed in roots than leaves and showed slight up-regulation during root development and during elevated CO^2 conditions. *OsNramp1* showed slight down regulation during salt overload. Apart from these data, no other *Nramps* were identified in other microarray experiments.

Table 4.7 also includes the results of searches of a number of proteomic databases available on the world wide web. However, no Nramps (and indeed no transport proteins in the majority of databases) were found in most of these databases. Searches of the Arabidopsis mitochondrial protein database

(AMPDB, http://www.ampdb.bcs.uwa.edu.au) provided results for all six AtNramps and indicated that none of these proteins are found in mitochondrial membranes.

Table 4.7. Microarray and Proteomic analysis data publicly available on the world wide web. Ratios given for microarray data indicate the ratio of signals from each dye on the chip. A positive value indicates an increase in expression while a negative value indicates a decrease in expression. A ratio of 2 or greater is considered the cut-off for actual changes in gene expression. TAIR (The *Arabidopsis* Information Resource): http://www.arabidopsis.org, OSMID (Osmotic Stress Microarray Information Database): http://www.osmid.org, AMPDB (*Arabidopsis* Mitochondrial Protein Database): http://www.ampdb.bcs.uwa.edu.au, AMPP (*Arabidopsis* Mitochondrial Proteome Project): http://www.gartenbau.uni-hannover.de/genetik/AMPP, PPDB (Plastid Proteome Database): http://ppdb.tc.cornell.edu, AtNoPDB (*Arabidopsis* Nucleolar Protein Database): http://bioInf.scri.sari.ac.uk.

Microarray data			
Database	**Gene**	**Experimental variable**	**Ratios**
AFGC data at TAIR	*AtNramp1*	Fe-deficiency 72 h	-0.5X, -0.3X, 0.4X
		Cd treatment	0.05X
		Root vs Leaf tissue	2.0X
		Root development	0.8X
		Elevated CO^2	0.9X
	AtNramp2	Cd treatment	0X
	AtNramp6	Zn treatment	0.4X
		Fe-deficiency 72 h	-0.8X
OSMID	*OsNramp1*	150mM NaCl stress	-0.51X, -0.59X
Proteomic data			
Database	**Protein**	**Result**	
AMPDB	AtNramp1-6	None found (not mitochondrial)	
AMPP		No transport proteins identified	
PPDB		No transport proteins identified	
AtNoPDB		No transport proteins identified	

Chapter 5. Heterologous expression of *AtNramps* in yeast.

5.1. Introduction.

The expression of plant proteins in yeast (heterologous expression) has been used in several studies to address function (Dreyer *et al.*, 1999). Eide *et al.* (1996) used this approach to isolate the cDNA for the *Arabidopsis* Fe transporter, IRT1, by screening cDNAs that rescued the *fet3/fet4* mutant, a Fe uptake-deficient yeast strain. As well as identifying previously unknown transporters the technique has also been used to help confirm the function of putative transporters such as the Na^+/H^+ exchanger 1 (AtNHX1) (Darley *et al.*, 2000). In many cases, putative transporters have been used to complement yeast mutants defective in a particular transport pathway and this has paved the way for measuring transport using radioactive tracers. Heterologous expression and functional complementation of yeast mutants can give a qualitative measure of substrate specificity for a transport protein, which can then be confirmed by more detailed kinetic studies using radiotracers. By knocking out previously characterised endogenous genes for certain functions (e.g. metal transporters) in the yeast and then expressing the genes of interest in these mutants it may be possible to rescue or "complement" the mutations. This then gives an indication that the gene of interest may have the ability to fulfil the role of the endogenous gene.

Yeast complementation has been used to demonstrate some of the transport characteristics of the Nramp1 and Nramp2 proteins from both mouse and human. Pinner *et al.* (1997) showed that mouse Nramp2 is capable of rescuing the low Mn and high pH phenotypes of the yeast *smf1/smf2* mutant while Tabuchi *et al.* (1999) investigated the functional activity of chimeric proteins made up of domains from human Nramp1 and Nramp2 by complementing the fission yeast *pdt1* mutant. The *pdt1* gene is the fission yeast Nramp homologue and cells lacking the gene are also disrupted in Mn transport and are pH sensitive (Tabuchi *et al.*, 1999, Maeda *et al.*, 2004). Replacement of the Nramp2 N-terminus with that from Nramp1 resulted in inactive chimeras although other regions were also suggested to be important. Previous work using the *fet3/fet4* Fe uptake-deficient yeast mutant transformed with *AtNramp1*, *AtNramp3* and *AtNramp4* has shown that these cDNAs are capable of rescuing the *fet3/fet4* mutant when expressed using a variety of vectors (Curie *et al.*,

2000; Thomine *et al.,* 2000.). Preliminary experiments in our laboratory (Pittman and Williams, unpublished) also indicated that AtNramp3 and AtNramp5 could rescue the *fet3/fet4* Fe uptake mutant, the *zrt1/zrt2* Zn-uptake mutant and the *smf1/smf2* Mn-uptake mutant. This suggested that the AtNramp3 and AtNramp5 proteins may have the ability to transport Fe, Mn and Zn. It is also possible that some of the AtNramps are capable of transporting other metals, such as Cd. Curie *et al.* (2000) found that AtNramp1, AtNramp3 and AtNramp4 were all able to transport Cd into wild-type yeast resulting in sensitivity to this metal. The ability of AtNramp5 and AtNramp6 to transport other metals such as Cd remains to be tested.

The aim of this chapter was to further investigate the ability of members of the *AtNramps* to functionally complement various yeast mutants and to attempt to characterise their functional activity in more detail using radioactive uptake assays.

5.2. Results.

5.2.1. Transformation of yeast with *AtNramps*.

The NEV N vector, NEV E vector, NEV E/*AtNramp3*, NEV N/*AtNramp5* and NEV E/*AtNramp6* cDNAs were prepared from *E. coli* stocks prepared and sequenced previously (Pittman *et al.,* unpublished). Yeast *fet3/fet4* Fe uptake double-mutants (strain DDY4) were then transformed with NEV N/*AtNramp5*, NEV E/*AtNramp6* and the empty NEV N and NEV E vectors using the PLATE solution method. The presence of the *AtNramp* genes was confirmed by carrying out PCR on selected colonies using specific *AtNramp5* and *AtNramp6* primers. Fig.5.1 shows the products obtained following PCR performed on colonies from cells transformed with NEV N/*AtNramp5* and NEV E/*AtNramp6*. In both cases a DNA fragment of the expected size (both approximately 1.6Kb) was amplified only from those cells transformed with *AtNramp5* or *AtNramp6*. No fragments were amplified from vector-only transformed yeast cells.

5.2.2 Functional complementation of yeast mutants with *AtNramps*.

The *fet3/fet4* Fe uptake mutant lacks both the high and low affinity uptake systems for Fe and so is unable to grow without supplemental Fe. Yeast *fet3/fet4* cells transformed with the empty vector are also unable to grow without supplemental Fe as

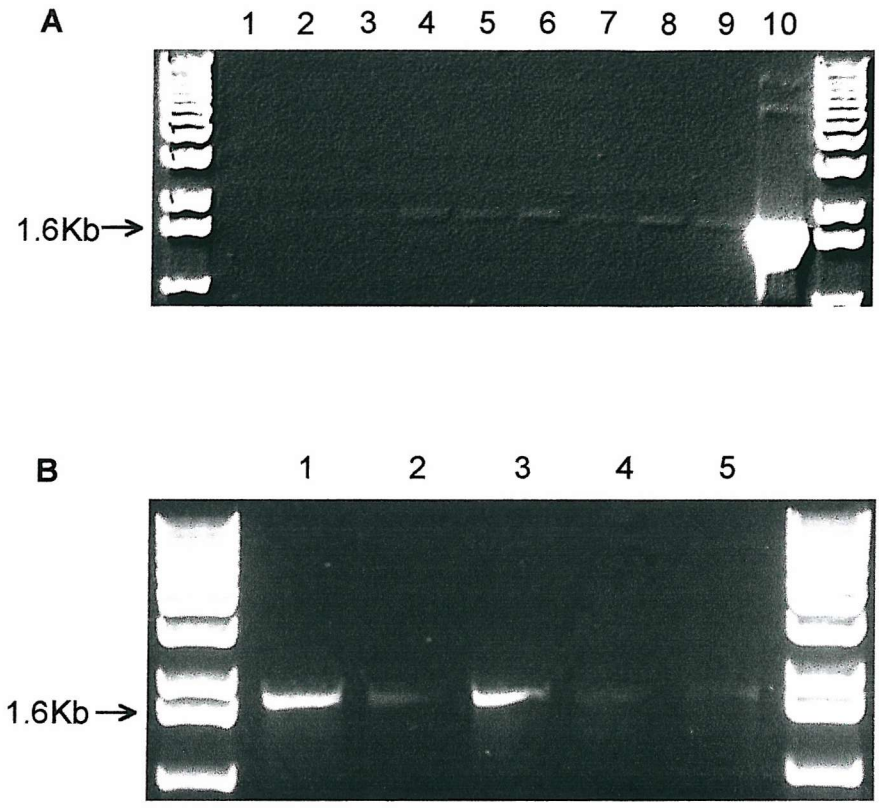

Fig.5.1. **A**: Agarose gel (1% w/v) electrophoresis of PCR products from *fet3/fet4* yeast transformed with NEVN (lanes 1 and 2) and NEVE empty vector (lane 3) or *AtNramp5* in NEVN (lanes 4 to 9). Lane 10 shows PCR performed on plasmid *AtNramp5* cDNA giving the expected size band at approximately 1.6Kb (positive control). **B**: Agarose gel electrophoresis of PCR products from *fet3/fet4* yeast transformed with *AtNramp6* in NEVE (lanes 2 to 5). Lane 1 shows PCR performed on plasmid *AtNramp6* cDNA giving the expected size band at approximately 1.7Kb (positive control). The 1.6Kb band of the DNA ladder contains 25 ng of DNA.

were those cells transformed with NEV N/*AtNramp5* or NEV E/*AtNramp6.* The *fet3/fet4* mutant also lacks the *URA3* gene and cannot synthesize uracil. This means that untransformed cells cannot grow even when given supplemental Fe if uracil is not supplied to them in the growth medium. The vectors used in this study contain the *URA3* gene allowing the vector transformed *fet3/fet4* mutant to produce uracil. Therefore, the transformed *fet3/fet4* mutant cells were plated onto synthetic complete (Sc) media without uracil (-uracil) and with 0, 50, 100 or 200 μM $FeCl_3$. These plates are shown in Fig.5.2. No differences can be seen between the growth of the mutants transformed with the NEV E or NEV N vectors and the mutant cells transformed with *AtNramp5* or *AtNramp6.* The presence of a ferrireductase at the yeast plasma membrane allows the cells to reduce Fe^{3+} to the more accessible Fe^{2+} form for uptake.

A lower concentration range was then chosen to see if any differences could be observed between the transformants. Transformed *fet3/fet4* mutant cells were plated onto SC -uracil media with 0, 1, 5, 15, 25 and 50 μM $FeCl_3$. Fig.5.3 shows the *fet3/fet4* yeast mutants transformed with *AtNramp5*, *AtNramp6* and the NEV vectors on the various concentrations of $FeCl_3$. Experiment 1 in Fig.5.3 shows that cells transformed with NEV N/*AtNramp5* do not grow at Fe concentrations lower than 25 μM while cells transformed with NEV N alone show growth down to 1 μM Fe. However, this was not seen in other experiments; in most cases the NEV N transformed cells only grew at Fe concentrations that supported growth of cells transformed with NEV N/*AtNramp5.* Cells transformed with NEV E/*AtNramp6* or the empty NEV E vector also did not grow well below 25 μM Fe. In experiment 2 (shown in Fig.5.3) cells transformed with NEV N/*AtNramp5* or the empty NEV N vector do not grow below 50 μM Fe. It also appears that cells transformed with NEV E/*AtNramp6* may grow better than the vector-only transformed cells at Fe concentrations between 15 and 25 μM. However, this result was not repeatable and was not seen in the other experiments. In most cases the cells transformed with the *AtNramps* were only able to grow at similar $FeCl_3$ concentrations to the cells lacking the *AtNramps.* All the cells were able to grow when supplemented with 50 μM $FeCl_3$. This suggests that neither *AtNramp5* nor *AtNramp6* are able to rescue the *fet3/fet4* mutant in these experiments when expressed in the NEV vectors. *AtNramp3* in the NEV E vector was also transformed into the *fet3/fet4* mutant for use as a control since *AtNramp3* has been shown previously to be capable

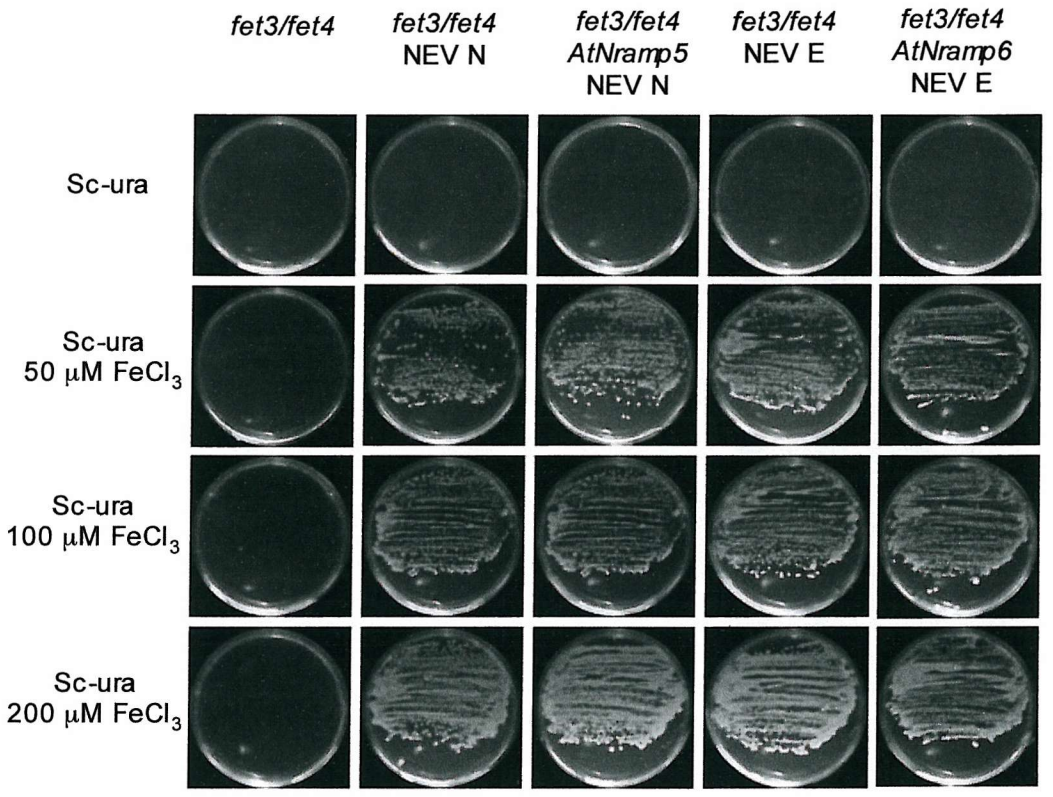

Fig. 5.2. The Fe uptake mutant *fet3/fet4* transformed with NEV E, NEV N, NEV N/*AtNramp5* and NEV E/*AtNramp6* plated onto Sc-uracil media with varying concentrations of $FeCl_3$. The untransformed *fet3/fet4* mutant is also shown.

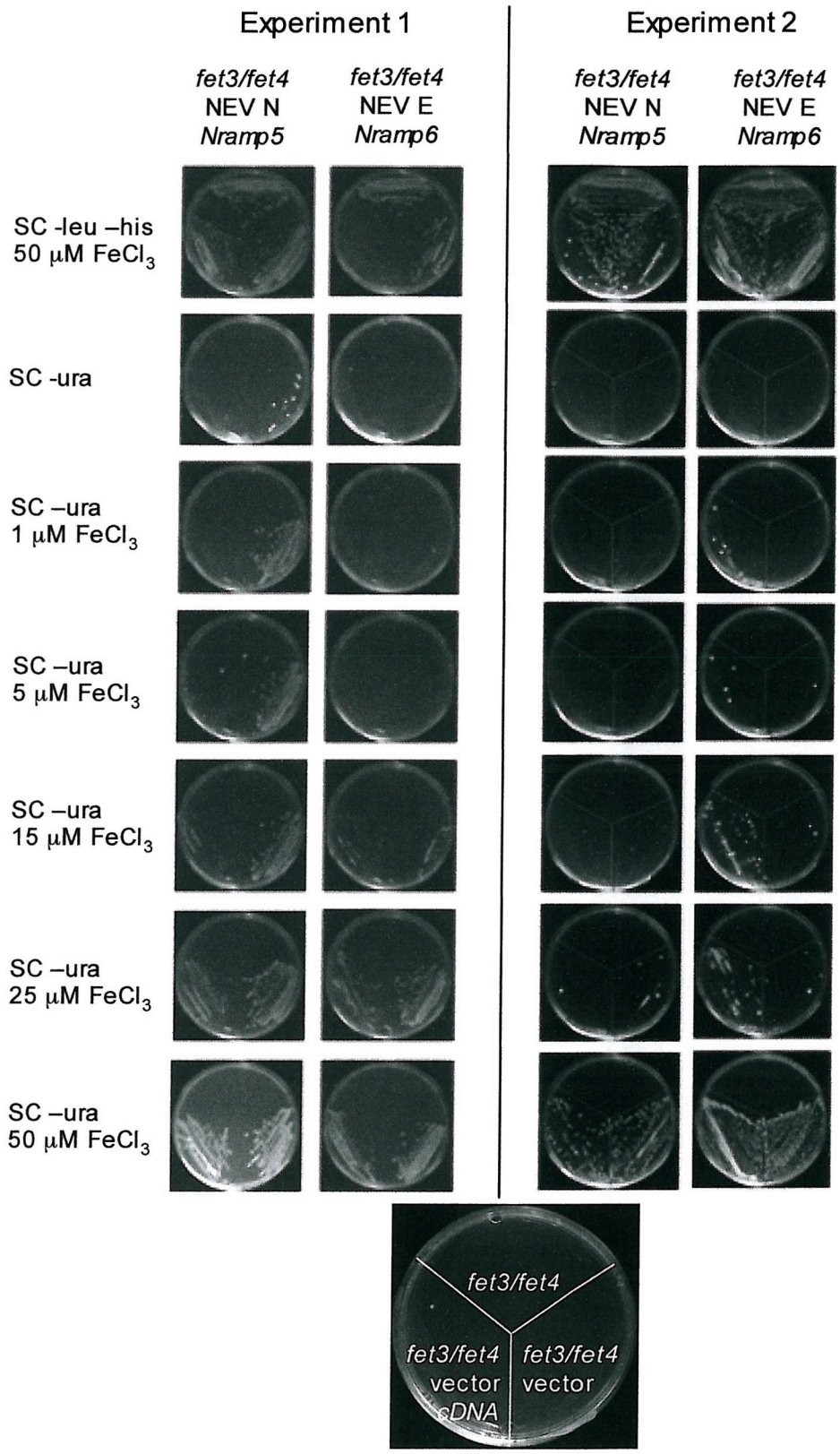

Fig. 5.3. Growth of the *fet3/fet4* Fe uptake-deficient yeast mutant transformed with *AtNramp5* or *AtNramp6* in the presence of varying concentrations of $FeCl_3$. Two representative experiments are shown. Yeast were grown on the plates for 72 h at 30°C before imaging using an Alpha Innotech imaging system.

of rescuing this mutant (Thomine *et al.*, 2000). With no supplemental Fe, NEV E/*AtNramp3* also failed to rescue the *fet3/fet4* mutant when compared to empty NEV E vector as shown in Fig.5.4. However, the cells transformed with NEV E/*AtNramp3* do grow well at 5 μM $FeCl_3$ whereas those with only the empty vector do not. This suggests that *AtNramp3* is capable of rescuing the *fet3/fet4* mutant under these conditions.

As a further check, pFL61/*IRT1*, pDR195/*AtNramp3* and pDR195/*AtNramp4* were obtained from Dr. Sebastien Thomine (Institut des Sciences Vegetal, Gif-sur-Yvette Cedex, France) and used to complement the *fet3/fet4* mutant. All three of these cDNAs have previously been shown to complement this yeast mutant (Eide *et al.*, 1996, Thomine *et al.*, 2000). *AtNramp5* was also cloned into the pDR195 vector at the *Sac*II site and the p426 vector at the *Sma*I site. Restriction digests were used to check for the presence of *AtNramp5.* A *Sac*II digest produces the correct sized band for the *AtNramp5* cDNA at 1.6Kb while a *Hin*dIII digests shows that *AtNramp5* is in the sense orientation by producing a 2Kb band as shown in Fig.5.5. Fig.5.5 also shows a restriction digest of p426/*AtNramp5* with *Eco*RI in which a 1.6KB band is produced indicating that *AtNramp5* is also in the sense orientation in this vector. All the constructs were transformed into the *fet3/fet4* Fe uptake deficient yeast mutant. PCR performed using *AtNramp5* specific primers on colonies of these transformed yeast are also shown in Fig.5.5. In each case the correct size 1.6Kb band representing *AtNramp5* is amplified from cells transformed with p426/*AtNramp5* or pDR195/*AtNramp5* but not from cells containing empty vector. Fig.5.5 also shows the vector maps of these plasmids and the position of the *AtNramps* within them. Plasmid vectors prepared by other groups that were used in this work are shown in Appendix I. Fig.5.6 shows the results of the complementation experiment using these new *AtNramp* cDNAs and vectors. While *IRT1*, *AtNramp3* and *AtNramp4* all rescue the mutant on media with no supplemental Fe, *AtNramp5* and *AtNramp6a* failed to rescue the mutant.

These constructs were also transformed into the *zrt1/zrt2* Zn uptake deficient yeast mutant. The results of complementation experiments on various concentrations of $ZnCl_2$ and EDTA are shown in Fig.5.7 and Fig.5.8. In Fig.5.7 growth of the mutant transformed with either empty vector or any of the cDNAs is only seen in SC media with supplemental Zn. In this case the cells transformed with the cDNAs appear to

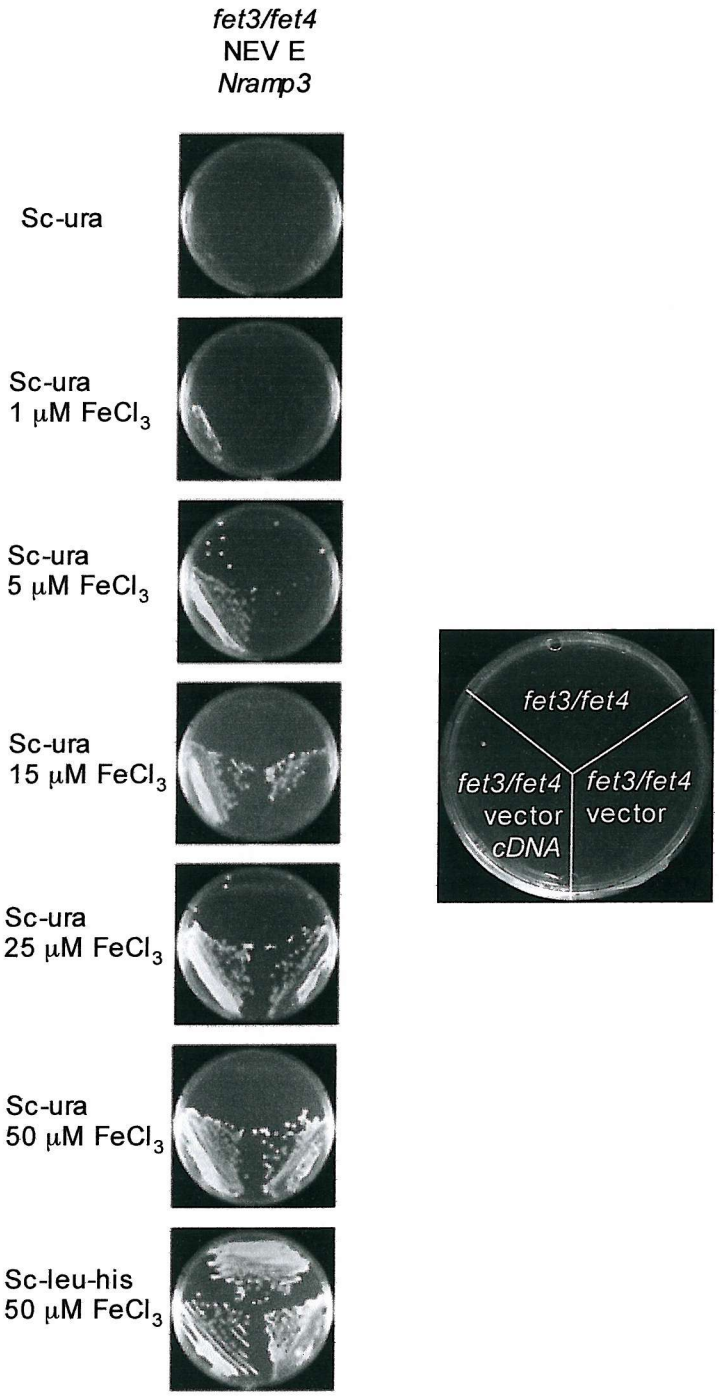

Fig. 5.4. Growth of the *fet3/fet4* Fe uptake-deficient yeast mutant transformed with *AtNramp3* in the presence of varying concentrations of $FeCl_3$. Yeast were grown on the plates for 72 h at 30°C before imaging using an Alpha innotech imaging system.

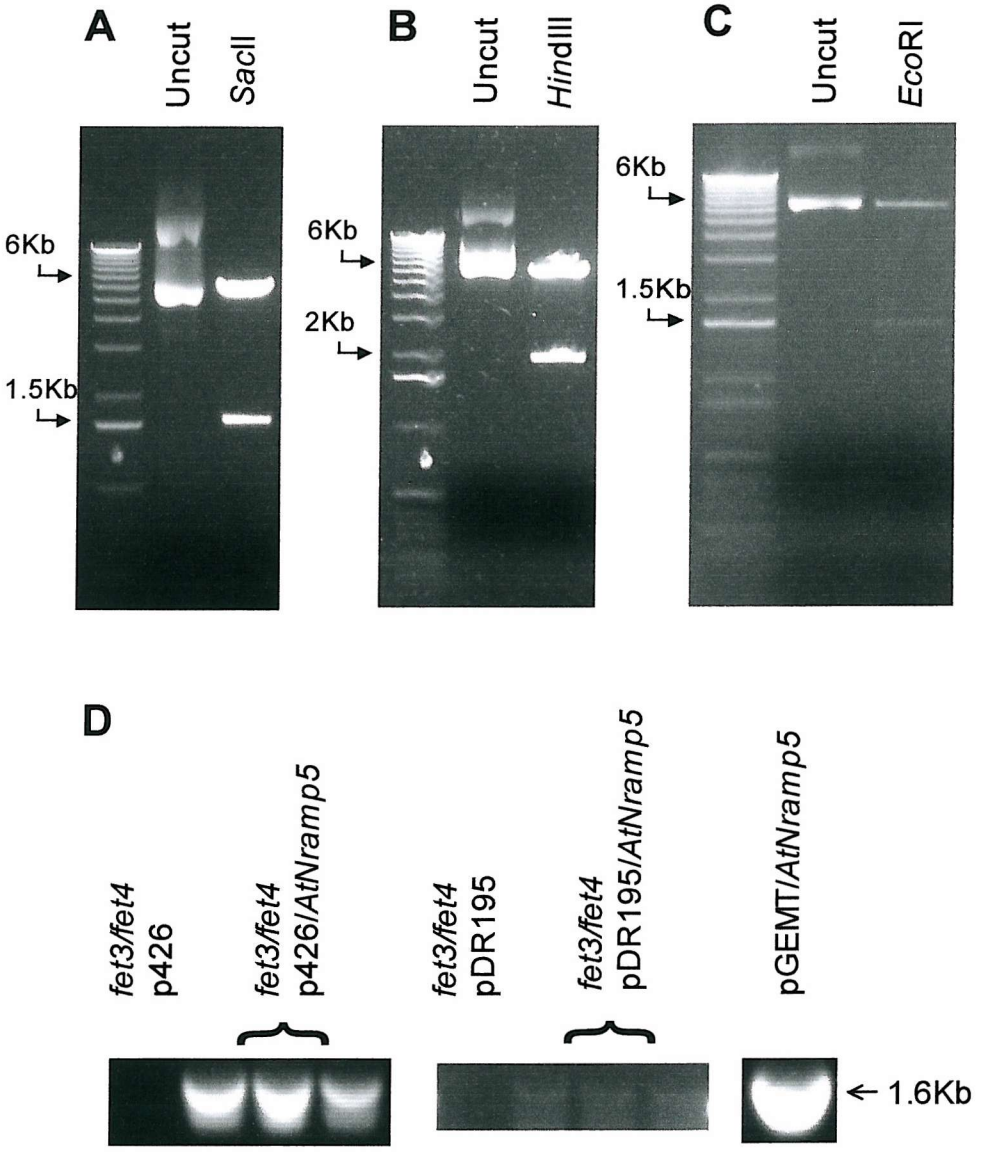

Fig. 5.5. Verification of ligation of *AtNramp5* cDNA into the pDR195 vector by restriction digest. **A**) *Sac*II digest of pDR195/*AtNramp5* ligation product. **B**) *Hin*dIII digest of pDR195/*AtNramp5* ligation product. **C**) EcoRI digest of p426/*AtNramp5* ligation product. Arrows indicate position of size markers. **D**) PCR performed on *fet3/fet4* colonies transformed with p426/*AtNramp5,* pDR195/*AtNramp5* or each of the empty vectors using *AtNramp5* specific primers. Also shown is PCR performed on pGEMT/*AtNramp5* cDNA (positive control). Arrows indicate position of 1.6Kb band representing *AtNramp5*.

E

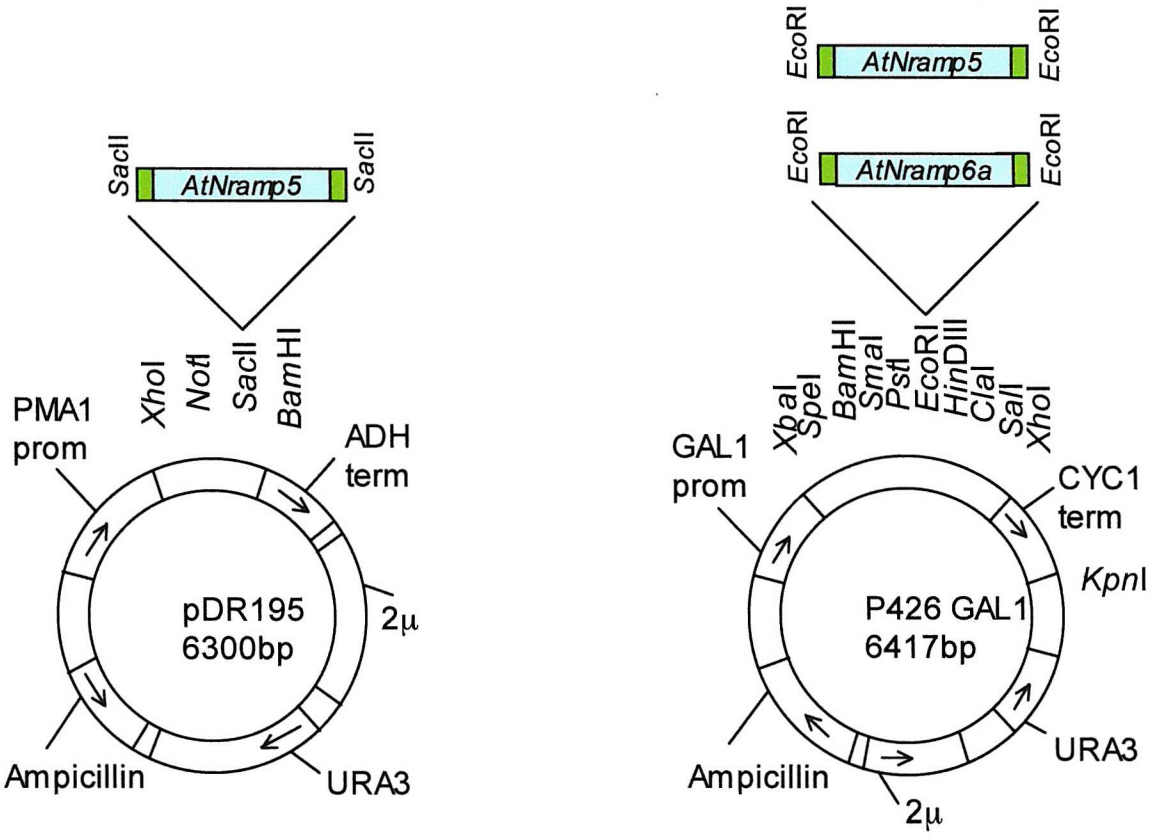

Fig. 5.5. **E**) Diagrammatic representation of plasmid constructs prepared for use in yeast expression. The *AtNramp* genes inserted into each plasmid are shown above each plasmid as blue bars (representing the coding region of each gene) with yellow bars representing the 5´ and 3´ untranslated regions. The restriction sites used are named at each end of the gene.

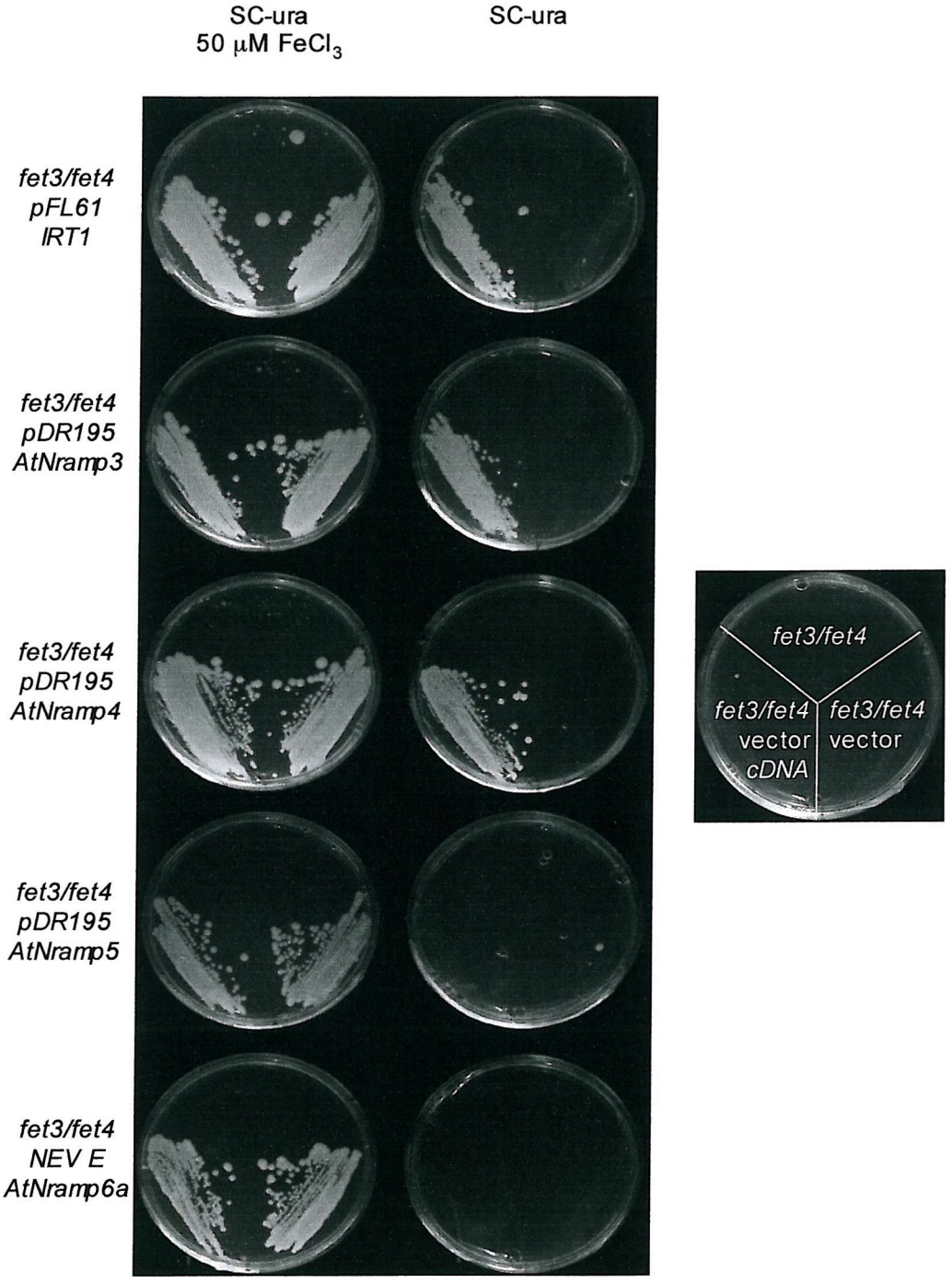

Fig. 5.6. Growth of the *fet3/fet4* Fe uptake-deficient yeast mutant transformed with *AtNramp3*, *AtNramp4*, *AtNramp5, AtNramp6a* or *IRT1* in the presence of varying concentrations of $FeCl_3$. The untransformed *fet3/fet4* cells are also shown. Yeast were grown on the plates for 72 h at 30°C before imaging using an Alpha Innotech imaging system.

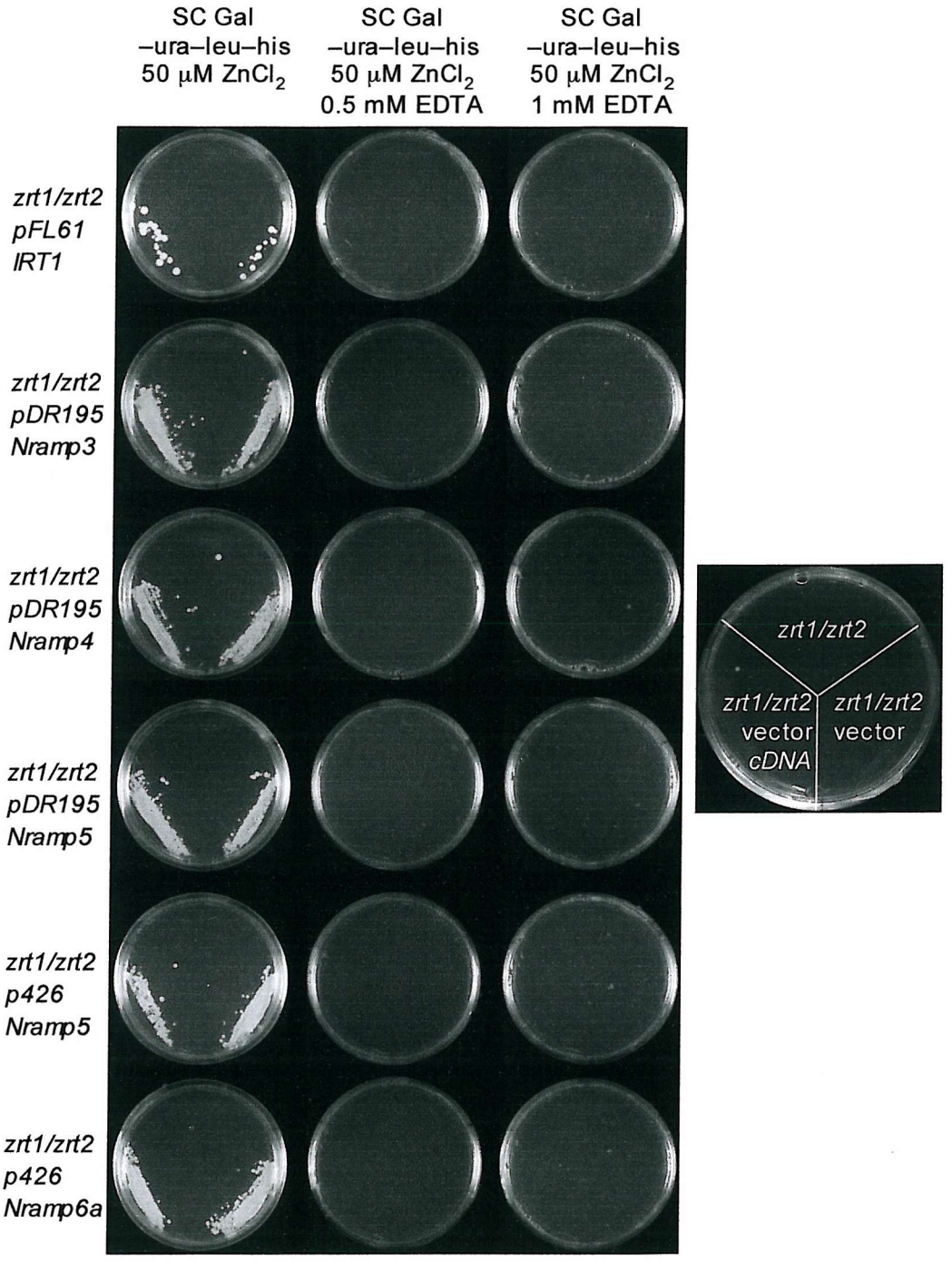

Fig.5.7. Growth of *zrt1/zrt2* Zn uptake mutant yeast transformed with *IRT1*, *AtNramp3*, *4*, *5* and *6a* on low Zn media. The untransformed *zrt1/zrt2* cells are also shown. *Yeast* were incubated at 30°C for 72 h before imaging using an Alpha Innotech imaging system.

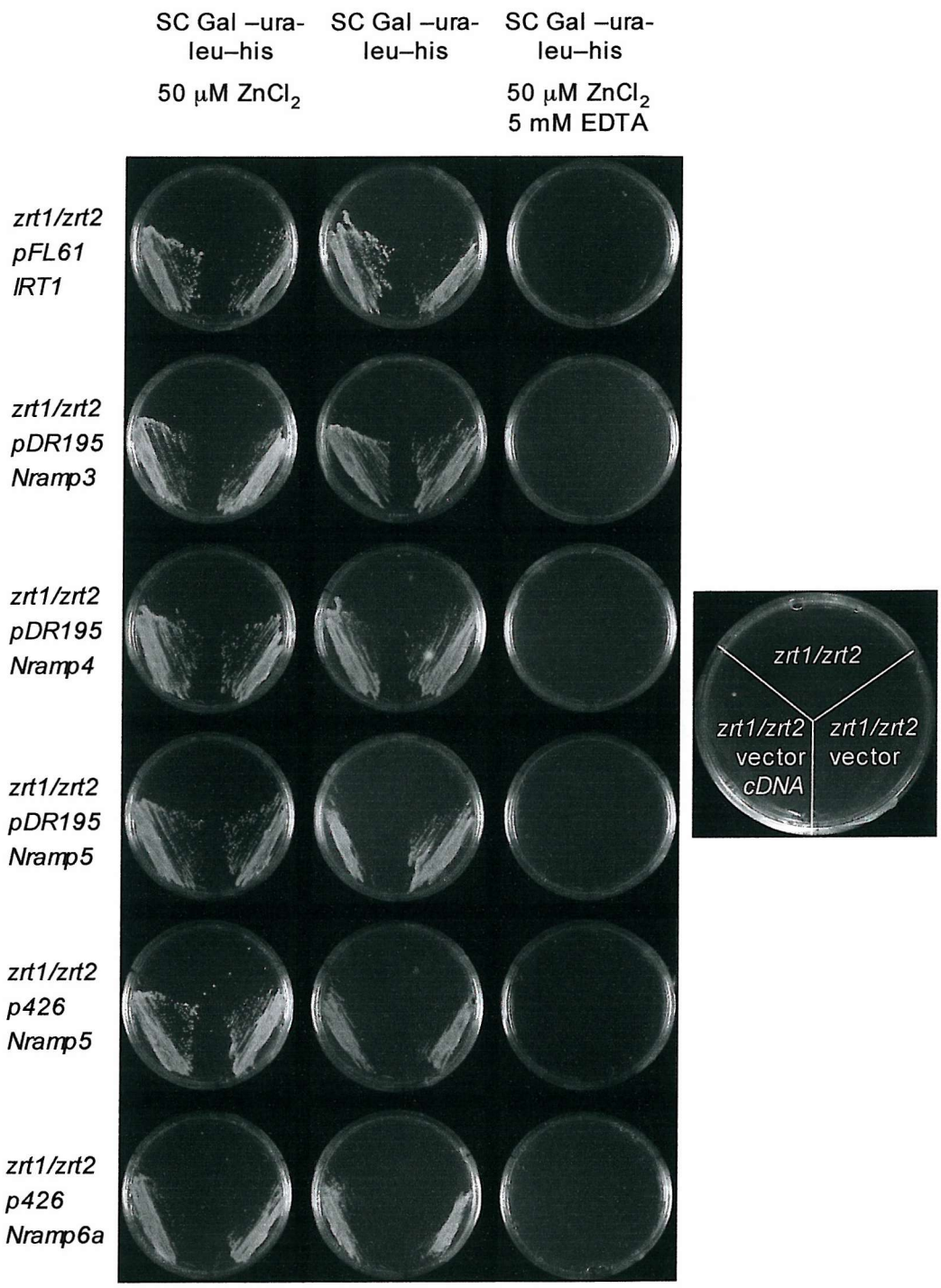

Fig.5.8. Growth of *zrt1/zrt2* Zn uptake mutant yeast transformed with *IRT1*, *AtNramp3*, *4*, *5* and *6a* on Zn replete and low Zn media. The untransformed *zrt1/zrt2* cells are also shown. Yeast were incubated at 30ºC for 72 h before imaging using an Alpha Innotech imaging system.

grow to the same degree as those transformed with only empty vector. On SC media with supplemental Zn and 0.5 mM or 1 mM EDTA no growth is observed from any of the cells. Fig.5.8 also shows the growth of these cells on SC media without supplemental Zn or EDTA. In this case the cells transformed with empty vector are still able to grow suggesting there is enough Zn in the SC media to support them. The *zrt1/zrt2* cells transformed with *IRT1* show slightly improved growth compared to those with empty vector. Cells transformed with *AtNramp4* or *AtNramp6* show similar growth to the empty vector transformed cells while those transformed with *AtNramp5* grow slightly less than those with the empty pDR195 vector. None of the transgenes appear able to complement this mutant in the presence of EDTA in these experiments. However, on SC media without additional $ZnCl_2$ or EDTA (shown in Fig.5.8, middle column), the cells transformed with *IRT1* grow better than those with only the empty vector. The cells transformed with *AtNramp3* and *AtNramp4* do not show a marked improvement over the cells transformed with the empty vector but grow more readily than cells transformed with *AtNramp5* and *AtNramp6*, which show no ability to improve the growth of this yeast strain.

The *zrt1/zrt2* yeast transformed with *IRT1*, *AtNramp3*, *4*, *5* and *6* were also grown in liquid cultures with 50 μM $ZnCl_2$ or 50 μM $ZnCl_2$ with 100 μM EDTA. The results of these experiments are shown in Fig.5.9, Fig.5.10 and Fig.5.11. Fig.5.9 shows the *zrt1/zrt2* yeast transformed with pDR195, *AtNramp3*, *4* and *5*. With no EDTA the cells transformed with the empty pDR195 vector grow more slowly than those transformed with pDR195/*AtNramp3* or pDR195/*AtNramp4* but more quickly than pDR195/*AtNramp5* transformed cells. With 50 μM $ZnCl_2$ and 100 μM EDTA none of the cells grow particularly well in the 30 h period. A very similar pattern of growth in the presence of EDTA is seen in the cells transformed with p426, *AtNramp5* and *AtNramp6* as shown in Fig.5.10. Fig.5.11 shows the results with *zrt1/zrt2* transformed with pFL61 and *IRT1*. In this case the cells transformed with the empty pFL61 vector reach similar optical densities as the cells transformed with the other constructs. However, those transformed with *IRT1* reach much higher densities. *IRT1* transformants also grow better than vector controls in the presence of 50 μM $ZnCl_2$ however. The *AtNramp* and *IRT1* constructs were also transformed into the *smf1/smf2* Mn uptake deficient yeast mutant and grown on media with varying concentrations of

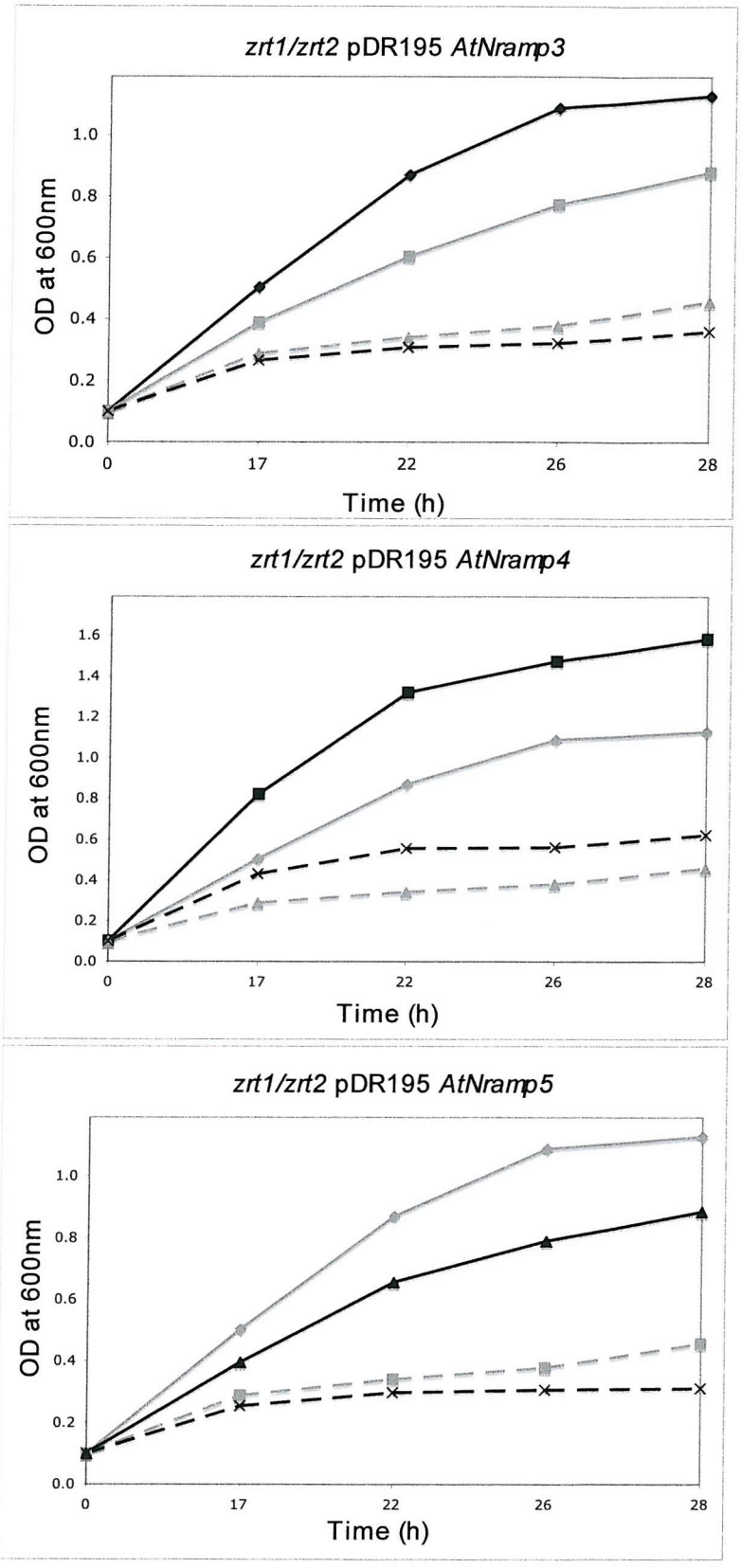

Fig.5.9. Growth of *zrt1/zrt2* yeast in SC -ura liquid culture. Yeast transformed with pDR195, pDR195/*AtNramp3*, pDR195/*AtNramp4* and pDR195/*AtNramp5* were grown at 30ºC. Black line: *AtNramp* transformed cells. Grey line: Vector transformed cells. Solid lines: 50 μM $ZnCl_2$. Dotted lines: 50 μM $ZnCl_2$ 100 μM EDTA.

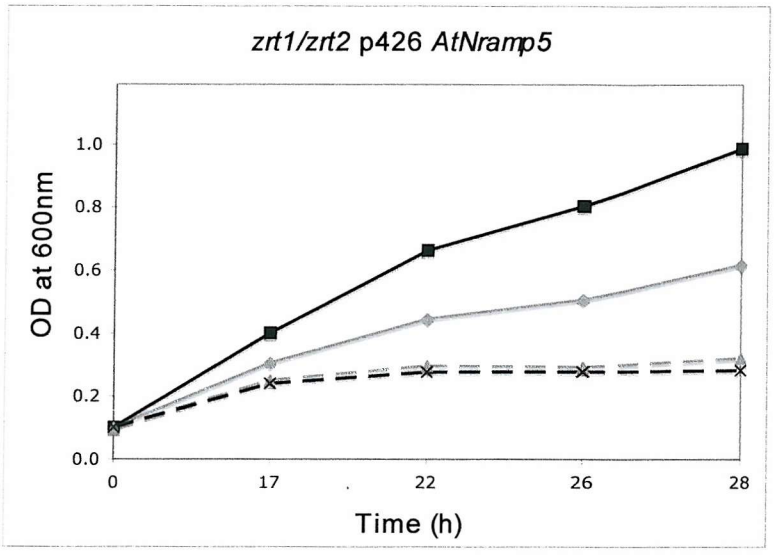

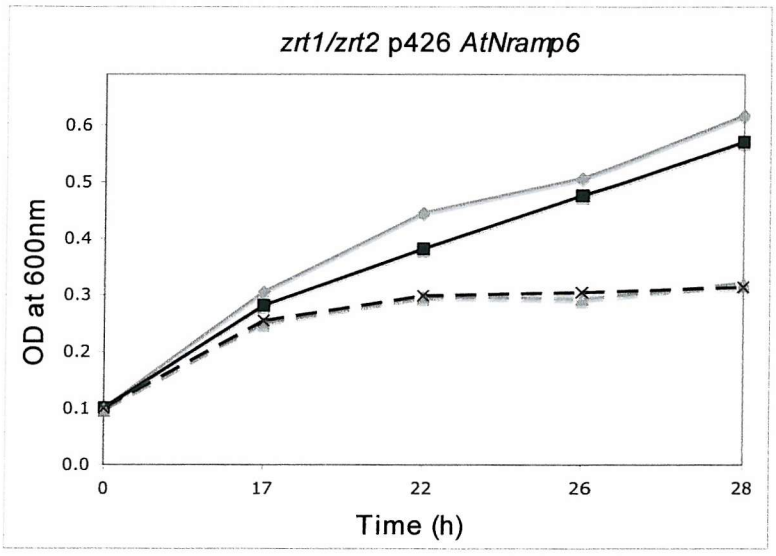

Fig.5.10. Growth of *zrt1/zrt2* yeast in SC -ura liquid culture. Yeast transformed with p426, p426/*AtNramp5*, and p426/*AtNramp6* were grown at 30°C. Black line: *AtNramp* transformed cells. Grey line: Vector transformed cells. Solid lines: 50 μM $ZnCl_2$. Dotted lines: 50 μM $ZnCl_2$ 100 μM EDTA.

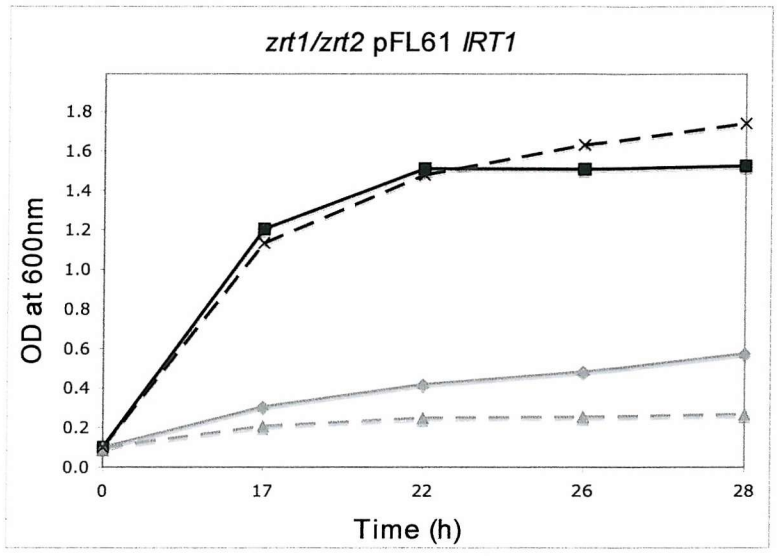

Fig.5.11. Growth of *zrt1/zrt2* yeast in SC -ura liquid culture. Yeast transformed with pFL61 and pFL61/*IRT1* were grown at 30ºC. Black line: *IRT1* transformed cells. Grey line: Vector transformed cells. Solid lines: 50 μM $ZnCl_2$. Dotted lines: 50 μM $ZnCl_2$ 100 μM EDTA.

Mn and EGTA. These results are shown in Fig.5.12. As with the other mutants, *AtNramp3* and *AtNramp4* are able to complement the *smf1/smf2* mutant when grown without supplemental Mn while *AtNramp5* and *AtNramp6* do not rescue this mutant. When grown on media with 50 μM $MnCl_2$ and 10 mM EGTA the cells transformed with *AtNramp6* appear to grow slightly better than those with only the empty vector. It should be noted that in this case the empty vector transformed cells did not grow as well as those on the other plates. The cells transformed with pFL61/*IRT1* did not grow well in this experiment suggesting it does not rescue the mutant.

5.2.3. Verification of transgene expression.

In order to check that the *AtNramp* genes were being expressed RNA was extracted from *fet3/fet4* yeast transformed with pDR195/*AtNramp4* or the pDR195 vector alone. A denaturing agarose gel of these RNA preparations is shown in Fig.5.13A. RT-PCR was performed using primers to the *AtNramp4* cDNA sequence. An agarose gel of this PCR is shown in Fig.5.13B. The correct size product of approximately 1.5Kb is amplified from the *fet3/fet4* pDR195/*AtNramp4* yeast RNA preparation while no product is amplified from *fet3/fet4* pDR195 RNA. Attempts to isolate RNA from *fet3/fet4* pDR195/*AtNramp5* cells proved unsuccessful preventing confirmation of the expression of *AtNramp5* within the yeast cells. RNA obtained from these cells was of both low yield and low quality making it unsuitable for RT-PCR.

AtNramp6a-GFP fusions were generated in our lab (Biggs and Williams, unpublished) and were transformed into the *zrt1/zrt2* yeast mutant in this project to allow the AtNramp6a protein to be localised within the cell. After growth on selection (-uracil) for 48 h the cells were visualised for GFP fluorescence. Fig.5.14 shows the result of these experiments. It can be seen that the cells are expressing GFP indicating that AtNramp6-GFP is being expressed at the protein level in these cells. It was also observed that after a further 48 h of growth on the same media very little fluorescence was detected. After re-streaking the cells to fresh media and growing new colonies the GFP signal was visible once more. However the resolution is not high enough to be certain whether the protein is being expressed at the plasma membrane or within the cytoplasm of the cells.

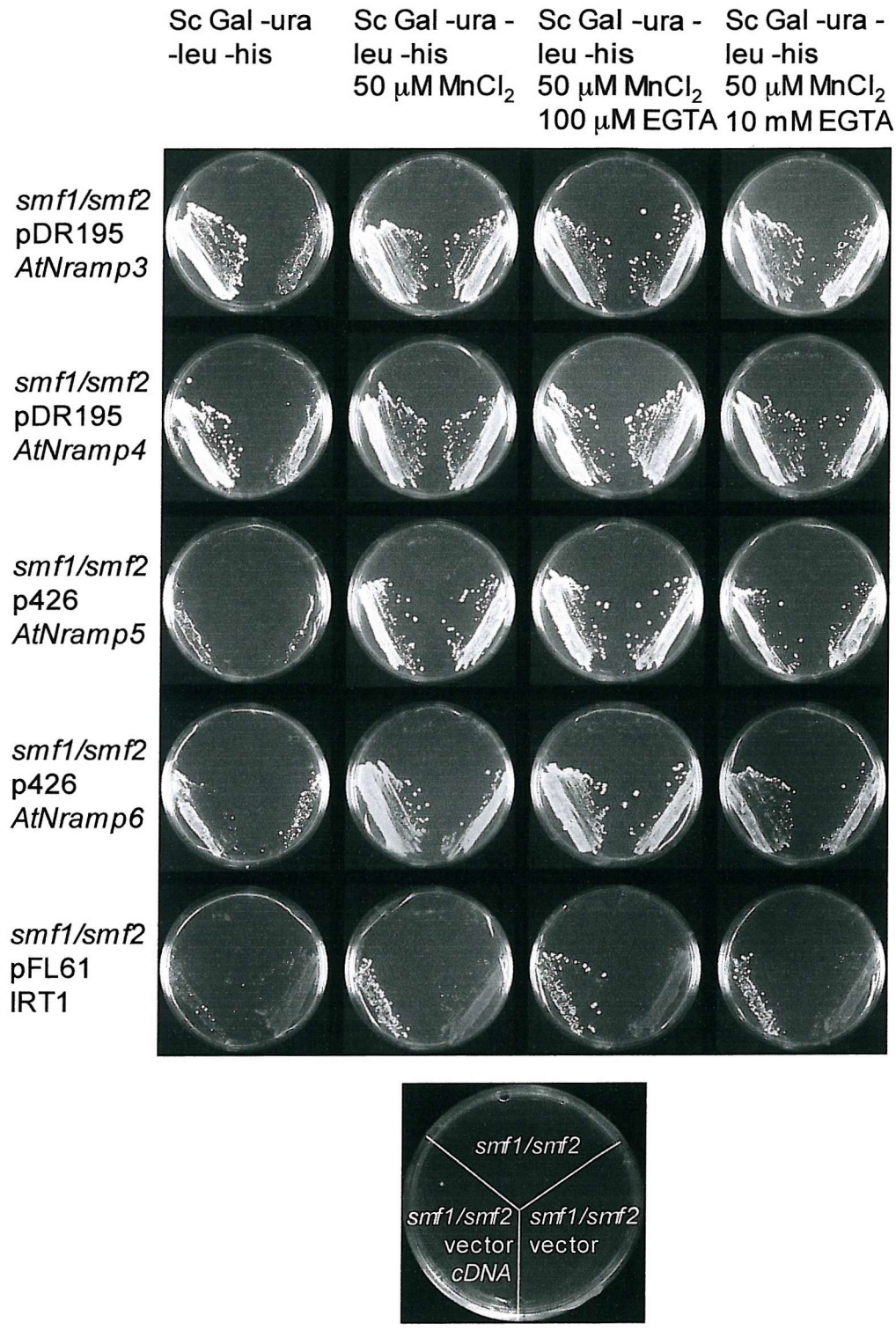

Fig.5.12. Growth of *smf1/smf2* Mn uptake deficient yeast mutant, transformed with *AtNramp3*, *AtNramp4*, *AtNramp5, AtNramp6* or *IRT1* in the presence of varying concentrations of $MnCl_2$. The untransformed *smf1/smf2* cells are also shown. Yeast were grown on the plates for 72 h at 30°C before imaging using an Alpha Innotech imaging system.

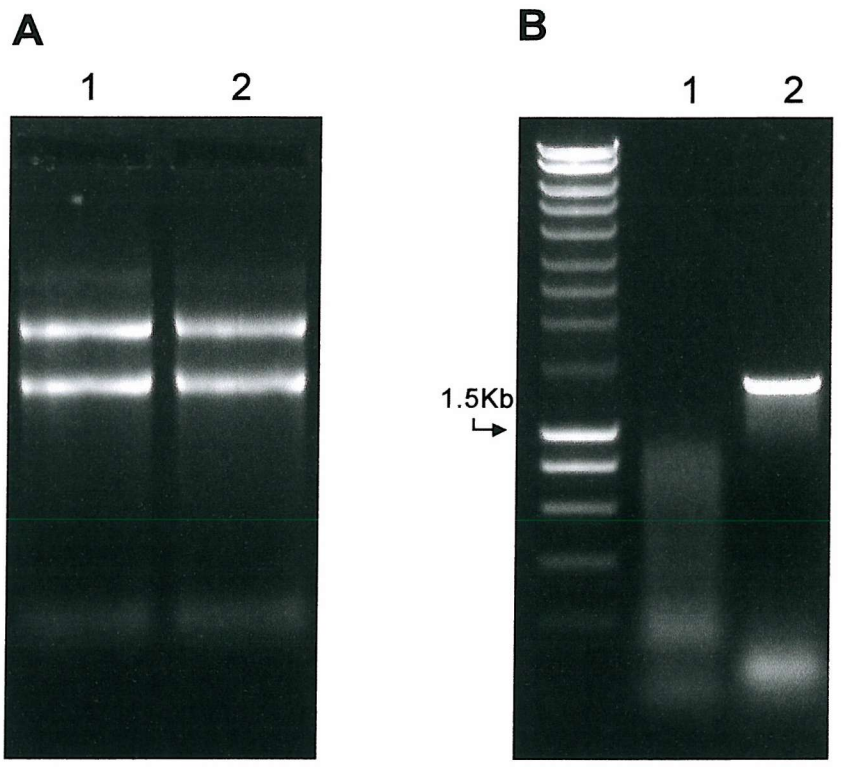

Fig.5.13. RNA and RT-PCR from *fet3/fet4* pDR195/AtNramp4 cells. **A:** Denaturing agarose gel electrophoresis of RNA extracted from *fet3/fet4* yeast transformed with: 1) pDR195 and 2) pDR195 *Nramp4*. **B:** Agarose gel electrophoresis of RT PCR using gene-specific primers for *AtNramp4* performed on RNA shown in A. RT PCR was performed using primers to the *AtNramp4* cDNA sequence. 1) product from RT PCR on RNA from *fet3/fet4* pDR195, 2) product from RT PCR on RNA from *fet3/fet4* pDR195 *AtNramp4*. Arrow indicates position of 1.5Kb marker.

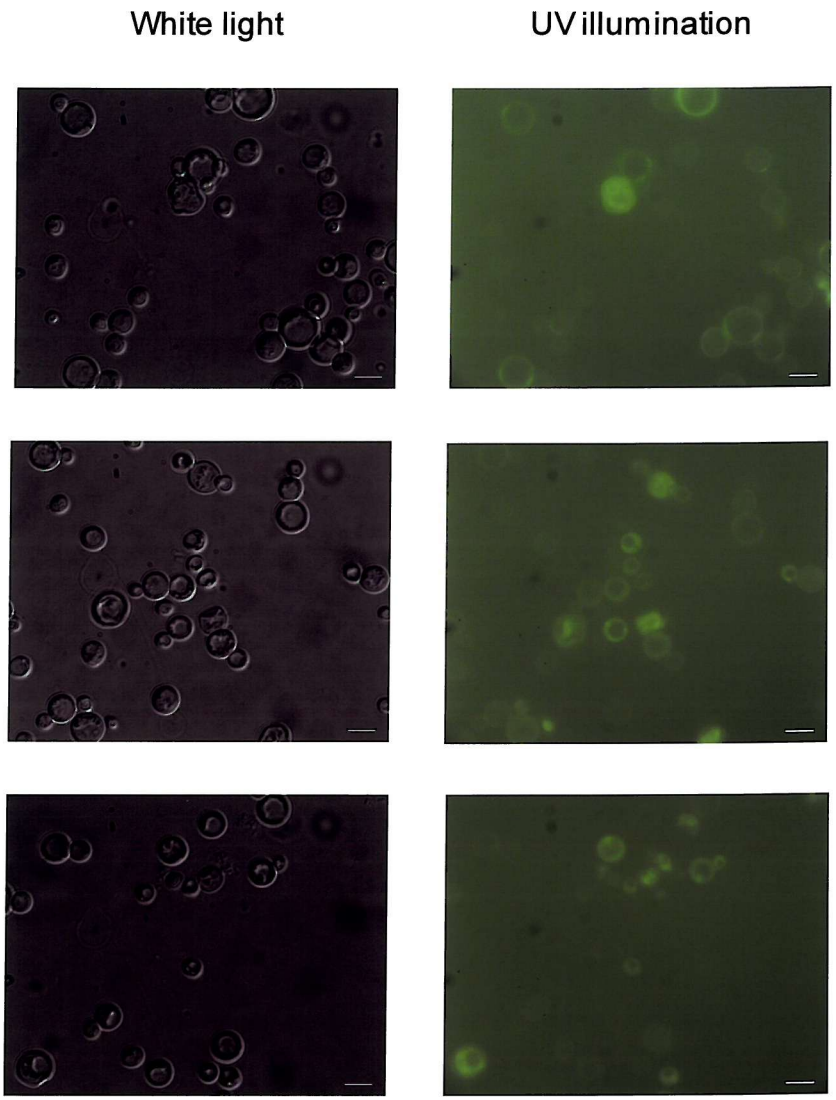

Fig. 5.14. AtNramp6a-GFP fluorescence in *zrt1/zrt2* yeast transformed with p426/AtNramp6a-GFP fusions. Images on the left show the cells under standard white light illumination while those on the right show the same field of view but under UV illumination. Bar = 10 μm.

5.2.4. Uptake of $^{55}FeCl_3$ into *fet3/fet4* yeast.

Initially, uptake of $^{55}FeCl_3$ into *fet3/fet4* pDR195/*AtNramp3* and *fet3/fet4* pDR195/*AtNramp4* cells was investigated over a 30 min time period. The result of this time course experiment is shown in Fig.5.15. Both the cells transformed with *AtNramp3* and *AtNramp4* accumulate more $^{55}FeCl_3$ than the cells transformed with empty pDR195. At 6 min the *fet3/fet4* pDR195/*AtNramp3* cells had accumulated more $^{55}FeCl_3$ than the *fet3/fet4* pDR195/*AtNramp4* cells. However, after this time point the *fet3/fet4* transformed with *AtNramp4* accumulated more $^{55}FeCl_3$ than those transformed with *AtNramp3*. Further time course experiments were performed with *AtNramp4* and *AtNramp5* in the pDR195 vector. The means and standard errors of these experiments are shown in Fig.5.16 and Fig.5.17. While *AtNramp4* transformed cells consistently accumulated more $^{55}FeCl_3$ than the empty vector control in all experiments performed, the cells transformed with *AtNramp5* were less consistent. Fig.5.17 shows the mean uptake from three replicates (in one experiment) in which some accumulation above that of the empty vector was observed. This shows that the level of $^{55}FeCl_3$ uptake was lower than that of *AtNramp4* transformed cells but still discernibly higher than the empty vector controls. In two other experiments no accumulation of $^{55}FeCl_3$ into *fet3/fet4* pDR195/*AtNramp5* cells was seen. The uptake of $^{55}FeCl_3$ into *fet3/fet4* yeast transformed with *AtNramp4* at varying pH was also investigated. The results of uptake experiments performed at pH values from 4.5 to 7.5 are shown in Fig.5.18. After 12 min it can be seen that cells incubated at pH 4.5 have accumulated the most $^{55}FeCl_3$. The uptake decreases with increasing pH up to pH 7 and then increases slightly at pH 7.5. This slight increase in uptake at pH 7.5 when compared to pH 7 occurred in all three replicates. Fig.5.19 shows the results of uptake experiments using the protonophore CCCP, which disrupts the proton gradient across the membrane. With or without CCCP, *AtNramp4* transformed cells accumulate more $^{55}FeCl_3$ than those transformed with the empty pDR195 vector. However, with 10 μM CCCP there is a slight increase in uptake of $^{55}FeCl_3$ in *AtNramp4* transformed cells when compared to the same cells incubated in standard uptake buffer or uptake buffer with EtOH.

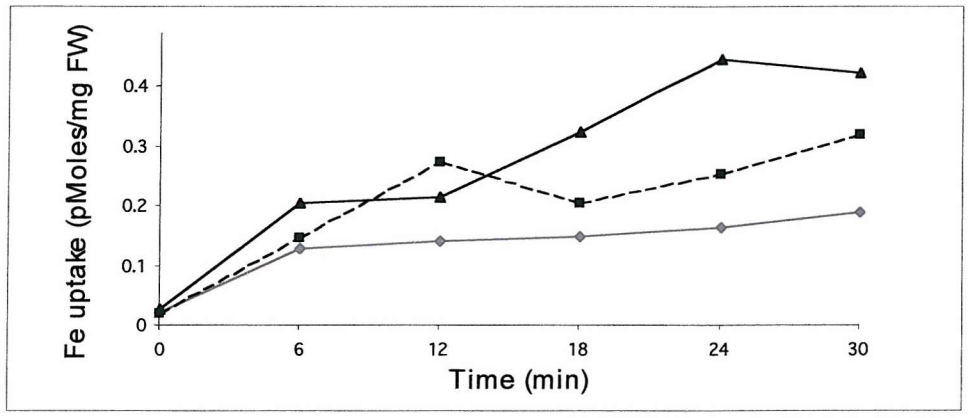

Fig.5.15. Time course for the uptake of radiolabelled Fe ($^{55}FeCl_3$) into *fet3/fet4* yeast transformed with pDR195/*AtNramp3* or pDR195/*AtNramp4* at 30°C. The $FeCl_3$ concentration was 50 μM. Dotted line: *fet3/fet4* pDR195/*AtNramp3*, Black line: *fet3/fet4* pDR195/*AtNramp4*, Grey line: *fet3/fet4* pDR195.

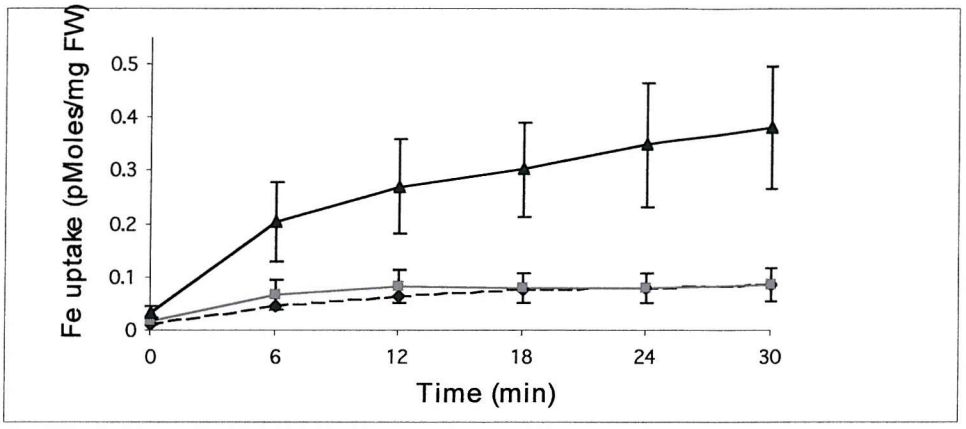

Fig.5.16. Time course for the uptake of radiolabelled Fe ($^{55}FeCl_3$) into *fet3/fet4* yeast transformed with pDR195/*AtNramp4* at 30°C. The $FeCl_3$ concentration was 50 μM. Black line: *fet3/fet4* pDR195/*AtNramp4*, Grey line: *fet3/fet4* pDR195, Dotted line: *fet3/fet4* pDR195 incubated on ice. Data shown are averages of six replicates from two experiments. Error bars indicate standard error.

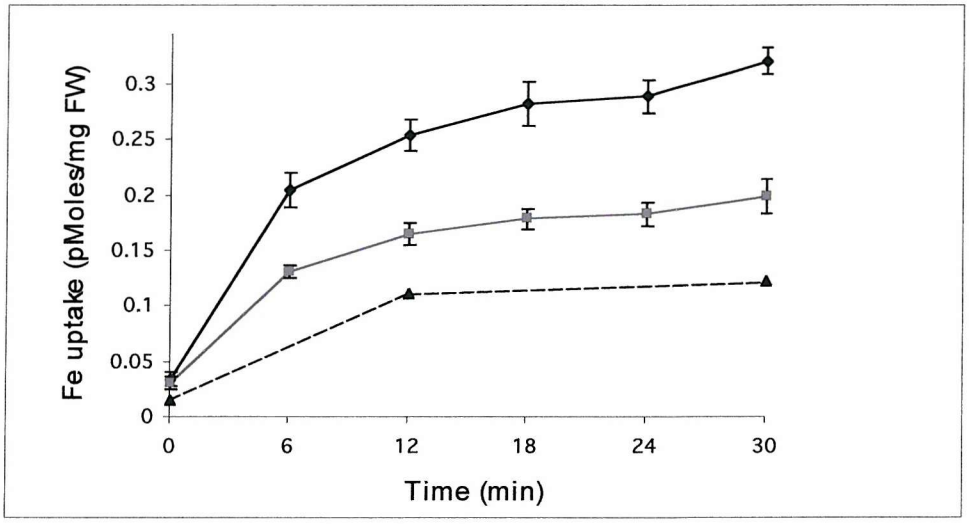

Fig.5.17. Time course for the uptake of radiolabelled Fe ($^{55}FeCl_3$) into *fet3/fet4* yeast transformed with pDR195/*AtNramp5* at 30°C. The $FeCl_3$ concentration was 50 μM. Black line: *fet3/fet4* pDR195/*AtNramp5*, Grey line: *fet3/fet4* pDR195, Dotted line: *fet3/fet4* pDR195 incubated on ice. Data shown are averages of three replicates except for those incubated on ice for which there was one replicate. Error bars indicate standard error.

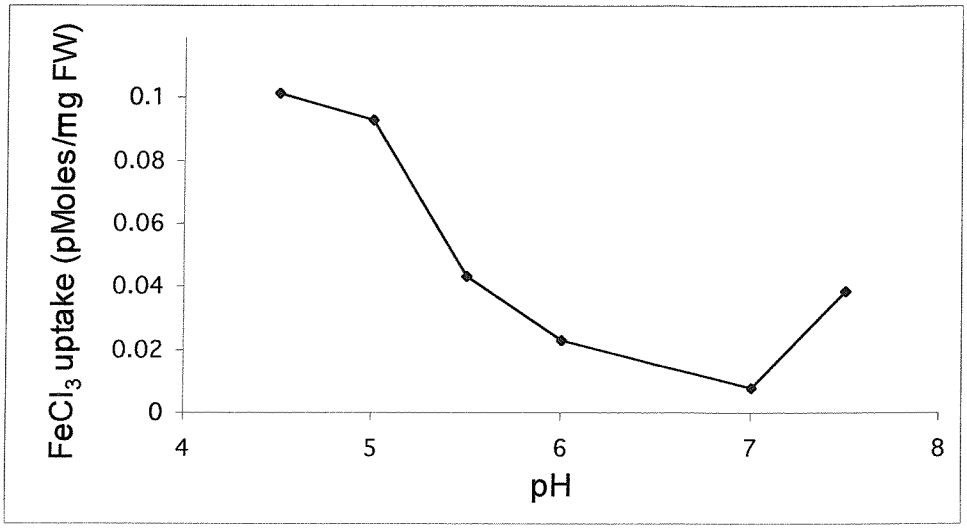

Fig.5.18. Accumulation of $^{55}FeCl_3$ in *fet3/fet4* yeast transformed with pDR195/*AtNramp4* at various pH values. Experiments were performed at 30ºC and samples taken for scintillation counting after 12 min. The $FeCl_3$ concentration was 50 μM. Data shown are the averages of three replicates and show the average uptake by cells transformed with pDR195/*AtNramp4* minus the average uptake by cells transformed with the empty pDR195 vector.

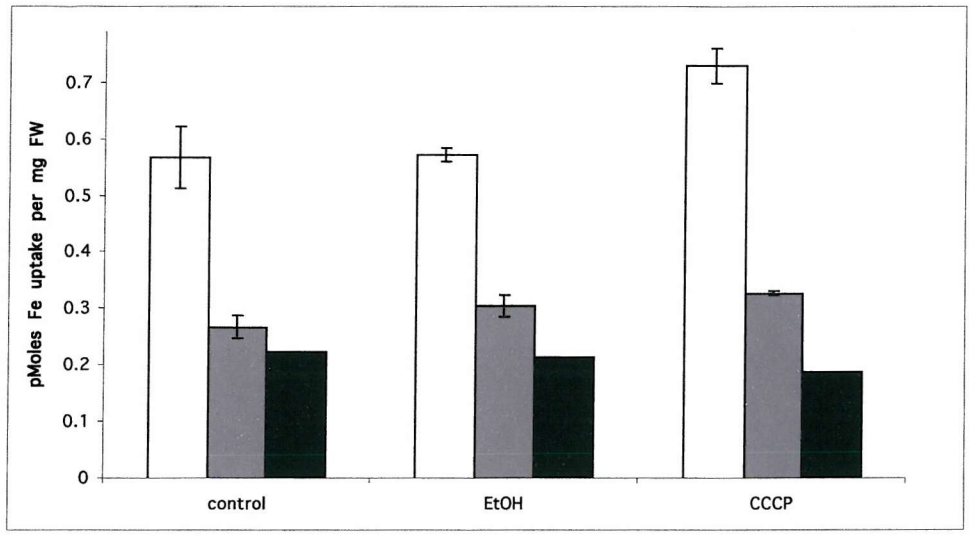

Fig.5.19. Accumulation of $^{55}FeCl_3$ in *fet3/fet4* yeast transformed with *AtNramp4* in the pDR195 vector incubated at 30°C for 12 min with 10μM CCCP. The $FeCl_3$ concentration was 50 μM. White bars: *fet3/fet4* pDR195/*AtNramp4*, Grey bars: *fet3/fet4* pDR195, Black bars: *fet3/fet4* pDR195 incubated on ice. Data shown are averages of three replicates except for those on ice for which one replicate is shown. Error bars indicate standard error.

5.3. Discussion.

Previous work using yeast mutants deficient in Fe, Zn and Mn uptake transformed with AtNramp1, 3 and 4 has indicated that these proteins are capable of transporting Fe, Zn and Mn under certain conditions (Curie *et al.,* 2000, Thomine *et al.,* 2000). However, the yeast complementation experiments presented here have so far been unable to show functional activity for AtNramp5 or AtNramp6 although some transport activity for AtNramp5 has been seen in radiolabelled Fe uptake experiments. Radiolabelled Fe uptake experiments presented in this work show that AtNramp4 is capable of transporting Fe and suggest that transport by AtNramp4 is dependent on pH since Fe accumulation at pH above 6 drops compared to lower pH values. PCR performed on yeast transformed with the *AtNramps* confirms the presence of the constructs while RNA extraction and RT-PCR has shown that *AtNramp4* is expressed so it seems unlikely that they are altogether not present in the yeast cells used. Also, p426/*AtNramp6-GFP* transformed cells do emit GFP fluorescence suggesting that the Nramp-GFP fusion protein is produced. It seems that for some reason, *AtNramp5* and *AtNramp6* are either not being expressed correctly by the yeast in these experiments or that under these conditions AtNramp5 and AtNramp6 are unable to function properly even if they are being expressed and targeted successfully to the plasma membrane of the yeast. There are many possible reasons why this may be occurring. Data from codon usage tables on the world wide web (http://www.kazusa.or.jp/codon/) suggest that *Saccharomyces cerevisiae* and *Arabidopsis thaliana* share very similar codon usage meaning that yeast should be able to translate Arabidopsis cDNA sequences successfully. However, a single amino acid substitution in the mammalian Nramp1 from Gly to Asp at position 105 is enough to prevent the protein from functioning. If one or more amino acids are translated differently by the yeast due to unknown variation in codon usage it may be possible that a non-functional protein could be produced. It seems unlikely that this would occur separately in AtNramp3, AtNramp5 and AtNramp6 unless the amino acid change was positioned in a conserved area in all three proteins. Mutations could also occur in the *AtNramp* genes when growing stock cultures of *E.coli* to obtain the *AtNramp* cDNA sequences for use in the yeast transformations. Again, it would be unlikely for a deleterious mutation to occur separately in all three of the *AtNramps* used in these experiments. Although

yeast are eukaryotes and are therefore capable of adding post-translational modifications to proteins, it may also be possible that some modifications such as glycosylation or N-myristoylation are not made to the AtNramps after translation under these conditions. This could result in the lack of function of the protein due to improper folding or targeting to an internal membrane (Drickamer and Taylor, 1998).

Assuming that the proteins are correctly translated, modified and targeted to the appropriate membrane of the yeast cells it is possible that the conditions under which these experiments were conducted were not suitable for the proper function of the AtNramps. Since it has been shown that the mammalian Nramps are driven by the proton gradient across the membrane (Gunshin *et al.,* 1997) it is conceivable that the pH of 5.5 or 5 used in these experiments was perhaps not low enough to allow the AtNramps to function efficiently in this particular yeast strain. Experiments using a range of media with different pH values should help to identify if this is the case. However, the Fe uptake experiments performed with AtNramp4 indicate that this protein is functional at pH 5 and 5.5 and is only slightly more active at pH 4.5 suggesting that pH 5 should be sufficient for activity. In some cases heterologous expression of a foreign gene fails because other proteins are required to regulate or interact with the protein of interest. In yeast the *BSD2* gene product is important in regulating SMF1 activity by redirecting the yeast Nramp SMF1 to the vacuole when metal ions are abundant (Liu and Culotta, 1999a and b). It may be that a similar interaction may be preventing the expression of the *AtNramps* in these yeast cells although this seems unlikely since *AtNramp1, AtNramp3* and *AtNramp4* have been expressed previously in the *fet3/fet4* mutant (Thomine *et al.,* 2000, Curie *et al.,* 2000, Pittman and Williams, unpublished) and *AtNramp3* and *AtNramp4* successfully complement the *fet3/fet4* and *smf1/smf2* mutants in the experiments shown in this work. The possibility exists that *AtNramp6a* did partially rescue the *smf1/smf2* mutant in these experiments but the poor growth of the vector only controls makes this uncertain. More experiments are required to verify this result.

RT-PCR performed on RNA extracted from *fet3/fet4* pDR195 *Nramp4* yeast produced a band of the correct size (see Fig.5.12), suggesting that *AtNramp4* is being expressed in the mRNA of the yeast. This is to be expected since *AtNramp4* does rescue this mutant on low Fe media, meaning it is likely to be expressed and translated to protein. RNA extraction from *fet3/fet4* pDR195 *Nramp5* yeast did not yield RNA of a suitable amount or quality to allow RT-PCR to be used to check the

expression of *AtNramp5*. This means it is impossible to rule out the possibility that *AtNramp5* is not being expressed by these yeast cells and it is therefore unable to rescue the mutant for this reason. *AtNramp6a-GFP* fusions transformed into the *zrt1/zrt2* mutant suggest that the yeast cells are correctly expressing the transgene since GFP fluorescence can be detected in some cells. From the images obtained it cannot be accurately determined whether the signal is coming from the plasma membrane or the cytoplasm. Some of the cells appear to possess a thin band of fluorescence at the plasma membrane but this could represent the cytoplasm between the cell vacuole and the plasma membrane. Other cells appear to fluoresce mainly within the cytoplasm. This means that while it cannot be ruled out that the AtNramp6a-GFP fusion protein is being expressed at the plasma membrane, it seems likely that many of the cells are not targeting the AtNramp6a-GFP fusion protein to the plasma membrane and it is instead residing in the cytoplasm. This could also be the case with the *AtNramp6a* and *AtNramp5* transgene products and would explain why little or no functional activity has been observed.

Fe uptake in *AtNramp4* transformed cells suggests that this protein is capable of transporting Fe. Also, it seems that AtNramp5 can transport Fe but to a lesser degree than AtNramp4. This did not occur in all the experiments performed however, so it may be that the expression of *AtNramp5* in these yeast mutants is not particularly stable or varies between individual yeast colonies. This could help to explain why *AtNramp5* has not been able to rescue the yeast mutants when grown on plates or in liquid culture: the transport activity may be too low to alleviate the limitations on growth of these mutants. The effect of pH on Fe uptake by AtNramp4 indicates that this protein may require protons for transport activity and could be proton driven in the same way as DCT1 (Gunshin *et al.*, 1997, Tandy *et al.*, 2000). However, the addition of 10 μM CCCP, a protonophore that should disrupt the proton-gradient, did not produce a drop in transport activity in AtNramp4 as would be expected. This could be due to many factors such as insufficient time for CCCP to have an effect, too low a concentration of CCCP or other effects on the cell. It is also possible that AtNramp4 is not proton coupled and the slight increase with added CCCP is not anything more than variation in the experiment. The effect of pH could be due to other mechanisms being affected. Further experiments with varying concentrations of CCCP, various time periods and other inhibitors of the proton gradient are required to confirm or reject the hypothesis that the transport activity of AtNramp4 is proton coupled.

Chapter 6. Insertional mutants and over-expression of the *AtNramps*.

6.1. Introduction.

A useful experimental approach towards discovering the function of a particular gene or family of genes is that of reverse genetics. This involves using mutant individuals in which the gene (or genes) of interest is non-functional. The effects of loss of function of particular genes on the phenotype of the individual mutants can then be studied. This data may in turn suggest a possible role for the gene of interest and point the way for further study using other techniques such as heterologous expression. Hussain *et al.* (2004) made use of plants in which the metal transporters *AtHMA2* and *AtHMA4* were both non-functional to show that the two genes may have a role in Zn nutrition and homeostasis. Since plants in which only one of the genes were non-functional showed no obvious phenotype it was also proposed by the authors that both genes share a similar function in Zn homeostasis and that there is some functional redundancy between them.

One way of generating mutant *Arabidopsis thaliana* plants is to use *Agrobacterium tumefaciens* mediated transformation to introduce a T-DNA insertion at a random point in the plant genome. By performing the transformation on many different plants a library of plants can be built up, each of which contains the T-DNA at a different position in the genome. By screening all the different plants produced, an individual in which the T-DNA lies within the coding region of the gene of interest may be found. As the number of plants transformed increases so does the probability of finding a T-DNA within the gene of interest. In order to make large numbers of transformed plants available to researchers a number of facilities are now producing many lines of plants with random T-DNA insertions that may be screened using PCR based techniques. One such facility exists at the University of Wisconsin, Madison, WI, U.S.A. as described by Krysan *et al.* (1996, 1999). Krysan *et al.* (1996) were able to screen the lines of T-DNA insertion mutants they created to find mutant plants which lacked various genes involved in signal transduction and ion transport such as CPK-9, a member of the calmodulin-domain protein kinase family.

The Arabidopsis Knockout facility at the University of Wisconsin now offers the opportunity to screen their lines of T-DNA transformed *Arabidopsis* plants for insertions in particular genes of interest. The facility uses gene-specific primers designed by users and their own primers to the T-DNA. PCR using these primers is carried out by the facility on 30 "super pools", each one containing genomic DNA from 2025 lines of plants transformed with the T-DNA. The PCR products are then returned to the users and screened for T-DNA inserts in the genes of interest using labelled-DNA probes. The products identified are then sequenced. Should any T-DNA inserts be found in one of the "super pools" a second round of PCR can then be performed on the 9 smaller pools that make up each super pool. Once the hit is narrowed down to one of these pools, which contains 225 lines of plants, seed can be ordered from the Arabidopsis Biological Resource Centre (ABRC) and the line containing the T-DNA insert identified by sequencing the genomic DNA from the plant. Once identified, seed from the plant containing the T-DNA insert can be collected and grown to produce a number of plants homozygous for the T-DNA insert. The phenotype of these plants can then be studied under various environmental conditions, potentially giving an insight into the function of the gene of interest if a successful knock-out is produced.

Other databases of insertional mutants of *Arabidopsis* also exist, for example SALK (http://signal.salk.edu/cgi-bin/tdnaexpress), Syngenta (http://www.tmri.org/en/partnerships/sail_collection.aspx) and GABI-kat (http://mpiz.koeln.mpg.de/GABI-Kat). In these cases sequence data for the position of each T-DNA insertion is made available on the respective database websites greatly accelerating the selection process. This enables the immediate identification of lines that contain an insertion within the gene of interest. Once obtained, these lines must still be checked by PCR to verify the presence and exact location of the T-DNA. Finally, plants that are homozygous for the insertion must be identified and selected before being used in studying the phenotype of the mutant line.

An alternative method to study gene function *in planta* is to make use of over-expression of the gene of interest. This can be achieved by cloning the cDNA of the gene of interest into a vector that, once transformed into the plant, allows the cDNA to be strongly and constitutively expressed within the plant. This should lead to an abnormally high expression level of the protein and the effect of this can give an indication as to its function. For example, Connolly *et al.* (2002) over-expressed the Fe

transporter *IRT1* in *Arabidopsis* and showed that these plants accumulated more Cd and Zn than wild-type plants, indicating that IRT1 is also capable of transporting these metals in the plant.

The aim of the experiments presented in this chapter was to identify potential insertional mutants of the *AtNramps*, verify the T-DNA insertions and attempt to characterise their effects. The effect of over-expression of *AtNramp5* in *Arabidopsis* was also to be investigated under varying conditions.

6.2. Results.

6.2.1. Wisconsin T-DNA insertion lines.

6.2.1.1. Primer design and testing.

Primers were designed to the untranslated regions of *AtNramp5* and *AtNramp6* genomic sequences as specified by the Arabidopsis Knockout Facility's guidelines at http://www.biotech.wisc.edu/Arabidopsis/default.htm on the world wide web. Primers were designed to be 29 base pairs long with a GC content between 34 and 50% using the primer3 program at http://www-genome.wi.mit.edu/cgi-bin/primer/primer3_www.cgi on the World Wide Web. The primer sequences and PCR conditions used are shown in Table 6.1. The primers were tested by performing PCR on *Arabidopsis* Col 0 genomic DNA using the Arabidopsis Knockout facility's suggested conditions. The PCR products were then run on an agarose gel shown in Fig.6.1. As can be seen, the expected sized bands were produced, indicating the primers were functioning correctly. The *AtNramp5* forward and reverse primers produced a 2.2Kb band from *Arabidopsis thaliana* Col 0 genomic DNA while the *AtNramp6* forward and reverse primers produced a 3Kb band.

These primers were sent to the Wisconsin facility for use in PCR alongside the T-DNA border primers on pools of genomic DNA from *Arabidopsis thaliana* plants transformed with the T-DNA.

Table 6.1. Primers and conditions used for PCR based screening of mutant lines from the Arabidopsis Knockout Facility at the University of Wisconsin. Primers were designed to the 3' and 5' untranslated regions of *AtNramp5* and *AtNramp6* according to the guidelines on the Arabidopsis Knockout Facility's website at http://www.biotech.wisc.edu/Arabidopsis/default.htm. JL202 primes to the left border of the T-DNA. The sequence of this primer was supplied by the Arabidopsis Knockout Facility.

Primer name	Primer sequence	Initial melting step.	Melting step.	Annealing step.	Elongation step.	Final elongation step.
AtNramp5 forward	5'-TAAGGGATTTTGTA ATTTAACCGGTTCTG-3'	96°C 5mins.	94°C 15sec.	65°C 30sec.	72°C 2mins.	72°C 4mins.
AtNramp5 reverse	5'-TTTTGCTCAGATAA GTTGTAAGGGTTGAA-3'	96°C 5mins.	94°C 15sec.	65°C 30sec.	72°C 2mins.	72°C 4mins.
AtNramp6 forward	5'-TGATGTTGGCATTA TAGATAGGGAGAGAA-3'	96°C 5mins.	94°C 15sec.	65°C 30sec.	72°C 2mins.	72°C 4mins.
AtNramp6 reverse	5'-CGTTTGATGGATTT TGTAGTCAAGTCTTC-3'	96°C 5mins.	94°C 15sec.	65°C 30sec.	72°C 2mins.	72°C 4mins.
JL202	5'-CATTTTATAATAACG CTGCGGACATCTAC-3'	96°C 5mins.	94°C 15sec.	65°C 30sec.	72°C 2mins.	72°C 4mins.

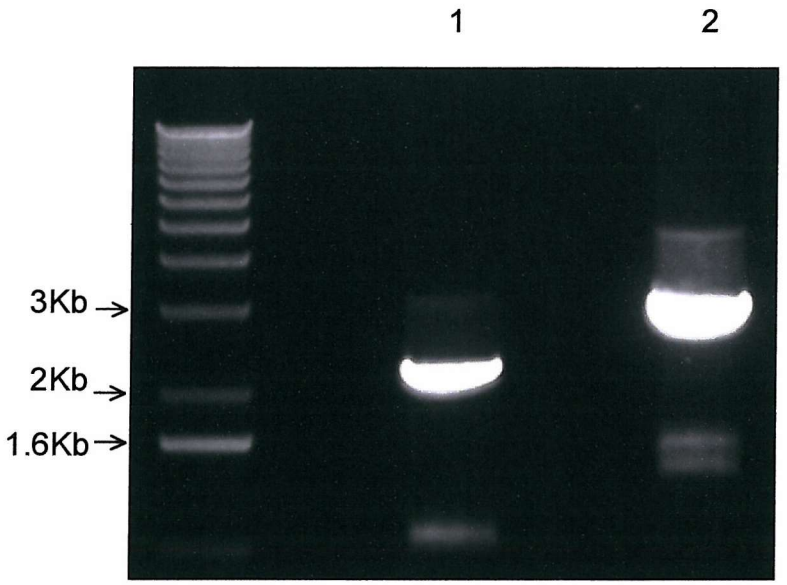

Fig. 6.1. Agarose gel electrophoresis of PCR products obtained using the primers designed for use in locating insertional mutants from the Wisconsin facility. *AtNramp5* (lane 1) and *AtNramp6* (lane 2) primers were used to amplify these products from *Arabidopsis thaliana* Col 0 genomic DNA as template. The expected size for *AtNramp5* amplified from genomic DNA is 2.2Kb while that of *AtNramp6* is 3Kb. A 1% agarose gel was used. The 1.6Kb band of the DNA ladder contains 25ng of DNA.

6.2.1.2. Preparation and testing of digoxygenin-labelled probes.

The bands produced when testing the *AtNramp5* and *AtNramp6* primers (Fig.6.1) were then cut from the agarose gel, purified and used to prepare the *AtNramp5* and *AtNramp6* digoxygenin-labelled probes by PCR using the same primers. The control reactions (using distilled water instead of the digoxygenin label) from this PCR were run on an agarose gel to check that the PCR was successful. This gel is shown in Fig.6.2. An incorporation check was then made on the digoxygenin-labelled probes by blotting 2 μl of each directly onto the DNA membrane, baking at 85°C and then proceeding with the detection steps. The exposed films are shown in Fig.6.3, which indicates that both the probes have successfully incorporated the digoxygenin label. The probes were also tested for specificity to the desired *AtNramp* by preparing a membrane blotted with different *AtNramp* cDNA or genomic DNA fragments. *AtNramp3* cDNA, *AtNramp5* genomic DNA, *AtNramp6* genomic DNA and NEV N plasmid DNA were applied in approximately 50 ng amounts. The membranes were then probed with either the *AtNramp5* or *AtNramp6* digoxygenin-labelled probes and X-ray film exposed to the membranes. The films are shown in Fig.6.4. While the *AtNramp6* probe does not appear to hybridise with the other DNA sequences it seems that the *AtNramp5* probe will also hybridise to the *AtNramp3* cDNA sequence albeit to a lesser degree than to the *AtNramp5* DNA sequence.

6.2.1.3. Screening for insertional mutants.

The first round of PCR using the *AtNramp5* and *AtNramp6* gene-specific primers and the T-DNA primer on the 30 "super pools" of genomic DNA from T-DNA transformed *Arabidopsis thaliana* plants was performed by the Wisconsin facility. Four sets of PCR were performed on the 30 super pools. The first set used the *AtNramp5* forward primer with the T-DNA left border primer. The second set used the *AtNramp5* reverse primer with the T-DNA left border primer. The third set used the *AtNramp6* forward primer and T-DNA left border primer while the fourth set used the *AtNramp6* reverse primer and T-DNA left border primer. Control reactions (sample no. 31 in each set of reactions) were performed using both forward and reverse gene-specific primers and the T-DNA left border primer. The PCR products were returned and run

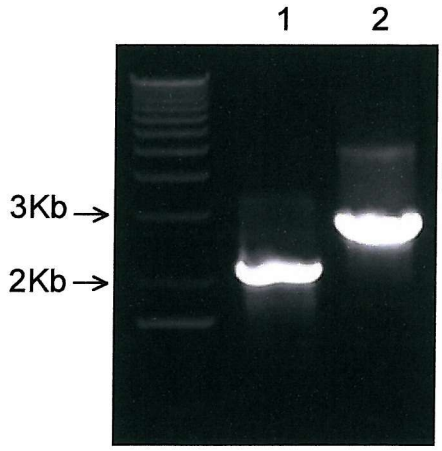

Fig.6.2. Agarose gel electrophoresis of control PCR products from digoxygenin labelling PCR on gel extracted DNA. The expected size bands were amplified in both cases. Lane 1 shows the PCR using *AtNramp5* primers in which a band of approximately 2.2Kb was produced, while lane 2 shows the PCR using *AtNramp6* primers in which a 3Kb band was produced. A 1% agarose gel was used. The 1.6Kb band of the 1Kb DNA ladder contains 25 ng of DNA.

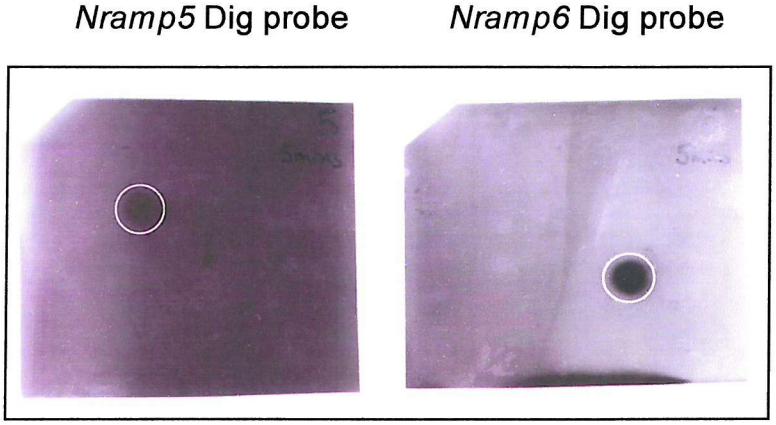

Fig.6.3. Digoxygenin incorporation by *AtNramp5* and *AtNramp6* specific probes generated by PCR from *Arabidopsis thaliana* COL 0 genomic DNA. The probes were spotted onto the membrane and digoxygenin detection steps carried out in order to check that digoxygenin had been incorporated into the probes. The position of the spotted probes is circled in white.

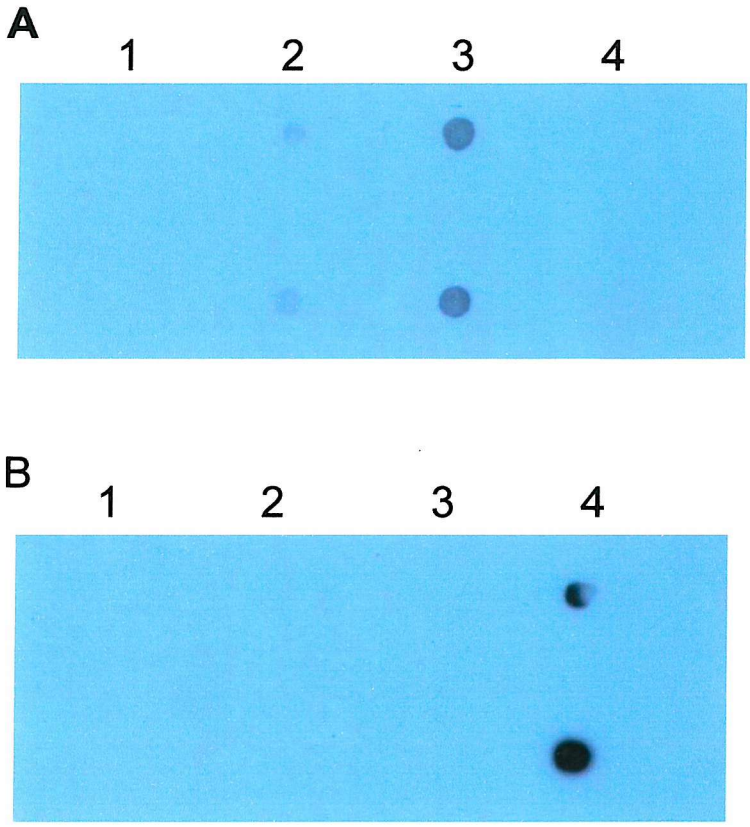

Fig.6.4. Dot blot to test the specificity of the digoxygenin-labelled probes to *AtNramp5* (**A**) and *AtNramp6* (**B**). Approximately 50ng of 1) NEV E plasmid DNA, 2) *AtNramp3* cDNA, 3) *AtNramp5* gDNA, 4) *AtNramp6* gDNA were applied to the hybond membrane and probed with the *AtNramp5* digoxygenin probe (**A**) or *AtNramp6* probe **(B).** The X-ray film was exposed to the membrane for 5 min.

on agarose gels. The *AtNramp5* forward primer reactions are shown in Fig.6.5, while the *AtNramp5* reverse reactions are shown in Fig.6.6. The *AtNramp6* forward primer reactions are shown in Fig.6.7 and the *AtNramp6* reverse primer reactions in Fig.6.8. The gel pictures show that a number of different sized bands were produced, often more than one band in each lane. The PCR products were then transferred from the gels to DNA membranes and probed using the *AtNramp5* or *AtNramp6* digoxygenin-labelled probes. The *AtNramp5* blots are shown in Fig.6.9 and 6.10. The *AtNramp6* blots are shown in Fig.6.11.

Initially, only bands that appeared after hybridisation with the appropriate digoxygenin-labelled probe and that were smaller in size than the genomic size of *AtNramp5* and *AtNramp6* were chosen for analysis. This is because any bands larger than the genomic size of the *AtNramps* would be unlikely to contain the T-DNA insertion within the coding region for either gene. The bands that were gel extracted and sequenced are listed in Table 6.2. More of these PCR products were again run on a gel and the selected bands cut out and gel extracted. The *AtNramp5* PCR products were first cycle sequenced but no sequence was obtained possibly due to insufficient amounts of the gel extracted PCR products used as template. A second PCR was therefore performed on the gel extracted *AtNramp5* bands using either the *AtNramp5* forward or reverse primer combined with the T-DNA primer to bulk up the amount of template available. These products were run on a 1% agarose gel, purified from the gel and used in cycle sequencing. The same procedure was carried out on the *AtNramp6* bands. To date, sequencing of these PCR products has proved unsuccessful with no readable sequence being obtained.

6.2.2. SALK insertion lines.

6.2.2.1. SALK database searching.

Putative *AtNramp* insertion mutants were identified by searching the SALK database using the protein entry code for each *AtNramp*. The SALK web interface T-DNA Express (http://signal.salk.edu/cgi-bin/tdnaexpress) was used to perform all searches. A number of different lines were identified with putative insertion events in

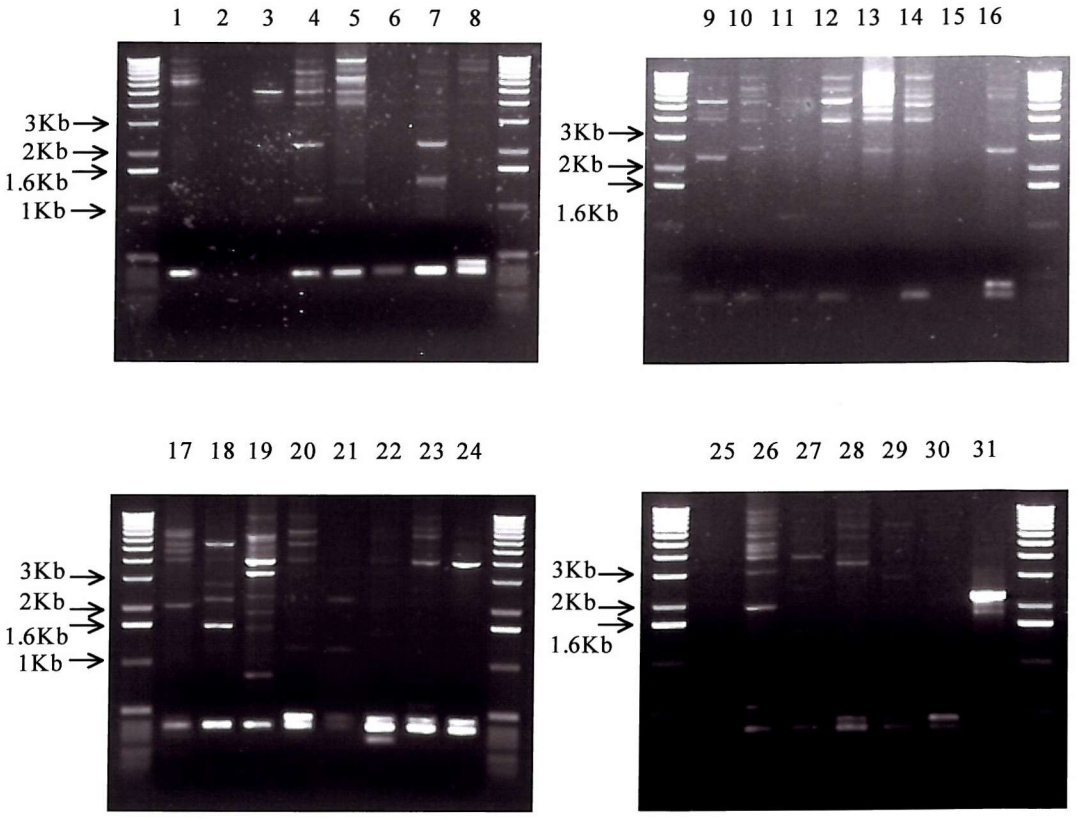

Fig.6.5. Gel electrophoresis of PCR performed on super pools 1 to 30 from the Arabidopsis Knockout Facility using *AtNramp5* forward and T-DNA specific primers. Lane 31 shows a control PCR performed using *AtNramp5* forward, *AtNramp5* reverse and the T-DNA primers giving a 2.2Kb sized band which is the correct size for the genomic sequence of *AtNramp5*.

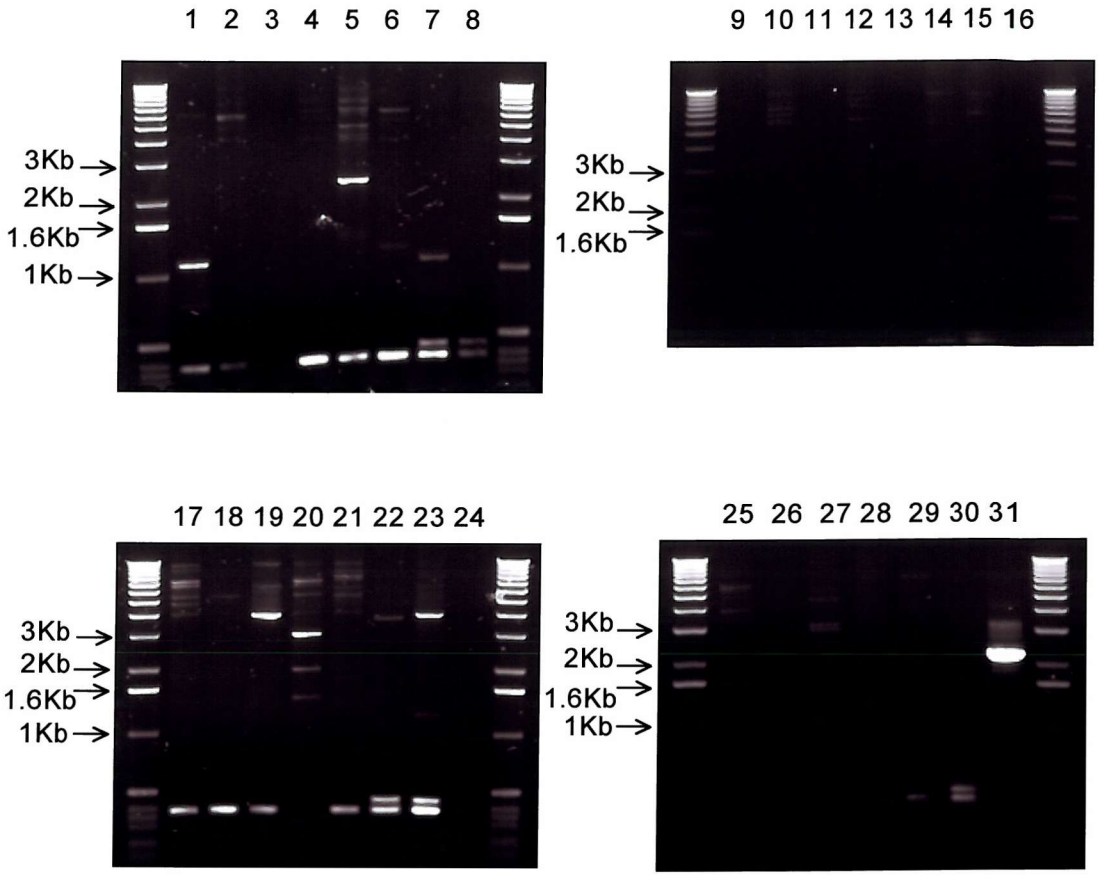

Fig. 6.6. Gel electrophoresis of PCR performed on super pools 1 to 8 from the Arabidopsis Knockout Facility using *AtNramp5* reverse and T-DNA specific primers. Lane 31 shows a control PCR performed using *AtNramp5* forward, *AtNramp5* reverse and the T-DNA primers giving a 2.2Kb sized band, which is the correct size for the genomic sequence of *AtNramp5*.

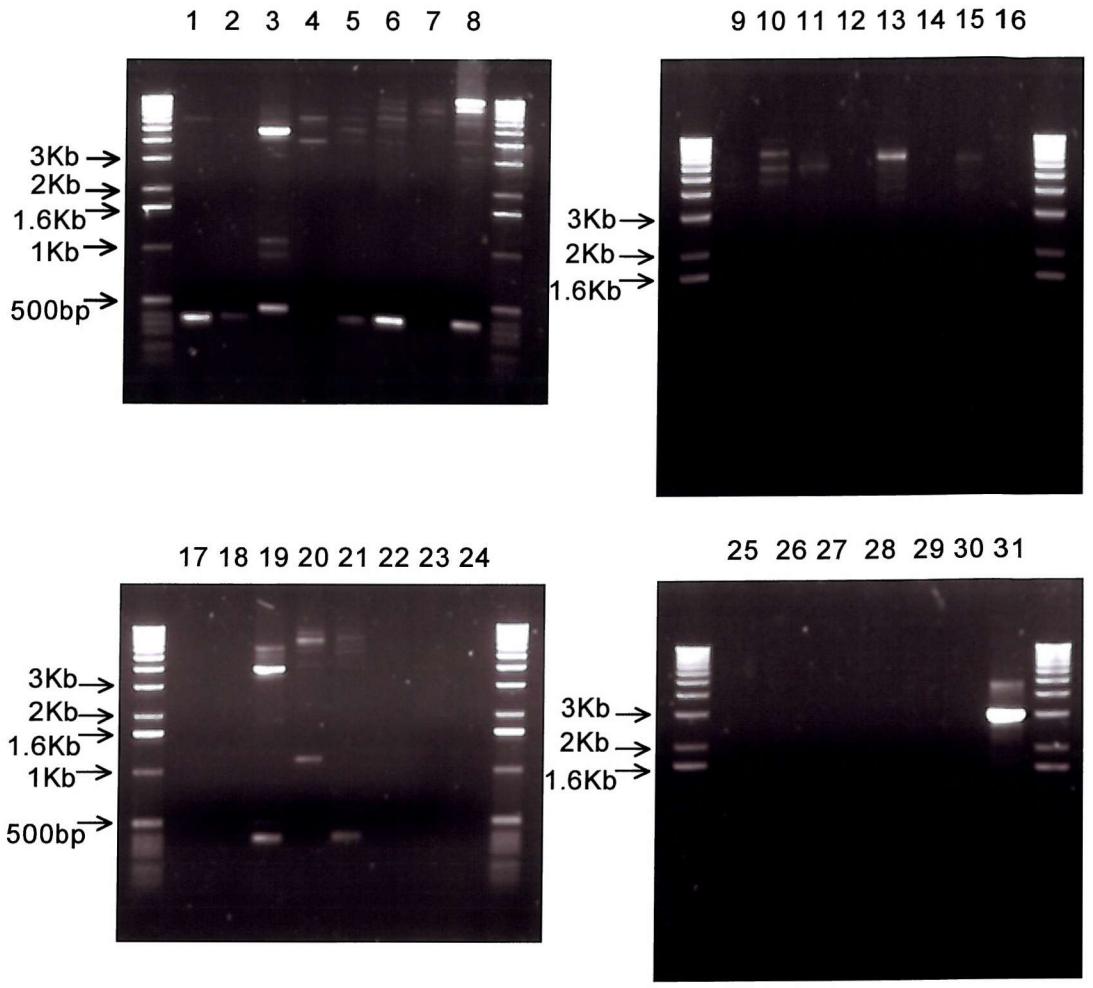

Fig. 6.7. Gel electrophoresis of PCR performed on super pools 1 to 30 from the Arabidopsis Knockout Facility using *AtNramp6* forward and T-DNA specific primers. Lane 31 shows a control PCR performed using *AtNramp6* forward, *AtNramp6* reverse and the T-DNA primers giving a 3Kb sized band which is the correct size for the genomic sequence of *AtNramp6*.

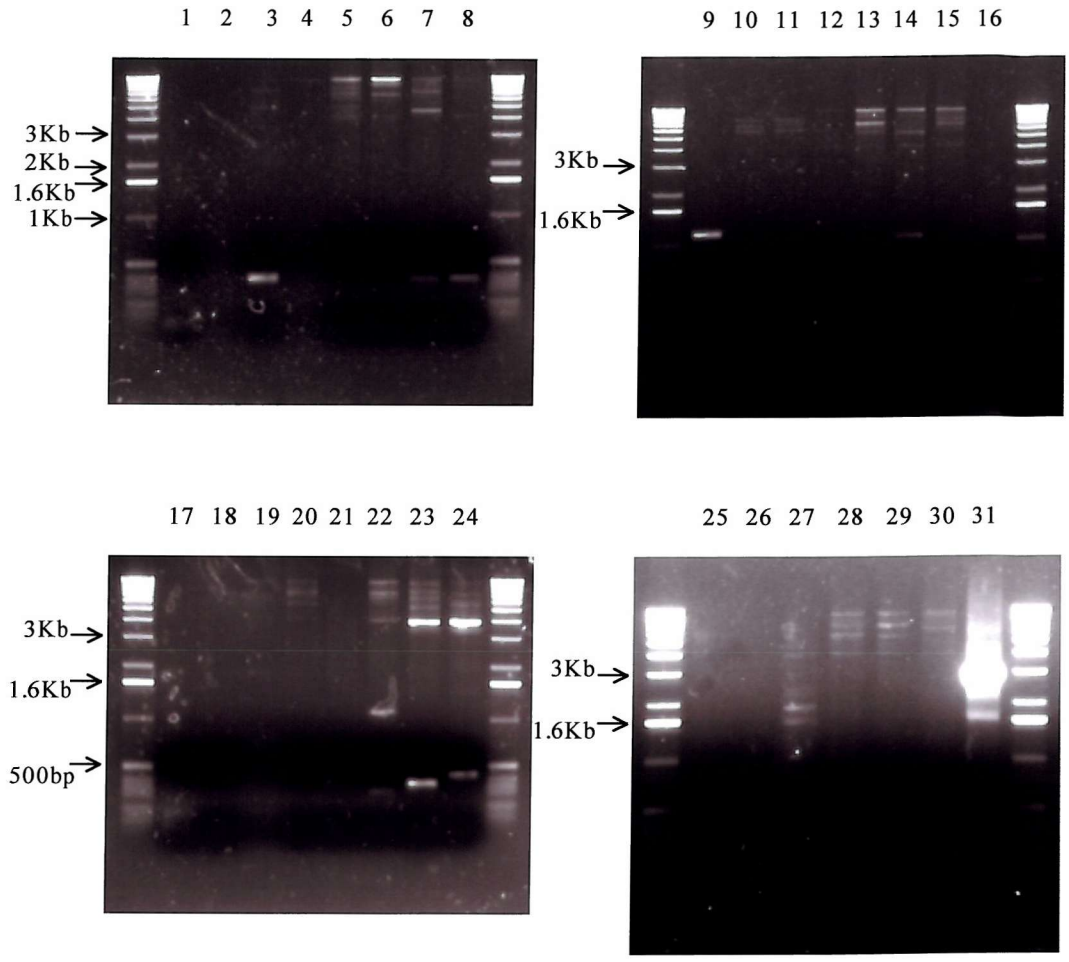

Fig.6.8. Gel electrophoresis of PCR performed on super pools 1 to 30 from the Arabidopsis Knockout Facility using *AtNramp6* reverse and T-DNA specific primers. Lane 31 shows a control PCR performed using *AtNramp6* forward, *AtNramp6* reverse and the T-DNA primers giving a 3Kb sized band, which is the correct size for the genomic sequence of *AtNramp6*.

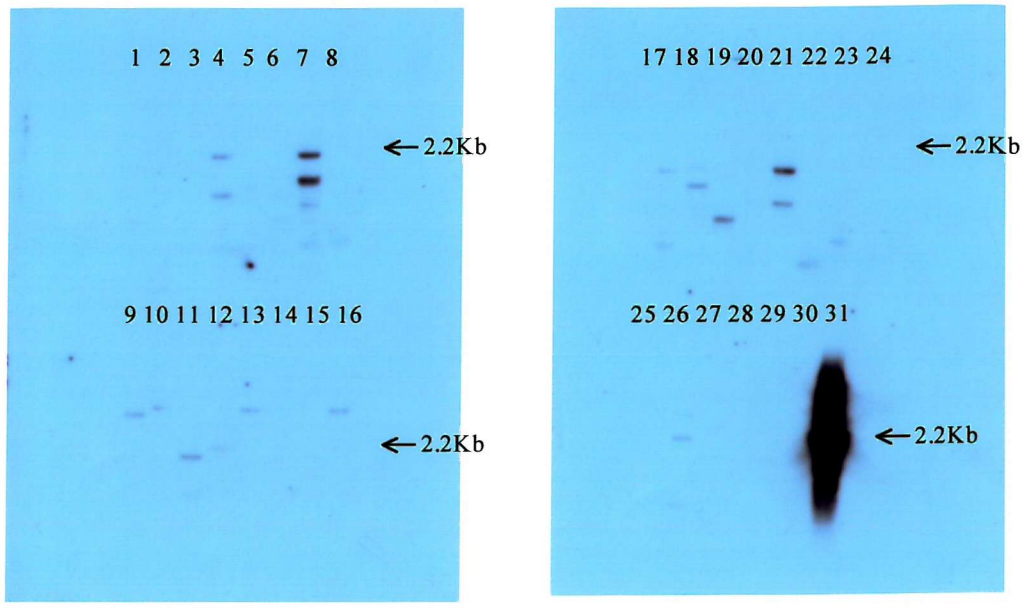

Fig. 6.9. Membranes hybridised with digoxygenin labelled probe to *AtNramp5*. *AtNramp5* forward primer PCR reactions performed by the Wisconsin facility were transferred to the membranes. Kodak X-ray film was exposed for 15h.

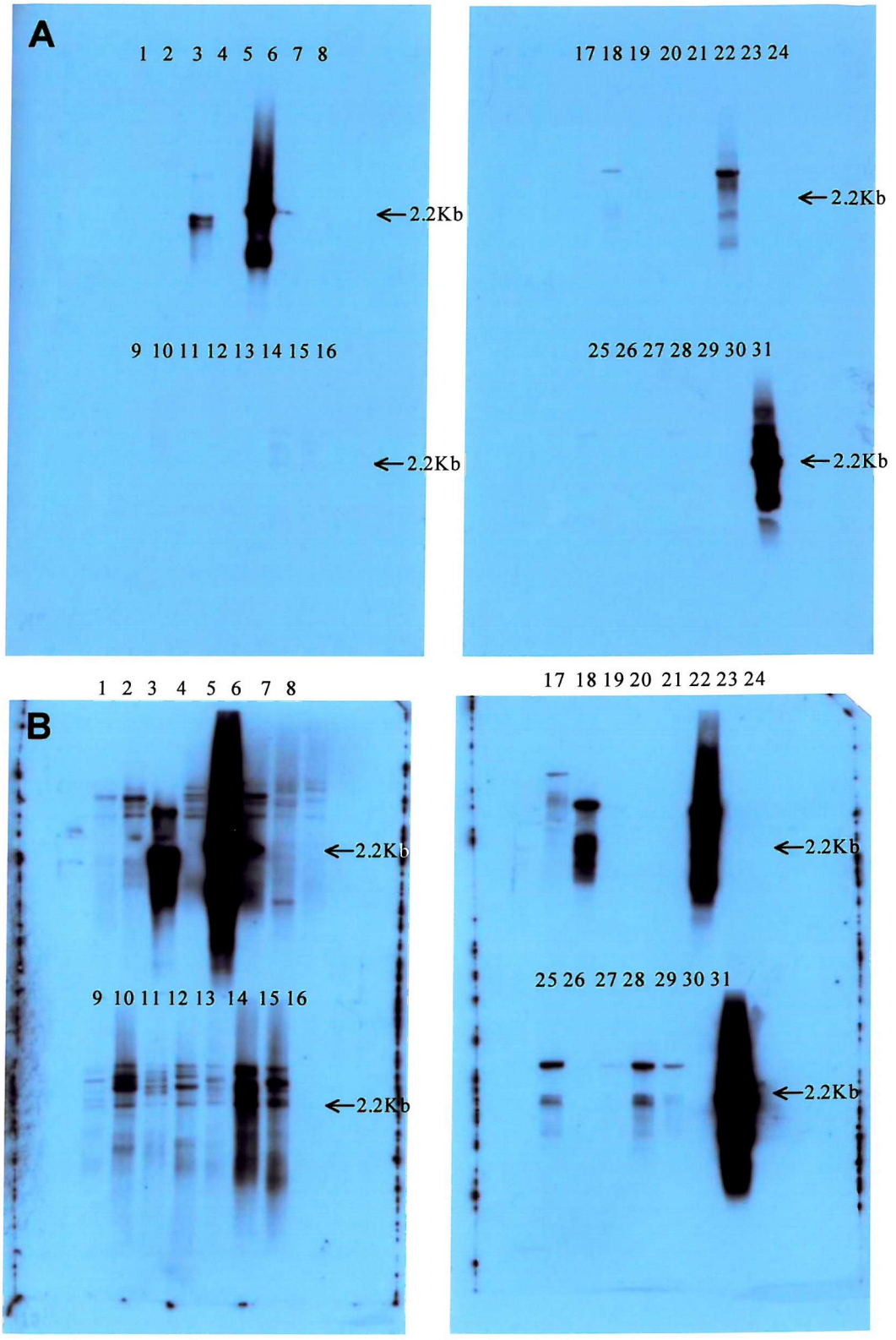

Fig. 6.10. Membranes hybridised with digoxygenin labelled probe to *AtNramp5*. *AtNramp5* reverse primer PCR reactions performed by the Wisconsin facility were transferred to the membranes. **A**: Kodak X-ray film was exposed for 25 min. **B**: Kodak X-ray film was exposed for 15h.

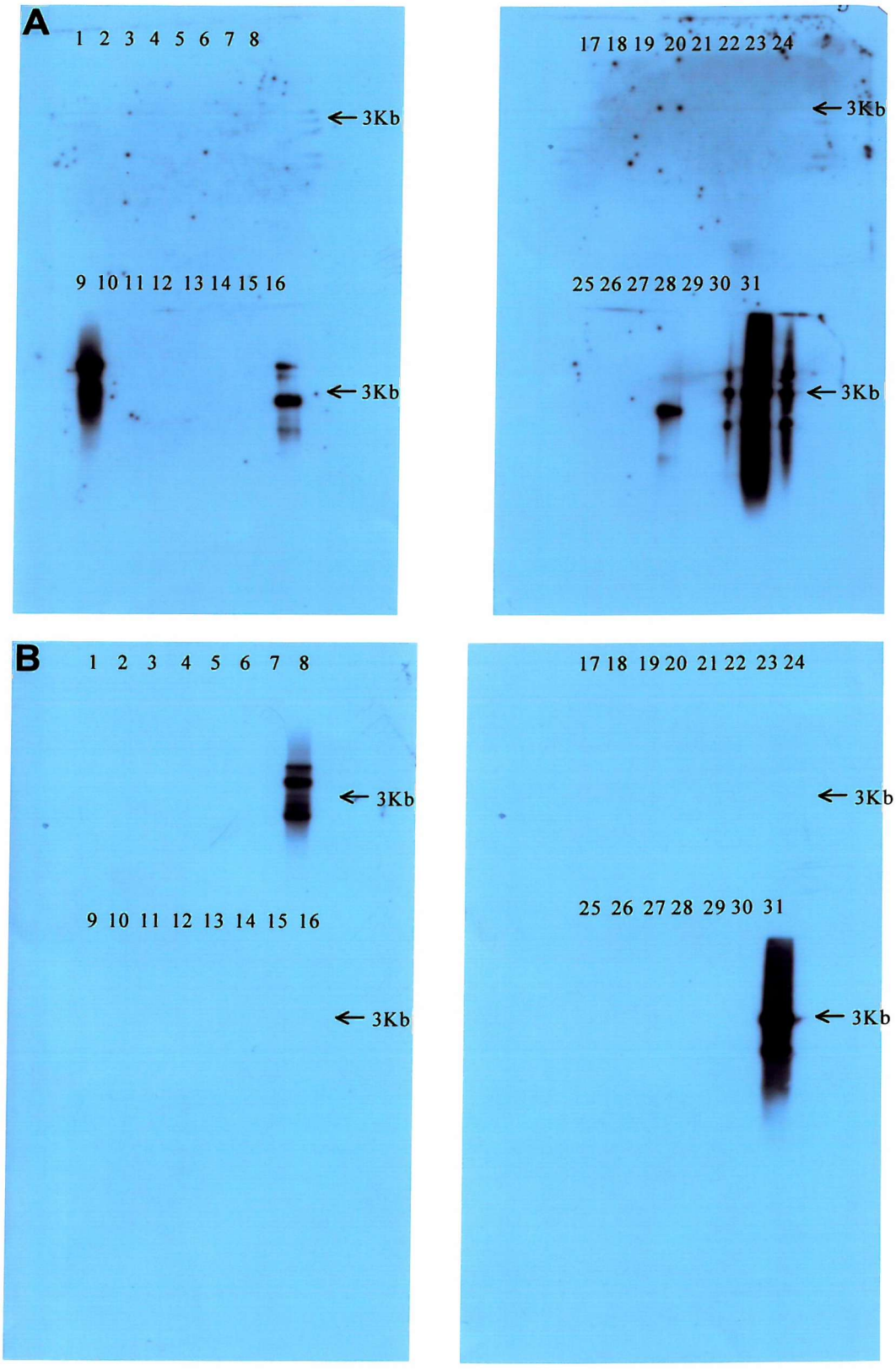

Fig. 6.11. **A**: Membranes hybridised with digoxygenin labelled probe to *AtNramp6. AtNramp6* forward primer PCR reactions performed by the Wisconsin facility were transferred to the membranes. Kodak X-ray film was exposed for 15h. **B**: Membranes hybridised with digoxygenin labelled probe to *AtNramp6. AtNramp6* reverse primer PCR reactions performed by the Wisconsin facility were transferred to the membranes. Kodak X-ray film was exposed for 5 mins.

Table.6.2. DNA fragments selected for gel extraction and sequencing after being identified as possible positives for containing T-DNA inserts. The approximate size of each band refers to the sizes identified using *AtNramp5* or *AtNramp6* specific digoxygenin probes to probe the PCR products from the Arabidopsis Knockout Facility at the University of Wisconsin.

Reaction primer	Super pool number	Approx. size of band gel extracted
AtNramp5 forward	4	1Kb
AtNramp5 forward	7	1.3Kb
AtNramp5 forward	19	800bp
AtNramp5 forward	21	1.1Kb
AtNramp5 forward	26	1.9Kb
AtNramp5 reverse	3	2Kb
AtNramp5 reverse	5	1.6Kb
AtNramp5 reverse	18	1.6Kb
AtNramp5 reverse	22	1Kb
AtNramp5 reverse	22	1.9Kb
AtNramp6 forward	9	2.5Kb
AtNramp6 forward	9	3Kb
AtNramp6 forward	16	2.5Kb
AtNramp6 forward	28	2.2Kb
AtNramp6 reverse	7	2.2Kb

AtNramp1, *2*, *3*, *4* and *5*. Sequence data supplied with each hit enabled the approximate location of the T-DNA to be identified to within 300bp (this allows for variation in the distance between the sequence obtained and the actual T-DNA itself.). These results are summarised for each line in Table 6.3. While many of the lines contain the T-DNA within the coding region of the *AtNramp* (for example the lines for *AtNramp1*, *4* and *5*) some of the lines have the T-DNA in the 5' untranslated regions or the promoter (*AtNramp2* and *3*).

6.2.2.2. Segregation analysis.

Table 6.4 summarises the data from segregation analysis performed on seed from each of the SALK lines obtained. Very few seeds were produced by the putative *AtNramp5* knockout lines and so these could not be used for segregation analysis. Each of the remaining lines appears to contain individual plants that are heterozygous and homozygous for the T-DNA insertion since some segregate in a 3:1 ratio or 75% survival (heterozygous parent) while others show approximately 100% survival (homozygous parent). None of the seed from the *AtNramp2* line survived on selection.

6.2.2.3. PCR analysis.

Fig.6.12 shows the results of PCR performed using *AtNramp5* gene-specific primers and the SALK left border primer LBb1 on genomic DNA extracted from six individual plants of the SALK N616205 line. PCR using the *AtNramp5* gene-specific primers produces genomic sized bands in only four of the plants (lanes 4 to 7) while PCR using the *AtNramp5* forward primer and the SALK LBb1 primer result in only a 450bp band being amplified. This product is known to occur when using the LBb1 primer on wild-type genomic DNA with certain *Taq* polymerases and does not indicate the presence of the T-DNA itself (http://signal.salk.edu/tdna_FAQs.html). However, a band of approximately 1.4Kb is produced when using the *AtNramp5* reverse and SALK LBb1 primers from genomic DNA of one of the plants (Lane 1 in Fig.6.12 C). As noted above, two of the genomic preparations gave no wild-type sized band with the

Table 6.3. Summary of *AtNramp* insertion mutant lines from the SALK facility. SALK and Nottingham Arabidopsis Stock Centre (NASC) codes are given, along with the % identity of the T-DNA border sequence with each *AtNramp* sequence. The proposed location of each T-DNA insertion was calculated on the basis of where the obtained sequence aligned to each gene, but the actual position may vary by up to 300bp from the positions given here.

AtNramp1 At1g80830			
SALK No.	**NASC code**	**% KO seq ID**	**Proposed location of SALK seq**
SALK_053236.56.00	N553236	100 (404bp)	Exon 9 pos 1881 after ATG (gen DNA seq)
SALK_053226.50.90	N553226	97.9 (327bp)	Exon 9 pos 1954 after ATG (gen DNA seq)
AtNramp2 At1g47240			
SALK No.	**NASC code**	**% KO seq ID**	**Proposed location of SALK seq**
SALK_027921.38.35.x	N527921	56 (48/86)	5' UTR 187bp before ATG (gen DNA seq)
AtNramp3 At2g23150			
SALK No.	**NASC code**	**% KO seq ID**	**Proposed location of SALK seq**
SALK_056666.41.15	N556666	99 (242bp)	Promoter 721bp before ATG
SALK_023049.45.35	N523049	100 (459bp)	Promoter 379bp before ATG
AtNramp4 At5g67330			
SALK No.	**NASC code**	**% KO seq ID**	**Proposed location of SALK seq**
SALK_003737.40.60	N503737	100 (460bp)	Exon 3 pos 1319 after ATG (gen DNA seq)
SALK_085986.35.95	N585986	95 (243bp)	Intron 1 pos 634 after ATG (gen DNA seq)
AtNramp5 At4g18790			
SALK No.	**NASC No.**	**% KO seq ID**	**Proposed location of SALK seq**
SALK_109028.41.90	N609028	100 (28bp)	Exon 1 pos 64 after ATG (gen DNA seq)
SALK_116205.16.55.n	N616205	89 (176/197)	Intron 1 pos 644 after ATG (gen DNA seq)

Table 6.4. Summary of segregation analysis of *AtNramp* insertion mutant plants from SALK. A minimum of 100 seeds were used from each plant and the results converted to percentage survival compared to the total number of seeds plated and to the total number of seeds germinating.

gene	line/plant	surviving as % of germinated	surviving as % of total
AtNramp1	N553226 no1	0	0
	N553226 no2	73	61.3
	N553226 no3	75	46.6
	N553226 no4	0	0
	N553226 no5	98.6	63.6
	N553236 no1	75.3	66.3
	N553236 no2	76.7	55
	N553236 no3	79.8	68
AtNramp2	N527921 no1	0	0
	N527921 no2	0	0
	N527921 no3	0	0
	N527921 no4	0	0
	N527921 no5	0	0
AtNramp3	N556666 No.1	67.5	90.3
	N556666 No.2	74.7	78.1
	N556666 No.3	93.8	95.1
	N556666 No.4	97.4	100
AtNramp4	N503737 no1	0	0
	N503737 no2	0	0
	N503737 no3	56.6	25.9
	N503737 no4	87.2	36.9
	N585986 no1	100	79.3
	N585986 no2	82.1	64.5
	N585986 no3	0	0
	N585986 no4	100	88.9
	N585986 no5	100	100

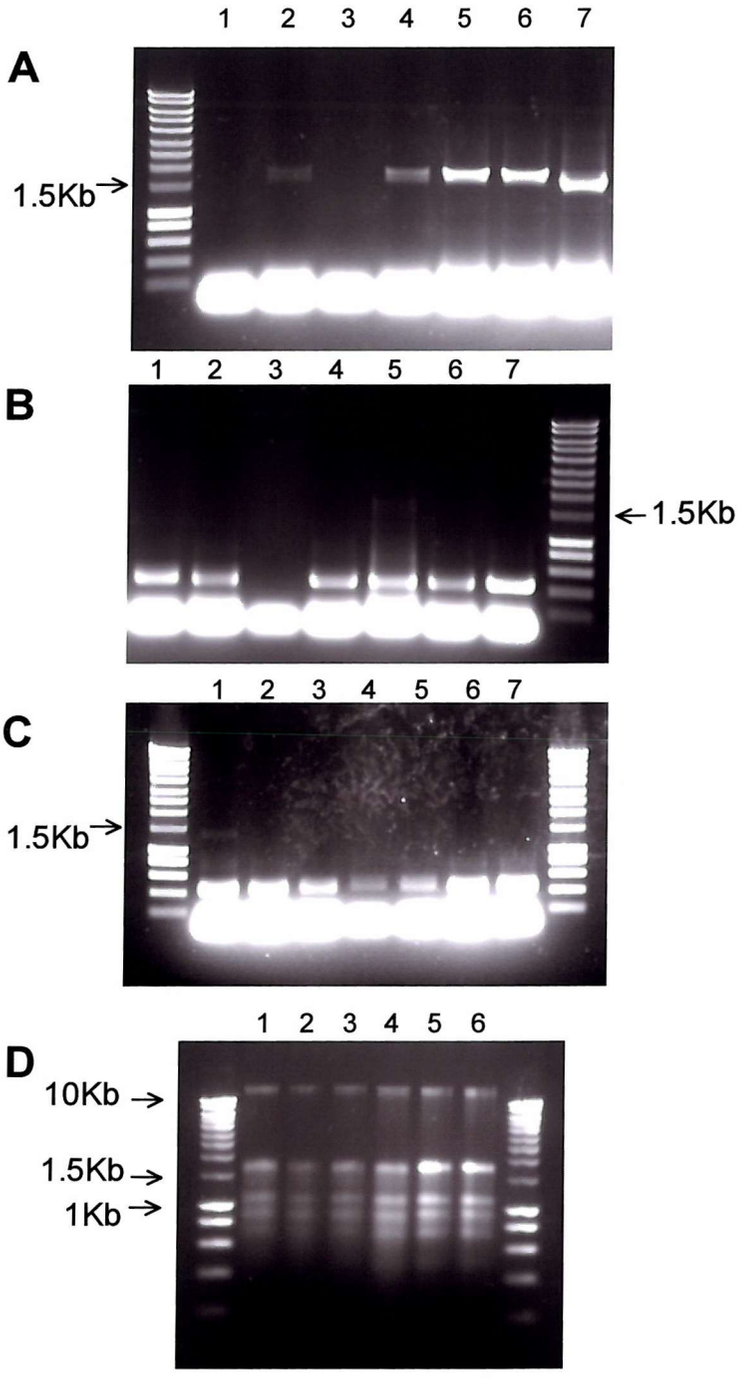

Fig. 6.12. Gel electrophoresis of PCR products using *AtNramp5* gene-specific primers and the SALK LBb1 left border T-DNA primer on genomic DNA extracted from SALK N616205 plants (lanes 1 to 6). These primer combinations used on Col 0 wild type genomic DNA are shown in lane 7. **A**: PCR using both *AtNramp5* forward and reverse gene specific primers, **B**: PCR using the *AtNramp5* forward and SALK LBb1 primers, **C**: PCR using the *AtNramp5* reverse and the SALK LBb1 primers. **D**: Gel electrophoresis of genomic DNA extracted from six plants of the putative *AtNramp5* knock-out SALK line N616205. Intact gDNA is visible in all preparations above the 10Kb marker. Other bands around 1 - 2Kb represent RNA.

AtNramp5 gene-specific primers. Preparation 1 (lane 1 in Fig.6.12 A) is one of these two, which suggests that this plant may be homozygous for the insertion and contain no wild-type copy of *AtNramp5.* However, at this stage it is impossible to know whether this plant is homozygous or heterozygous since the PCR may simply have failed in this case.

6.2.3. GABI-kat insertion lines.

6.2.3.1. GABI-kat database searches.

Putative AtNramp insertion mutants were located within the GABI-kat database by searching using the protein entry codes for each *AtNramp*. Five of the *AtNramps* were identified as containing a T-DNA, each with one or more insertion events: *AtNramp1*, *2*, *3*, *4* and *6*. This data is summarised graphically in Fig.6.13. In the absence of segregation data it is assumed that each line contains only one insertion event. This means that for some of the *AtNramps* there is more than one line, labelled on Fig.6.13 above each sequence. The colour of each label for each insertion point indicates how well the sequence obtained from the T-DNA border aligns with the genome sequence in that location. This gives an idea of how likely it is that the T-DNA is in the gene indicated, the lower the value, the better the hit. *AtNramp2*, *4* and *6* each have lines that contain T-DNA insertion events with sequence data that aligns strongly to the respective genes. For *AtNramp1* there are two lines with good hits and one more with a lower sequence identity. For *AtNramp3* there are two lines, both with moderate sequence alignments. Since insertion mutant lines for *AtNramp1*, *2*, *3* and *4* were already obtained from SALK only the *AtNramp6* GABI-kat mutant line 550D06 was ordered.

6.2.3.2. Segregation analysis.

Seed from the *AtNramp6* GABI-kat insertion line 550D06 were first plated onto standard MS media in order to bulk up the number of seed available for this line. Of 12 seeds plated only 3 germinated and survived with only 2 of these producing seed.

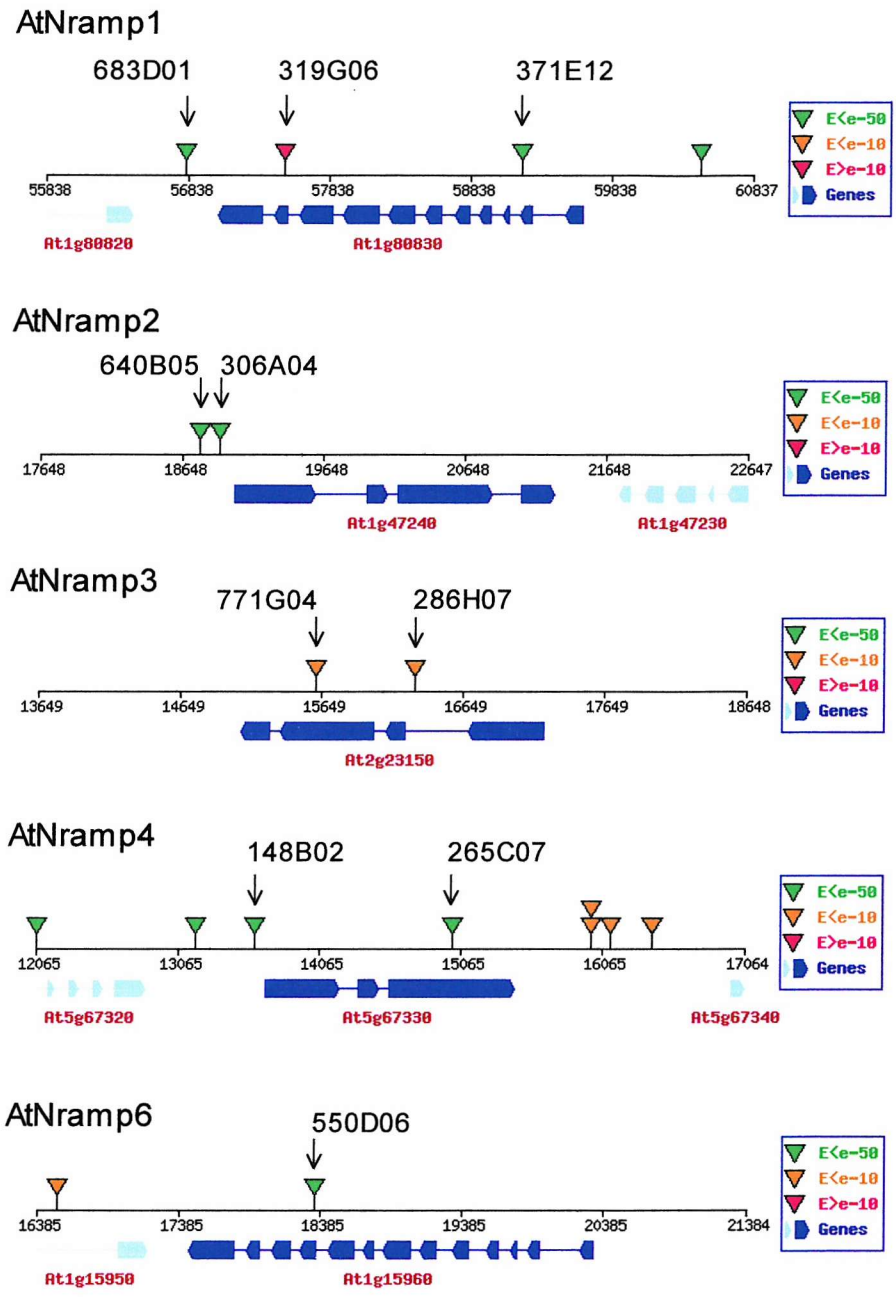

Fig. 6.13. Graphical summary of *AtNramp* genes with T-DNA insertions from the GABI-Kat database. Line codes are given above each insertion. The colour of each insertion indicates the identity between the sequence obtained from the T-DNA borders and the gene sequence when aligned using BLAST. Adapted from GABI-kat simple search results obtained by searching with AtNramp protein entry codes (http://mpiz.koeln.mpg.de/GABI-Kat).

Seed from these two plants was then plated onto MS media with sulfadiazine for selection. 100% survival of seedlings was observed in seed from plant 1 while 90% survival was observed in seed from plant 2. Prior to sending the order, the GABI-kat facility confirmed the presence of the T-DNA insertion in the predicted position within *AtNramp6* and performed a single segregation experiment with 50 seeds from the 550D06 line. Their results were similar in that only 7 seeds of a batch of 50 germinated but all 7 survived the selection. From this data the GABI-kat facility suggested that the line gives a 100% survival ratio indicative of the presence of two or more insertion events within the genome.

6.2.4. Over-expression of *AtNramp5.*

6.2.4.1. Verification of presence of pBECKS/*AtNramp5* construct.

Arabidopsis thaliana Col 0 plants transformed with pBECKS/*AtNramp5* were prepared previously in the lab and one plant was shown to be homozygous for the pBECKS/*AtNramp5* DNA (Biggs and Williams, unpublished). This plant was designated "1b". Two other plants also showed resistance to the selection designated "1f" and "2a". Seed from these plants were grown and genomic DNA extracted. PCR was then performed using gene-specific primers to *AtNramp5.* The gel electrophoresis of these PCR products is shown in Fig.6.14. The correct sized band is amplified from the cDNA control (lane 9) at 1.6Kb. A band at 2Kb is amplified from the genomic DNA control (lane 10). PCR performed on the genomic DNA from plants transformed with pBECKS/*AtNramp5* results in both of these bands being amplified in the same sample suggesting that the pBECKS/*AtNramp5* construct is present in plants 1b, 1f and 2a (lanes 3&4, 5&6 and 7&8 respectively). A slightly smaller band at approximately 1.5Kb is also amplified from some of the samples. One of the pBECKS empty vector transformed plants also amplifies bands at similar sizes to *AtNramp5* cDNA and genomic DNA.

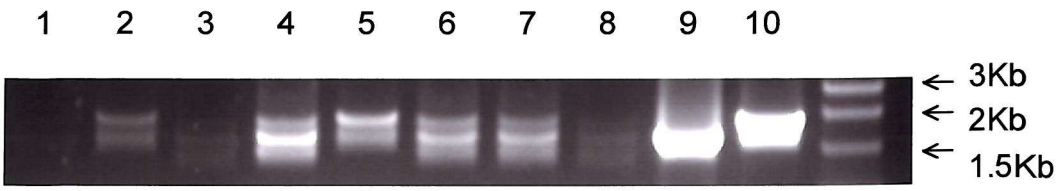

Fig. 6.14. Gel electrophoresis of PCR performed on genomic DNA from plants transformed with *AtNramp5*/pBECKS. 1&2: Col 0 pBECKS (6a) genomic DNA, 3&4: Col 0 pBECKS/*AtNramp5* (1b) genomic DNA, 5&6 Col 0 pBECKS/*AtNramp5* (1f) genomic DNA, 7&8: Col 0 pBECKS/*AtNramp5* (2a) genomic DNA, 9: PCR performed on NEV N/*AtNramp5* as a cDNA sized control, 10: PCR performed on Col 0 WT genomic DNA.

6.2.4.2 Growth of seedlings on Fe and Cd.

Initially, Col 0, Col 0 pBECKS/*AtNramp5* (1b), Col 0 pBECKS/*AtNramp5* (1f) and Col 0 pBECKS/*AtNramp5* (2a) *Arabidopsis* seedlings were analysed for growth on standard MS agar plates, plates with 50 μM FeEDTA or plates with 100 μM ferrozine. The fresh and dry weights of these seedlings after 10 d of growth are shown in Fig.6.15. While Col 0 and Col 0 pBECKS/*AtNramp5* (1b) plants show very slight growth improvements on FeEDTA and ferrozine, the other two pBECKS/*AtNramp5* transformed seedlings show reduced weights compared to standard MS media. This effect is more pronounced in Col 0 pBECKS/*AtNramp5* (1f) seedlings. This experiment was performed again, this time including Col 0 pBECKS (6a) seedlings as a transformation control. The data from this experiment is shown in Fig.6.16. This time, little difference in weight is seen between the seedlings and the treatments except for Col 0 pBECKS/*AtNramp5* (1f) seedlings which were again larger when grown on ferrozine but smaller on FeEDTA than when plated on standard MS. The Col 0 pBECKS (6a) seedlings also seem to follow this pattern but to a lesser degree. Seedlings were then plated onto MS media with a higher concentration of FeEDTA of 600 μM. The results of this experiment are shown in Fig.6.17. This time an extra Col 0 pBECKS empty vector control was added (6e). All of the seedlings showed extremely reduced growth at 600 μM FeEDTA compared to 50 μM or zero FeEDTA but there were no obvious differences between the potential over-expressing lines and the control seedlings. The seedlings were also grown on plates with either 10 μM $CdSO_4$ or 25 μM $CdSO_4$. This data is shown in Fig.6.18. Growth on $CdSO_4$ at either concentration was reduced compared to standard MS by approximately the same degree. On standard MS the Col 0 pBECKS (6e) control seedlings seemed considerably larger than the others, which was not seen in the previous experiments. This excess growth was reduced to WT levels on $CdSO_4$ however.

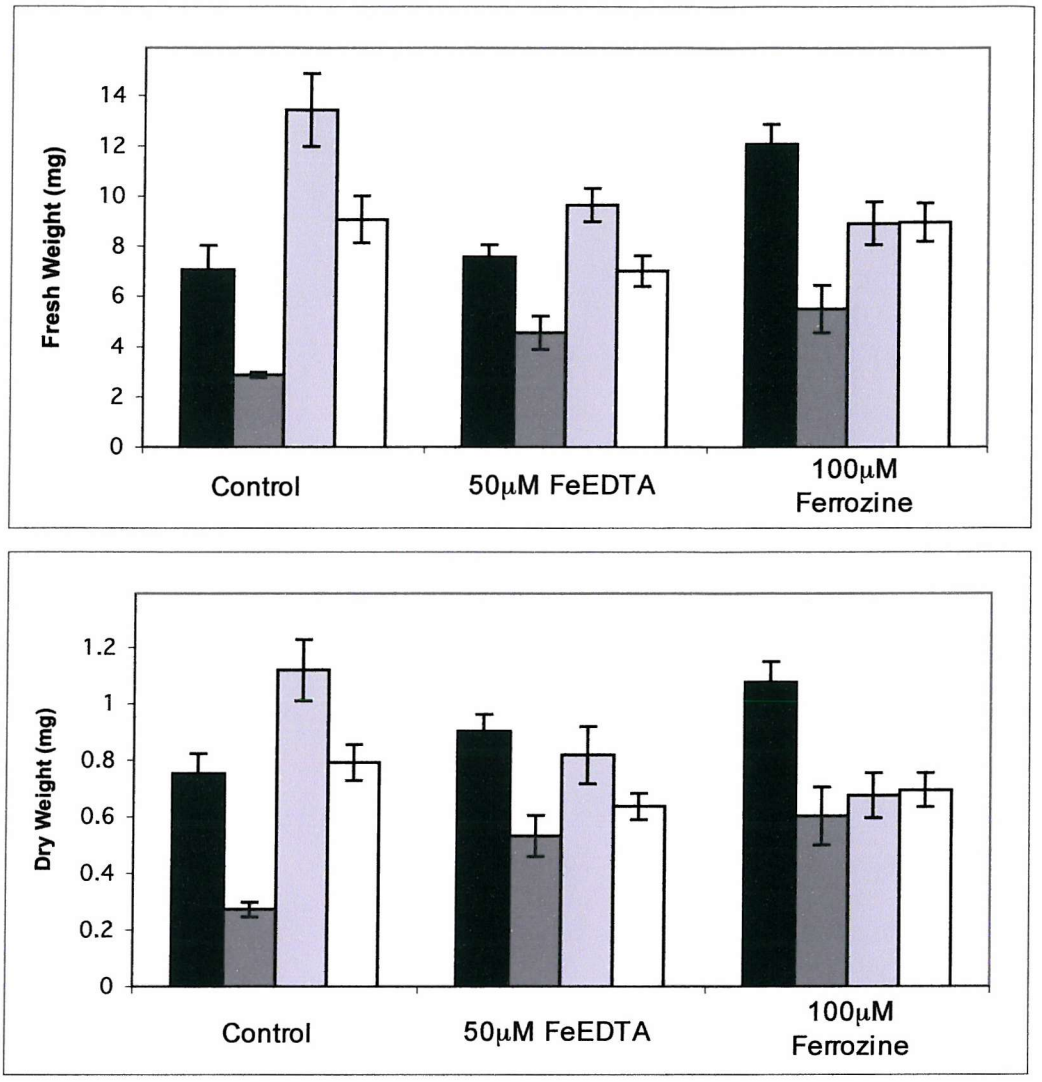

Fig. 6.15. Fresh and dry weights of 2 week old Col 0 *Arabidopsis* seedlings transformed with *AtNramp5*/pBECKS. Black: Col 0 untransformed. Dark grey: Col 0 *AtNramp5*/pBECKS 1b, Light grey: Col 0 *AtNramp5*/pBECKS 1f, White: Col 0 *AtNramp5*/pBECKS 2a. Control plants were grown on standard MS plates.

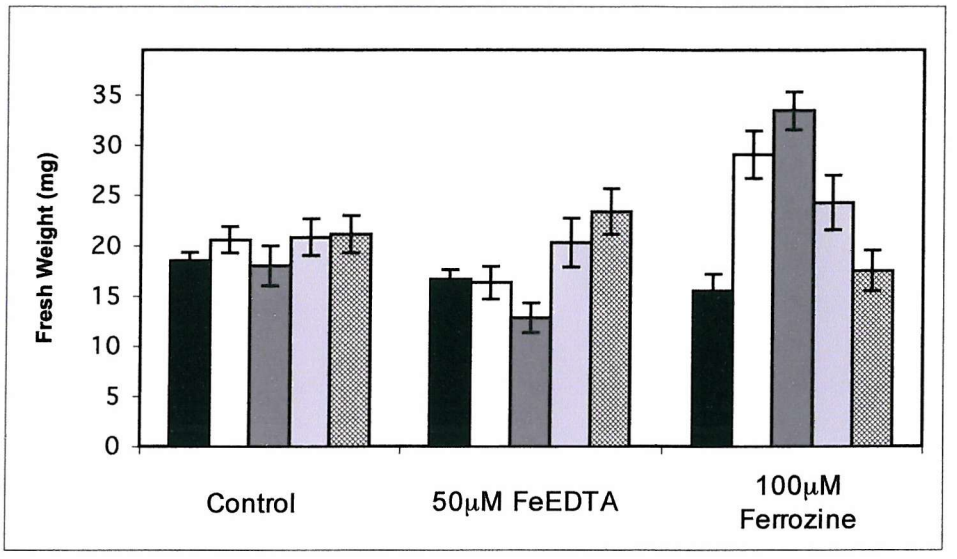

Fig. 6.16. Fresh weights of 2 week old Col 0 *Arabidopsis* seedlings transformed with *AtNramp5*/pBECKS. Black: Col 0 untransformed, White: pBECKS (6a), Dark grey: Col 0 *AtNramp5*/pBECKS (1f), Light grey: Col 0 *AtNramp5*/pBECKS (2a), Hatched: Col 0 *AtNramp5*/pBECKS (1b). Control plants were grown on standard MS plates.

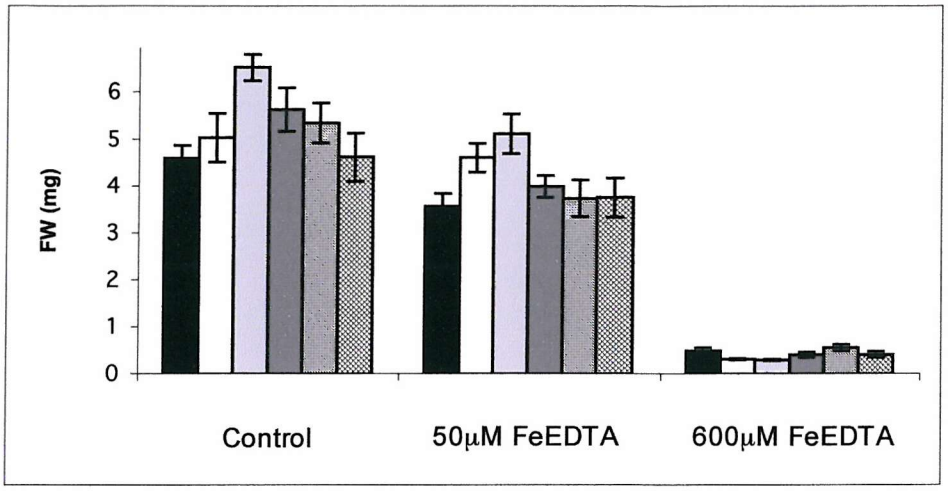

Fig. 6.17. Fresh weights of 2 week old Col 0 *Arabidopsis* seedlings transformed with *AtNramp5*/pBECKS. Black: Col 0 untransformed. White: Col 0 pBECKS (6a), Light grey: Col 0 pBECKS (6e), Dark grey: Col 0 *AtNramp5*/pBECKS 1b, Slashed: Col 0 *AtNramp5*/pBECKS 1f, Hatched: Col 0 *AtNramp5*/pBECKS 2a. Control plants were grown on standard MS plates.

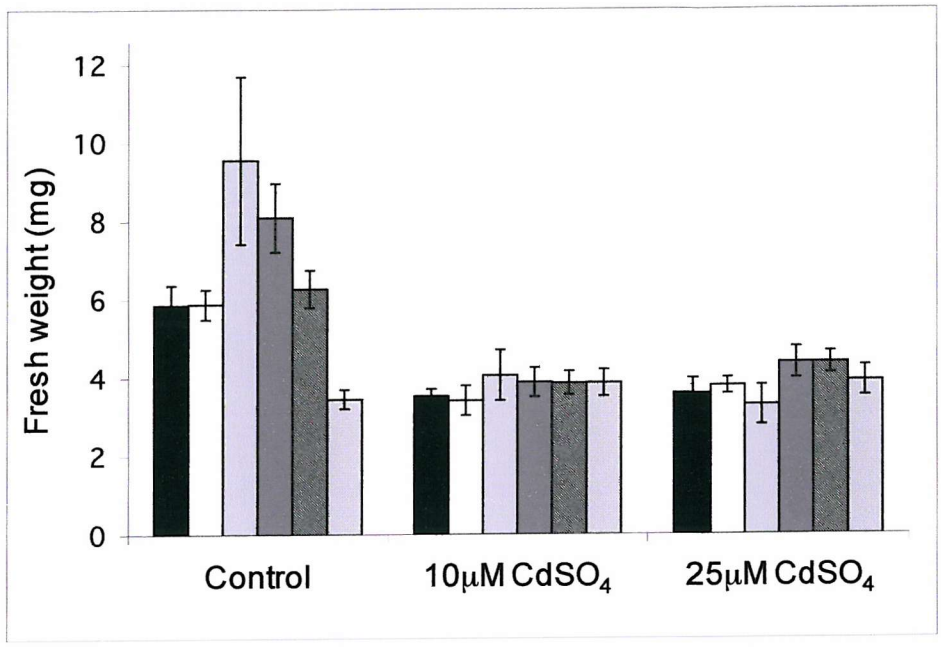

Fig. 6.18. Fresh weights of 2 week old Col 0 *Arabidopsis* seedlings transformed with pBECKS/*AtNramp5*. Black: Col 0 untransformed. Dark grey: Col 0 pBECKS 6a, Light grey: Col 0 pBECKS 6e, White: Col 0 pBECKS/*AtNramp5* 1b, Diagonal line: Col 0 pBECKS/*AtNramp5* 1f, Hatched: Col 0 pBECKS/*AtNramp5 2a*. Control plants were grown on standard MS plates.

6.3. Discussion.

The use of insertional mutants in the study of gene function has been widely exploited in animal and micro-organism systems but the large number of individual lines required has only relatively recently become available in plants such as *Arabidopsis thaliana.* The larger the number of lines screened the greater the chance of finding a T-DNA insertion in the gene of interest. Digoxygenin-labelled probes to the genomic sequences of *AtNramp5* and *AtNramp6* were generated in order to probe the PCR samples returned from the Arabidopsis Knockout Facility at the University of Wisconsin. The specificity of these probes was tested against different sequences and although they hybridised strongly to the correct sequences there was some indication that they may also hybridise with other, closely related DNA sequences. This presents a problem since the Nramp family in *Arabidopsis* is highly conserved at the DNA level. Although the *AtNramp5* probe did not hybridise to the *AtNramp6* genomic DNA sequence and vice versa, the *AtNramp5* probe did hybridise to the *AtNramp3* cDNA sequence. Since *AtNramp2*, *3, 4* and *5* are quite closely related it is possible that the *AtNramp5* probe is unable to distinguish between some or all of these genes. This means that any positive pools identified by digoxygenin-labelled probes must first be confirmed as positives by sequencing before proceeding with the second round of PCR-based screening.

Although some positive pools have been identified by digoxygenin probing of the PCR products, sequencing these products has so far proven to be unsuccessful with almost no readable sequence and large regions of unresolvable bases. The sequence obtained after gel extraction and purification of the positive PCR products, and the subsequent re-amplification of these products by PCR, is still of low quality, possibly due to the presence of multiple sequences or contaminated template. Cleaning up the products before sequencing has made no improvement on the sequence obtained however. It is possible that the re-amplification by PCR of the positive products following gel extraction is generating unwanted products, which in turn prevent successful sequencing. The re-amplification step was introduced due to the low yields obtained after gel extraction. In all cases it seems the yields were too low to sequence from directly since no signal was detected after sequencing. It may be necessary to

run more of the initial PCR products on an agarose gel so that yields will be higher following gel extraction and allow sequencing to be performed without re-amplification. It may also be possible that two or more DNA fragments of almost the same size are being amplified and then gel extracted from the first round of PCR performed by the *Arabidopsis* Knockout Facility. This could also result in sequencing being unsuccessful due to the presence of multiple sequences. However, this does not seem a likely explanation since a number of different DNA fragments from different pools have failed to produce any readable sequences and it is unlikely that multiple fragments of the same length but of different sequence would be produced in all the various reactions performed using both *AtNramp5* and *AtNramp6* primers. The data presented here does suggest the possibility that there are insertion events in *AtNramp5* and *AtNramp6* within the Wisconsin lines but further work will be required in order to be certain.

A number of lines have been identified in the SALK database of insertional mutants that contain T-DNA insertions within members of the *AtNramp* family. Of these, the two lines with insertions in *AtNramp5* are the most important for this work. Segregation analysis of these lines has proved to be difficult in the light of few seed being produced by these plants. However, genomic DNA extraction and PCR using gene-specific and T-DNA left border primers does suggest that the T-DNA is present and, since amplification was only achieved with the gene-specific reverse primer, that the T-DNA is in the orientation suggested by the SALK sequencing facility. The lack of a WT-sized product in this PCR suggests that the plant used for the extraction is homozygous but it is impossible to rule out other factors contributing to the failure of the PCR. Further PCR and segregation analysis will be required to ascertain this before these plants can be used in studying the phenotype of this potential knock-out. The lack of seed production from these plants could possibly be an effect of loss of function of *AtNramp5*, since it is expressed in the flowers but without knowing whether these plants were heterozygous or homozygous it is difficult to draw conclusions from this observation. It is also possible that any loss of function of *AtNramp5* may be masked by the activity of other members of the *AtNramp* family so further work with multiple knock-outs in the same individual may be required. However, an insertion in *AtNramp3* has been shown to give enhanced resistance to Cd (Thomine *et al.*, 2000) and an increased accumulation of Mn and Zn under Fe deficiency (Thomine *et al.*,

2003) so individual AtNramps can have a particular function not shared with the other Nramps. Of the other lines from SALK, heterozygous and homozygous individuals have been identified for insertions within *AtNramp1*, *3* and *4*. However, it would still be useful to check the insertions by PCR to ascertain more precisely where the T-DNA is located and therefore understand how effective the knockout could potentially be. The *AtNramp2* line showed no survival when selected for the resistance marker suggesting one of two possibilities: either the T-DNA is not present in the plants supplied from this line or silencing of the resistance marker gene has occurred, a phenomenon that SALK report in the FAQ section on their website. As with the other lines, further investigation using PCR methods is necessary to ascertain whether the T-DNA is present or not.

A number of lines have also been identified in the GABI-Kat database of insertional mutants with T-DNA insertions in *AtNramp1*, *2*, *3*, *4* and *6*. Seedlings from the *AtNramp6* line (550D06) all show resistance to the sulfadiazine selection, which would suggest that these are homozygous for the insertion. However, seed supplied from GABI-kat should be from a T2 segregating pool and should give nearer to a 3:1 ratio of survival (75% surviving). This raises the question as to whether there is a second (or more) T-DNA insertion within the genome of plants from this line. If a second T-DNA were present then the segregation ratio would be closer to 14:1 (93.33% survival), which perhaps fits the observed segregation ratio better. A backcross to a WT plant would be required in order to segregate out any secondary insertions.

Data is also presented here for the fresh weights of seedlings containing an over-expression construct of *AtNramp5* grown on media with varying Fe or Cd concentrations. Curie *et al.* (2000) showed that over-expression of AtNramp1 led to increased resistance to normally toxic Fe concentrations (600 μM). Thomine *et al.* (2000) have shown that over-expression of *AtNramp3* results in Cd hypersensitivity and increased Fe uptake and more recently showed that it down-regulates Mn accumulation and the expression of *IRT1* and *FRO2*, genes involved in Fe acquisition (Thomine *et al.*, 2003). The data for the potential *AtNramp5* over-expressing plants shows no obvious differences between these plants and WT on low or high Fe concentrations or on Cd. The seedlings do not seem to be sensitive to Cd or resistant to high Fe concentrations when compared to Col 0 wild-type seedlings. This is not

altogether unexpected considering the expression profile for *AtNramp5*. Being expressed only in flowers suggests that it may not be functional at earlier developmental stages or may require other factors to be present that may not be produced in other tissues or at the seedling stage of development. It is also possible that other members of the *Nramp* family are altered in their expression profiles in these plants, masking any effects of over-expression of *AtNramp5*. Of course, it may turn out that AtNramp5 is not involved in the transport of Fe or Cd within the plant but is required for some other function. Further checks, such as performing RT-PCR or northern analysis on these plants, are still required to show that *AtNramp5* is being over-expressed and that other *Nramps* (or *IRT1*) are being expressed normally before these questions can be addressed.

Chapter 7. General Discussion.

The genome of *Arabidopsis thaliana* contains at least six members of the Nramp family identified to date. They appear to be 12 transmembrane domain proteins of between 509 and 532 amino acids and contain a motif implicated in transport activity. The AtNramp sequences are highly similar to Nramps from other organisms leading to the hypothesis that they are also involved in transition metal transport and homeostasis. Evidence has already been accumulated that this is the case. Transport of Fe, Cd, Mn and Zn by AtNramp3 has been shown by Thomine *et al.* (2000, 2003). Phylogenetic analysis indicates that there may be a division in the Nramp family into two sub-groups. In the AtNramp family, AtNramp1 and 6 form one sub-group on the tree while AtNramp2, 3, 4 and 5 comprise a second sub-group. The data from yeast complementation studies suggests that the function of the AtNramps is not mirrored by their sub-groupings since *AtNramp1*, *AtNramp3* and *AtNramp4* all complement an Fe uptake deficient yeast mutant (Thomine *et al.*, 2000) and are expressed in same tissues. Also, *AtNramp5* is expressed in different tissues to *AtNramp2*, *3* and *4* and does not rescue the same yeast mutant despite falling in the same sub-group in the phylogenetic tree. *AtNramp3* is upregulated on Fe starvation but no changes are seen in the other *AtNramps* except *AtNramp6* in the stem. The expression pattern of *AtNramp1*, *2*, *3* and *4* suggests there may be some redundancy in the function of these proteins although this has not been verified and needs further investigation. Thomine *et al.* (2004) have reported a phenotype for *AtNramp3*/*AtNramp4* double knockout plants not observed in single knockouts, adding support to the theory that some of the *AtNramps* may encode functionally redundant proteins. Lending further support to this theory is the fact that both AtNramp3 and AtNramp4 reside in the tonoplast (Thomine *et al.*, 2003, Shimaoka *et al.*, 2004). Although the functional data does not indicate it, it is still possible that the two groups differ in some way not yet identified. For example, it is possible that although expressed at the mRNA level, AtNramps from the different groups may be regulated at the protein level in different ways, allowing their activity to be tailored to the nutrient status of the plant. This has not yet been investigated and so it is still not known whether the proteins follow the expression pattern of the mRNA or if post-translational regulation of protein stability or activity is taking place in some cases.

Uptake of radiolabelled Fe by *fet3/fet4* yeast transformed with *AtNramp3* or *AtNramp4* has been demonstrated previously by Thomine *et al.* (2000). The work presented here is in accordance with this previous work. However, the data presented here also suggests that, at least for AtNramp4, the uptake of radiolabelled Fe in these cells is dependent on the external pH being more acidic than the cytoplasm. This points to the hypothesis that AtNramp4 is a proton driven co-transporter of Fe. However, experiments using the protonophore, CCCP, were inconclusive and did not show a reduced uptake of Fe when CCCP was introduced. CCCP is not specific to the plasma membrane and can also disrupt proton gradients across other membranes, notably the mitochondrial membrane. The effects of this kind of change in the cells is not easily predicted and further experiments will be required in order to better interpret the result. It is also possible that Nramp4 function is dependent on the protein remaining in a certain conformation that is dependent on low pH but that its activity is not dependent on the proton gradient across the membrane. Some Fe uptake above that of controls was observed in *fet3/fet4* yeast transformed with *AtNramp5* but at a low level. Perhaps AtNramp5 requires other factors in order for it to be fully active or it does not have a high affinity for Fe and transports another cation in its normal role within the plant. The possibility of transport of other metals by the AtNramps seems likely. *AtNramp3* and *AtNramp4* both rescue Fe, Mn, Zn deficient yeast although *AtNramp5* and *AtNramp6* did not do so in the experiments presented here. Uptake with other radiolabelled metals such as Zn, Cd and Mn would give more detailed information and allow competition assays to be performed to identify the specificities for each. The human Nramp2 (DMT1) has also been shown to transport Cu (Tennant *et al.*, 2002). Transport of Cu by AtNramp4, AtNramp5 or AtNramp6 was not investigated in this work but would give more information since the specificity of the AtNramps for various metals has not yet been determined. The broad range of metals transported by AtNramp3 and AtNramp4 also reinforces the theory that they encode redundant proteins since if each AtNramp specifically transported a different substrate then their similar expression profiles would not be indicative of redundancy. Since they each seem to transport a broad range of metals and are expressed in the same tissues, there may well be an overlap in their functions. It is possible that certain environmental conditions not investigated here may trigger the activity of one of the Nramps and not others, reducing any overlap between them. The *AtNramps* may be expressed in all tissues but may not be functional in all of them or there may be more subtle

differences in their distribution not identified in these experiments using whole tissues. For example, IRT1 and IRT2 are both expressed in the roots, up-regulated upon Fe starvation and both complement Fe uptake deficient yeast indicating that they both transport Fe but it appears that they are not functionally redundant (Vert *et al.*, 2001). The authors suggested that the two proteins are expressed in different cell layers of the root and therefore do not necessarily share identical functions. This shows that uptake and homeostasis of Fe (and other metals) is a complex process and that genes with apparently identical expression patterns and functions can play different roles.

AtNramp5 did not rescue Fe, Mn or Zn uptake-deficient yeast mutants under the conditions tested. Radiolabelled uptake into Fe uptake-deficient yeast transformed with *AtNramp5* did indicate a low level of Fe uptake. This suggests that AtNramp5 is a transport protein but may require different conditions or a different substrate to *AtNramp3* and *4* in order to function. It was possibly not active enough to enable the yeast to grow without supplemental Fe on plates but enough to be detected using the radiolabelled Fe uptake assay. Seedlings over-expressing *AtNramp5* did not show any clear differences to wild type plants grown on high Cd or Fe as has been previously shown for *AtNramp3* (Thomine *et al.*, 2000). *AtNramp5* was detected in flowers by RT-PCR and quantitative PCR implicating AtNramp5 in the transport of metals specifically in flowers. Honys and Twell (2003) analysed the pollen transcriptome by using a microarray approach. While their work concentrated on the most highly expressed genes in mature pollen grains, the raw data from the microarray experiment shows that *AtNramp5* is among the list of transcripts present only in pollen (the male gametophyte tissues) of the flower. This suggests that AtNramp5 performs a highly specialised function needed only in this particular part of the plant, in providing metal transport to the developing pollen for example. It also raises the question as to what causes *AtNramp5* to be expressed in a specific tissue while *AtNramp2*, *3* and *4* are found throughout the plant even though they share a high degree of identity. The most obvious possibility is the presence of a particular motif located within the promoter causing expression only in pollen or a site in the 5' untranslated region that is recognised by other molecules to prevent degradation of the mRNA only in pollen.

AtNramp6 also did not rescue Fe, Mn or Zn uptake-deficient yeast mutants, although the result with Mn is not clear. *AtNramp6* seems to be expressed in above ground parts of the plant although the transcript may be expressed in roots but at low levels (it was undetectable in roots with RT-PCR but quantitative PCR shows some

amplification). *AtNramp6* seems to be up-regulated in stem following 72hrs treatment with ferrozine suggesting some role in Fe transport. The lack of functional complementation in yeast is not conclusive evidence that AtNramp6 cannot transport Fe in the plant. The significance of AtNramp6b is unclear. In mice two isoforms of Nramp2 are present, one of which contains an Iron Responsive Element (IRE) that the other does not (Tchernitchko *et al.*, 2002). The two isoforms differ in their subcellular localisation. The same arrangement is seen in monkey (Zhang *et al.*, 2000), human and rat Nramp2 (DMT1) (Hubert and Hentze, 2002); in each case one isoform contains the IRE while the other does not.

AtNramp6b seems to be expressed at a low level, which could perhaps represent a "leaky" splicing system where particular intron sequences are susceptible to being left in situ. The protein product of *AtNramp6b* cDNA is unlikely to produce a functional protein due to its truncated nature. Unlike *AtNramp6a*, *AtNramp6b* is not dramatically up-regulated in stem after 72h ferrozine treatment, which perhaps indicates that the signal is only affecting the correctly spliced *AtNramp6a* form. If *AtNramp6b* was solely a product of inefficient splicing then it would be logical that *AtNramp6b* should increase with increased *AtNramp6a* production. However, it is not strictly alternative splicing since almost the whole intron is left in place. Alternative splicing involves the production of two different mRNA sequences from the same gene by splicing out different parts of the sequence to give two functionally different proteins. In the case of AtNramp6b the protein is likely to be non-functional since it would not contain the consensus transport signature and only four transmembrane domains. It has been suggested that inefficient splicing does occur in a subset of genes in most plants so the situation with *AtNramp6* is not unique (Lorkovic *et al.*, 2000). It has been suggested that inefficient splicing of an intron can be controlled by polyadenylation, which could present a mechanism for controlling expression by leaving some introns in place, resulting in a non-functional protein. Macknight *et al.* (1997) observed that the occurrence of an intron remaining in the *FCA* gene increased greatly when it was over-expressed in *Arabidopsis* plants and suggested that polyadenylation in intron 3 of this gene was used to control levels of the fully spliced transcript to regulate flowering time. It is possible that a similar system is in place to regulate the activity of AtNramp6. An example of an Nramp undergoing post-translational regulation exists in yeast. The *BSD2* gene product is activated when the cell is Mn replete and causes the SMF1 protein to be degraded in the vacuole. When

the cell is Mn deficient BSD2 is switched off and its absence allows SMF1 to be targeted to the plasma membrane to allow uptake of Mn from the environment (Liu and Culotta, 1999). It is perhaps possible that some analogous system is present in plants although BLAST searches using the yeast BSD2 cDNA or protein sequence do not detect any homologous sequences within the Arabidopsis genome. However, other proteins, unrelated to BSD2 may be present so this scenario cannot be ruled out. If identified, this could represent a mechanism for giving the AtNramps tissue specific functions even when they are expressed in all tissues. The recognition event between BSD2 and SMF1 has not yet been elucidated so it is not possible to compare Arabidopsis and yeast sequences for any similarities that could hint at the presence of this type of post-translational regulation.

The data presented in this work adds further evidence to the hypothesis that the AtNramps are transport proteins with a broad metal specificity. Radiolabelled Fe uptake studies in yeast also suggest that at least AtNramp4 may be a proton driven transporter like the Nramps from mammals (Gunshin *et al.*, 1997, Goswami *et al.*, 2001). The expression pattern of the *AtNramps* shows that they are generally expressed in all tissues of the plant under metal replete and Fe deficient conditions with the exception of *AtNramp5*, which is expressed only in flowers, suggesting a function removed from that of the other Nramps in *Arabidopsis.*

Many key elements in plant metal uptake and distribution have now been identified (Fox and Guerinot, 1998, Guerinot, 2000, Williams *et al.,* 2000, Maser *et al.*, 2001, Hall and Williams, 2003). However, much still remains to be understood and there are a number of possible roles for the Nramps. In terms of Fe uptake, the principle mechanism of uptake in strategy I plants from the soil has been identified (in *Arabidopsis*) as the IRT1 protein, which functions in the uptake of Fe^{2+} following its reduction from the Fe^{3+} from by the ferric reductase FRO2 at the root cell epidermis (Eide *et al.*, 1996, Robinson *et al.,* 1999, Vert *et al.,* 2002). IRT1 has also been found in other plant species indicating that this is a common mechanism (Berecksy *et al.,* 2003). Reduction is aided by the acidification of the rhizosphere by the Arabidopsis H^+ ATPase 2 (AHA2). AtIRT2 has also been localised to the outer cell layers of the root subapical zone where it may also function in the uptake of Fe from the soil in tandem with AtIRT1 (Vert *et al.*, 2001). AtIRT2 does not replace the function of AtIRT1 however and seems to transport a more specific subset of metals compared to AtIRT1. Strategy II plants (the grasses) make use of phytosiderophores (such as mugineic

acid) synthesised from nicotianamine (NA) to chelate Fe^{3+} in the extracellular soil environment (Romheld and Marschner, 1986, Von Wiren *et al.*, 1999). The Fe-phytosiderophore or Fe-NA complex is then taken up by a specific transport protein, termed YS1 (Curie *et al.*, 2001, Roberts *et al.*, 2004).

Within the plant Fe is released from the phytosiderophore complex (Schmidt, 2003) and is generally transported in all plants within the xylem and phloem as a complex with specific molecules such as NA (predominantly in phloem) or citrate (xylem) (Briat *et al.*, 1995, Von Wiren *et al.*, 1999). Also present in the phloem is the iron transport protein 1 (ITP1), which may be involved in the movement of Fe^{3+} within the phloem, although it can also chelate Cd, Zn and Mn (Curie and Briat, 2003). Specific transport systems for the movement of Fe from the epidermal cells through to loading into the xylem have not yet been fully identified and this is an area where some of the Nramps may be important. A candidate for export of Fe from root cells to the xylem vessels is suggested to be ferroportin (FPT1, also known as IREG1 or MTP1) since it is found in vascular bundles (Schmidt, 2003) but this does not exclude the Nramps from this or similar roles. Recently, Colangelo and Guerinot (2004) identified an Fe-induced transcription factor (FIT1) expressed in the outer cell layers of the root. This transcription factor is increased with Fe-deficiency and regulates IRT1 at the protein level and FRO2 at the mRNA level. *AtNramp1* was also found to be dependent on FIT1 for its expression in roots (Colangelo and Guerinot, 2004). This suggests that AtNramp1 may play a role in Fe transport in the outer cell layers of the root. The fact that *AtNramp1* is also expressed in shoots, while *FIT1* is not, perhaps points to different roles for AtNramp1 in roots and shoots. *AtNramp1* expression is probably increased only in roots under certain Fe-deficiency conditions from a steady state expression level present in all tissues of the plant since *FIT1* is only expressed in roots. An increase above a basal level of *AtNramp1* in roots following Fe-deficiency while shoot expression remains constant has been reported (Curie *et al.*, 2000). This demonstrates how a protein can be expressed in all parts of the plant but might carry out a more specific role due to a regulatory factor expressed only in certain tissues. This suggests that AtNramp1 may play a housekeeping role in most tissues under Fe-replete conditions but also plays a specific role in roots under Fe-deficiency. It is also possible that the basal level of AtNramp1 expression may not be high enough to provide transport activity in shoots and roots until it is up-regulated by FIT1 upon Fe-deficiency. Microarray analysis has also shown that *AtNramp1* may be more strongly

expressed in roots (Koo and Ohlrogge, 2002). Koo and Ohlrogge (2002) and Ferro *et al.* (2002) have also performed *in silico* proteomic analysis to identify potential *Arabidopsis* plastid inner envelope membrane proteins, one of which was identified as AtNramp1.

Once Fe has reached the tissues where it is required it must then be unloaded from the xylem vessels and this is again an area that remains to be studied in detail. The mRNA of the pea *Ferric Reductase 1* (*FRO1*) has been shown to be present in Fe-deficient shoots and this protein may be involved in the reduction of Fe^{3+} in the xylem to allow a transport protein to unload Fe to the shoot tissues (Waters *et al.*, 2002). Microarray data has shown that an increase in cDNA clones homologous to H^+ ATPases also occurs in shoots in response to Fe-deficiency (Thimm *et al.*, 2001), suggesting that a similar mechanism to that at the root epidermis may function at the site of xylem unloading, with apoplastic acidification solubilizing Fe and driving Fe transport processes across the cell plasma membranes. This is again a potential area where members of the Nramp family may be functional in Fe homeostasis. Recently DiDonato *et al.* (2004) identified a homologue of the maize *YS1* gene in *Arabidopsis* named *YSL2*, which they localised to the vascular tissues. YSL2 was shown to transport both Fe and Cu when these ions were chelated by NA suggesting it may function in loading and unloading of Fe-NA and Cu-NA complexes into and out of the vasculature. This mechanism would presumably not require ferric reductase activity at the vascular tissue since NA has been shown to be capable of binding the Fe^{3+} ion (Von Wiren *et al.*, 1999). It may be possible that both systems are present and take priority depending on Fe availability.

Following transport into individual cells Fe must then be partitioned into the various organelles where it is required. Since Fe is involved in electron transfer chains in photosynthesis (Arnon *et al.*, 1964) it must first be transported across the chloroplast envelope through the stroma and to the thylakoid membranes. Fe transport systems have not yet been identified in the chloroplast but clearly a mechanism must exist to allow this. The Fe storage protein ferritin is often found within plastids before they differentiate into chloroplasts and may represent a stored supply of Fe for the lifetime of the chloroplast (Briat and Lobreaux, 1997). Therefore, it is possible that Fe transporters may only be present before differentiation into mature chloroplasts when Fe is being actively accumulated for storage bound to ferritin. The potential plastid inner envelope membrane localisation of AtNramp1 (Ferro *et al.*, 2002, Koo and

Ohlrogg, 2002) and its regulation by the Fe-dependent transcription factor FIT1 (Colangelo and Guerinot, 2004) makes AtNramp1 a prime candidate for a role in Fe homeostasis within the plastid. Although AtNramp6 shares high homology with AtNramp1 it has not been identified in the same studies as AtNramp1 and so it seems unlikely that it shares a similar function. Transport to other organelles is also unclear although some candidate transporters for export from the vacuole have been identified. Thomine *et al.* (2003) found that AtNramp3 localises to the vacuolar membrane where it may function in mobilising vacuolar metal pools to the cytosol. Overexpression of *AtNramp3* resulted in the down-regulation of both *IRT1* and *FRO2*, which suggests that AtNramp3 may be exporting Fe, although the levels of Mn and Zn were also higher in the roots of these plants. Another protein, IDI7, a member of the ABC family of transporters has also been localised to the tonoplast and is induced upon iron-deficiency (Yamaguchi *et al.*, 2002). The substrate of IDI7 has not yet been identified however.

Remobilisation of Fe from storage organelles and its redistribution around the plant via the phloem will also require transport proteins to be present at the various cellular membranes present in this pathway, but this is an area where data is lacking. The members of the plant Nramps that are expressed throughout the plant are potential candidates for these types of roles. Further characterisation of their localisation within the plant should help to clarify these hypotheses.

The Nramps have not been implicated solely in the transport of Fe and most experimental evidence suggests that individual Nramps are capable of transporting a number of different metals, including Fe, Mn, Zn and Cd (Curie *et al.,* 2000, Thomine *et al.*, 2000, 2003). Therefore they may play more general roles in the movement of various metal ions through the plant.

The basic principles for uptake and distribution of other metals such as Zn and Mn remain the same as that for Fe. In the case of Zn, the available data suggests that AtZIP1 to 3 are responsible for uptake of this nutrient from the soil, since they are expressed in the roots of Zn-deficient plants and can complement the yeast Zn uptake mutant *zrt1/zrt2* (Grotz *et al.*, 1998, Guerinot, 2000). ZIP4 contains a putative chloroplast targeting sequence and may function in Zn transport at this site in shoots (Grotz *et al.*, 1998, Guerinot, 2000). However, AtIRT1 has also been shown to be capable of Zn transport and is down-regulated by Zn treatment when plants are Fe-deficient (Connolly *et al.*, 2002). MTP1 of *Arabidopsis thaliana* is localised at the

tonoplast and is thought to function in transporting Zn into the vacuole in order to reduce toxic effects from excess Zn (Kobae *et al.*, 2004, Kramer, 2005). A number of other plant genes have been identified as Zn transporters or are regulated by Zn but their precise functions have not yet been ascertained.

In *Thlaspi caerulescens* two ZIPs have been identified, TcZNT1 and 2, and have been localised to the roots but were not Zn regulated (Assuncao *et al.*, 2001). However, TcZNT1 has also been localised in both roots and shoots and was regulated by Zn levels (Pence *et al.*, 2000). AtHMA4 has also been found in a range of tissues and can restore Zn transport in Zn-efflux defective *E.coli* (Mills *et al.*, 2003) and restores growth of the Zn hypersensitive *zrc1/cot1* yeast strain on high Zn media (Mills *et al.*, 2005). It is also up-regulated in response to high Zn levels in the soil. Becher *et al.* (2004) performed a microarray based comparison of the gene expression profiles of *A. thaliana* and the closely related Zn hyperaccumulator, *A. halleri*. The authors identified a number of highly and constitutively expressed genes and went on to express them in mutant yeast strains hypersensitive to Zn. Their data suggested that AhHMA3 (a P-type ATPase), AhCDF1-3 (Cation Diffusion Facilitators) and AhNAS3 (Nicotianamine Synthase) are able to function in Zn detoxification. They also suggested that ZIP family members, ZIP6 and 9, function in elevated Zn uptake from the soil in *A. halleri*. While many of these proteins do seem to be involved in Zn transport it remains unclear what their precise roles are and there are still gaps in our understanding of Zn distribution within the plant following uptake from the soil. Since AtNramp3 is localised at the tonoplast and capable of transporting Zn it may function in mobilising Zn (and other metals) from the vacuole (Thomine *et al.*, 2003). It is therefore possible that other members of the Nramp family also function in Zn transport at other membranes within the cell or in specific organs.

The uptake of Mn is less well understood although there is some evidence that AtIRT1 is also able to transport Mn (Vert *et al.*, 2001). The P-type ATPase, endoplasmic reticulum-type calcium ATPase 1 (ECA1), has also been suggested to transport Mn in plants and is localised at the endoplasmic reticulum (Wu *et al.*, 2002). ECA1 is proposed to function in the transport of Ca and Mn, since mutant plants lacking the functional protein are intolerant to high Mn levels and it provides increased tolerance to Mn in yeast mutants normally sensitive to this metal (Wu *et al.*, 2002). In tomato, a Mn binding protein that may function in the distribution of Mn within plant cells has been identified and named LeGLP1 (Takahashi and Sugiura, 2001). They

were able to show an increase in Mn binding in tobacco expressing *LeGLP1* using radioactive tracers and suggested that Mn may be bound by LeGLP1 at the plasma membrane of root cells to facilitate uptake of Mn into the plant.

Due to the apparent broad specificity of the Nramps it is possible that they may perform a role in Mn transport, alongside other transition metals. In addition to Fe and Zn, AtNramp3 may also function in Mn mobilisation from the vacuole since Mn uptake in roots was observed to decrease when AtNramp3 was overexpressed, due to vacuolar metal ion pools being mobilised (Thomine *et al.,* 2003). Some of the Nramp family members from *S. cerevisiae,* the SMF proteins, have been shown to be involved in the uptake of Mn (Supek *et al.*, 1996, Chen *et al.*, 1999, Cohen *et al.*, 2000) and it is possible that some members of the AtNramps may also perform a similar function in the plant, potentially in the uptake of Mn from the soil or in its transport within the plant.

In summary, it appears that AtNramp1 may have a potential function in Fe homeostasis in plastids while AtNramp3 and AtNramp4 function in the mobilisation of metal ions from the cell vacuole. The tissue localisation of AtNramp5 in pollen suggests a specialised role in metal homeostasis to or within the pollen grains. A summary of how the Nramps may function together with other proteins involved in Fe, Zn and Mn homeostasis is shown diagrammatically in Fig. 7.1. and Fig. 7.2. However, there are still many potential roles for the other Nramps present in plants such as uptake from the soil, loading and unloading of the vascular tissues or transport across other internal membranes. The apparent broad specificity for Fe, Zn, Mn and Cd suggests that some Nramps may be involved in the homeostasis of a number of the transition metals but further experimental evidence is required to identify these roles.

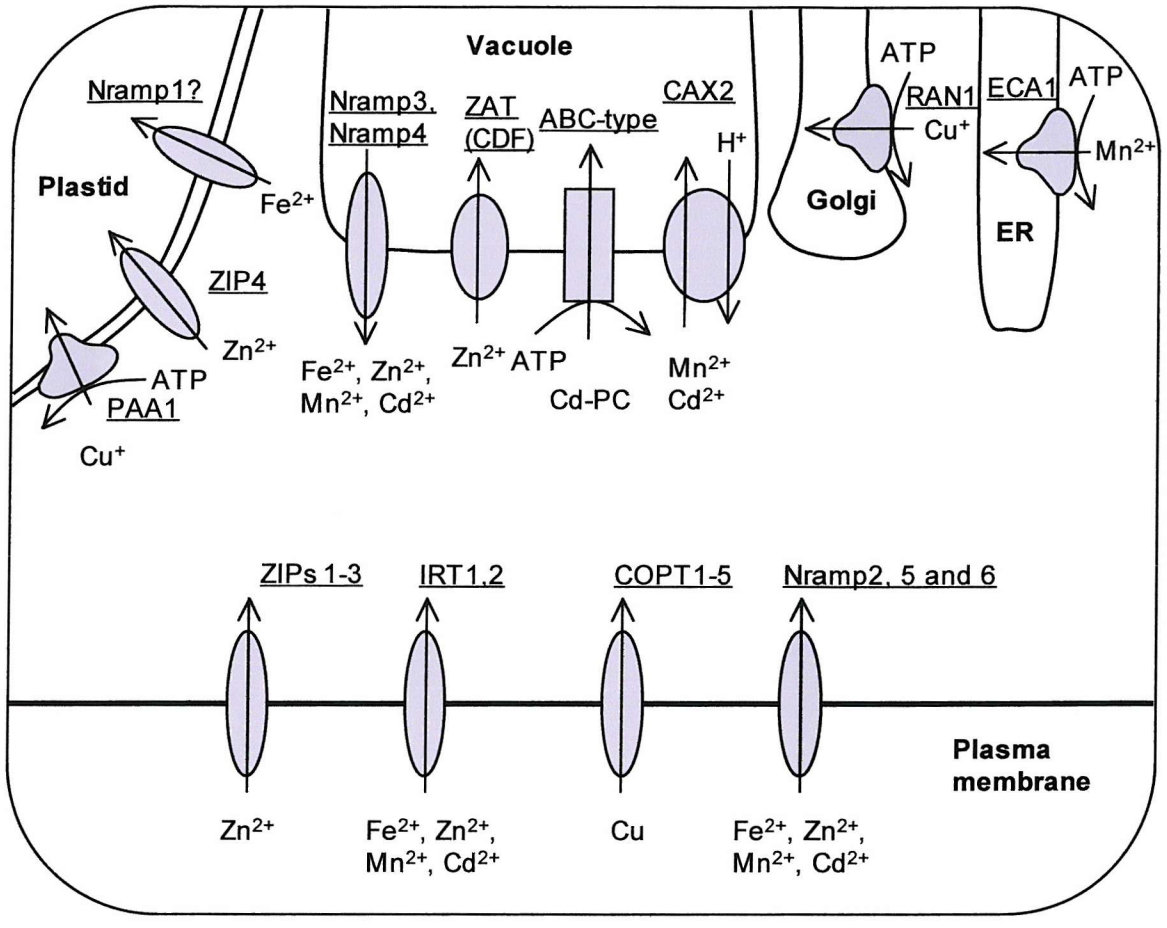

Fig. 7.1. Summary of putative transition metal transporters and their potential localisation within the plant cell. Modified after Hall and Williams (2003).

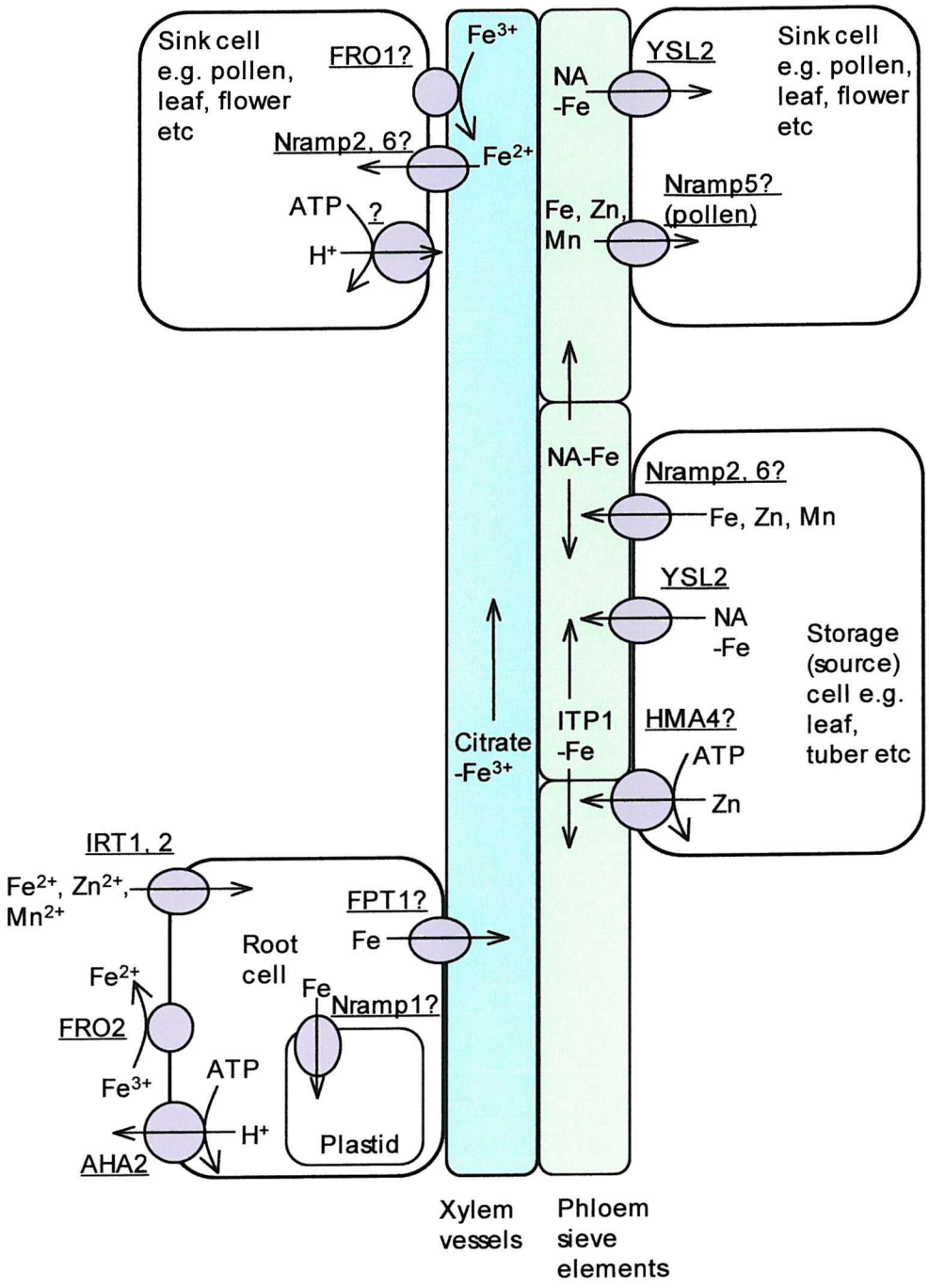

Fig. 7.2. Summary of the potential roles that members of the Nramp family may play in transition metal transport and distribution around the plant. The function and localisation of many of these proteins remains to be confirmed experimentally.

References

Abdel-Ghany, S., Muller-Moule, P., Niyogi, K., Pilon, M., and Shikanai, T. (2005). Two P-type ATPases are required for copper delivery in *Arabidopsis thaliana* chloroplasts. Plant Cell **17,** 1233-1251.

Agranoff, D., Monahan, I., Mangan, J., Butcher, P., and Krishna, S. (1999). *Mycobacterium tuberculosis* expresses a novel pH-dependent divalent cation transporter belonging to the nramp family. J. Exp. Med. **190,** 717-724.

Alonso, J., Hirayama, T., Roman, G., Nourizadeh, S., and Ecker, J. (1999). EIN2, a bifunctional transducer of ethylene and stress responses in *Arabidopsis.* Science. **284,** 2148-2152.

Arazi, T., Sunkar, R., Kaplan, B., and Fromm, H. (1999). A tobacco plasma membrane calmodulin-binding transporter confers Ni^{2+} tolerance and Pb^{2+} hypersensitivity in transgenic plants. Plant J. **20,** 171-182.

Arnon, D., Tsujimoto, H., and McSwain, B. (1964). Role of ferredoxin in photosynthetic production of oxygen and phosphorylation by chloroplasts. Proc. Natl. Acad. Sci. U.S.A. **51,** 1274-1282.

Arteca, R., and Arteca, J. (2000). A novel method for growing *Arabidopsis thaliana* plants hydroponically. Physiol. Plantarum **108,** 188-193.

Askwith, C., Eide, D., Van Ho, A., Bernard, P., Li, L., Davis-Kaplan, S., Sipe, D., and J, K. (1994). The *FET3* gene of S. cerevisiae encodes a multicopper oxidase required for ferrous iron uptake. Cell **76,** 403-410.

Assuncao, A., Martins, P., De Folter, S., Voojs, R., Schat, H., and Aarts, M. (2001). Elevated expression of metal transporter genes in three accessions of the metal hyperaccumulator *Thlaspi caerulescens.* Plant Cell Env. **24,** 217-226.

Axelsen, K., and Palmgren, M. (2001). Inventory of the superfamily of P-type ions pumps in *Arabidopsis.* Plant Physiol. **126,** 696-706.

Babcock, G., and Wikstrom, M. (1992). Oxygen activation and the conservation of energy in cell respiration. Nature **356,** 301-309.

Becher, M., Talke, I., Krall, L., and Kramer, U. (2004). Cross-species microarray transcript profiling reveals high constitutive expression of metal homeostasis genes in shoots of the zinc hyperaccumulator *Arabidopsis halleri.* Plant J. **37,** 251-268.

Belouchi, A., Cellier, M., Kwan, T., Saini, H., Leroux, G., and Gros, P. (1995). The macrophage-specific membrane protein Nramp contraolling natural resistance to infections in mice has homologues expressed in the root systems of plants. Plant Mol. Biol. **29,** 1181-1196.

Belouchi, A., Kwan, T., and Gros, P. (1997). Cloning and characterisation of the *OsNramp* family from *Oryza sativa*, a new family of membrane proteins possibly implicated in the transport of metal ions. Plant Mol. Biol. **33,** 1085-1092.

Bereczky, Z., Wang, H., Schubert, V., Ganal, M., and Bauer, P. (2003). Differential regulation of *nramp* and *irt* metal transporter genes in wild type and iron uptake mutants of tomato. J. Biol. Chem.

Bernard, C., Roosens, N., Czernic, P., Lebrum, M., and Verbruggen, N. (2004). A novel CPx-ATPase from the cadmium hyperaccumulator *Thlaspi caerulescens*. FEBS Lett. **569,** 140-148.

Bovet, L., Eggmann, T., Meylan-Bettex, M., Polier, J., Kammer, P., Marin, E., Feller, U., and Martinoia, E. (2003). Transcript levels of *AtMRPs* after cadmium treatment; induction of *AtMRP3*. Plant Cell Env. **26,** 371-381.

Briat, J.-F., Fobis-Loisy, I., Grignon, N., Lobreaux, S., Pascal, N., Savino, G., Thoiron, S., Wiren, N., and Wuytswinkel, O. (1995). Cellular and molecular aspects of iron metabolism in plants. Biol. Cell. **84,** 69-81.

Briat, J.-F., and Lobreaux, S. (1997). Iron transport and storage in plants. Trends In Plant Science. **2,** 187-193.

Bughio, N., Yamaguchi, H., Nishizawa, N., Nakanishi, H., and Mori, S. (2002). Cloning an iron-regulated metal transporter from rice. J. Exp. Biol. **53,** 1677-1682.

Caro, A., and Puntarulo, S. (1996). Effect of *in vivo* iron supplementation on oxygen radical production by soybean roots. Biochim. Biophys. Acta. **1291,** 245-251.

Cellier, M., Belouchi, A., and Gros, P. (1996). Resistance to intracellular infections: comparative genomic analysis of *Nramp*. TIG **12,** 201-204.

Cellier, M., Prive, G., Belouchi, A., Kwan, T., Chia, W., and Gros, P. (1995). Nramp defines a family of membrane proteins. Proc. Natl. Acad. Sci. U.S.A. **92,** 10089-10093.

Chen, X., Peng, J., Cohen, A., Nelson, H., Nelson, N., and Hediger, M. (1999). Yeast SMF1 mediates H^+-coupled iron uptake with concomitant uncoupled cation currents. J. Biol. Chem. **274,** 35089-35094.

Clarke, N., and Berg, J. (1998). Zinc fingers in *Caenorhabditis elegans*: Finding families and probing pathways. Science. **282,** 2018-2022.

Clemens, S. (2001). Molecular mechanisms of plant metal tolerance and homeostasis. Planta. **212,** 475-486.

Clemens, S., Palmgren, M., and Kramer, U. (2002). A long way ahead: understanding and engineering plant metal accumulation. Trends in Plant Science **7,** 309-315.

Clough, S., and Bent, A. (1998). Floral dip: a simplified method for *Agrobacterium*-mediated transformation of *Arabidopsis thaliana.* Plant J. **16,** 735-743.

Cohen, A., Nelson, H., and Nelson, N. (2000). The family of *SMF* metal ion transporters in yeast cells. J. Biol. Chem. **275,** 33388-33394.

Cohen, A., Nevo, Y., and Nelson, N. (2003). The first external loop of the metal ion transporter DCT1 is involved in metal ion binding and specificity. Proc. Natl. Acad. Sci. U.S.A. **100,** 10694-10699.

Cohen, C., Garvin, D., and Kochian, L. (2004). Kinetic properties of a micronutrient transporter from *Pisum sativum* indicate a primary function in Fe uptake from the soil. Planta. **218,** 784-792.

Colangelo, E., and Guerinot, M. (2004). The essential basic helix-loop-helix protein FIT1 is required for the iron deficiency response. Plant Cell **16,** 3400-3412.

Connolly, E., Fett, J., and Guerinot, M. (2002). Expression of the IRT1 metal transporter is controlled my metals at the levels of transcript and protein accumulation. Plant Cell **14,** 1347-1357.

Curie, C., Alonso, J., Le Jean, M., Ecker, J., and Briat, J.-F. (2000). Involvement of NRAMP1 from *Arabidopsis thaliana* in iron transport. Biochem. J. **347,** 749-755.

Curie, C., and Briat, J. (2003). Iron transport and signalling in plants. Annu. Rev. Plant Biol. **54,** 183-206.

Curie, C., Panaviene, Z., Loulergue, C., Dellaport, S., Briat, J.-F., and Walker, E. (2001). Maize *yellow stripe1* encodes a membrane protein directly involved in Fe(III) uptake. Nature **409,** 346-349.

Dancis, A., Haile, D., Yuan, D., and Klausner, R. (1994). The *Saccharomyces cerevisiae* copper transport protein (Ctr1p). J. Biol. Chem. **269,** 25660-25667.

Darley, C., Wuytswinkel, O., Woude, K., Mager, W., and Boer, A. (2000). *Arabidopsis thaliana* and *Saccharomyces cerevisiae NHX1* genes encode amiloride sensitive electroneutral Na^+/H^+ exchangers. Biochem. J. **351,** 241-249.

Davidson, J., Flanagan, C., Zhou, W., Becker, I., Elario, R., Emeran, W., Sealfon, S., and Millar, R. (1995). Identification of N-glycosylation sites in the gonadotrophin-releasing hormone receptor: role in expression but not ligand binding. Mol. Cell. Endocrin. **107,** 241-245.

Debus. (1992). The manganese and calcium-ions of photosynthetic oxygen evolution. Biochim. Biophys. Acta. **1102,** 269-352.

Delhaize, E., Kataoka, T., Hebb, D., White, R., and Ryan, R. (2003). Genes encoding proteins of the caion diffusion facilitator family that confer manganese tolerance. Plant Cell **15,** 1131-1142.

Deprez, R., Fijnvandraat, A., Ruijter, J., and Moorman, A. (2002). Sensitivity and accuracy of quantitative real-time polymerase chain reaction using SYBR green I depends on cDNA synthesis conditions. Analyt. Biochem. **307,** 63-69.

DiDonato, R., Roberts, L., Sanderson, T., Eisley, R., and Walker, E. (2004). *Arabidopsis Yellow Stripe-Like2* (*YSL2*): a metal-regulated gene encoding a plasma membrane transporter of nicotianamine-metal complexes. Plant J. **39,** 403-414.

Dix, D., Bridgham, J., Broderius, M., Byersdorfer, C., and Eide, D. (1994). The *FET4* gene encodes the low affinity Fe(II) transport protein of *Saccharomyces cerevisiae*. J. Biol. Chem. **269,** 26092-26099.

Dix, D., Bridgham, J., Broderius, M., and Elde, D. (1997). Characterisation of the FET4 protein of yeast. Evidence for a direct role in the transport of iron. J. Biol. Chem. **272,** 11770-11777.

Drager, D., Desbrosses-Fonrouge, A., Krach, C., Chardonnens, A., Meyer, R., Saumitou-Laprade, P., and Kramer, U. (2004). Two genes encoding *Arabidopsis halleri* MTP1 metal transport proteins co-segregate with zinc tolerance and account for high *MTP1* transcript levels. Plant J. **39,** 425-439.

Dreyer, I., Horeau, C., Lemaillet, G., Zimmermann, S., Bush, D., Rodriguez-Navarro, A., Schachtman, D., Spalding, E., Sentenac, H., and Gaber, R. (1999). Identification and characterisation of plant transporters using heterologous expression systems. J. Exp. Bot. **50,** 1073-1087.

Drickamer, K., and Taylor, M. (1998). Evolving views of protein glycosylation. Trends In Biochemical Sciences **23**.

Eide, D., Broderius, M., Fett, J., and Guerinot, M. (1996). A novel iron-regulated metal transporter from plants identified by functional expression in yeast. Proc. Natl. Acad. Sci. U.S.A. **93,** 5624-5628.

Eide, D., Davis-Kaplan, S., Jordan, I., Sipe, D., and Kaplan, J. (1992). Regulation of iron uptake in *Saccharomyces cerevisiae.* J. Biol. Chem. **267,** 20774-20781.

Eide, D., and Guarente, L. (1992). Increased dosage of a transcriptional activator gene enhances iron-limited growth of *Saccharomyces cerevisiae.* J. Gen. Microbiol. **138,** 347-354.

Epstein, E., and Bloom, A. (2005). Mineral nutrition of plants: Principles and perspective. 2nd Edn. (Sinauer Assoc.).

Evans, C., Harbuz, M., Ostenfeld, T., Norrish, A., and Blackwell, J. (2001). Nramp1 is expressed in neurons and is associated with behavioural and immune responses to stress. Neurogen. **3,** 69-78.

Faller, P., Kienzler, K., and Krieger-Liszkay, A. (2005). Mechanism of Cd^{2+} toxicity: Cd^{2+} inhibits photoactivation of Photosystem II by competitive binding to the essential Ca^{2+} site. Biochim. Biophys. Acta. **1706,** 158-164.

Felsenstein, J. (1985). Confidence-limits on phylogenies - An approach using the bootstrap. Evolution **39,** 783-791.

Ferro, M., Salvi, D., Riviere-Rolland, H., Vermat, T., Seigneurin-Berny, D., Grunwald, D., Garin, J., Joyard, J., and Rolland, N. (2002). Integral membrane proteins of the chloroplast envelope: Identification and subcellular localization of new transporters. Proc. Natl. Acad. Sci. U.S.A. **99,** 11487-11492.

Finkemeier, I., Kluge, C., Metwally, A., Georgi, M., Grotjohann, N., and Dietz, K. (2003). Alterations in Cd-induced gene expression under nitrogen deficiency in *Hordeum vulgare.* Plant Cell Env. **26,** 821-833.

Fleming, M., Romano, M., Su, M., Garrick, L., Garrick, M., and Andrews, N. (1998). *Nramp2* is mutated in the anemic Belgrade (*b*) rat: evidence of a role for Nramp2 in endosomal iron transport. Proc. Natl. Acad. Sci. U.S.A. **95,** 1148-1153.

Fox, T., and Guerinot, M. (1998). Molecular biology of cation transport in plants. Annu. Rev. Plant Physiol. Plant Mol. Biol. **49,** 669-696.

Goswami, T., Bhattacharjee, A., Babal, P., Searle, S., Moores, E., M, L., and Blackwell, J. (2001). Natural-resistance-associated macrophage protein 1 is an H^+/bivalent cation antiporter. Biochem. J. **354,** 511-519.

Graham, R., and Stangoulis, J. (2003). Trace element uptake and distribution in plants. J. Nutr. **133,** 1502-1505.

Gross, J., Stein, R., Fett-Neto, A., and Fett, J. (2003). Iron homeostasis related genes in rice. Genet. Mol. Biol. **26,** 477-497.

Grotz, N., Fox, T., Connolly, E., Park, W., Guerinot, M., and Eide, D. (1998). Identification of a family of zinc transporter genes from *Arabidopsis* that respond to zinc deficiency. Proc. Natl. Acad. Sci. U.S.A. **95,** 7220-7224.

Guerinot, M. (2000). The ZIP family of metal transporters. Biochim. Biophys. Acta. **1465,** 190-198.

Gunshin, H., Mackenzie, B., Berger, U., Gunshin, Y., Romero, M., Boron, W., Nussberger, S., Gollan, J., and Hediger, M. (1997). Cloning and characterization of a proton-coupled metal-ion transporter. Nature **388,** 482-488.

Hall, J. (2002). Cellular mechanisms for heavy metal detoxification and tolerance. J. Exp. Bot. **53,** 1-11.

Hall, J., and Williams, L. (2003). Transition metal transporters in plants. J. Exp. Bot. **54,** 2601-2613.

Hirayama, T., Kieber, J., Hirayama, N., Kogan, M., Guzman, P., Nourizadeh, S., Alonso, J., Dailey, W., Dancis, A., and Ecker, J. (1999). Responsive-to-antagonist 1, a Menkes/Wilson disease related copper transporter, is required for ethylene signalling in *Arabidopsis*. Cell **97,** 383-393.

Hirschi, K. (2001). Vacuolar H^+/Ca^{2+} transport; who's directing the traffic? Trends In Plant Science **6,** 100-104.

Hirschi, K., Korenkov, V., Wilganowski, N., and Wagner, G. (2000). Expression of *Arabidopsis CAX2* in tobacco. Altered metal accumulation and increased manganese tolerance. Plant Physiol. **124,** 125-134.

Hirschi, K., Zhen, R., Cunningham, K., Rea, P., and Fink, G. (1996). CAX1, an H^+/Ca^{2+} antiporter from *Arabidopsis*. Proc. Natl. Acad. Sci. U.S.A. **93,** 8782-8786.

Hoffman, C., and Winston, F. (1987). A 10-minute preparation from yeast efficiently releases autonomous plasmids for transformation of *Escherichia coli.* Gene **57,** 267-272.

Hofmann, K., and Stoffel, W. (1993). TMbase - A database of membrane spanning proteins segments. Biol. Chem. **374,** 166.

Honys, D., and Twell, D. (2003). Comparative analysis of the Arabidopsis pollen transcriptome. Plant Physiol. **132,** 640-652.

Hubert, N., and Hentze, M. (2002). Previously uncharacterised isoforms of divalent metal transporter (DMT)-1: Implications for regulation and cellular function. Proc. Natl. Acad. Sci. U.S.A. **99,** 12345-12350.

Hussain, D., Haydon, M., Wang, Y., Wong, E., Sherson, S., Young, J., Camakaris, J., Harper, J., and Cobbett, C. (2004). P-type ATPases heavy metal transporters with roles in essential zinc homeostasis in *Arabidopsis.* Plant Cell **16,** 1327-1339.

Jefferson, R., Burgess, S., and Hirsh, D. (1986). b-glucuronidase from Escherichia coli as a gene-fusion marker. Proc. Natl. Acad. Sci. U.S.A. **83,** 8447-8451.

Kaiser, B., Moreau, S., Castelli, J., Thomson, R., Lambert, A., Bogliolo, S., Puppo, A., and Day, D. (2003). The soybean NRAMP homologue, GmDMT1, is a symbiotic divalent metal transporter capable of ferrous iron transport. Plant J. **35,** 295-304.

Kampfenkel, K., Kushnir, S., Babiychuk, E., Inze, D., and Van Montagu, M. (1995). Molecular characterization of a putative *Arabidopsis thaliana* copper transporter and its yeast homologue. J. Biol. Chem. **270,** 28479-28486.

Kispal, G., Csere, P., Guiard, B., and Lill, R. (1997). The ABC transporter Atm1p is required for mitochondrial iron homeostasis. FEBS Lett. **418,** 346-350.

Kobae, Y., Uemura, T., Sato, M., Ohnishi, M., Mimura, T., Nakagawa, T., and Maeshima, M. (2004). Zinc transporter of *Arabidopsis thaliana* AtMTP1 is localized to vacuolar membranes and implicated in zinc homeostasis. Plant Cell Physiol. **45,** 1749-1758.

Koo, A., and Ohlrogge, J. (2002). The predicted candidates of Arabidopsis plastid inner envelope membrane proteins and their expression profiles. Plant Physiol. **130,** 823-836.

Kornfeld, R., and Kornfeld, S. (1985). Assembly of aspargine-linked oligosaccharides. Annu. Rev. Biochem. **54,** 631-664.

Krysan, P., Young, J., and Sussman, M. (1999). T-DNA as an insertional mutagen in Arabidopsis. Plant Cell. **11,** 2283-2290.

Krysan, P., Young, J., Tax, F., and Sussman, M. (1996). Identification of transferred DNA insertions within *Arabidopsis* genes involved in signal transduction and ion transport. Proc. Natl. Acad. Sci. U.S.A. **93,** 8145-8150.

Leng, Q., Mercier, R., Hua, B., Fromm, H., and Berkowitz, G. (2002). Electrophysiological analysis of cloned nucleotide-gated ion channels. Plant Physiol. **128,** 400-410.

Liu, X., and Culotta, V. (1999a). Mutational analysis of *Saccharomyces cerevisiae* Smf1p, a member of the Nramp family of metal transporters. J. Mol. Biol. **289,** 885-891.

Liu, X., and Culotta, V. (1999b). Post-translation control of nramp metal transport in yeast. Role of metal ions and the *BSD2* gene. J. Biol. Chem. **274,** 4863-4868.

Lorkovic, Z., Wieczorek Kirk, D., Lambermon, M., and Filipowicz, W. (2000). Pre-mRNA splicing in higher plants. Trends In Plant Science **5,** 160-167.

Luk, E., and Culotta, V. (2001). Manganese superoxide dismutase in *Saccharomyces cerevisiae* acquires its metal co-factor through a pathway involving the nramp metal transporter, Smf2p. J. Biol. Chem. **276,** 47556-47562.

Macknight, R., Bancroft, I., Page, T., Lister, C., Schmidt, R., Love, K., Westphal, L., Murphy, G., Sherson, S., Cobbett, C., and Dean, C. (1997). *FCA*, a gene controlling flowering time in *Arabidopsis*, encodes a protein containing RNA-binding domains. Cell **89,** 737-745.

Maeda, T., Sugiura, R., Kita, A., Saito, M., Deng, L., He, Y., Lu, Y., Fujita, Y., Takegawa, K., Shuntoh, H., and Kuno, T. (2004). Pmr1, a P-type ATPase, and Pdt1, an *Nramp* homologue cooperatively regulate cell morphogenesis in fission yeast: The importance of Mn^{2+} homeostasis. Genes To Cells **9,** 71-82.

Makui, H., Roig, E., Cole, S., Helmann, J., Gros, P., and Cellier, M. (2000). Identification of the *Escherichia coli* K-12 nramp ortholog (MntH) as a selective divalent metal ion transporter. Mol. Microbiol. **35,** 1065-1078.

Marjorette, M., Pena, O., Puig, S., and Thiele, D. (2000). Characterization of the *Saccharomyces cerevisiae* high affinity copper transporter Ctr3. J. Biol. Chem. **275,** 33244-33251.

Maser, P., Thomine, S., Schroeder, J., Ward, J., Hirschi, K., Sze, H., Talke, I., Amtmann, A., Maathius, F., Sanders, D., Harper, J., Tchieu, J., Gribskov, M., Persans, M., Salt, D., Kim, S., and Guerinot, M. (2001). Phylogenetic relationships within cation transporter families of Arabidopsis. Plant Physiol. **126,** 1646-1667.

McCormac, A., Elliott, M., and Chen, D. (1997). pBECKS. A flexible series of binary vectors for *Agrobacterium*-mediated plant transformation. Mol. Biotechnol. **8,** 199-213.

Meneghini, R. (1997). Iron homeostasis, oxidative stress and DNA damage. Free Rad. Biol. Med. **23,** 783-792.

Metwally, A., Safronova, V., Belimov, A., and Dietz, K. (2005). Genotypic variation of the response to cadmium toxicity in *Pisum sativum* L. J. Exp. Bot. **56,** 167-178.

Mills, R., Francini, A., Ferreira da Rocha, P., Baccarini, P., Aylett, M., Krijger, G., and Williams, L. (2005). The Plant P_{1B}-type ATPase AtHMA4 trnasports Zn and Cd and plays a role in detoxification of transition metals supplied at elevated levels. FEBS Lett. **579,** 783-791.

Mills, R., Krijger, G., Baccarini, P., Hall, J., and Williams, L. (2003). Functional expression of AtHMA4, a P_{1B}-type ATPase of the Zn/Co/Cd/Pb subclass. Plant J. **35,** 164-176.

Mori, S. (1999). Iron acquisition by plants. Curr. Opin. Plant Bio. **2,** 250-253.
Norvell, W., and Welch, R. (1993). Growth and nutrient uptake by Barley (*Hordeum vulgare* L. cv Herta): Studies using *N*-(2-Hydroxyethyl)ethylenedinitrilotriacetic acid-buffered nutrient solution technique. Plant Physiol. **101,** 619-625.

Ortiz, D., Kreppel, L., Speiser, D., Scheel, G., McDonald, G., and Ow, D. (1992). Heavy metal tolerance in the fission yeast requires an ATP-binding cassette-type vacuolar membrane transporter. EMBO J. **11,** 3491-3499.
Page, R. (1996). TREEVIEW: An application to display phylogenetic trees on personal computers. Comp. Appl. Biosci. **12,** 357-358.

Palmgren, M., and Axelsen, K. (1998). Evolution of P-type ATPases. Biochim. Biophys. Acta. **1365,** 37-45.

Papoyan, A., and Kochian, L. (2004). Identification of *Thlaspi caerulescens* genes that may be involved in heavy metal hyperaccumulation and tolerance. Characterization of a novel heavy metal transporting ATPase. Plant Physiol. **136,** 3814-3823.

Pascal, C., Roman, C., Frederic, V., and Cellier, M. (2003). Determination of the transmembrane topology of *Escherichia coli* Nramp ortholog. J. Biol. Chem. **279,** 3318-3326.

Patrick, J., and Offler, C. (2001). Compartmentation of transport and transfer events in developing seeds. J. Exp. Bot. **52,** 551-564.

Pence, N., Larsen, P., Ebbs, S., Letham, D., Lasat, M., Garvin, D., Eide, D., and Kochian, L. (2000). The molecular physiology of heavy metal transport in the Zn/Cd hperaccumulator *Thlaspi caerulescens*. Proc. Natl. Acad. Sci. U.S.A. **97,** 4956-4960.

Persans, M., Nieman, K., and Salt, D. (2001). Functional activity and role of cation-efflux family members in Ni hyperaccumulation in *Thlaspi goesingense*. Proc. Natl. Acad. Sci. U.S.A. **98,** 9995-10000.

Picard, V., Govoni, G., Jabado, N., and Gros, P. (2000). Nramp2 (DCT1/DMT1) expressed at the plasma membrane transports iron and other divalent cations into a calcein-accessible cytoplasmic pool. J. Biol. Chem. **275,** 35738-35745.

Pinner, E., Gruenheid, S., Raymond, M., and Gros, P. (1997). Functional complementation of the yeast divalent cation transporter family *SMF* by *Nramp2*, a member of the mammalian natural resistance associated macrophage protein family. J. Biol. Chem. **272,** 28933-28938.

Portnoy, M., Liu, X., and Culotta, V. (2000). *Saccharomyces cerevisiae* expresses three functionally distinct homologues of the nramp family of metal transporters. Mol. Cell. Biol. **20,** 7893-7902.

Ririe, K., Rasmussen, R., and Wittwer, C. (1997). Product differentiation by analysis of DNA melting curves during the polymerase chain reaction. Analyt. Biochem. **245,** 154-160.

Roberts, L., Pierson, A., Panaviene, Z., and Walker, E. (2004). Yellow Stripe1. Expanded roles for the maize iron-phytosiderophore transporter. Plant Physiol. **135,** 112-120.

Robinson, N., Procter, C., Connolly, E., and Guerinot, M. (1999). A ferric-chelate reductase for iron uptake from soils. Nature **397,** 694-697.

Rodrigues, V., Cheah, P., Ray, K., and Chia, W. (1995). *malvolio*, the *Drosophila* homologue of mouse NRAMP-1 (*Bcg*), is expressed in macrophages and in the nervous system and is required for normal taste behaviour. EMBO J. **14,** 3007-3020.

Romheld, V., and Marschner, H. (1986). Evidence for a specific uptake system for iron phytosiderophores in roots of grasses. Plant Physiol. **80,** 175-180.

Salier, J.-P. (2000). Chromosomal location, exon/intron organization and evolution of lipocalin genes. Biochim. Biophys. Acta. **1482,** 25-34.

Sancenon, V., Puig, S., Mira, H., Thiele, D., and Penarrubia, L. (2003). dentification of a copper transporter family in *Arabidopsis thaliana.* Plant Mol. Biol. **51,** 577-587.

Sauer, K., and Yachandra, V. (2004). The water-oxidation complex in photosynthesis. Biochim. Biophys. Acta. **1655,** 140-148.

Schmidt, W. (2003). Iron homeostasis in plants: Sensing and signalling pathways. J. Plant Nutr. **26,** 2211-2230.

Schulze, W., Weise, A., Frommer, W., and Ward, J. (2000). Function of the cytosolic N-terminus of sucrose transporter AtSUT2 in substrate affinity. FEBS Lett. **485,** 189-194.

Shigaki, T., Pittman, J., and Hirschi, K. (2003). Manganese specificity determinants in the *Arabidopsis* metal/H^+ antiporter CAX2. J. Biol. Chem. **278,** 6610-6617.

Shikanai, T., Muller-Moule, P., Munekage, Y., Niyogi, K., and Pilon, M. (2003). PAA1, a P-type ATPase of *Arabidopsis*, functions in copper transport in chloroplasts. Plant Cell **15,** 1333-1346.

Shimaoka, T., Ohnishi, M., Sazuka, T., Mitsuhashi, N., Hara-Nishimura, I., Shimazaki, K., Maeshima, M., Yokota, A., Tomizawa, K., and Mimura, T. (2004). Isolation of intact vacuoles and prteomic analysis of tonoplast from suspension-cultured cells of *Arabidopsis thaliana.* Plant Cell Physiol. **45,** 672-683.

Solioz, M., and Vulpe, C. (1996). CPx-type ATPases: a class of P-type ATPases that pump heavy metals. Trends Biochem. Sci. **21,** 237-241.

Sonnhammer, E., Eddy, S., Birney, E., Bateman, A., and Durbin, R. (1998). Pfam: multiple sequence alignments and HMM-profiles of protein domains. Nucl. Acids Res. **26,** 320-322.

Srivastava, S., Ansari, N., Liu, S., Izban, A., Das, B., Szabo, G., and Bhatnagar, A. (1989). The effects of oxidants on biomembranes and cellular metabolism. Mol. Cell. Biochem. **91,** 149-157.

Stearman, R., Yuan, D., Yamaguchilwai, Y., Klausner, R., and Dancis, A. (1996). A permease-oxidase complex involved in high-affinity iron uptake in yeast. Science. **271,** 1552-1557.

Supek, F., Supekova, L., Nelson, H., and Nelson, N. (1996). A yeast manganese transporter related to the macrophage protein involved in conferring resistance to mycobacteria. Proc. Natl. Acad. Sci. U.S.A. **93,** 5105-5110.

Supek, F., Supekova, L., Nelson, H., and Nelson, N. (1997). Function of metal-ion homeostasis in the cell division cycle, mitochondrial protein processing, sensitivity to mycobacterial infection and brain function. J. Exp. Biol. **200,** 321-330.

Tabata, K., Kashiwagi, S., Mori, H., Ueguchi, C., and Mizuno, T. (1997). Cloning of a cDNA encoding a putative metal-transporting P-type ATPase from *Arabidopsis thaliana*. Biochim. Biophys. Acta. **1326,** 1-6.

Tabuchi, M., Yoshida, T., Takegawa, K., and Kishi, F. (1999). Functional analysis of the human NRAMP family expressed in fission yeast. Biochem. J. **344**.

Takahashi, M., and Sugiura, M. (2001). Strategies for uptake of a soil micronutrient, manganese, by plant roots. RIKEN Review **35,** 76-77.

Tandy, S., Williams, M., Leggett, A., Lopez-Jimenez, M., Dedes, M., Rameshi, B., Srai, S., and Sharp, P. (2000). Nramp2 expression is associated with pH-dependent iron uptake across the apical membrane of human intestinal Caco-2 cells. J. Biol. Chem. **275,** 1023-1029.

Tchernitchko, D., Bourgeois, M., Martin, M., and Beaumont, C. (2002). Expression of the two mRNA isoforms of the iron transporter nramp2/DMT1 in mice and function of the iron responsive element. Biochem. J. **363,** 449-455.

Tennant, J., Stansfield, M., Yamaji, S., Srai, S., and Sharp, P. (2002). Effects of copper on the expression of metal transporters in human intestinal CaCO-2 cells. FEBS Lett. **527,** 239-244.

Tester, M., and Leigh, R. (2001). Partitioning of nutrient transport processes in roots. J. Exp. Bot. **52,** 445-457.

Theodoulou, F. (2000). Plant ABC transporters. Biochim. Biophys. Acta. **1465,** 79-103.

Thimm, O., Essigmann, B., Klosker, S., Altmann, T., and Buckhout, T. (2001). Response of *Arabidopsis* to iron deficiency stress as revelaed by microarray analysis. Plant Physiol. **127,** 1030-1043.

Thomine, S., Lanquar, V., Lelievre, F., Vansuyt, G., Curie, C., Kramer, U., and Barbier-Brygoo, H. (2004). AtNramp3 and AtNramp4 encode redundant metal transporters involved in the mobilization of vacuolar iron pools. In 13th International Workshop on Plant Membrane Biology (Montpellier, France).

Thomine, S., Lelievre, F., Debarbieux, E., Schroeder, J., and Barbier-Brygoo, H. (2003). AtNramp3, a multispecific vacuolar metal transporter involved in plant responses to iron deficiency. Plant J. **34,** 685-695.

Thomine, S., Wang, R., Ward, J., Crawford, N., and Schroeder, J. (2000). Cadmium and iron transport by members of a plant metal transporter family in *Arabidopsis* with homology to *Nramp* genes. Proc. Natl. Acad. Sci. U.S.A. **97,** 4991-4996.

Thompson, J., Higgins, D., and Gibson, T. (1994). CLUSTAL W: improving the sensitivity of progressive multiple sequence alignment through sequence weighting, positions-specific gap penalties and weight matrix choice. Nucl. Acids Res. **22,** 4673-4680.

Van der Zaal, B., Neuteboom, L., Pinas, J., Chardonnens, A., Schat, H., Verkleij, J., and Hooykaas, P. (1999). Over-expression of a novel *Arabidopsis* gene related to putative zinc-transporter genes from animals can lead to enhanced zinc resistance and accumulation. Plant Physiol. **119,** 1047-1055.

Vert, G., Briat, J.-F., and Curie, C. (2001). *Arabidopsis* IRT2 gene encodes a root periphery iron transporter. Plant J. **26,** 181-189.

Vert, G., Grotz, N., Dedaldechamp, F., Gaymard, F., Guerinot, M., Briat, J.-F., and Curie, C. (2002). IRT1, an *Arabidopsis* transporter essential for iron uptake from the soil and for plant growth. Plant Cell **14,** 1223-1233.

Vidal, S., Malo, D., Vogan, K., Skamene, E., and Gros, P. (1993). Natural resistance to infection with intracellular parasites: isolation of a candidate for *Bcg.* Cell **73,** 469-485.

von Heijne, G. (1992). Membrane protein structure prediction: hydrophobicity analysis and the 'positive inside' rule. J. Mol. Biol. **225,** 487-494.

Von-Wiren, N., Klair, S., Bansal, S., Briat, J.-F., Khodr, H., Shioiri, T., Leigh, R., and Hider, R. (1999). Nicotianamine chelates both Fe^{III} and Fe^{II}. Implications for metal transport in plants. Plnat Physiol. **119,** 1107-1114.

Wang, S., Yang, Z., Yang, H., Lu, B., Li, S., and Lu, Y. (2004). Copper-induced stress and antioxidative responses in roots of *Brassica juncea* L. Bot. Bull. Acad. Sin. **45,** 203-212.

Waters, B., Blevins, D., and Eide, D. (2002). Characterization of FRO1, a pea ferric-chelate reductase involved in root iron acquisition. Plant Physiol. **129,** 85-94.

Weckx, J., and Clijsters, H. (1996). Oxidative damage and defense mechanisms in primary leaves of *Phaseolus vulgaris* as a result of root assimilation of toxic amounts of copper. Physiol. Plantarum **96,** 506-512.

Williams, L., Pittman, J., and Hall, J. (2000). Emerging mechanisms for heavy metal transport in plants. Biochim. Biophys. Acta. **1465,** 104-126.

Wittwer, C., Ririe, K., Andrew, R., David, D., Gundry, R., and Balis, U. (1997). The lightcycler: a microvolume multisample fluorimeter with rapid temperature control. Biotechiques **22,** 176-181.

Woeste, K., and Kieber, J. (2000). A strong loss-of-function mutation in *RAN1* results in constitutive activation of the ethylene response pathway as well as a rosette-lethal phenotype. Plant Cell **12,** 443-455.

Wood, M., VanDongen, H., and VanDongen, A. (1995). Structural conservation of ion conduction pathways in K channels and glutamate receptors. Proc. Natl. Acad. Sci. U.S.A. **92,** 4882-4886.

Wu, Z., Liang, F., Hong, B., Young, J., Sussman, M., Harper, J., and Sze, H. (2002). An endoplasmic reticulum-bound Ca^{2+}/Mn^{2+} pump, ECA1, supports plant growth and confers tolerance to Mn^{2+} stress. Plant Physiol. **130,** 128-137.

Yamaguchi, H., Nishizawa, N., Nakanishi, H., and Mori, S. (2002). IDI7, a new iron-regulateed ABC transporter from barley roots, localizes to the tonoplast. J. Exp. Bot. **53,** 727-735.

Yamaji, S., Tennant, J., Tandy, S., Williams, M., Srai, S., and Sharp, P. (2001). Zinc regulates the function and expression of the iron transporters DMT1 and IREG1 in human intestinal Caco-2 cells. FEBS Lett. **507,** 137-141.

Zhang, L., Lee, T., Wang, Y., and Soong, T. (2000). Heterologous expression, functional characterisation and localisation of two isoforms of the monkey iron transporter nramp2. Biochem. J. **349,** 289-297.

Zhao, H., and Eide, D. (1996a). The yeast *ZRT1* gene encodes the zinc transporter protein of a high-affinity uptake system induced by zinc limitation. Proc. Natl. Acad. Sci. U.S.A. **93,** 2454-2458.

Zhao, H., and Eide, D. (1996b). The *ZRT2* gene encodes the low affinity zinc transporter in *Saccharomyces cerevisiae*. J. Biol. Chem. **271,** 23203-23210.

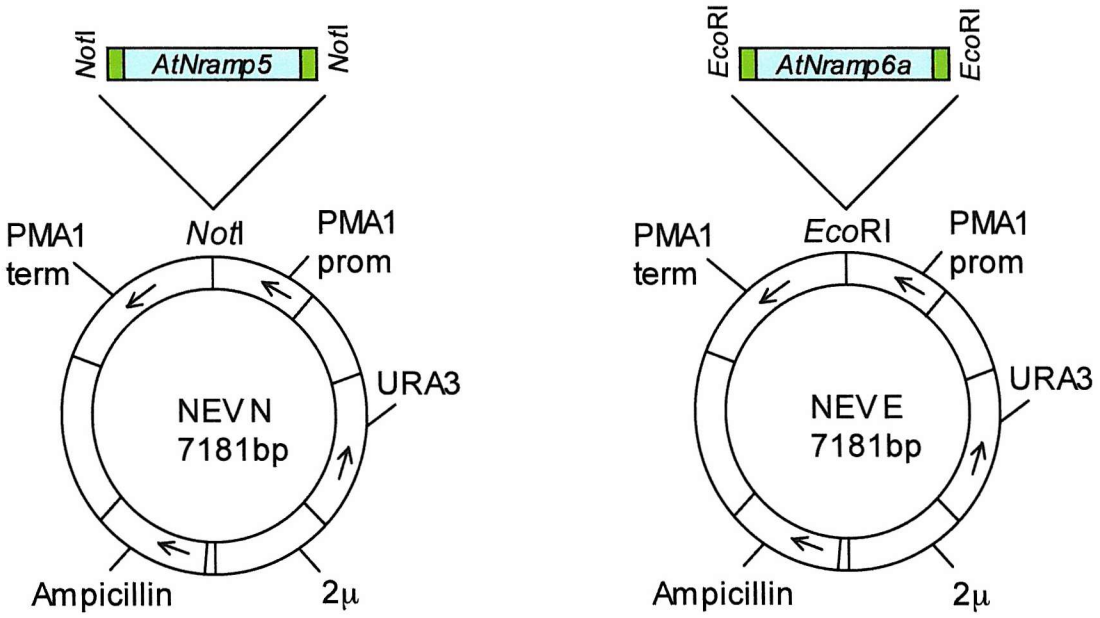

Appendix I (A). Diagrammatic representation of plasmid constructs prepared for use in yeast expression. The *AtNramp* genes inserted into each plasmid are shown above each plasmid as blue bars (representing the coding region of each gene) with yellow bars representing the 5´ and 3´ untranslated regions. The restriction sites used are named at each end of the gene. NEVN/*AtNramp5* and NEVE/*AtNramp6a* plasmid constructs were created in our laboratory (Pittman and Williams, unpublished).

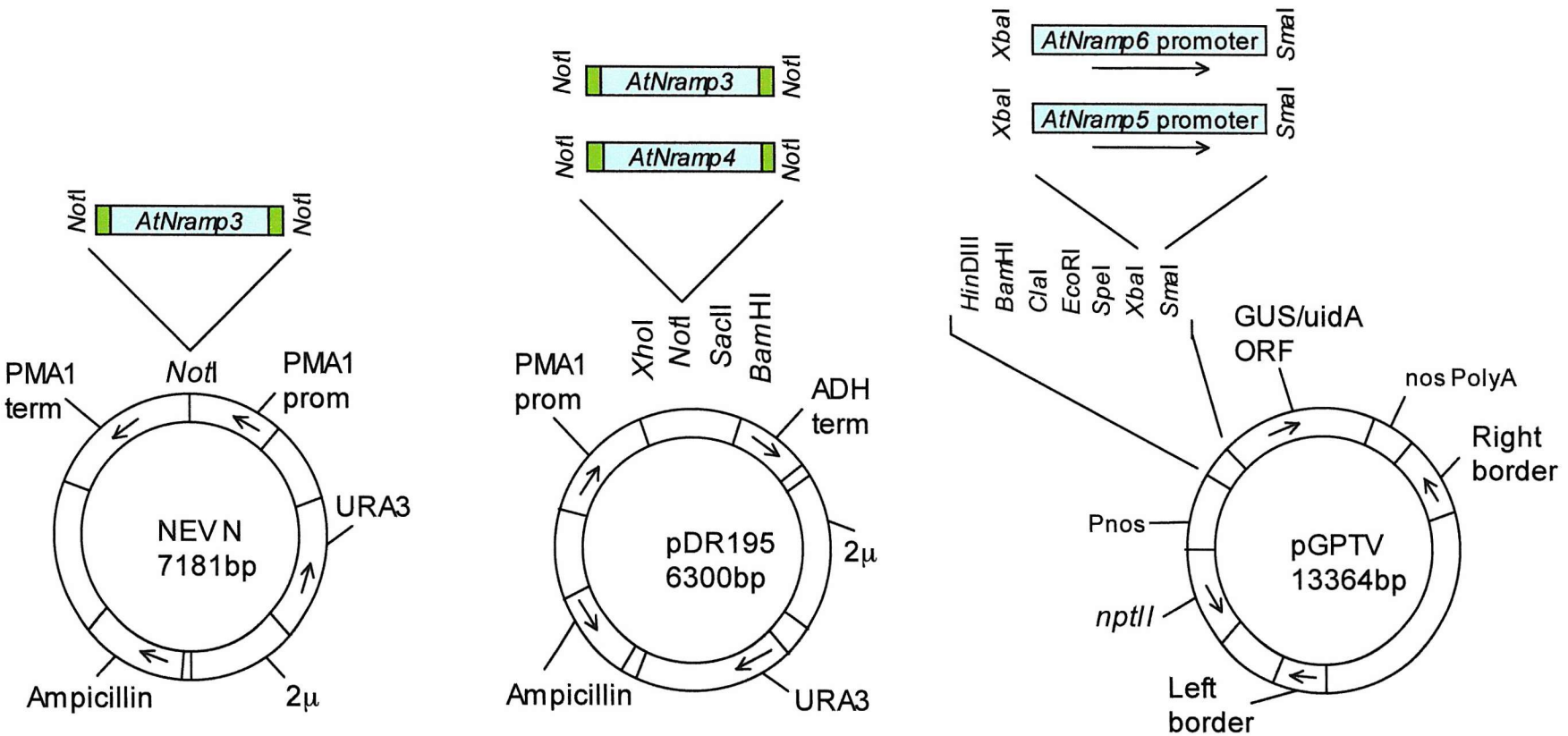

Appendix I (B). Plasmid vectors used in heterologous expression of *AtNramps* in yeast (NEVN and pDR195) and *AtNramp* promoter driven expression of β-glucuronidase in *Arabidopsis thaliana* and tobacco (pGPTV). NEVE/*AtNramp3*, pGPTV/*AtNramp5* promoter and pGPTV/*AtNramp6* promoter constructs were created in our laboratory (Pittman and Williams, unpublished). pDR195/*AtNramp3* and pDR195/*AtNramp4* were provided by Dr. Sebastien Thomine (Institut des Sciences Vegetal, Gif-sur-Yvette Cedex, France).

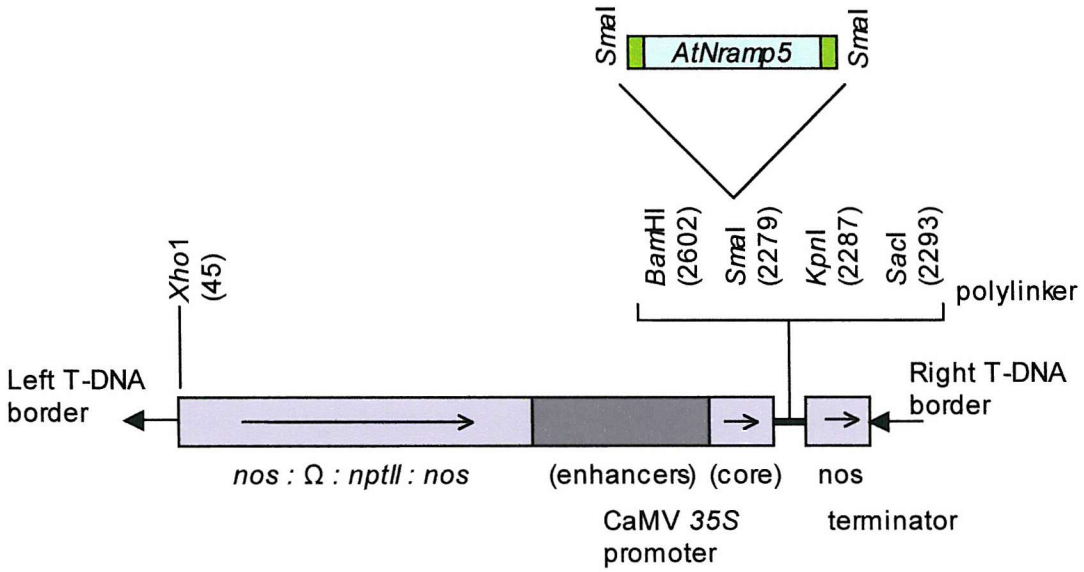

pBECKS$_{400.6}$

Appendix I (C). Vector map of pBECKS$_{400.6}$ (McCormac *et al.*, 1997) used for constitutive overexpression of the cDNA of *AtNramp5* under the control of the CaMV *35S* promoter. Cloning of *AtNramp5* into this vector was performed in our laboratory (Biggs and Williams, unpublished).